

Investigations of Tetraspanin Functions Using Large Extracellular Loops

by

Christopher C. Liu

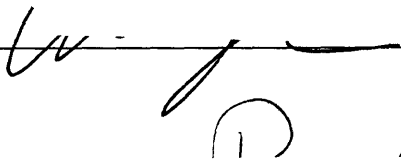
B.A. Biology
Washington University in St. Louis, 1997

SUBMITTED TO THE DEPARTMENT OF BIOLOGY IN PARTIAL FULFILLMENT
OF THE REQUIREMENTS FOR THE DEGREE OF

DOCTOR OF PHILOSOPHY IN BIOLOGY
AT THE
MASSACHUSETTS INSTITUTE OF TECHNOLOGY

SEPTEMBER 2005

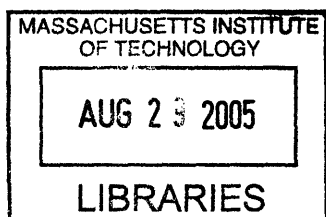
© 2005 Massachusetts Institute of Technology
All Rights Reserved

Signature of Author:  _____
Department of Biology
June 13, 2001

Certified by: _____
Peter S. Kim
Professor of Biology
Thesis Supervisor

Certified by: _____
Richard O. Hynes
Professor of Biology
Thesis Supervisor

Accepted by: _____
Stephen P. Bell
Professor of Biology
Graduate Committee Chairperson



ARCHIVES

Investigations of Tetraspanin Functions Using Large Extracellular Loops

Christopher C. Liu

**Submitted to the Department of Biology on June 13th, 2005 in Partial
Fulfillment of the Requirements for the Degree of Doctor of Philosophy**

Abstract

This thesis describes our characterization of a specific tetraspanin domain: the large extracellular loop (LEL). Tetraspanins are involved in cellular migration, adhesion, and metastasis, sperm-egg fusion, and viral infectivity. The large extracellular loop domain is the major extracellular domain of tetraspanins and the binding of a monoclonal antibody against the tetraspanin CD9 serves to inhibit fertilization, consistent with the CD9-null mouse model. The first area of focus in this thesis is the characterization of the murine CD9-LEL domain. We present a methodology to express and purify the mCD9-LEL to homogeneity. Biophysical characterization of the mCD9-LEL protein reveals that it is an autonomously folding, α -helical dimer. Mutagenesis over much of the mCD9-LEL protein reveals that it is composed of two subdomains: a dimerization subdomain and a variable subdomain proposed to mediate heterotypic interactions. These results suggest both a means for exploring endogenous tetraspanins functions and a mechanism by which tetraspanins may oligomerize. Surprisingly, we were not able to detect oligomerization of the intact CD9 molecule, in discordance with our biophysical data on the mCD9-LEL. In the latter part of this thesis, we expand our methodology to purify and characterize three different tetraspanins-LELs, the hCD9-LEL, the hCD63-LEL, and the hCD81-LEL. These tetraspanins-LELs all exhibit similar characteristics to the mCD9-LEL, consistent with a published crystal structure of the hCD81-LEL. Lastly, we demonstrate the ability of our tetraspanin-LEL proteins to bind integrins, to inhibit sperm-egg fusion, and to inhibit hepatitis C viral infectivity. Taken as a whole, these studies present novel, biophysically validated tetraspanins-LELs that lend insight into endogenous tetraspanins functions.

Thesis Co-Supervisor: Peter S. Kim
Title: Professor of Biology
Thesis Co-Supervisor: Richard O. Hynes
Title: Professor of Biology

Acknowledgments

This thesis has been the culmination of efforts not only on my part, but also those of countless others. In many ways, this section is not so much acknowledgments as many thanks to all those mentioned and unmentioned who have set me on the right path throughout the years.

First and foremost I would like to thank the people most directly involved in this body of work: my co-advisors Peter Kim and Richard Hynes. They have given me enthusiastic support and encouragement throughout this process. Their respective laboratories were also instrumental in both my development as a scientist and as a person. Although I initiated an ambitious experiment outside the core expertise of the Kim lab, the laboratory learned quickly about sperm-egg fusion and proceeded to enthusiastically critique my ideas. As I brought my project to the Hynes lab, the laboratory also excitedly learned about tetraspanins.

Most of all, I would like to thank my family and friends for their support and numerous visits to Boston over the years. I thank my wife, Mariette, for her unrelenting encouragement over the years. And finally, for my cat Sophie, who was the only one who saw the whole thing through.

Contents

Chapter 1: Introduction.....7

The Tetraspanin Family.....	8
Sequence Conservation of The Tetraspanin Large Extracellular Loops.....	9
Structural Studies of the human CD81-LEL.....	11
Recombinant Tetraspanin-LELs.....	15
Heterotypic Tetraspanin Interactions.....	18
Tetraspanins and Integrins.....	20
Homotypic Tetraspanin Interactions.....	23
Genetic Studies of Tetraspanins.....	25
Viral Membrane Fusogens.....	28
Cell-cell fusion.....	30
Sperm-Egg Fusion.....	32

Chapter 2: Purification and Characterization of the Murine CD9 Large Extracellular Loop.....42

Introduction.....	43
Materials and Methods.....	44
Results.....	47
Expression and Partial Purification of the mCD9-LEL Protein.....	47
Isolation and Characterization of Two mCD9-LEL Protein Species.....	47
Circular Dichroism and Sedimentation Equilibrium Analysis of mCD9-LEL Protein Species.....	48
Disulfide-Shuffling of mCD9-LEL Protein Variants.....	49
Discussion.....	41
Figures.....	53

Chapter 3: Structural Studies of the murine CD9 Large Extracellular Loop.....59

Introduction.....	60
Materials and Methods.....	62
Results.....	64
Protein Crystallization Trials of the mCD9-LEL.....	64
Nuclear Magnetic Resonance Studies of the mCD9-LEL.....	64
Homology Model Construction of the hCD9-LEL.....	65
Discussion.....	66
Figures.....	68

Chapter 4: Molecular Biological Studies of the Murine CD9 Large Extracellular Loop.....76

Introduction.....77
Materials and Methods.....79
Results.....84
 The Folding Stability of the mCD9-LEL Dimer.....84
 Epitope-Mapping of the KMC8/mCD9-LEL Binding Site.....85
 Binding of KMC8 Fab Fragments to the mCD9-LEL.....86
Discussion.....87
Figures.....90

Chapter 5: Oligomerization Studies of the CD9 Protein.....100

Introduction.....101
Materials and Methods.....103
Results.....107
 Detergent Stability of CD9 Homooligomers.....107
 Gel Filtration Analysis of the CD9 Protein.....107
 Native-Blue Electrophoresis Analysis of the CD9 Protein.....108
 Cross-Linking Analysis of CD9 Protein.....109
 Detergent Stability of mCD9-LEL Dimers.....110
Discussion.....111
Figures.....113

Chapter 6: Purification and Characterization of Human Tetraspanin-Large Extracellular Loops.....118

Introduction.....119
Materials and Methods.....121
Results.....124
 Exprssion of Human Tetraspanin-LEL Proteins.....124
 Purification and Characterization of Four Cysteine-Containing Tetraspanin-LEL Proteins.....124
 Purification and Characterization of Six Cysteine-Containing Tetraspanin-LEL Proteins.....125
 Heterodimer Formation of Tetraspanin-LEL Proteins.....126
Discussion.....128
Figures.....131

Chapter 7: The Role of Tetraspanins in Cell-Cell Fusion.....140

Introduction.....141
Materials and Methods.....143

Results.....	146
CD9-LEL Inhibition Studies of Fertilization.....	146
CD9 Rescue Studies of CD9-Null Eggs.....	146
Characterization of Non-Fertilization Permissive CD9.....	147
Immunoprecipitation of mCD9-LEL Oocyte Binding Partners.....	147
The Effects of Tetraspanin-LELs on Myoblast Fusion.....	148
The Effects of Tetraspanin-LELs on Macrophage Fusion.....	149
Discussion.....	150
Figures.....	154

Chapter 8: Tetraspanins and Integrin Interactions.....162

Introduction.....	163
Materials and Methods.....	165
Results.....	167
Cation-Dependence of Tetraspanin/Integrin Binding.....	167
Integrin Tail-Release of Tetraspanin/Integrin Binding.....	168
Antibody Inhibition of Tetraspanin/Integrin α IIb β 3 Binding.....	169
Tetraspanin Specificity in Tetraspanin/Integrin Binding.....	169
Anti- β 4 Integrin Antibody Modulation of Interaction.....	170
Specificity of anti- β 4 Integrin Antibody Modulation of Binding.....	170
Discussion.....	171
Figures.....	172

Chapter 9: Conclusions and Future Directions.....187

Introduction.....	188
Tetraspanin Extracellular Domains.....	188
Inhibitory Effects of Soluble Tetraspanin-LELs.....	190
Tetraspanin Interactions in the Membrane.....	192

Appendices.....197

A) Specific hCD81-LEL Inhibition of Hepatitis C Viral Infection	
B) Publications	
Residues SFQ (173-175) in the Large Extracellular Loop of CD9 are Required for Gamete Fusion	
Complete Replication of Hepatitis C Virus in Cell Culture	

References

Chapter 1

Introduction

All chapters were written by Christopher C. Liu, with editing and comments by Mariette Vogelezang, Sunny Wong, and Richard O. Hynes. All opinions and errors are my own.

Introduction.

Tetraspanins are cell surface membrane proteins comprising a family of over twenty-five genes sharing a characteristic membrane topology. Tetraspanins have been identified in both vertebrates and invertebrates, suggesting the early evolutionary development of these proteins (Levy and Shoham 2005). Furthermore, tetraspanins have been implicated in a wide range of functions involving the immune and nervous systems, development, cancer progression (Hemler 2003), and infectious diseases. These functions have been identified through function-inhibiting anti-tetraspanin antibodies, modulation of tetraspanin expression levels, recombinant, soluble mimics of tetraspanins, and genetics. However, the molecular mechanisms by which tetraspanins mediate these effects are unknown. Strong sequence and structural conservation among all tetraspanins suggest the existence of a generalized tetraspanin function. This function, which we propose is to regulate affinity and/or avidity at the cell surface, is propagated through protein-protein interactions specific to each biological system. In the body of this thesis, we describe our attempts to probe the role of tetraspanin large extracellular loops, the major extracellular domain of tetraspanins. Towards these ends, we have developed novel reagents that enhance our understanding of both the role of CD9 in sperm-egg fusion in particular and tetraspanin functions in general. This introduction serves to introduce tetraspanins and their multitude of effects, with specific emphasis on biochemical studies of tetraspanins and their roles in membrane fusion. Ultimately, this thesis strives towards enabling us to understand how tetraspanins function at the cell membrane.

The Tetraspanin Family

The first sequence characterization of a tetraspanin protein, CD63, was identified in the late 1980s as an antigen associated with melanoma tumor progression (Hotta, Ross et al. 1988). Subsequently, sequence identification of another tetraspanin, CD81, as the target of an anti-proliferative antibody by Shoshana Levy's group in 1990 established tetraspanins as a family of conserved proteins (Oren, Takahashi et al. 1990). Tetraspanins have been identified in fungi (but not yeast), sponges, schistosomes, *Caenorhabditis elegans*, *Drosophila melanogaster*, zebrafish, and all mammals. With the

advent of whole-genome sequencing, 28 human (Figure 1.1B), 37 *Drosophila* (Todres, Nardi et al. 2000), and 20 *C. elegans* tetraspanins (Moribe, Yochem et al. 2004) have been identified. All mammalian cells, except for erythrocytes, express tetraspanins and it has been estimated that 20 individual tetraspanins are expressed in the immune system (Levy and Shoham 2005).

Tetraspanins are small, ranging between 250 and 350 amino acids in length (Figure 1.1A). SDS-PAGE analysis reveals that many tetraspanins (although not CD9 or CD81) are heavily glycosylated, resulting in the addition of 20-50 kDas of additional molecular weight (Boucheix and Rubinstein 2001). As their name suggests, tetraspanins are a family of proteins that have four transmembrane domains. Conserved, polar amino acid residues exist in each of the transmembrane domains (Figure 1.1A)(Stipp, Kolesnikova et al. 2003), resulting in hypotheses suggesting that tetraspanins may oligomerize to form channels (Horejsi and Vlcek 1991). However, no experimental evidence has supported these suggestions and this role for tetraspanins has been discounted. At this time, it is not clear what role conserved residues in the transmembrane regions serve.

Tetraspanin proteins share a common membrane topology, having intracellular amino- and carboxyl-termini and four transmembrane segments delimiting two extracellular loops of unequal size (Figure 1.2A). Transmembrane segments one and two delimit a short extracellular loop (~20 amino acids) and transmembrane segments three and four delimit a large extracellular loop (~80 to 140 amino acids). Lastly, an absolutely conserved cysteine motif, CCG, and two other conserved cysteine residues in the large extracellular loops define the tetraspanin family. It is worth noting that not all four transmembrane containing proteins (L6, MM3, PERP, claudins) contain these signature motifs and likely have different functions from tetraspanins.

Sequence Conservation Of the Tetraspanin Large Extracellular Loop

When we started working on tetraspanins, a number of functions had already been assigned to them, most commonly in the haematopoietic and hemostasis systems (Hemler 2001). As with the cloning of CD63 and CD81, a number of monoclonal antibodies recognize tetraspanins and induce dramatic cellular changes (Boucheix and

Rubinstein 2001). The tetraspanin CD9 was first cloned as the antigen of an antibody which inhibits cell motility (Miyake, Koyama et al. 1991). To date, all function-inhibiting anti-tetraspanin antibodies bind to the tetraspanin large extracellular loop (Stipp, Kolesnikova et al. 2003), suggesting the critical importance of this domain to tetraspanin function.

Tetraspanin large extracellular loops (LELs) vary between 70 and 120 amino acids in length. Overall, there is quite low homology (5-40%) between tetraspanin-LELs, with an average pairwise homology of 15% (Seigneuret, Delaguillaumie et al. 2001). As tetraspanin-LELs vary greatly in length, alignment of this region results in significant gaps. Even with low sequence homology, there are sufficient conserved residues to allow LELs to be aligned with one another (Figure 1.2A). Tetraspanins almost all contain either four, six, or eight cysteines which are presumed to oxidize to form intramolecular disulfide bonds. In the case of outlying tetraspanin family members such as RDS and ROM, there is an additional cysteine which may participate in an intermolecular covalent bond (Loewen and Molday 2000).

The tetraspanin large extracellular loops (LELs) have a conserved cysteine residue pattern, including a tri-amino-acid sequence of cysteine-cysteine-glycine (CCG). Strikingly, the distance between transmembrane segment three and this CCG motif, which is always the most N-terminal of LEL cysteines, is conserved at approximately 40 amino acids. Secondary structural analysis of these forty amino acids predicts that they form two α -helices in all tetraspanins. Furthermore, the last cysteine residue in all tetraspanin-LELs is positionally conserved at approximately ten amino-acids N-terminal to transmembrane segment four. These ten amino acids are also predicted to form an α -helix (Seigneuret, Delaguillaumie et al. 2001). Predicted solvent accessibility of these two segments, the most N-terminal and C-terminal portions of the LEL, revealed a hydrophobic periodicity in a roughly 3-4 residue pattern, also suggestive of the helical nature of these regions (Seigneuret, Delaguillaumie et al. 2001). These regions are not predicted to form coiled-coils (Wolf, Kim et al. 1997) (C.C.L., data not shown).

The two described α -helical segments bracket a variable region. This region contains the CCG motif that is a defining characteristic of tetraspanins (Figure 1.2A). All tetraspanins contain four or more cysteines in this region and the position of these

cysteine residues has allowed the classification of tetraspanins into 3 groups containing four, six, or eight cysteines (Seigneuret, Delaguillaumie et al. 2001). Among tetraspanin orthologues, which contain approximately 70% identity, this region contains the majority of amino-acid substitutions (Hemler 2001). Studies mapping epitopes of function-inhibiting anti-tetraspanin antibodies (including one described in this thesis) have all identified this region as particularly antigenic. Furthermore, functional studies of tetraspanin-LELs have suggested that this variable region is important in sperm-egg fusion and the binding of tetraspanins to integrins (Zhu, Miller et al. 2002). Only recently, through biophysical analysis of recombinant tetraspanin-LELs and the solution of a crystal structure of the human CD81-LEL (Figure 1.2B) (Kitadokoro, Bordo et al. 2001), has the role of sequence conservation in tetraspanin-LEL oligomerization been revealed. In fact, historically, the series of sequence analyses described in this section were conducted after this tetraspanin-LEL structure was solved.

Structural Studies of the hCD81-LEL

In 2001, the Bolognesi group solved the structure of the human CD81-LEL, a tetraspanin-LEL containing four cysteines (Figure 1.2B) (Kitadokoro, Bordo et al. 2001). Ultimately, the Bolognesi group found that the hCD81-LEL protein crystallized into two similar, but non-identical forms: a monoclinic form solved as pdb ID: 1G8Q and a hexagonal form solved as pdb ID: 1IV5 (Kitadokoro, Ponassi et al. 2002). Both of these structures had two molecules in the crystallographic asymmetric unit and formed similar, superimposable structures (Figure 1.3A), although the crystal contacts were dramatically different. In fact, the second structure (1IV5) was solved through molecular replacement with the first structure (1G8Q).

The CD81-LEL molecule consisted of five α -helices, consistent with secondary structure predictions of the protein sequence. There were two α -helices N-terminal of the variable region (designated helix A and B), two α -helices formed by the variable region (designated helix C and D), and a single α -helix C-terminal of the variable region (designated helix E). The N- and C-termini fall in close proximity to one another and extend to transmembrane segments three and four respectively (Kitadokoro, Bordo et al.

2001). Two disulfide bridges stretch in opposite directions from the conserved CCG motif and serve to stabilize the structure (Figure 1.2B).

Surprisingly, the CD81-LEL structure was solved with two molecules in the crystallographic asymmetric unit. These two molecules assemble around a local two-fold axis in an anti-parallel fashion. A large hydrophobic region of approximately 1000 Å² mediates CD81-LEL dimerization and no water molecules were observed at the dimer interface. Each monomer adopts a similar tertiary structure of five helical regions as described and helices A, B, and E all contribute to form the hydrophobic dimerization interface. These three helices have been called a “stalk” or dimerization subdomain and are predicted to be conserved among all tetraspanin homologues (Figure 1.2A and Figure 1.2B).

The remaining two helices, helices C and D, constitute a head subdomain and present a second, smaller, low polarity region. As noted previously, this variable region of approximately 30 amino acids is where function-blocking antibody epitopes have been localized (Figure 1.2A and B). The antiparallel nature of CD81-LEL dimer serves to present the head subdomains at apposing ends of the molecules (Figure 1.2B), with a distance of approximately 30 Å between the two small hydrophobic patches (Kitadokoro, Bordo et al. 2001).

Both CD81-LEL structures contain a similar dimerization sub-domain mediated through helices A, B, and E. However, the head sub-domain is slightly altered between the two structures with helices C and D presented at different angles respective to one another. The disparities in the head sub-domain are most likely due to dramatically different crystal packing contacts (Kitadokoro, Ponassi et al. 2002). Analysis of average mass-weighted fluctuation of all atoms in each molecule suggests that under physiological conditions, the hCD81-LEL quarternary structure is plausible, with some flexibility in the head sub-domain (Neugebauer, Klein et al. 2004). This molecular dynamics study of both hCD81-LEL crystal structures also suggests that the latter crystal structure (1IV5) is more accurate (Neugebauer, Klein et al. 2004). As the first, monoclinic 1G8Q, CD81-LEL structure was solved concurrent with our biophysical analysis of the mCD9-LEL protein; we refer to this structure of the CD81-LEL

exclusively in the body of this thesis. Close analysis of both isoforms of the hCD81-LEL structures suggests that the structures are interchangeable for our level of analysis.

Spurred on by crystallographic studies of the hCD81-LEL, several groups (including our studies in Chapter 3) have modeled other tetraspanin-LEL domains, both in isolation and with the transmembrane domains, onto the hCD81-LEL structure. Conjead *et al.* used the hCD81-LEL crystal structure, homology alignments, and secondary structure predictions to predict the disulfide connectivities of tetraspanin-LELs (Figure 1.3C) (Seigneuret, Delaguillaumie et al. 2001). They present a compelling body of evidence for structural conservation among all tetraspanin dimerization subdomains mediated by the conserved helices A, B, and E. They further classified all tetraspanin-LELs into three classes based upon signature patterns of cysteine residues in the variable subdomain (Figure 1.3C). The variable subdomain is not predicted to be structurally conserved among tetraspanin-LELs (Seigneuret, Delaguillaumie et al. 2001).

In an ambitious study, Bienstock and Barrett attempted to model the transmembrane-intact CD82 molecule (Bienstock and Barrett 2001). The tetraspanin CD82, also called Kai1, has been functionally identified as a metastasis suppressor (Dong, Lamb et al. 1995), although its mechanism of action is unclear. Bienstock and Barrett modeled each domain of the CD82 molecule individually and then combined each domain to form the intact molecule (Figure 1.3B). To model the transmembrane regions of CD82, an alignment of tetraspanin transmembrane proteins was created. Helical hydrophobic moments were calculated to predict the orientation of each transmembrane region with respect to one another. Molecular models of the short intracellular segments, the short extracellular loop, and large extracellular loop, were constructed, assembled, and energy minimization and molecular dynamics simulations of the intact molecule were performed (Bienstock and Barrett 2001). As expected, the hCD82-LEL model adopts a global fold similar to the hCD81-LEL (Figure 1.3B). However, there are many caveats to this model.

All of the tetraspanin-LEL models described (including ours) have been modeled onto a monomeric CD81-LEL molecule. As described above, the CD81-LEL contains a desolvated, 1000 \AA^2 , hydrophobic region that lies at the interface between each monomer (Kitadokoro, Bordo et al. 2001). Deconvoluting the dimer and computationally exposing

this region to solvent serves to artificially minimize the dimerization interface (Bienstock and Barrett 2001) (Seigneuret, Delaguillaumie et al. 2001). As a result, these models most likely do not accurately represent intersubunit contacts between tetraspanin homodimers.

Furthermore, the model of the hCD82 molecule does not take into account the effects of glycosylation on the hCD82 molecule. Although all tetraspanins have a predicted molecular weight of between 22 and 30 kDa, CD82 is observed to be especially glycosylated (Boucheix and Rubinstein 2001). SDS-PAGE analysis of CD82 reveals bands ranging from 50 to 80 kDas, suggesting that glycosylation may double or triple the molecular weight of CD82. No studies on tetraspanin glycosylation have been reported and currently, it is not clear what are the functions of sugar residues.

Most importantly, sequence, structural, and our biophysical studies strongly suggest an intrinsic, dimeric nature to all tetraspanin-LELs. Barrett's model of the whole CD82 molecule displays the CD82-LEL as projecting in a perpendicular manner to the cellular membrane (Figure 1.3C) (Bienstock and Barrett 2001). Extrapolating from the antiparallel CD81-LEL dimer, only a CD82 trans dimer, or a dimer traversing two apposing lipid bilayers, would seem plausible and serve to cap the large, hydrophobic dimerization interface. It is plausible that the angle between helix A and transmembrane 3 (presented as $\sim 180^\circ$ in this figure) is highly flexible and that the CD82-LEL lies in a more planar fashion to the lipid bilayer. This model would allow the formation of a cis tetraspanin dimer, or a dimer existing on the same lipid bilayer. Although currently no trans tetraspanin/tetraspanin interactions have been observed, the antiparallel nature of the CD81-LEL dimer is plausible either in cis or in trans.

The functional relevance of tetraspanin-LEL-mediated oligomerization remains a contentious issue in the field. A common misgiving lies in reconciling the orientation of the CD81-LEL antiparallel dimer with its endogenous, adjacent, transmembrane domains (Levy and Shoham 2005). The hCD81-LEL structure does not rule out the formation of a cis antiparallel tetraspanin dimer (in the same lipid bilayer). As in many crystal structures, several amino acid residues at the distal N- and C-termini of the hCD81-LEL protein were disordered in the crystal structure. Given the α -helical nature of residues proximal to these termini, the addition of each helical amino acid to the α -helix would

twist the orientation of the adjacent transmembrane domains 100° (Branden and Tooze 1999). This helical nature of both N- and C-termini allow almost any orientation of the tetraspanin transmembrane segments three and four relative to the dimeric structure, as long as they are in close proximity to the N- and C- termini. To date, these issues have not been resolved and misgivings about the biological relevance of the hCD81-LEL structure have not been laid to rest.

In summary, crystallization of the CD81-LEL has identified two subdomains: a dimerization region and a variable region whose organization is predicted to be conserved among all tetraspanin-LELs. The CD81-LEL structure matches predicted secondary structural elements of tetraspanins. Furthermore, previously identified functional residues and antigenic regions were surface-exposed and clustered to the variable region. By these criteria, the CD81-LEL meets the benchmark of all crystal structures: “does this structure make sense?” Although many homology models of tetraspanin-LELs based upon the CD81-LEL structure have been constructed, they are not completely accurate. As a result, it would be highly desirable to determine atomic level structures for a number of other tetraspanin-LELs. In lieu of these detailed structural studies, biophysical characterizations of tetraspanin-LELs in solution are clearly necessary.

Recombinant Tetraspanin-LELs

Both anti-tetraspanin antibody and mutagenesis studies have underscored the importance of tetraspanin-LELs. As a result, tetraspanin-LELs have been expressed, purified, and studied in a variety of ways. For the crystallization studies described above, the human CD81-LEL was expressed as a fusion sandwiched between the IgG binding domain of *Staphylococcus Aureus* Protein A, which was subsequently removed, and a hexahistidine tag, which was not ordered in the crystal structure (Kitadokoro, Bordo et al. 2001). The Grandi group, which collaborated on the CD81-LEL structure, has also successfully expressed the CD81-LEL as both a thioredoxin fusion (Pileri, Uematsu et al. 1998) and also as a glutathione-S-transferase (GST) fusion (Petracca, Falugi et al. 2000). Removal of the GST tag resulted in a single CD81-LEL species as assessed by reverse-phase HPLC, which was shown to inhibit Hepatitis C viral entry (Petracca, Falugi et al. 2000). Inhibition of hepatitis C viral fusion was also shown with a GST-CD81-LEL

fusion protein constructed by the Monk group, albeit with decreased efficacy (Flint, Maidens et al. 1999).

The GST fusion system has been used by the Monk group to express the CD9-LEL (Higginbottom, Takahashi et al. 2003), the CD81-LEL (Flint, Maidens et al. 1999), and the CD63-LEL (personal communication). This GST-fused CD9-LEL has been shown to inhibit lymphocyte transendothelial migration by the Sanchez-Madrid group (Barreiro, Yanez-Mo et al. 2005). The Primakoff group has also used a GST-CD9-LEL fusion to inhibit sperm-egg fusion (Zhu, Miller et al. 2002) (see Chapter 7 and Appendix). On the other hand, the Mekada group has shown a pro-fusogenic effect on macrophage fusion with both GST-fused CD9-LEL and CD81-LEL (Takeda, Tachibana et al. 2003).

The Levy group has expressed the CD81-LEL as fusions with Fc, GST, or maltose-binding protein fusion (MBP) (Maecker, Todd et al. 2000; Nakajima, Cocquerel et al. 2005). By surface plasmon resonance, they measured the binding kinetics of both GST-fused and MBP-fused CD81-LEL constructs to soluble, recombinant hepatitis C glycoproteins. Analysis of the oligomeric states of these two fusion proteins by both gel filtration and sedimentation equilibrium yielded surprising results (Nakajima, Cocquerel et al. 2005). Both assays revealed that the GST-CD81-LEL protein was dimeric and the MBP-CD81-LEL protein was monomeric. As the GST protein is dimeric and the MBP protein is monomeric, their data suggest that the CD81-LEL fusion partner is monomeric. These results are antithetical both to our understanding of tetraspanin-LELs as a family and to results presented in Chapter 6 of this thesis, suggesting that more detailed biophysical analysis of fusion GST and MBP fusion proteins is required. No other detailed biophysical analysis of tetraspanin-LELs has been published. Lastly, when these tetraspanin-LEL proteins were used as antigens to generate polyclonal antibodies, the resulting antibodies were never immunoreactive to the intact CD9 molecule, also suggestive that the fusion proteins may be misfolded, even after repeated trials (Shoshana Levy, personal communication).

Almost all soluble, recombinant, tetraspanin-LEL-mediated inhibitions of function match the effects observed when anti-tetraspanin antibodies are added.

Nevertheless, soluble, recombinant tetraspanin-LELs are an important and increasingly utilized tool to probe endogenous tetraspanin functions.

In this thesis, we describe our own studies with soluble, recombinant tetraspanins (Figure 1.1B). Complementary to the studies described above, we show that it is unnecessary to fuse tetraspanin-LELs to a large carrier protein to achieve high protein expression. By utilizing a short, C-terminal hexahistidine tag and the nickel and reverse-phase chromatographic systems these fusions make tractable, we are readily able to express and purify to conformational homogeneity the CD9-LEL, the CD81-LEL, and the CD63-LEL (see Chapter 6). These conformationally pure proteins exhibit significantly greater potency of inhibition (except for the study of the CD81-LEL (Petracca, Falugi et al. 2000) in all assays tested to date (see Chapter 7 and 9). Given the nearly ubiquitous binding nature of tetraspanins (described below), the importance of pure, validated reagents is increasingly appreciated. The reagents described in this thesis are rapidly becoming the touchstone of tetraspanin-LEL biology.

More importantly, the lack of a large fusion partner allows detailed biophysical characterization of tetraspanin-LELs which may lend insight into their functional mechanisms. Concurrently with the crystal structure of the CD81-LEL described above (Kitadokoro, Bordo et al. 2001), our biophysical analysis of the murine CD9-LEL revealed that it is an autonomously folding, α -helical dimer. Our empirical estimate of secondary structure content matched secondary structure predictions of the CD9-LEL and we observed that proper disulfide-connectivities were critical for achieving α -helical content. Sedimentation equilibrium analysis also revealed that the murine CD9-LEL is a stable dimer (Chapter 2). Our extension of these analytical techniques to the CD81-LEL and the CD63-LEL proteins revealed that these proteins are also autonomously folding α -helical dimers (Chapter 7).

The development of a rapid, biochemical and biophysical methodology to express, purify, and analyze tetraspanin-LELs allowed us to identify the determinants of the folding stability of the murine CD9-LEL. Mutational analysis based upon a structural homology model of the mCD9-LEL (Chapter 3) confirmed the presence of two subdomains: a dimerization subdomain and an antigenic, variable region in solution (Chapter 4). Furthermore, we show that the variable region of the mCD9-LEL is discrete

from the dimerization subdomain and hypothesize that function-inhibiting anti-tetraspanin antibodies have no effect on mCD9-LEL-mediated homooligomerization (Chapter 4). These results, combined with the structural studies of the CD81-LEL and inhibition of tetraspanin functions by soluble tetraspanin-LELs (Chapter 7), reinforce the importance of tetraspanin-LELs to endogenous tetraspanin functions. Although the significance of tetraspanin-LELs is undisputed, their precise contribution to endogenous tetraspanin functions is still unclear.

Heterotypic Tetraspanin Interactions

Many classes of proteins have been hypothesized to complex with tetraspanins (Figure 1.4) (Boucheix and Rubinstein 2001). These interactions vary highly in their composition, strength of their interaction, and the stoichiometry of complex formation (Hemler 2003). For simplicity, we have codified these interactions by their components. We refer to tetraspanin/non-tetraspanin interactions as heterotypic interactions and tetraspanin/tetraspanin interactions as homotypic interactions. Furthermore, oligomerization of individual tetraspanins is described as homooligomerization. Heterotypic interactions have been further classified by the detergent sensitivity of macromolecular complex formation. In most instances, it is necessary to use mild detergent conditions, such as Brij 96, Brij97, or CHAPS before these complexes can be immunoprecipitated (Charrin, Manie et al. 2003).

Detergent solubilization is often an essential step to isolate transmembrane proteins. However, any experiment that requires the addition of detergent is fraught with the possibility of artifacts. Detergent solubilization of membranes often results in incomplete membrane protein isolation, leaving large patches of the native lipid bilayer that can be visualized by electron microscopy. Furthermore, detergent treatment often brings about fusion of disparate portions of the membrane, fusing fragments into continuous sheets (Mayor and Maxfield 1995). It is essential to be careful with the interpretation of detergent-solubilized protein complexes (Chamberlain 2004). It is only necessary to look to the lipid raft or detergent-resistant microdomain field to realize how contentious detergent solubilization of membrane proteins may be (Simons and Vaz 2004).

To overcome these controversies, we will focus this introduction on only robust tetraspanin heterotypic interactions which have been shown to interact in either TX-100 or digitonin and characterized as primary interactions. By restricting this introduction to robust tetraspanin interactions (Hemler 2003), we do not focus on the vast majority of weaker, and possibly artifactual, tetraspanin complexes. Although we do not wish to discount the validity of these complexes, we deem them to be controversial. Under weak detergent conditions, tetraspanins associate both with one another (homotypic interactions) and with numerous non-tetraspanin proteins (Rubinstein, Le Naour et al. 1996), raising the likelihood of large, indirect macromolecular interactions and possibly artifactual results. Severely restricting the focus of this introduction in this manner also eliminates any direct involvement of tetraspanins in mediating signals across the cellular membrane. Tetraspanins have been shown to mediate FAK (Berditchevski and Odintsova 1999) and PI4-kinase-dependent signalling pathways (Yauch and Hemler 2000) and protein kinase C (Zhang, Bontrager et al. 2001); however, it is unclear whether these effects are direct or mediated through intermediaries. The large number of identified binding partners to tetraspanins under mild detergent conditions is confusing, at best.

A limited number of primary, robust, heterotypic tetraspanin complexes have been observed. The most striking primary tetraspanin complexes are with uroplakins, distant relatives to canonical tetraspanins. These tetraspanins, uroplakin 1a and uroplakin 1b, associate heterotypically with uroplakin II and uroplakin III (Wu, Medina et al. 1995). These proteins are expressed exclusively on the bladder epithelium and have been suggested to play a role in uropathogenic *E. coli* infection (Wu, Sun et al. 1996; Mulvey, Lopez-Boado et al. 1998). Uroplakins are expressed at such high concentrations that they form hexagonal, two-dimensional lattices that can be visualized and resolved using Cryo-EM techniques (Min, Zhou et al. 2003). Presently, these techniques are not at sufficient resolution to model the predicted dimerization and variable subdomains of the uroplakin-LEL.

On the surface of B-lymphocytes, CD81 has been shown to associate in a complex with CD19, CD21, and Leu-13 (Levy, Todd et al. 1998) (Horvath, Serru et al. 1998). Monoclonal antibodies against CD81, CD19, CD21 and Leu-13 share similar

effects on B-cell co-stimulation, proliferation, and homotypic aggregation, suggesting that this complex is functionally relevant (Cherukuri, Shoham et al. 2004). Targeted deletion of CD81 in a mouse model also reduces all components of this complex, making it difficult to assign individual functions to each member of the complex (Shoham, Rajapaksa et al. 2003). A large number of weak, heterotypic interactions in the immune system have been identified and are extensively reviewed elsewhere (Levy and Shoham 2005).

A third, robust complex, between the tetraspanin CD9 and the precursor of heparin-binding epidermal growth factor (Nakamura, Mitamura et al. 2000), which is also the diphtheria toxin receptor, has been observed (Iwamoto, Higashiyama et al. 1994). Overexpression of CD9 serves to increase diphtheria toxin binding. The tetraspanins CD9 and CD81 have also been shown to interact with the immunoglobulin superfamily members EWI-2 (also called PGRL) (Stipp, Kolesnikova et al. 2001) (Charrin, Le Naour et al. 2003) and EWI-F (also called CD9P-1 or FPRP) (Stipp, Orlicky et al. 2001). This interaction is TX-100 resistant and of high stoichiometry (Charrin, Le Naour et al. 2001). To date, the functions of these proteins and the biological relevance of their association with CD9 and CD81 is unknown.

Lastly, tetraspanins have been shown to associate with integrins (Figure 1.5), consistent with observed roles for tetraspanins in cellular motility and metastasis (Boucheix, Duc et al. 2001) (Berdichevski 2001).

Tetraspanins and Integrins

Integrins are obligate cell-surface heterodimers that mediate cellular adhesion to the extracellular matrix and play major roles in immune functions, leukocyte traffic, and human disease (Hynes 2002). Each integrin subunit is a class 1 transmembrane domain and their N-terminal regions are in close association to form a head domain consisting of a beta-propeller (in the α subunit) (Springer 1997) and a Rossman fold (in the β subunit) (Takagi and Springer 2002). Carboxy-terminal to the head domain are elongated legs leading to the transmembrane domains and cytoplasmic tails. Integrins have the ability to change conformation (affinity) (Takagi, Petre et al. 2002), cluster (avidity) (Li, Babu et al. 2001) (Luo, Springer et al. 2004), and to bind the cytoskeleton (anchoring) (van der

Flier and Sonnenberg 2001). A recent crystal structure of the $\alpha v\beta 3$ extracellular domain raised the prospect of global conformational changes in this domain to mediate integrin affinity (Xiong, Stehle et al. 2001). A series of molecular design (Luo, Springer et al. 2003) and electron micrographic (Takagi, Petre et al. 2002) studies revealed that integrins undergo both global and local (in the head domain) conformational changes, reinforcing the notion that regulation of integrin affinity is complex (Takagi and Springer 2002).

Artificially, integrin affinity can be modulated by cations (EDTA decreases, Mn^{++} increases), monoclonal antibodies (to both increase and decrease), and peptidomimetics of integrin ligands (cyclic RGD peptides). Biologically, integrin affinity can be modulated by binding to natural ligands (outside-in signaling) or separation of the cytoplasmic tails (inside-out signaling) both resulting in the separation of integrin transmembrane and stalk domains and affinity upregulation (Hynes 2002).

Recently, it was shown that integrin transmembrane domains may play a role in both modulating integrin affinity and avidity (Li, Mitra et al. 2003). Individual α integrin and β integrin transmembrane domains were shown to spontaneously homooligomerize. It is enticing to envision an extended lateral network of α/β integrin heterodimers coupled with α/α and β/β oligomeric transmembrane domains, although avidity regulation by integrin transmembrane domains remains controversial (Luo, Carman et al. 2005). Biologically, the ability of integrins to cluster into large, extended, high-avidity complexes has been observed for some time (Hynes 2002). It is plausible that tetraspanins may participate in integrin affinity regulation, avidity regulation, or both through binding either extracellularly or within the lipid bilayer.

Although fairly ubiquitous binding between tetraspanins and integrins have been observed (Figure 1.5), only a small subset of these heterotypic interactions have been documented under stringent detergent conditions. Of these, the best-characterized interaction is between the tetraspanin CD151 and integrin $\alpha 3\beta 1$ (Yanez-Mo, Alfranca et al. 1998; Stipp and Hemler 2000). Through chimeric molecule and mutagenesis experiments, it was shown that this interaction requires the CD151-LEL and stalk domain of the $\alpha 3$ integrin subunit and it is presumed that this is the heterotypic interaction domain (Yauch, Kazarov et al. 2000; Berditchevski, Gilbert et al. 2001). Domain swapping between the $\alpha 3$ (CD151-binding permissive) and $\alpha 5$ (CD151-binding non-

permissive) of their respective transmembrane and cytoplasmic domains did not disrupt the robust CD151/ α 3 β 1 association (Yauch, Kazarov et al. 2000).

When detergent stringency is lowered, a wide array of tetraspanin/integrin interactions is observed (Charrin, Manie et al. 2003). As observed pairwise interactions are a subset of expressed, potential tetraspanin/integrin interactions, these observed interactions have been classified as low-affinity, specific interactions (Berditchevski, Zutter et al. 1996). Again, due to widespread co-immunoprecipitation of tetraspanins under these conditions, it is difficult to assess if these interactions are specific or artifactual. The ability to cross-link pairwise detergent-solubilized tetraspanin/integrin complexes, although technically distinct from immunoprecipitation experiments, is subject to the same detergent-induced experimental caveats described above.

Tetraspanin/integrin association under mild detergent conditions is not affected by changes in integrin conformation. The addition of divalent cations, function-blocking, and function-inducing anti-integrin antibodies had no effect on tetraspanin/integrin interactions (Mannion, Berditchevski et al. 1996) (Longhurst, White et al. 1999). Ligand-binding also had no effect on the association of tetraspanins and integrins under mild detergent conditions (Yanez-Mo, Tejedor et al. 2001).

In the studies described in this thesis, we circumvent potential problems of detergent-induced lipid domain fusion by testing pairwise interaction of soluble tetraspanin-LELs with a panel of integrins (see Chapter 8). Contrary to the published literature, we observed a strong influence of cations on tetraspanin/integrin interactions, but could not decipher a specific pair-wise binding pattern (see Chapter 8). To reconcile the disparity between our own and published data, we speculate that mild detergent conditions may have dual effects. Mild detergent may serve both to disrupt low-affinity extracellular-mediated tetraspanin/integrin interactions (which we observe in Chapter 8) and also serve to constitutively bring tetraspanins and integrins together, thus obscuring preferential, conformation-dependent interactions. As a result, observed, constitutive tetraspanin/integrin interactions under mild detergent conditions would obscure the integrin-conformational dependence of these interactions. Strong detergents may serve to completely disrupt these low-affinity tetraspanin/integrin interactions.

In summary, this hypothesis suggests that lateral association on the cellular membrane is necessary to form a high avidity tetraspanin/integrin complex. Formation of this complex (which may be mediated by both transmembrane regions and tetraspanin palmitoylation) brings the extracellular tetraspanin and integrin domains into close proximity and allows tetraspanin-LEL regulation of extracellular integrin activation. Indeed, the ability of anti-tetraspanin antibodies and tetraspanin expression levels to induce integrin-mediated signaling (Zhang, Bontrager et al. 2001), adhesion (Lammerding, Kazarov et al. 2003), and cellular motility (Sugiura and Berditchevski 1999) strongly suggests the influence of tetraspanins (and tetraspanin-LELs in particular) on integrin-related cellular functions. This hypothesis, which postulates that both tetraspanin transmembrane regions and dimeric tetraspanin-LELs are necessary for heterotypic tetraspanin interactions, is consistent with the notion of both the tetraspanin web and transmembrane-enriched microdomains (discussed below). Furthermore, this hypothesis is consistent with our biophysical observations that the tetraspanin-LEL form two functional domains: a large hydrophobic interface that mediates homodimerization and a much smaller hydrophobic interface that mediates heterotypic interactions (Chapter 4).

Homotypic Tetraspanin/tetraspanin Interactions

As described previously, our biophysical analysis of multiple tetraspanin-LELs and the structure of the hCD81-LEL strongly suggested a conserved role for tetraspanin-LELs to mediate tetraspanin dimer formation. These observations raised two attractive possibilities: tetraspanin-LELs may mediate homo- and/or hetero-dimerization. The combinatorial assembly of homo- and hetero- oligomers is a common phenomenon in biology that serves to increase the number of potential interactions in an exponential fashion (Newman and Keating 2003) (Klemm, Schreiber et al. 1998). For example, homodimerization of the known mammalian tetraspanin genes would result in 28 homotypic tetraspanin interactions that would in turn bind to 28 heterotypic partners. If tetraspanin heterodimers were to exist, the potential number of homotypic tetraspanin complexes rises dramatically to 28^2 , or 784, potential tetraspanin complexes. These

complexes, in turn, could interact heterotypically to bind any number of non-tetraspanin partners.

In the limited number of pair-wise tetraspanin-LELs tested, potential heterooligomers were not observed (Chapter 6). Even more discouragingly, we did not observe homooligomerization of intact CD9 molecules under strong detergent conditions, although we did observe homooligomerization under weak detergent conditions (Chapter 5). The requisite use of detergents when working with the intact CD9 molecule precluded an accurate estimate of the CD9 oligomerization state. Although surprising to us, the inability to observe homooligomerization under strong detergent conditions was neither surprising to the tetraspanin field nor inconsistent with the published results described above. Although we did not observe robust detergent resistance of tetraspanin-LEL-mediated homooligomerization, it is quite possible that the presence of other tetraspanin domains serves to abrogate tetraspanin-LEL mediated oligomerization (discussed further in Chapter 5).

On the other hand, a large number of homotypic, tetraspanin/tetraspanin, oligomers have been observed in mild, but not strong, detergent conditions (Rubinstein, Le Naour et al. 1996). The ubiquitous nature of tetraspanin interactions under mild detergent, and the observation that antibodies against different tetraspanin may induce similar effects, has resulted in the proposal of a tetraspanin web on the cell surface (Rubinstein, Poindessous-Jazat et al. 1997). This model, that extracellular tetraspanin-LELs mediate heterotypic interactions and tetraspanin hydrophobic domains (both transmembrane domains and palmitoylation) mediate homotypic tetraspanin interactions. Inhibition endogenous tetraspanin palmitoylation may serve to impair homotypic tetraspanin interactions (Berditchevski, Odintsova et al. 2002; Charrin, Manie et al. 2002; Yang, Claas et al. 2002). Again, it is difficult to interpret these results. The presence or absence of hydrophobic palmitate groups may influence the non-specific recruitment of individual tetraspanins into detergent solubilized complexes. Given the large number of observed interactions under mild detergent conditions, it is impossible to decipher direct and indirect tetraspanin interactions.

To further complicate matters, ubiquitous observations of tetraspanin palmitoylation (Yang, Kovalenko et al. 2004) has led to the proposal that they may

constitute a new form of rafts on the cellular membrane. However, detergent solubilization of tetraspanins reveals that they only partially exhibit traditional raft-like characteristics (Cherukuri, Shoham et al. 2004) (Claas, Stipp et al. 2000). As these results are more ambiguous (and indirect) than the contentious characterization of lipid-rafts (Simons and Vaz 2004), it is difficult to fully ascertain the biological relevance of these experiments. We feel that without further, rigorous characterization, the current hypotheses of the tetraspanin web and tetraspanin-enriched microdomains, which are core concepts in the tetraspanin field, will remain unresolved. Detailed analysis of homotypic and heterotypic tetraspanin oligomerization will most likely require more detailed biophysical methods, such as fluorescence resonance energy transfer (FRET) and fluorescence recovery after photobleaching (FRAP) of purified, reconstituted tetraspanins and their mutants.

Lastly, we note that our hypothesis: mild-detergent solubilization of lipid bilayers serving to artificially coalesce disparate tetraspanin complexes into a single, large complex (Chamberlain 2004), is sufficient to explain both the ubiquitous interactions seen in the tetraspanin literature and the notion of a tetraspanin web and lipid-raft-like tetraspanin-enriched microdomains.

Our characterization of tetraspanin-LELs, and their ability to disrupt endogenous tetraspanin functions on the cell surface, suggest that tetraspanin-LEL mediated oligomerization is biologically relevant. The most fascinating of these inhibition studies is for the mCD9-LEL to inhibit the role of CD9 in sperm-egg fusion (Stein, Primakoff et al. 2004). This unique function of CD9, which until recently was the only gene shown to be necessary for sperm-egg fusion, was the result of various genetic studies on tetraspanins.

Genetic Studies of Tetraspanins

Tetraspanin-null organisms have been generated in a number of model organisms by targeted deletion of genes, siRNA, and mutagenesis screening. In the nematode *C. elegans*, all twenty predicted tetraspanin molecules have been sequentially targeted with small interfering RNAs with no significant consequences. Only one, tsp-15, has been shown to have a defect in epithelial cell integrity, leading to blistering of the hypodermis

(Moribe, Yochem et al. 2004). The *Drosophila* tetraspanin, latebloomer, had a delay in synaptic contacts at the neuromuscular junction (Kopczynski, Davis et al. 1996). However, latebloomer is not essential for embryo viability. Genetic deletion of nine (out of 37 predicted) drosophila tetraspanins had no effect on the *Drosophila* lifecycle (Fradkin, Kamphorst et al. 2002). Recently, deletion of another non-essential *Drosophila* tetraspanin, sunglasses, results in light-induced retinal degeneration (Xu, Lee et al. 2004).

Human genetics has identified a number of tetraspanin-deficiency related diseases. Similar to the drosophila sunglasses deletion mutant, mutation of peripherin/RDS in humans leads to several retinal diseases (Kohl, Giddings et al. 1998). Although phenotypically similar, RDS and *Drosophila* sunglasses (which is most related to CD63) are not orthologues. A series of missense mutation in the RDS large extracellular loop, as well as deletion mutants, result in the onset of retinopathies. In mouse model systems, targeted deletion of RDS (Sanyal, De Ruiter et al. 1980) or its closest homologue, ROM (Clarke, Goldberg et al. 2000), lead to abnormal photoreceptor morphogenesis. Lastly, the tetraspanin, TM4SF2, is associated with mental retardation in humans (Zemni, Bienvenu et al. 2000). Either truncation of the protein or a single missense mutation, P172H (which lies in the large extracellular loop), is sufficient for onset of the phenotype.

A number of tetraspanin-null mice have been generated which result in mild immune defects (Figure 1.1B). Deletion of CD37 results in slight defects of B-cell humoral responses and B-and T-cell interactions (Knobeloch, Wright et al. 2000). Targeted deletion of the CD81 gene also resulted in a slight reduction of B-cell humoral responses but had no effect on T lymphocyte development (as expected from antibody inhibition experiments) (Maecker and Levy 1997; Miyazaki, Muller et al. 1997; Tsitsikov, Gutierrez-Ramos et al. 1997). On the other hand, deletion of the tetraspanin Tssc6 resulted in normal B cell development but a slight elevation in T cell receptor-dependent proliferation (Tarrant, Groom et al. 2002). CD151-deleted mice also exhibit an increase in T-cell mediated hyperproliferation (Wright, Geary et al. 2004). Furthermore, CD151 deletion results in hemostasis problems, including prolonged bleeding times, due to defects in mild defects in α IIb β 3 integrin signaling (Lau, Wee et

al. 2004). Targeted deletions of the tetraspanins, CD37, CD81, CD151, and Tssc6 in mouse models were viable and fertile (Hemler 2001).

In the central nervous system, deletion of either CD9 or CD81 results in mice that have enlarged brains due to increased numbers of glia and astrocytes (Geisert, Williams et al. 2002). Neuronal binding to CD81 on astrocytes inhibits astrocyte proliferation (Kelic, Levy et al. 2001). As a result, deletion of CD81 results in astrocytic hyperproliferation. Puzzlingly, in vitro experiments show that antibodies against CD81 serve to suppress astrocyte proliferation, suggesting a case where antibody binding to a tetraspanin is the reverse of the null-phenotype (Geisert, Yang et al. 1996; Dijkstra, Geisert et al. 2001). In the central nervous system, CD9 has also been shown to be essential for proper paranodal maintenance and saltatory conductance in the axon (Ishibashi, Ding et al. 2004).

Unexpectedly, the only dramatic tetraspanin-null phenotype was due to deletion of the CD9 gene. The CD9 molecule has proposed roles in cellular migration (Scherberich, Giannone et al. 2002), adhesion (Rubinstein, Le Naour et al. 1994), metastasis (Ikeyama, Koyama et al. 1993). It has been shown to bind both $\beta 1$ integrins and the platelet integrin $\alpha IIb\beta 3$ under mild detergent conditions (Longhurst, White et al. 1999). Targeted deletion of the CD9 gene did not result in dramatic effects in any of these systems. On the other hand, CD9, which is expressed on the oocyte, was shown to be essential for fertilization (Kaji, Oda et al. 2000; Le Naour, Rubinstein et al. 2000; Miyado, Yamada et al. 2000). CD9 is expressed on oocytes (Kaji, Oda et al. 2000) and CD9-null oocytes bind normally, but can not fuse with sperm (Le Naour, Rubinstein et al. 2000). Bypassing the sperm-egg fusion event using intracytoplasmic sperm injection resulted in normal onset of development (Miyado, Yamada et al. 2000). The CD9-null phenotype is mimicked by the exogenous addition of an antibody against CD9 (Chen, Tung et al. 1999; Miller, Georges-Labouesse et al. 2000).

Given the dramatic effects induced by the addition of antibodies against tetraspanins, the mild phenotypes described above were surprising. Except for the case of astrocytic hyperproliferation, deletion of a tetraspanin gene mimics the binding of antibodies to the tetraspanin-LEL, albeit with a milder effect. Perhaps in the case of null-mice, these non-deleted tetraspanins may serve to compensate for one another through

the formation of novel tetraspanin complexes. Only in specific biological systems, such as fertilization, is compensation insufficient to make up for the loss. We further hypothesize that antibody addition serves to rapidly disrupt cell-surface tetraspanin macromolecular complexes mediated by the tetraspanin-LEL. This effect is rapid and eclipses the rate of de novo complex formation, which results in the near wild-type phenotypes observed in tetraspanin-null mice.

Viral Membrane Fusogens

Only one gene, CD9, has been shown to be essential for sperm-egg fusion (another gene, izumo, was just recently shown to be essential (Inoue, Ikawa et al. 2005)). Since the invention of the microscope, sperm and egg cells have been the focus of intense biological interest. The regulated fusion of these two cells restores diploidy and marks the beginning of a new embryo. Functionally, this fascinating biological event is most analogous to viral-cell fusion and this functional similarity served as the basis for our interest into this field.

Virions are inert particles with a wide range of sizes and shapes (Fields 2001). Like spermatozoa, virions are terminally differentiated and do not have the ability to self-replicate without external assistance. Virions encapsulate genomic material (either DNA or RNA), contain structural proteins (and possibly polymerases), and a set coat proteins that mediate virion entry (Eckert and Kim 2001). Like the sperm cell, virions need to recognize that they are in proximity to a potential host cell, bind to it, and release its genomic material into the cytoplasm of the host cell. In the case of the sperm cell, this host cell is also a fully differentiated gamete, the egg (Talbot, Shur et al. 2003). Carrying genetic material from one location to another is the central purpose of both sperm cells and virions. In fact, both sperm and viruses generate huge numbers of these genetic packages, many orders of magnitude in excess of what ultimately is needed. In the case of human fertilization, a typical male ejaculate contains about 100 million sperm, only about 100 of which reach the upper reproductive tract, and only one of which fuses with the egg. The dynamics of both virus infectivity and sperm competition is an actively investigated field of research (Brikhead and Moller 1998; Nowak and May 2000).

Membrane lipid bilayers are stable structures that do not fuse spontaneously. Furthermore, cell membranes do not have spontaneous curvature and are fully hydrated (Tanford 1980). To overcome the barriers to lipid mixing, a wide variety of membrane fusogens have evolved to catalyze this event, which is central to fertilization, vesicle trafficking, muscle development, and viral entry (Earp, Delos et al. 2005). The most well characterized protein catalysts of membrane-fusion are viral fusion proteins.

As obligate intracellular parasites, it is essential for viruses to enter and infect host cells. This entry event is controlled and catalyzed by large, extracellular viral surface proteins (fusogens) that have been structurally classified into two groups. Class I fusion proteins are synthesized as a single protein precursor that is subsequently activated and cleaved. This proteolytic processing creates a metastable trimeric structure that is conserved among several classes of virions and forms a “spike” on the surface of the virion (Figure 1.6) (Eckert and Kim 2001). Activation of these metastable proteins through either receptor binding or pH changes results in global conformational changes and the insertion of an amphipathic fusion peptide into the target membrane, creating a fusion intermediate (Carr and Kim 1993). Subsequent formation of a thermodynamically stable six-helical bundle, termed a “trimer of hairpins” (Figure 1.6), likely provides the energy for bringing apposing phospholipids into close proximity and mediating fusion (Chan, Fass et al. 1997). A similar membrane fusion mechanism, utilizing the formation of a stable alpha-helical coiled-coil structure to mediate lipid mixing has also been shown for SNAP/SNARE mediated vesicle fusion (Jahn, Lang et al. 2003).

Structurally, class II fusion proteins are quite dissimilar from the conserved alpha-helical class I fusion proteins (Earp, Delos et al. 2005). The most studied models of class II fusion proteins (which include Hepatitis C virus) are the tick-borne encephalitis (TBE) and Semliki Forest Virus (SFV) virions. Unlike the α -helices characteristic of class I fusion proteins, the TBE (Rey, Heinz et al. 1995) and SFV envelope (Lescar, Roussel et al. 2001) proteins both adopt a predominantly beta-strand structure. The TBE glycoprotein forms an antiparallel dimer that lies flatly on the viral surface (Figure 1.7). A putative amphipathic fusion peptide (which inserts into the target membrane) is internal, unlike class I fusion proteins (Allison, Schlich et al. 2001). Upon activation under acidic conditions, the homodimer globally rearranges into an elongated homotrimer

that lies perpendicular to the virion surface (Allison, Schlich et al. 1995; Ferlenghi, Clarke et al. 2001; Stiasny, Allison et al. 2001; Bressanelli, Stiasny et al. 2004), possibly allowing the fusion peptide to insert into the target membrane (Figure 1.7). Although no detailed structural analysis of the hepatitis C viral glycoproteins is available, they have been proposed to adopt and undergo similar conformational changes as their closely related flaviviridae family members TBE and SFV (Garry and Dash 2003).

In conclusion, although class I and class II viral fusion proteins are structurally dissimilar, they share many conserved features. They are synthesized in a metastable state that upon activation, undergo global oligomerization rearrangements to catalyze lipid mixing (Chan and Kim 1998). This membrane fusion event, similar to most cell-cell fusion events is irreversible and unlike vesicle fusion, does not require recycling of fusion proteins (Sudhof 2004). Extrapolating from known fusogens in these diverse membrane fusion systems, tetraspanins do not appear to directly catalyze lipid mixing and fusion. The extracellular domains of tetraspanins are relatively small and few known trans binding partners are known. The studies described in this thesis indicate that the CD9-LEL exists as a stable, α -helical dimer and does not adopt multiple conformations (Chapter 2). Furthermore, inhibition of fertilization by soluble, recombinant mimics of the CD9-LEL show that the major role of the egg CD9 is to act in cis (Zhu, Miller et al. 2002), on the egg surface, and not to function in trans, with the sperm cell (Chapter 7). So why is CD9 essential for membrane fusion? First we review other cell-cell fusion systems.

Cell-Cell Fusion

A number of genetic and biochemical screens have attempted to probe the molecular mechanisms of membrane fusion. As a- and alpha- type yeast mating involves membrane apposition and fusion, a screen for yeast fusogens was conducted by the Walter laboratory. They identified a single protein, Prmp1, which showed normal membrane apposition and decreased fusion. However, deletion of the prmp1 gene yielded ambiguous results, where membrane fusion was only reduced 50% (Heiman and Walter 2000). Given the ease and elegance of yeast genetics, it is unclear why this screen has been unsuccessful to date.

Recently, the *C. elegans* protein Eff-1 has been identified as a potential epithelial fusogen (Mohler, Shemer et al. 2002), although it has no effect on sperm-egg fusion (del Campo, Opoku-Serebuoh et al. 2005). The Eef-1 protein is a novel type 1 transmembrane protein with no orthologues in other sequenced organisms (Mohler, Shemer et al. 2002). Similar to canonical membrane fusion proteins (syncytia review), ectopic expression of Eef-1 in non-fusogenic cell is sufficient to induce cell-cell fusion, although its mechanism of action is unclear (Shemer, Suissa et al. 2004). Without the presence of orthologues, it is unlikely that the identification of eef-1 will lend insight into mammalian cell-cell fusion. A *C. elegans* screen for fertilization-incompetent sperm specific mutations has yielded spermatogenesis and gamete binding defects, but not fusion defects (L'Hernault, Shakes et al. 1988; Singson, Mercer et al. 1998). A systematic screen of *C. elegans* genes using RNAi (Kamath, Fraser et al. 2003) did not yield a sperm-egg fusogen. However, often RNAi does not work in *C. elegans* gametes (L'Hernault, personal communication).

Genetic screens have implicated a variety of genes in the fusion of drosophila myoblasts to form myotubes (Schnorrer and Dickson 2004). These screens have identified intracellular small GTPases, GTPase exchange factors (GEFs), and adaptor proteins as essential genes in myoblast fusion. Furthermore, identification of cell-surface proteins containing immunoglobulin-domains are thought to function in homotypic myoblast recognition and adhesion and not to directly mediate fusion. At this time a myoblast fusogen has not been identified.

Recently, a review has noted the widespread identification of IgG superfamily proteins playing essential roles in a wide variety of cell-cell fusion events (Chen and Olson 2005). As a result, they have proposed that α -helical structures are non-essential for catalysis of membrane fusion. As described above, although α -helical coiled-coil structures are widely used to catalyze membrane fusion, other β -strand glycoproteins (class II viral fusogens) may also serve to mediate membrane fusion (Earp, Delos et al. 2005). The common mechanism underlying all known membrane fusion events is the presence of metastable proteins that undergo global, oligomeric, conformational changes. This specific class of proteins does not include either tetraspanins or the immunoglobulin superfamily of proteins. Although putative cell-cell fusogens have yet to be identified,

we are optimistic that in time the mechanisms underlying heterotypic and homotypic cell-cell membrane fusion events will converge with those already known.

Sperm-Egg Fusion

Like many researchers in the tetraspanin field, our interest in tetraspanins was sparked in other cell-biological systems. CD9 first came to our attention through work by Brent Miller in Paul Primakoff's laboratory, who showed that a monoclonal antibody against CD9, clone KMC8, could specifically inhibit sperm-egg fusion (Miller, Georges-Labouesse et al. 2000). As CD9 was thought to be complexed with integrin $\alpha 6 \beta 1$ on the egg surface, these results were striking, but fit the paradigm for a central role of egg-surface integrins interacting with the sperm-surface ADAM family members (Chen, Tung et al. 1999).

The ADAM family of molecules were first identified as the targets of a monoclonal antibody, PH-30, that inhibited sperm-egg binding and fusion (Blobel, Wolfsberg et al. 1992) (Primakoff and Myles 2000). PH-30 was especially striking as its antigen was spatially restricted to the equatorial region of murine sperm, a subdomain of the sperm head that had been observed to mediate sperm-egg binding and fusion (Primakoff and Myles 1983). After a decade of intense research, mouse genetics revealed that targeted deletion of a PH-30 antigen, ADAM2, had minimal effects on sperm-egg binding and no effect on sperm-egg fusion (Cho, Bunch et al. 1998). Subsequently, mouse genetics studies showed that integrins also played a non-essential role in sperm-egg binding and fusion (He, Brakebusch et al. 2003). Currently, the molecular mechanism underlying sperm-egg binding is not known.

Concurrently, three groups independently presented mouse genetic experiments illustrating that CD9 is essential for sperm-egg fusion, with no role in sperm-egg binding (Kaji, Oda et al. 2000; Le Naour, Rubinstein et al. 2000; Miyado, Yamada et al. 2000). These results are striking. Sperm-egg fusion was specifically blocked and the phenotype was 98% penetrant. This surprising role for the tetraspanin CD9 raises several intriguing questions. Are there other factors that mediate sperm-egg fusion? Furthermore, no other major effects have been observed with any tetraspanin-null mice to date as it is believed

that many tetraspanins may compensate for one another. Why does this not occur at the egg surface?

The functional nature of the clone KMC8 targeted our fertilization studies to the extracellular domain of the protein CD9. Our inhibition results with the soluble, recombinant mCD9-LEL protein further suggest that CD9 functions on the egg surface, and not as a receptor for sperm. This result suggests against experiments to probe the sperm-surface for a CD9 receptor, which we have contemplated.

A recent finding that CD9 may bind in trans to pregnancy-specific glycoprotein 17 (PSG17) is puzzling (Ellerman, Ha et al. 2003). PSG proteins are members of the immunoglobulin superfamily, synthesized by the placenta during pregnancy, and secreted into the maternal circulation. They are hypothesized to play a role in the immune system and may function in inhibiting maternal rejection of the foetus (Ha, Waterhouse et al. 2005). Consistent with this role, PSG17 has been shown to interact with CD9 on macrophages (Waterhouse, Ha et al. 2002). It is not certain if PSG17 is present on mature spermatogonia and their expression pattern does not match that expected for a protein with a role in sperm-egg fusion. On the other hand, the Primakoff lab showed binding specificity of PSG17 to the murine CD9-LEL; the introduction of non-fusogenic permissive mutations abolished the interaction. Interestingly, it was shown that transient binding of PSG17 (washing out PSG17 prior to gamete mixing) was insufficient to inhibit sperm-egg fusion (wash-out experiments were not attempted with our mCD9-LEL protein inhibition), suggesting that the CD9-LEL is not involved in priming the egg for sperm entry (Ellerman, Ha et al. 2003). These results also suggest that CD9 does not serve to hold a fusogen in a metastable state.

Although we have identified CD9 as acting in cis on the egg surface, the molecular mechanisms underlying sperm-egg fusion remain opaque. It is possible that CD9 functions as a chaperone to assist in the maintenance of an egg fusogen in a metastable state. However, transient inhibition results with the PSG17 protein suggest against this. It is also possible that CD9 functions only to provide a high-affinity or high-avidity scaffold for either a egg-bound membrane fusogen or a receptor to a sperm-bound fusogen. A role for CD9 in mediating affinity or avidity is consistent with its proposed roles in other cellular contexts.

Recently, a gene on the sperm cell, izumo, was also characterized as a necessary protein to sperm-egg fusion (Inoue, Ikawa et al. 2005). Izumo is the antigen to a sperm-egg fusion-blocking antibody and is localized to the posterior head of sperm (the membrane domain where fusion occurs). Targeted deletion of izumo was results in a specific defect in sperm-egg fusion and bypassing this event with izumo-null spermatozoa resulted in normal development. Izumo is a small type 1 transmembrane protein with a single, extracellular, immunoglobulin fold with no predicted homology to other characterized proteins. Izumo does not directly bind CD9 (Okabe, personal communication). It is striking that the only two known essential genes for membrane fusion are small with unknown functions.

Motivated by evidence for the role of CD9 in sperm-egg fusion, we focused our studies on the CD9-LEL. This approach both targets our approach to the domain recognized by a fertilization-inhibiting antibody and also circumvents the issues of detergent solubility problematic for transmembrane proteins. In this thesis, I describe the purification and characterization of the mCD9-LEL. This methodology is expandable to some, but not all, tetraspanins-LELs. Using our biophysical characterization of the mCD9-LEL as a model, we explore both the oligomerization of intact CD9 molecules and the interactions of tetraspanins-LELs with integrins. Lastly, we demonstrate the inhibitory activity of our panel of soluble tetraspanins-LELs in a number of biological contexts, including fertilization and hepatitis C viral infectivity.

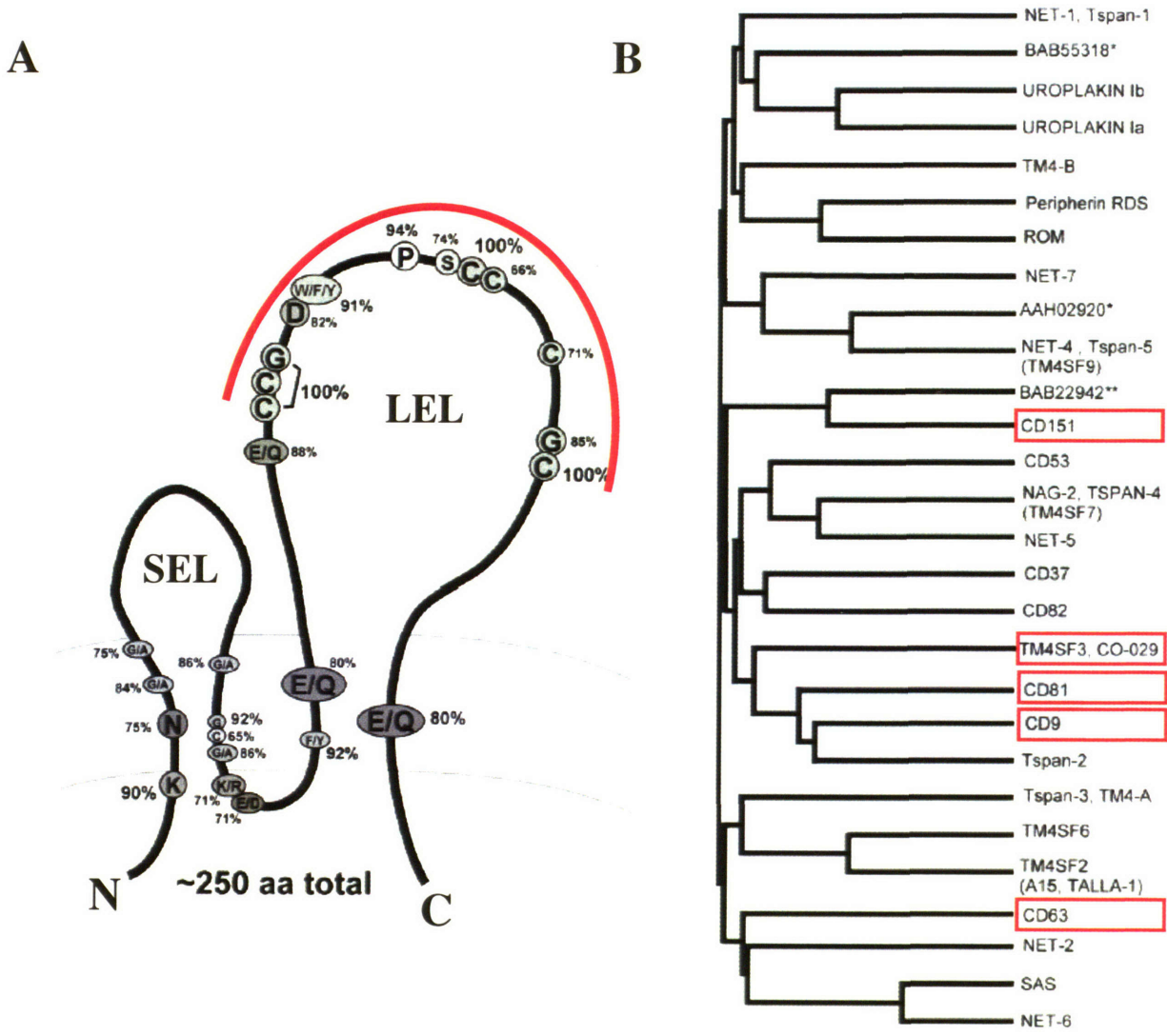


Figure 1.1 Sequence conservation and phylogeny of tetraspanin proteins. A) Conserved amino acids among 28 known human tetraspanin and 37 *Drosophila* tetraspanins. The short extracellular loop (SEL) and large extracellular loop (LEL) are labeled. The non- α -helical variable region is indicated with a red bar. The predicted, conserved, α -helical lies N- and C-terminal of this region, extending to transmembrane segment 3 and transmembrane segment 4. B) Twenty-seven human and one murine tetraspanin sequence were aligned. The murine sequence is indicated with “***”. Shaded genes are mutated tetraspanins in humans or targeted deletions in mouse. Tetraspanins with a red box are studied in more detail in Chapter 6

(from Martin Hemler, *Journal of Cell Biology*, 155(7) 1103-1107, 2001)

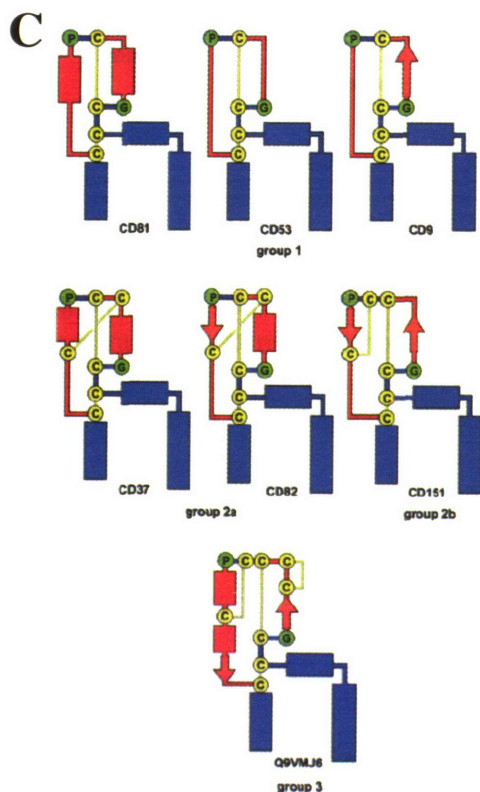


Fig 1.3 Homology Analysis of the hCD81-LEL structure A) Superposition of the monoclinic 1G8Q (green) and hexagonal 1IV5 (red) crystal structures. B) Model of the intact CD82 molecule using the hCD81-LEL structure as a template. Helical elements are shown in red. Disulfide bonds are shown in yellow. C) Predicted disulfide-bond connectivities of tetraspanin-LELs containing two disulfide bonds (Group 1; top) three disulfide bonds (Group 2; middle) and four disulfide bonds (Group 3). Conserved helical structures comprising the dimerization subdomain are shown in blue. The variable subdomain is shown in red and key conserved residues are indicated in green.

(From A) Neugebauer et. al. *Bioorg Med Chem Lett* 14: 1765-1769 (2004) B) Bienstock and Barrett *Mol Carcin.* 32: 139-153 (2001) C) Seigneuret et. al. *JBC* 267 (43) 40055-40064 (2001))

Tetraspanin	Species	Cell type	Associated molecules
CD9	Human	Platelets	$\alpha 11\beta 3$ (CD41/CD61) integrin (mAb-induced association)
		HeLa cells	$\alpha 6\beta 1$ integrin, $\alpha 3\beta 1$ integrin and CD81 or CD63
		NALM-6, HEL cell lines	$\beta 1$ integrins
	Monkey	Platelets	25–26 kDa G-proteins
		Vero cells	diphtheria toxin receptor proHB-EGF and $\alpha 3\beta 1$ integrin
CD37	Rat	Schwann cell line S-16	$\alpha 3\beta 1$, $\alpha 6\beta 1$ integrins
CD53	Human	B cells	MHC class II
	Human	Hematopoietic cell lines	$\alpha 4\beta 1$ integrin
CD63	Rat	Lymph node; thymoma	An unknown phosphatase
		B cells	MHC class II
	Human	NK cell line, T cells	CD2
CD81	Human	Hematopoietic cell lines	$\alpha 4\beta 1$ integrin
		HeLa cells, melanoma cell lines	$\alpha 3\beta 1$ integrin and CD81 or CD9
	Rat	Multiple cell lines	$\alpha 3\beta 1$ and $\alpha 6\beta 1$ integrins
CD82	Human	Neutrophils	LFA-1
		Basophilic leukemia cell line	An unknown phosphatase
		B cells	CD19/CD21/Leu-13 complex
	Rat	T cells	MHC class II
CD82	Human	Hematopoietic cell lines	CD4, CD8, and CD82
		T cells	$\alpha 4\beta 1$, $\alpha 4\beta 7$ integrins
		Hematopoietic cell lines	$\alpha 6\beta 1$ integrin, $\alpha 3\beta 1$ integrin, and CD9 or CD63
Rom-1	Cow	B cells	CD4, CD8, and CD81
Peripherin	Human	Photoreceptor cells	$\alpha 4\beta 1$ integrin
		Photoreceptor cells	$\alpha 3\beta 1$, $\alpha 6\beta 1$ integrins
UPIa	Cow	Bladder epithelium	MHC class II
UPIb	Cow	Bladder epithelium	Peripherin
UPIa	Cow	Bladder epithelium	Rom-1
UPIb	Cow	Bladder epithelium	UPIb, UPII, UPIII
	Cow	Bladder epithelium	UPIa, UPII, UPIII

Figure 1.4 A table of observed tetraspanin heterotypic interactions circa 1997. Listed are the tetraspanin family members (left), species, cell type where the interaction was observed and associated molecules. The list includes tetraspanin binding partners under both robust and non-robust detergent conditions

(from Maecker et. al. *FASEB J.* 11 (6) 428-42 (1997).

Table 1. Integrin-tetraspanin complexes

Tetraspanin	Integrin	Cells	References
CD9	$\alpha 1\beta 1$	Epithelia (cervix)	Lozahic et al., 2000
	$\alpha 2\beta 1$	Vascular smooth muscle, keratinocytes	Scherberich et al., 1998; Jones et al., 1996
	$\alpha 3\beta 1$	Epithelia (skin, breast, endometrium, colon and kidney), trophoblasts, endothelia, Schwann cells, vascular smooth muscle, fibrosarcoma, melanoma	Scherberich et al., 1998; Jones et al., 1996; Berditchevski et al., 1996; Hadjiargyrou, et al., 1996, Yáñez-Mó et al., 1998; Yáñez-Mó et al., 2001; Hirano et al., 1999; Nakamura et al., 1995; Park et al., 2000; Serru et al., 1999
	$\alpha 4\beta 1$	B cells, T cells	Rubinstein et al., 1994
	$\alpha 5\beta 1$	B cells, myocytes, trophoblasts	Rubinstein et al., 1994; Hirano et al., 1999; Tachibana and Hemler, 1999
	$\alpha 6\beta 1$	Epithelia (breast, endometrium), trophoblasts, fibrosarcoma	Berditchevski et al., 1996; Hirano et al., 1999; Park et al., 2000
	$\alpha 7\beta 1$	Myocytes	Tachibana and Hemler, 1999
	$\alpha 6\beta 4$	Keratinocytes	Jones et al., 1996
	$\alpha IIb\beta 3$	Platelets	Slupsky et al., 1989
	CD53	$\alpha 4\beta 1$	T cells
CD63	$\alpha 3\beta 1$	Epithelial (breast), fibrosarcoma	Berditchevski et al., 1996
	$\alpha 4\beta 1$	T cells	Mannion et al., 1996
	$\alpha 6\beta 1$	Epithelial (breast), fibrosarcoma	Berditchevski et al., 1996
	$\alpha M\beta 2$	Neutrophils	Skubitz, et al., 1996
	$\alpha IIb\beta 3$	Platelets	Israels et al., 2001
CD81	$\alpha 3\beta 1$	Epithelia (breast, cervix), fibrosarcoma, neurites, myocytes	Berditchevski et al., 1996; Serru et al., 1999, Tachibana and Hemler, 1999; Stipp and Hemler, 2000
	$\alpha 4\beta 1$	T cells, B cells, erythroleukaemia, myocytes	Tachibana and Hemler, 1999, Mannion et al., 1996
	$\alpha 5\beta 1$	Myocytes	Tachibana and Hemler, 1999
	$\alpha 6\beta 1$	Epithelia (breast), fibrosarcoma, Rhabdomyosarcoma	Berditchevski et al., 1996; Mannion et al., 1996
	$\alpha 7\beta 1$	Myocytes	Tachibana and Hemler, 1999
CD82	$\alpha 3\beta 1$	Epithelia (breast)	Berditchevski and Odmtsova, 1999
	$\alpha 4\beta 1$	T cells, B cells, rhabdomyosarcoma	Mannion et al., 1996
	$\alpha 5\beta 1$	Hamster ovary	Ono et al., 2000
	$\alpha 6\beta 1$	Rhabdomyosarcoma	Mannion et al., 1996
CD151	$\alpha 3\beta 1$	Epithelia (skin, breast, cervix, kidney, colon), endothelia, neurites, fibrosarcoma	Yáñez-Mó et al., 1998; Yáñez-Mó et al., 2001, Serru et al., 1999; Stipp and Hemler, 2000, Berditchevski and Odmtsova, 1999; Yauch et al., 1998; Sterk et al., 2000
	$\alpha 4\beta 1$	Megakaryocytes, erythroleukaemia	Fitter et al., 1999
	$\alpha 5\beta 1$	Megakaryocytes, T cells, erythroleukaemia, endothelia	Fitter et al., 1999; Sincock et al., 1999, Hasegawa et al., 1998
	$\alpha 6\beta 1$	Epithelia (cervix, colon), B-cells, fibrosarcoma, megakaryocytes, endothelia, erythroleukaemia	Serru et al., 1999; Yauch et al., 1998, Fitter et al., 1999; Sincock et al., 1999
	$\alpha 6\beta 4$	Keratinocytes, endothelia	Sterk et al., 2000, Sincock et al., 1999
	$\alpha II\beta 3$	Erythroleukaemia	Fitter et al., 1999
Nag2/Tspan4	$\alpha 3\beta 1$	Epithelia (breast), fibrosarcoma	Tachibana et al., 1997
	$\alpha 6\beta 1$	Epithelia (breast), fibrosarcoma	Tachibana et al., 1997
Tspan3	$\alpha \beta 1$	Oligodendrocytes	Tiwari-Woodruff et al., 2001
CO-029	$\alpha 3\beta 1$	Epithelia (colon, pancreatic)	Serru et al., 1999; Claas et al., 1998
	$\alpha 6\beta 1$	Epithelia (colon, pancreatic)	Serru et al., 1999; Claas et al., 1998

Only original reports describing a particular integrin-tetraspanin association in a particular cell type are cited.

Figure 1.5 A table of observed tetraspanin integrin interactions circa 2001. Listed are the tetraspanin family members (left), integrin heterodimer, cell type where the interaction was observed and references where the interaction was initially observed. This list includes tetraspanin binding partners under both robust and non-robust detergent conditions and illustrated the rapid curation of tetraspanin heterotypic binding partners.

(from Berditchevski *J of Cell Sci.* 114, 4143-4151 (2001).

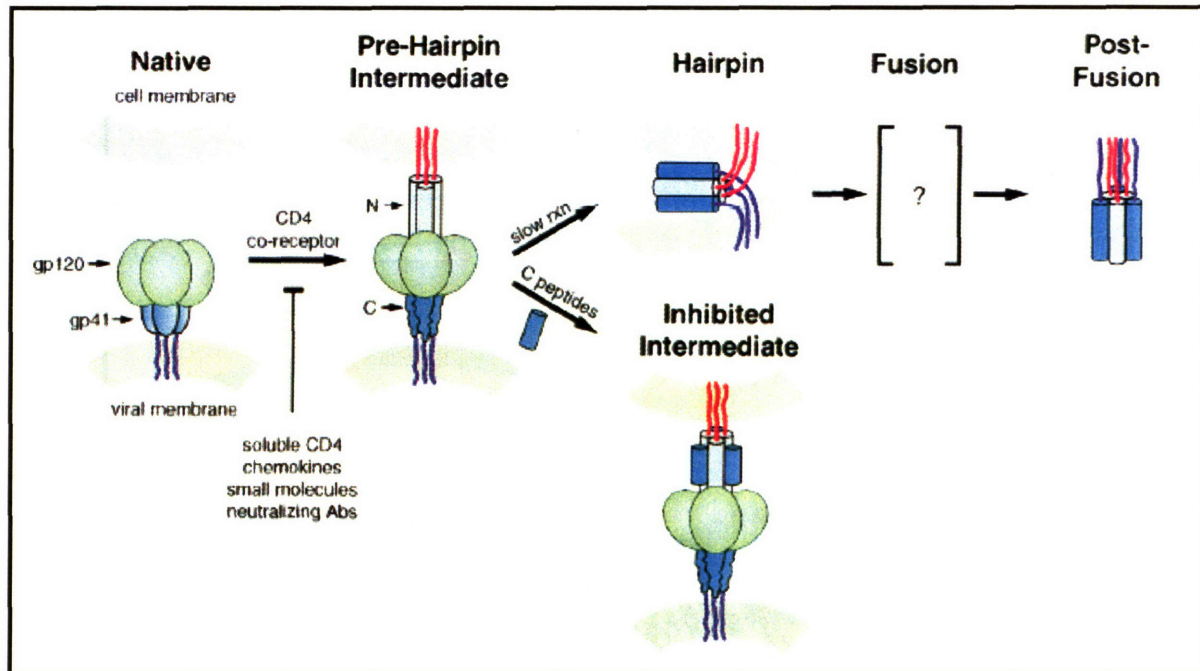


Figure 1.6 A model of HIV (Class I) Membrane Fusion. The native state of the HIV glycoprotein is depicted on the left. Binding to cellular receptors induces insertion of a fusion peptide (red) into the host target membrane, forming a pre-hairpin intermediate. This inhibition is long-lived and susceptible to multiple inhibition. The pre-hairpin intermediate then collapses to a hairpin structure, where trimeric N peptide coiled coils (gray) form a six bundle with helical C peptides (blue). This global conformational rearrangement results in membrane apposition and fusion. Ultimately, both fusion peptide (red) and the transmembrane segments (purple) are in the same membrane.

(from Chan DC and Kim PS Cell 93, 681-684 (1998)).

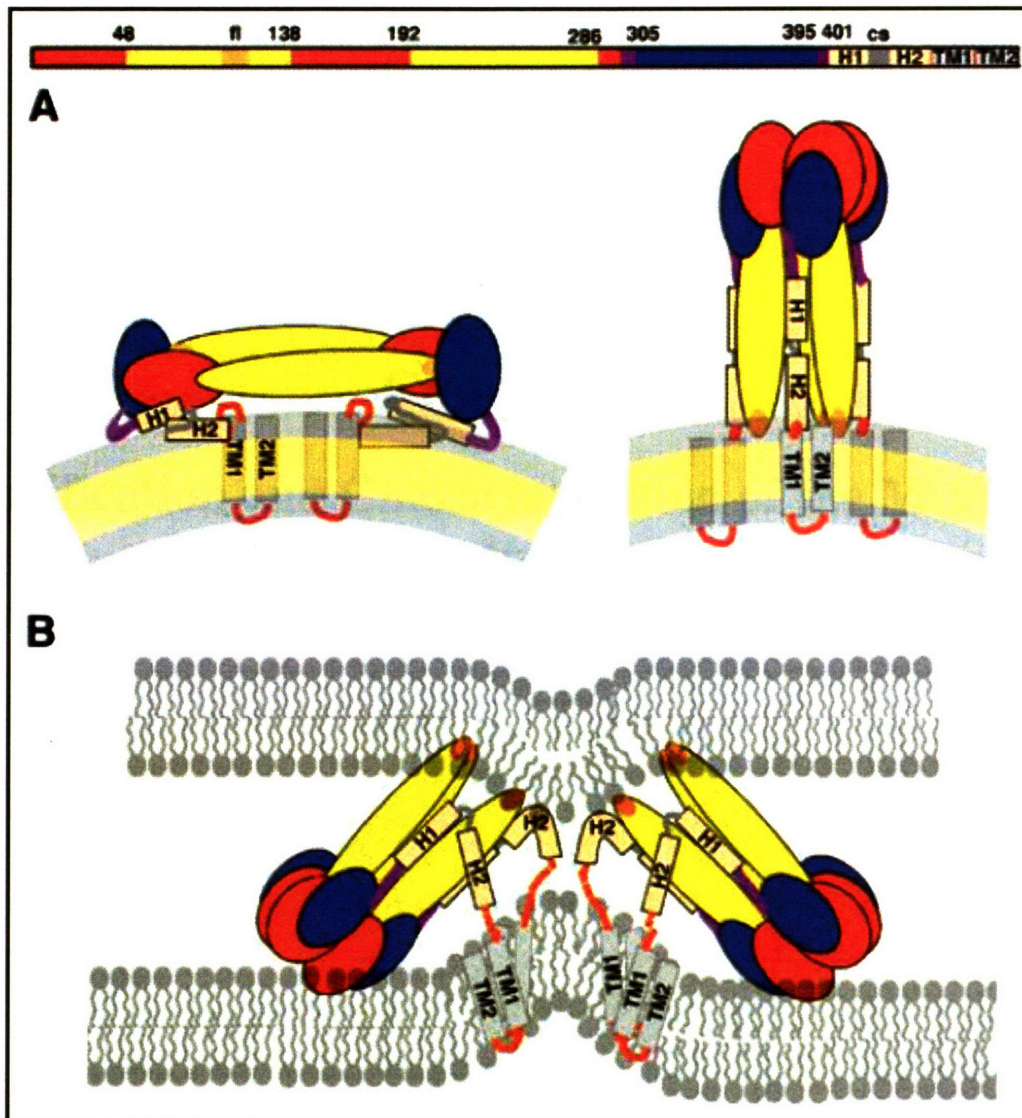


Figure 1.7 A model of TBE (Class II) Membrane Fusion. The primary domain structure of the TBE glycoprotein is depicted with regions color coordinated to the domain structure below. Transmembrane segments are in gray towards the C- termini and the internal fusion peptide is in orange towards the N-termini. A) A cartoon of the native TBE glycoproteins as planar antiparallel dimers on the left. A cartoon of the final post-fusion TBE glycoprotein as a trimer that sits orthogonal to the lipid bilayer on the right. B) A cartoon of the TBE glycoprotein hairpin structure with fusion peptides inserted into the target membrane. This intermediate structure is formed upon receptor activation of the native TBE glycoprotein (A left) and ultimately resolves into the post-fusion TBE glycoprotein (A right)

(from Bressanelli et.al.EMBO J. 23, 728-738 (2004).

Chapter 2

Purification and Characterization of the Murine CD9 Large Extracellular Loop

These experiments were conceived by Christopher C. Liu and Peter S. Kim. All experiments were carried out by Christopher C. Liu. We thank Michael W. Burgess for technical assistance with chromatography and David L. Akey for technical assistance with both biophysical instrumentation and analysis of data. All errors are my own.

Introduction

Tetraspanins have been implicated in a wide variety of cell biological effects. Surprisingly, knockout mouse models of several tetraspanin proteins have resulted only in mild immune phenotypes (Hemler 2001). In contrast, female CD9-null mice are infertile, and this phenotype was pinpointed to a defect in sperm-egg fusion (Kaji, Oda et al. 2000; Le Naour, Rubinstein et al. 2000; Miyado, Yamada et al. 2000). Lack of CD9 does not affect either sperm-egg binding or subsequent development of the zygote, when sperm-egg fusion is artificially bypassed. Exogenous addition of an antibody against murine CD9, clone KMC8, mimics the CD9-null mutant (Chen, Tung et al. 1999; Miller, Georges-Labouesse et al. 2000). This antibody specifically inhibits sperm-egg fusion and has no effect on gamete binding.

Due to our interest in cell-cell membrane fusion, we chose to focus our studies on the murine CD9-large extracellular loop (mCD9-LEL). By focusing on the extracellular domain of the murine CD9 molecule, we targeted our experiments to the protein domain recognized by a fertilization-blocking monoclonal antibody (Miller, Georges-Labouesse et al. 2000). Furthermore, restricting our studies to this domain also circumvented issues of solubility and aggregation commonly associated with the biophysical characterization of membrane proteins.

In this chapter, we describe our method to express and purify to conformational homogeneity a single disulfide-bonded species of the murine CD9-LEL. Furthermore, we show that this mCD9-LEL species is specifically recognized by the fertilization-blocking monoclonal antibody KMC8 and biophysical analysis reveals that it is an autonomously folding α -helical dimer. Lastly, we present evidence of the critical importance in the contribution of proper-disulfide bond formation to the stability and function of this mCD9-LEL species.

Materials and Methods

Cloning and Expression of the Murine CD9-LEL.

Fresh, primary bone marrow cells were flushed from the long-bones of a BL6 mouse. Total ribonucleic acid (RNA) was prepared from bone marrow cells using the RNA STAT-60 total RNA purification kit (Tel-Test, Friendswood, TX). Total RNA was reverse-transcribed using oligo-dT primers with the Superscript Preamplification System (Gibco BRL, Grand Island, NY). The oligonucleotide primers CL34 and CL35 (Research Genetics, Huntsville, AL) were designed to amplify the murine CD9-LEL:

CL34 = 5'-CCCGCTAGCACCCACAAGGATGAGGTGATTAAAGAACTGC-3'

CL35, = 5'-CCCCTCGAGGATGTGGAACCTTGTTGTTGAAGACCTCAC-3'

PCR was performed in a Robocycler (Stratagene, La Jolla, CA) with a 45–65°C gradient. The amplified product was inserted into the *NheI*–*XhoI* restriction site of the carboxy-terminal hexahistidine expression vector pET24a (Novagen, Madison, WI). Proper plasmid construction was confirmed by DNA sequencing through the open reading frame and referenced to the NCBI database.

Purification of the Murine CD9-LEL

The resulting plasmid, denoted recmCD9-LEL, was transformed into *E. coli* BL21/pLysS competent cells for protein expression. Cells were grown in Luria-Bertani medium to an optical density of 0.2 at 600 nm. Protein expression was induced with 1 mM isopropyl-beta-D-thiogalactopyranoside, and cells were harvested after 5 hours.

Cells were lysed in a French press and separated into soluble and insoluble fractions by centrifugation. The insoluble portion was resuspended in 6 M guanidine-HCl, and subsequently clarified by both centrifugation and filtration. The recombinant protein was purified by nickel-nitrilotriacetic acid metal-affinity chromatography (Qiagen, Chatsworth, CA), followed by reverse-phase HPLC (Waters, Milford, MA) using a Vydac C18 preparative column (Vydac, Hesperia, CA) with a water/acetonitrile gradient of 0.05%/min in the presence of 0.1% trifluoroacetic acid.

Protein samples were analyzed by reverse-phase HPLC connected to an LCQ electrospray mass spectrometer (Finnigan-MAT, San Jose, CA). Proteins were centrifuged under vacuum to remove the acetonitrile, lyophilized, and resuspended in PBS (pH 7.4); all protein concentrations were determined by absorbance at 280 nm in 20 mM phosphate-buffered 6M guanidine-HCl (pH 6.5) (Edelhoch 1967).

Western Blot Analysis

Lyophilized samples were resuspended in PBS and analyzed by 18% SDS-PAGE under non-reducing and reducing conditions and Coomassie Blue staining (Lu, Blacklow et al. 1995). Gels were transferred onto Hybond-C membrane (Amersham-Pharmacia, Piscataway, NJ) in 10 mM CAPS/10% MeOH (pH 11.0). Membranes were blocked for 2 hours at room temperature in 4% non-fat dry milk/TBS/0.1% Tween-20. A monoclonal antibody against mCD9, clone KMC8 (BD Pharmingen, San Diego, CA), was used as the primary probe at a 1:1000 dilution. Horseradish peroxidase (HRP)-conjugated goat anti-rat (BD Pharmingen) at a 1:1000 dilution was used to detect the presence of KMC8. The membrane was developed using the ECL system (Amersham-Pharmacia) and exposed to film.

Quantitation of Free Thiols.

Free thiols were quantified using Ellman's Reagent (Pierce, Rockford, IL) as per the manufacturer's instructions. In brief, resuspended protein was added to a fresh 0.08 mg/ml solution of Ellman's reagent in 100 mM sodium phosphate, pH 8.0. Absorbance was measured at 412 nm using an extinction coefficient of 14,000.

Circular Dichroism Spectroscopy

Circular dichroism (CD) spectra were measured at 10 μ M protein concentration in PBS buffer with an AVIV 62A DS CD spectrometer (Aviv Associates, Lakewood, NJ) as described (Wu and Kim 1997). Thermal melts were performed over a temperature range from 0–80°C in 2°C increments. Protein samples were equilibrated for 90 seconds and data were acquired over 30 seconds. The midpoint of the thermal unfolding transition (T_m) reported is the maximum of the first derivative of the thermal melt data.

Sedimentation Equilibrium Analysis

Sedimentation equilibrium analysis was performed on a Beckman XLA-90 analytical ultracentrifuge (Beckman Instruments, Palo Alto, CA). Samples were dialyzed overnight against PBS and spun at 20,000 and 30,000 rpm. Protein samples were analyzed at concentrations of 10, 20, and 50 μ M. Data were collected at three wavelengths per rotor speed after spinning for 24 hours at 25°C. For all speeds and time points, a second data set was acquired 3 hours after the first. The two data sets were compared to ensure that the samples were at equilibrium. A single ideal species model was fit to the data and the partial specific volume was calculated from the residue-weighted average of the amino acid sequence. Solvent density was calculated from the solvent composition (Laue, Shah et al. 1992).

Disulfide-Shuffling of the Murine CD9-LEL protein

The murine CD9-LEL was expressed, purified, and eluted from a Ni-NTA column under denaturing conditions. This protein fraction was diluted 10-fold into PBS (for a final concentration of .6M guanidine-HCl) containing the specified concentrations of reduced or oxidized glutathione. The protein solution was shaken at room temperature for 5 hours, and simulated disulfide shuffling was stopped with the addition of neat HOAc to a final concentration of 5% (pH 2.0). Each solution was clarified by both centrifugation and filtration and analyzed by reverse-phase HPLC on a Vydac C18 analytical column. Protein content was monitored at 229 nm.

Results

Expression and Partial Purification of the Murine CD9-LEL construct.

To study the mCD9-LEL we isolated primary murine bone marrow cells by flushing the long bones of a mouse. Total RNA was extracted and first-strand cDNA synthesis was used to create a template pool containing the murine CD9 cDNA. The oligonucleotides CL34 and CL35 were designed to amplify the mCD9-LEL, corresponding to murine CD9 residues 110-193 with an *NheI* and *XhoI* site inserted 5' and 3' of the LEL respectively for subcloning purposes. The large extracellular loop portion of the CD9 cDNA was successfully amplified and inserted into pET24a, excising almost the entire multiple-cloning site, and verified by DNA sequencing. The plasmid was designed to contain a C-terminal hexahistidine tag in frame with the mCD9-LEL (Figure 2.1A).

The recmCD9-LEL plasmid was transformed into BL21/pLysS cells for protein expression. Overnight cultures were diluted 1:100 into Luria-Bertani growth medium and protein expression was induced with 1mM isopropyl-beta-D-thiogalactopyranoside when cells were at an optical density of 0.2 at 600nm. It should be noted that no protein expression was observed when cells were induced at higher optical densities. Post-induction, *E. coli* cells continued to grow in near-logarithmic phase, as monitored at OD600 nm, and induced cells were harvested after 5 hours.

The mCD9-LEL protein was highly expressed and sequestered into inclusion bodies. The mCD9-LEL protein was solubilized, air-oxidized under denaturing conditions, and partially purified using metal-ion chromatography (Figure 2.1B). Non-reducing SDS-PAGE analysis of the nickel-purified mCD9-LEL protein revealed several higher order oligomers which collapsed to the monomeric form upon addition of 10% beta-mercaptoethanol prior to loading onto SDS-PAGE (data not shown). This suggests that nickel-purified higher order oligomers are intermolecular disulfide-bonded variants of the mCD9-LEL protein.

Isolation and Characterization of Two mCD9-LEL Protein Species

Nickel-purified mCD9-LEL protein was diluted 10-fold into PBS, acidified, and clarified by both centrifugation and filtration. The sample was loaded onto a reverse-

phase C18 HPLC and protein content was monitored at 229nm. We observed and isolated two mCD9-LEL species, designated mP1 and mP2, respectively, which were chosen for further characterization (Figure 2.2A). Mass spectrometry revealed the molecular weights of each of mP1 and mP2 to be 10,989.5 +/- 0.3 Da. These data matched the predicted molecular weight of mCD9-LEL (for the oxidized species) with the N-terminal methionine residue cleaved, but no further modifications. Using Ellman's reagent, we detected no free sulfhydryls in either mP1 or mP2 (data not shown).

Western blot analysis revealed that only the mP1 protein was recognized by a fertilization-blocking monoclonal antibody, clone KMC8 (Figure 2.2B). Residual KMC8 immunoreactivity of the mP2 protein may be due to traces of mP1 in the protein prep. Reduced mP1 was weakly recognized by KMC8 at the same low levels as reduced mP2, suggesting that KMC8 recognizes only a single, oxidized isomer of the mCD9-LEL protein. Sandwich ELISA studies revealed that the C-terminal hexahistidine tag did not interfere with KMC8 binding (data not shown). These results suggest that the hexahistidine epitope is discrete from the KMC8 epitope and that the hexahistidine tag may be utilized to probe KMC8 function (Chapter 7).

Circular Dichroism and Sedimentation Equilibrium Analyses of mCD9-LEL Protein Species.

The mP1 protein folds into an α -helical structure in PBS as determined by circular dichroism analysis (Figure 2.3A), with characteristic minima at 208 nm and 222 nm (Chen, Yang et al. 1974). Our measurement of a mean molar ellipticity at 222nm of approximately $-11,000$ empirically corresponds to approximately one-third global, helical content. The mP1 protein undergoes a cooperative, reversible, thermal unfolding transition, with a T_m value of approximately 58°C . Conversely, circular dichroism experiments reveal that mP2 does not have a well-folded structure. At 80°C , when mP1 is thermally denatured, both mP1 and mP2 have the same CD signal at 222 nm (Figure 2.3B). When mP1 was thermally denatured to 100°C and then renatured, it did not regain native levels of α -helicity. As a result, all subsequent thermal denaturation/renaturation analysis was done to 80°C .

Sedimentation equilibrium analyses clearly indicate that mP1 is a dimer in solution (Figure 2.4A). Residuals (deviations) from the predicted molecular dimeric weight were randomly distributed (Laue, Shah et al. 1992). These data are consistent at concentrations of 10, 20, and 50 μM in PBS (pH 7.4). The dimerization state of mP1 was confirmed by gel filtration chromatography (see Chapter 4). Sedimentation equilibrium experiments with the mP2 protein reveal that it is a slightly aggregated monomer (Figure 2.4B). The best linear fit for mP2 was estimated at a molecular weight of 1.14 times that of the monomeric molecular weight. Lastly, there was a high degree of auto-correlation in the residuals, indicative of a poor fit to a linear molecular weight model (Laue, Shah et al. 1992). This sedimentation equilibrium result is consistent with the unstructured nature of mP2.

Disulfide-Shuffling of the mCD9-LEL Protein Variants.

The presence of two variants of the mCD9-LEL (P1 and P2) that had identical masses, but different chromatographic properties allowed us to hypothesize that these proteins were disulfide-bonded variants. However, the presence of two adjacent cysteine residues (Figure 1A) frustrated attempts to map the disulfide-bond connectivities by tryptic proteolysis followed by mass spectral analysis (data not shown). To explore the role of cysteine residues in the P1 and P2 variants of the mCD9-LEL protein, we turned to simulated disulfide-shuffling conditions (Tu and Weissman 2004).

It has been shown that a mix of reduced and oxidized glutathione can simulate the redox environment of the endoplasmic reticulum (Tu and Weissman 2004). In our purification scheme, the mCD9-LEL protein is oxidized as it is solubilized by 6M Guanidine-HCl from the insoluble portion of *E. coli* cells. This oxidation occurs under denaturing conditions, which is consistent with the approximately equimolar ratio between the mCD9-LEL P1 and P2 (Figure 2.2A). We rapidly diluted equivalent quantities of fully oxidized, denatured mCD9-LEL into non-denaturing conditions containing various ratios of reduced and oxidized glutathione. In most cases, significant amounts of protein precipitate formed within several minutes. After 5 hours, we stopped the redox reaction by lowering the pH and monitored mCD9-LEL P1 and P2 quantities with an analytical C18 column .

We observed that the presence of a glutathione mix significantly increased the yield of both the mCD9-LEL P1 and P2 proteins (Figure 2.5). Under all redox conditions, there was more mCD9-LEL P1 than mCD9-LEL P2, suggesting that the mCD9-LEL is the preferred disulfide-bonded state. The ability of a redox reaction to increase mCD9-LEL P1 yields emphasizes the contribution of a proper disulfide-bond connectivity both to the thermodynamic stability and the α -helical nature of the mCD9-LEL. Lastly, the identification of redox conditions that optimize protein yield may be critical for the extension of our methodology to other tetraspanin-LELs. For studies in Chapter 6, we selected the redox condition consisting of 2mM GSH/0.5mM GSSG as it both optimized yield and minimized off-pathway tetraspanin-LEL isomers (Figure 2.5C).

Discussion

In this chapter we present evidence that the LEL of mCD9, a prototypical tetraspanin, is an independently folding domain. mCD9-LEL can be expressed without a large fusion partner. The properly oxidized species can be purified to homogeneity and is approximately one-third α -helical and dimeric. The α -helical, dimeric nature of the mCD9-LEL protein most likely depends on attaining of a proper disulfide-bonding pattern.

We chose to restrict our studies of the murine tetraspanin CD9 to a single domain of the molecule: the large extracellular loop. This strategy allows significant technical simplification, as subsequent experiments are not complicated by the necessity of adding detergents. All of our biophysical characterization is done in phosphate-buffered saline. However, we note that this strategy excludes the transmembrane regions, which not only constitute a significant portion of the tetraspanin molecule but also has distinguishing sequence conservation (Stipp, Kolesnikova et al. 2003), implying evolutionary significance beyond anchoring the protein in the lipid bilayer of the cell. Furthermore, this strategy does not allow the exploration of the short extracellular loop, which has largely been ignored by the tetraspanin community. Lastly, it also does not allow the exploration of post-translational modifications. Most importantly, palmitoylation has been shown to play significant roles in tetraspanin function (Yang, Kovalenko et al. 2004). These issues will be further addressed in Chapter 5.

Regardless, our experiments illustrate a straightforward investigative avenue to explore tetraspanin function in general, and CD9 in particular. By expressing the mCD9-LEL protein in *Escherichia coli*, we are readily able to express and purify milligram quantities of pure protein. Although using a prokaryotic expression system precludes the inclusion of glycosaccharides (the CD9-LEL has no predicted glycosylation sites), it allows fast and cheap expression of mutant constructs (see Chapter 4). An attempt to express the CD9-LEL in S2 insect cells has not been successful to date (Jack Lawler, personal communication). Using a hexahistidine purification tag, we eliminate the necessity to add a large fusion partner such as glutathione-S-transferase (Zhu, Miller et al. 2002) or maltose binding protein. Although the hexahistidine tag is not ideal for immunoprecipitation experiments (as it binds many metal-chelating proteins), it adds

little molecular weight to the protein of interest, further simplifying subsequent biophysical analysis. Lastly, the use of a hexahistidine tag allows the purification of recombinant proteins under denaturing conditions.

A critical component of our purification strategy is the use of reverse-phase HPLC. By purifying our nickel-purified mCD9-LEL protein over C18 chromatography, we were able to eliminate contaminating higher order oligomers, bringing our protein purity up significantly (as assessed by SDS-PAGE). In actuality, the purity of the nickel-purified mCD9-LEL protein (which was estimated at 85% in Figure 2.1B) significantly overestimated protein purity. As assayed over a C18 column with a fine elution gradient, the KMC8 immunoreactive mCD9-LEL species (P1) was estimated to be a mere 20%. We were pleasantly surprised that a C18 reverse-phase column could separate protein species with identical molecular weight but different disulfide-connectivities at pH 2. It should be noted that for a protein the size of the mCD9-LEL (~11kDa), the suggested reverse-phase column is either C4 or C8, as C18 is recommended for shorter synthetic peptides. We have not tested the chromatographic performance of the mCD9-LEL protein on C4 or C8 reverse-phase columns.

Circular dichroism analysis proved to be a powerful analytical tool for the study of the mCD9-LEL. Our circular dichroism measurement of the mCD9-LEL protein, with a θ_{222} of approximately -11,000 corresponds to one-third average, global helical content (Chen Yang). For example, coiled-coils, which contain almost complete α -helicity, exhibit a circular dichroism θ_{222} of between -30,000 and -35,000 (O'Shea, Rutkowski et al. 1989). These circular dichroism measurements of the mCD9-LEL protein are consistent with predictions of its secondary structure content.

As all tetraspanins-LELs are predicted to have significant α -helicity, circular dichroism may allow us to identify well-folded tetraspanin-LEL species, even without clearly defined, conformation-specific antibodies such as the clone KMC8. By monitoring the α -helicity of the mCD9-LEL protein over a range of temperatures, we concluded that the mCD9-LEL protein is a very stable protein. Thermal denaturation data may allow us a rapid, if qualitative, methodology to assay the stability of mCD9-LEL variants. Most importantly, it directly suggests that the mCD9-LEL protein is folded at physiological temperatures (37°C), which is critically important in analysis of

inhibition data (Chapter 7). Thermal renaturation data also allow us to identify incubation times and temperatures where the mCD9-LEL will no longer be folded (ie. $>80^{\circ}\text{C}$) which may prove useful in later experiments (Chapter 6). Lastly, the autonomously folding nature of the mCD9-LEL suggests that there are no kinetic traps in the folding landscape of the mCD9-LEL (Pain 1994).

Our sedimentation equilibrium suggests that the mCD9-LEL protein behaves as a globular, ideal protein species (Laue, Shah et al. 1992). Although this experimental method is tedious, it allows us to characterize carefully the oligomerization of the mCD9-LEL under equilibrium conditions (versus gel filtration). Empirically, the minimum sequence size for a protein to exhibit a stable tertiary structure is approximately 50 amino acids (Dyson and Wright 1991). Evidence of a dimeric mCD9-LEL may explain the relatively high thermal stability of the 83-amino acid protein.

Although our attempts to map the disulfide connectivities was not technically tractable, the isolation of two mCD9-LEL species with identical molecular weights suggested that the difference in the chromatographic properties of these variants lay in their disulfide connectivities. The ability of a redox mix to significantly alter the yields of the two mCD9-LEL species (relative to random oxidation) strongly suggests that disulfide connectivities result in the observed shift in reverse-phase elution times. Equimolar yields of the two mCD9-LEL species under random oxidation (due to denaturing conditions) also points to the importance of disulfide connectivity in determining α -helicity. Lastly, the greater yield of mCD9-LEL P1 under redox conditions suggests that the α -helical mCD9-LEL species is in a lower thermodynamic state than its disulfide-shuffled variants. For the remainder of this thesis, we will refer to the mCD9-LEL P1 species as the mCD9-LEL protein.

A soluble, properly folded form of the mCD9-LEL protein and the general methodology described in this chapter may assist both in studying the intrinsic nature of the mCD9-LEL protein, its cell biological roles, and the functions of other tetraspanin-LELs. In this thesis, we both build upon and expand the methods and results described within this chapter.

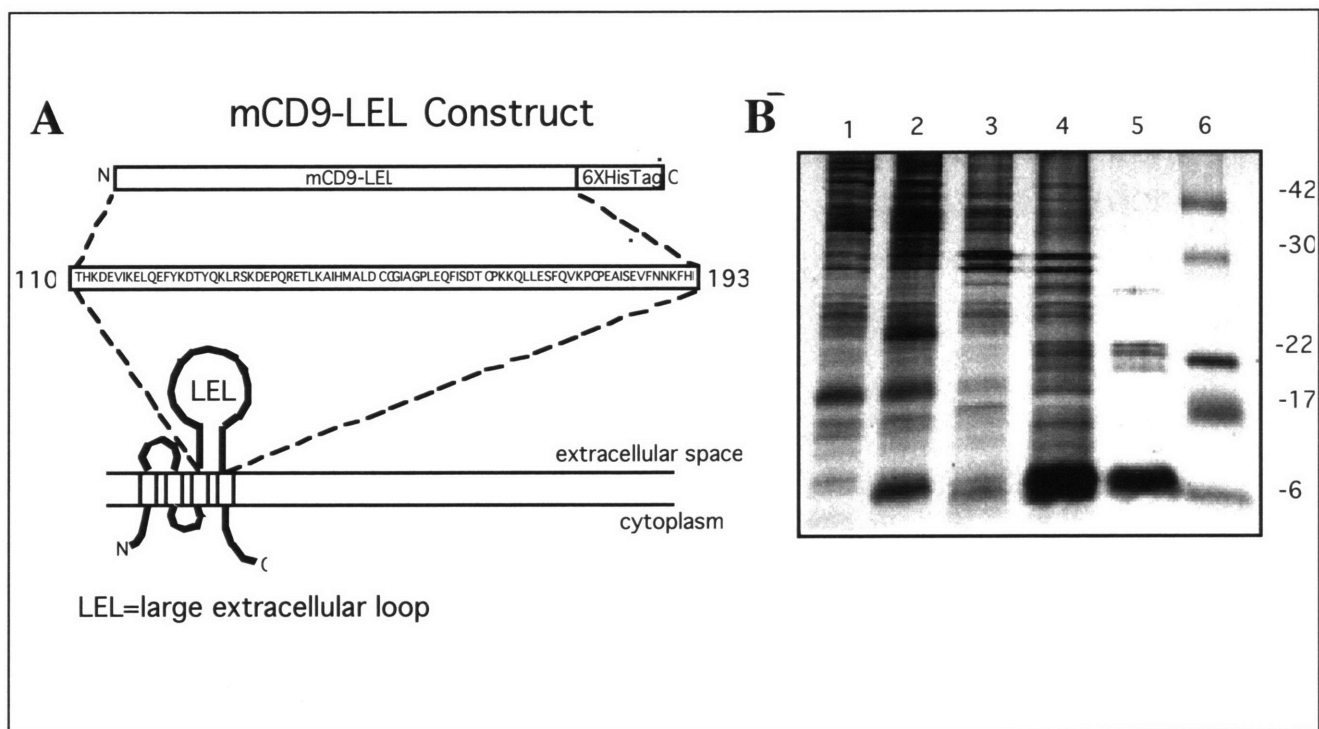


Figure 2.1 Preparation of Recombinant CD9-LEL. A) Schematic diagram of the mCD9-LEL protein sequence. The region encoding the murine CD9-large extracellular loop (LEL) was amplified by PCR and inserted in the pET24a expression vector with a C-terminal hexahistidine tag. B) The mCD9-LEL protein was partially purified using Ni-column chromatography and analyzed by nonreducing SDS-PAGE: Lane 1) preinduced BL21/pLysS cells; Lane 2) induced BL21/pLysS cells; Lane 3) insoluble fraction; Lane 4) 6 M guanidine-HCl solubilized fraction; Lane 5) elution from Ni-column; Lane 6) molecular weight marker.

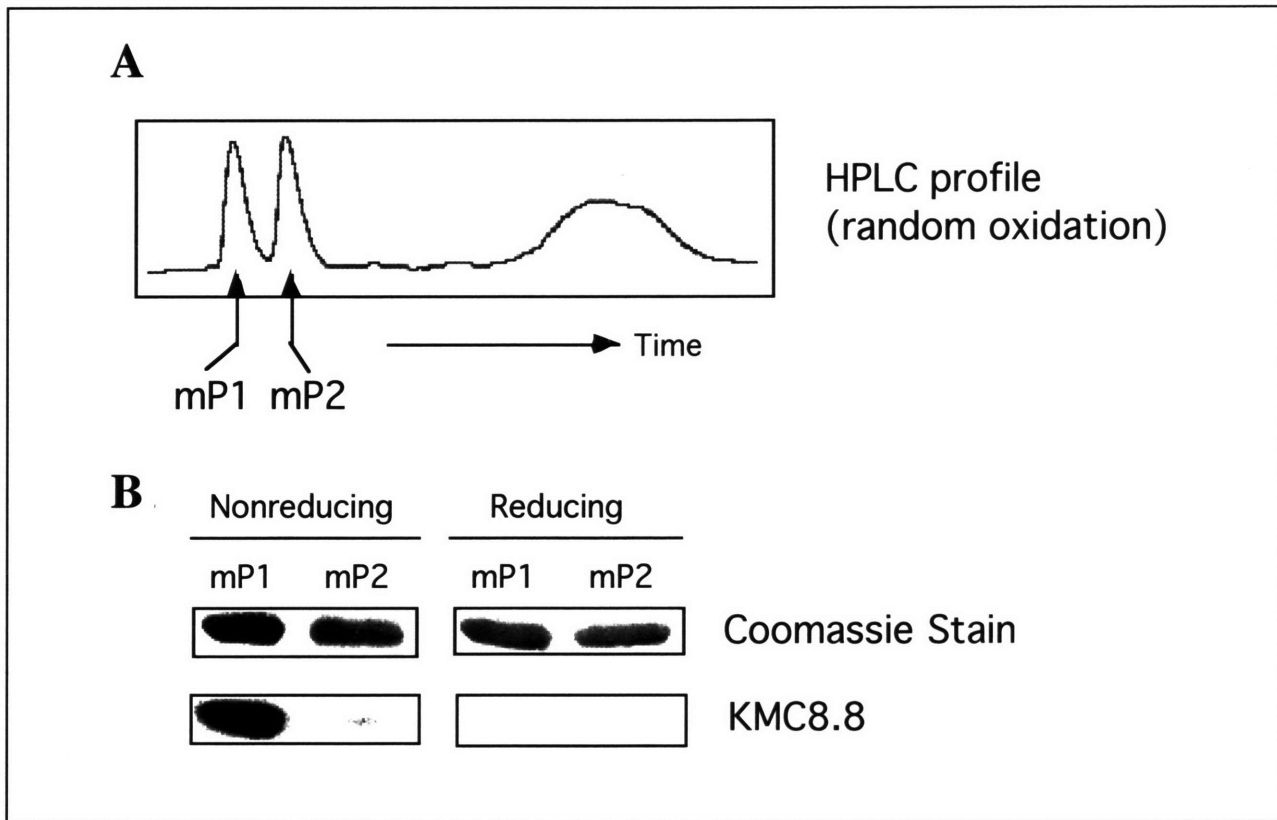


Figure 2.2 HPLC Purification and Analysis of mCD9-LEL. A) HPLC purification profile of Ni-purified mCD9-LEL. Three peaks corresponding to oxidized mCD9-LEL were identified. The first two eluted proteins, designated mP1 and mP2, were analyzed further. B) Peaks were analyzed by Coomassie blue staining and Western blotting. Equal amounts of protein were loaded onto 18% SDS-PAGE under reducing or non-reducing conditions, and blotted onto Hybond-C. Blots were probed with KMC8 and HRP-conjugated anti-rat secondary antibody. KMC8 recognizes only the nonreduced form of mP1.

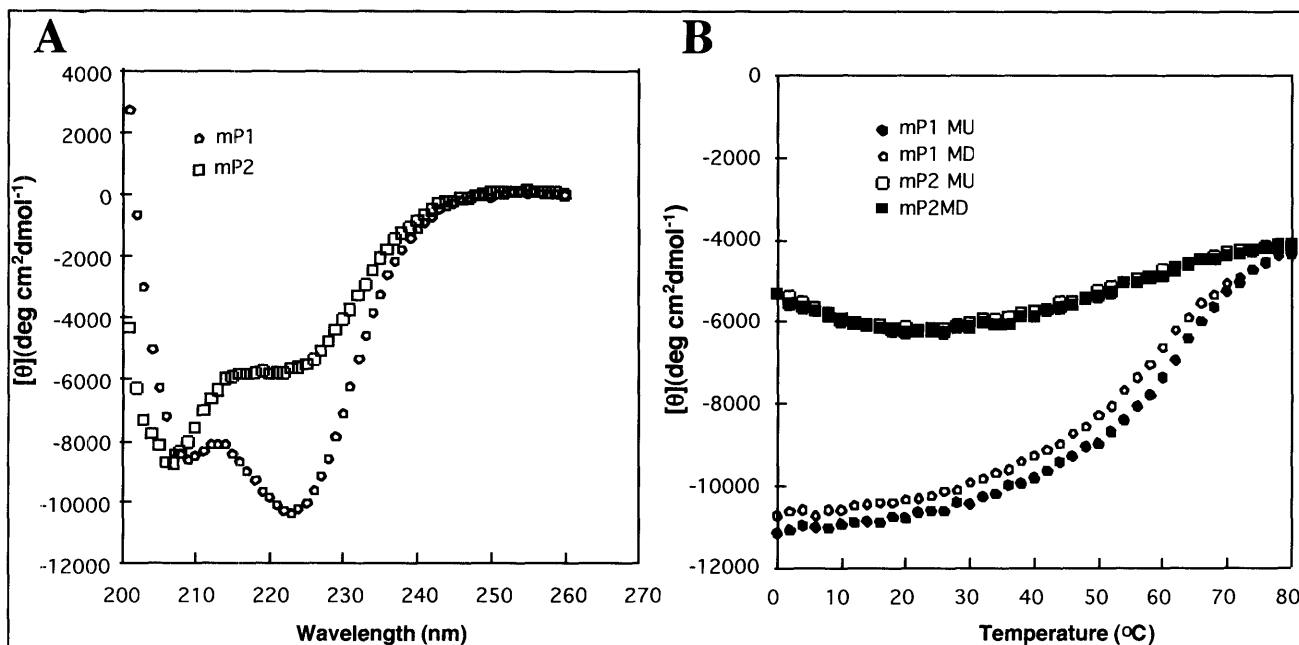


Figure 2.3 Circular Dichroism Characterization of mCD9-LEL Isomers. A) CD spectra of 10 μM mP1 (O) or mP2 (\square) at 25 $^{\circ}\text{C}$ in PBS. The minima at 208 and 222 nm for mP1 indicate that the protein is highly helical. B) Temperature dependence of the CD signal at 222 nm for the mP1 (O) and mP2 (\square) species. Thermal denaturation is indicated by the filled symbols and thermal renaturation is indicated by the open symbols. Protein concentrations were 10 μM in PBS. mP2 has little organized structure, whereas mP1 has a significant α -helical structure that unfolds at high temperature and refolds upon cooling.

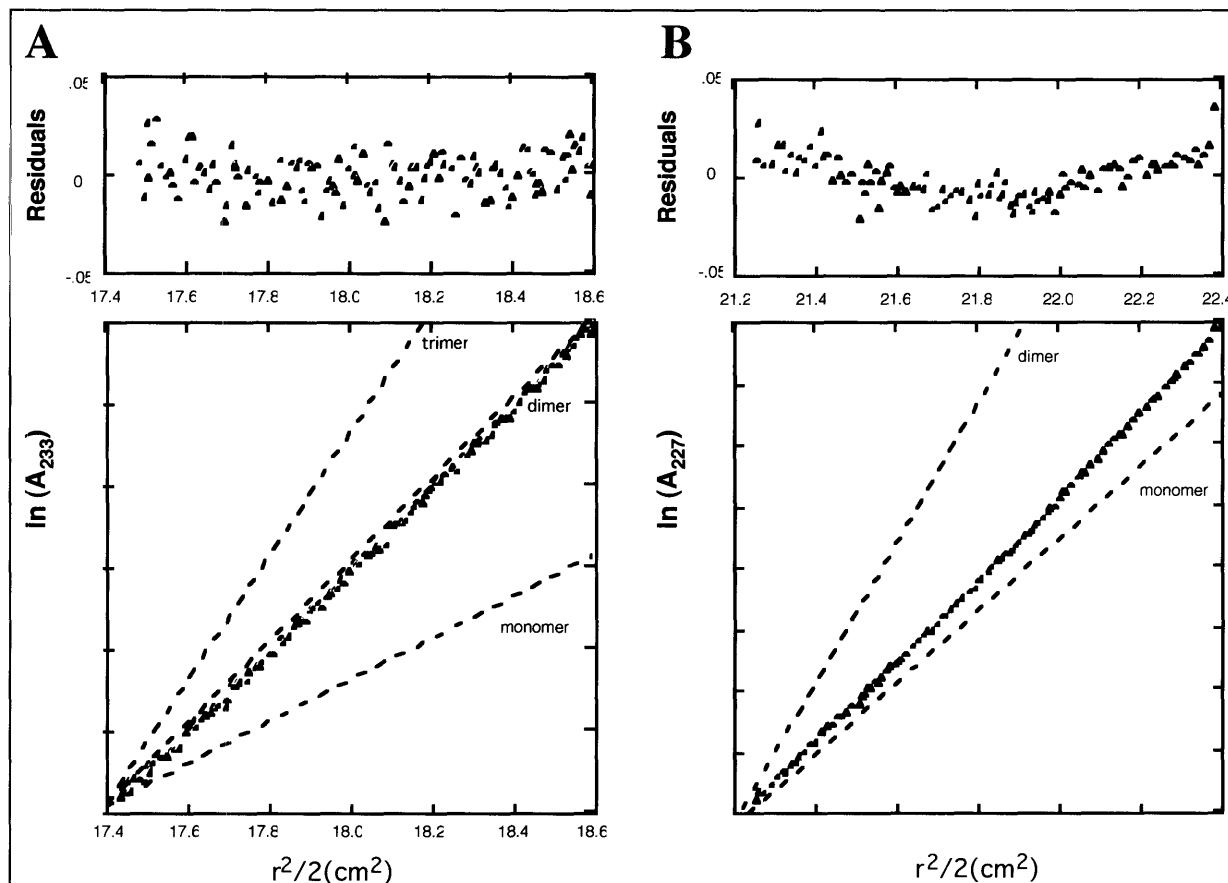


Figure 2.4 Equilibrium Sedimentation of mP1 and mP2 at 25°C in PBS at 20,000 rpm. If the experimental data fit a single species model, a single experimental molecular weight can be derived by comparing the radius²/2 versus log absorbance (ln). Deviation from the predicted oligomeric molecular weight is revealed by the residuals from this line. In an idealized case, residuals off the predicted slope should be random. The deviations in the data from the linear fit are plotted (upper). A) mP1 data closely fit a dimer model with random residuals around the predicted dimeric molecular weight. B) mP2 data reveal an oligomerization state of 1.16 with nonrandom residuals, indicating a predominantly monomeric species with some aggregation. Lines expected for monomeric, dimeric, and trimeric oligomerization states are indicated for comparison.

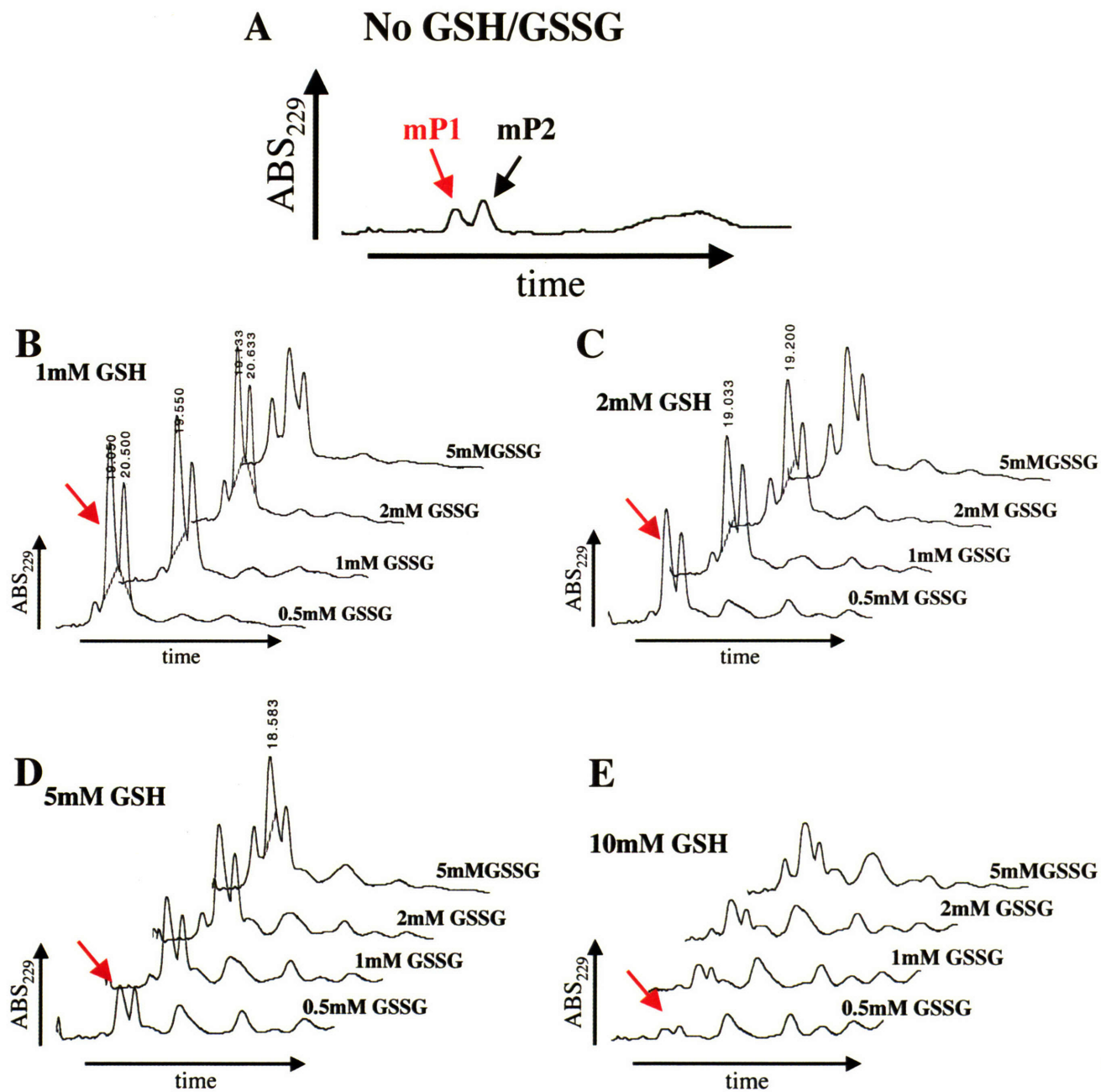


Figure 2.5 Glutathione Reduction/Oxidation Mix Effects on mCD9-LEL Variant Yields. Equivalent quantities of oxidized, reduced mCD9-LEL in denaturing buffer was rapidly diluted into redox conditions. Protein samples were mixed for 5 hours, acidified, and analyzed by reverse-phase HPLC. Protein content, as monitored at 229 nm, was analyzed over time to collect an HPLC profile. Reduced glutathione (GSH) concentrations are indicated in the upper-left corner of each set of HPLC profiles. Oxidized glutathione (GSSG) concentrations are indicated to the right of each individual HPLC trace. Under conditions with no reduced or oxidized glutathione present, mP1 and mP2 are indicated. mP1, which is the α -helical dimeric mCD9-LEL variant is indicated in red. Under conditions with a reduced/oxidized glutathione mix, the mP1 protein peak is indicated with red arrow. As these samples were analyzed in an automated fashion, protein abundance (as assessed by area under the peak) is quantitative and may be directly compared between HPLC traces.

Chapter 3

Structural Studies of the Murine CD9 Large Extracellular Loop

These experiments were conceived by Christopher C. Liu and Peter S. Kim. All experiments were carried out by Christopher C. Liu. We thank Vladimir Malashkevich for technical assistance with protein crystal trials, Peter Carr for technical assistance with both NMR instrumentation and analysis of data, and Steve Johnston for technical assistance with structural homology modeling. All errors are my own.

Introduction:

We have described a methodology by which we can express and purify to homogeneity a single disulfide-bonded species of the murine CD9-LEL. The mCD9-LEL is autonomously folding, α -helical, and dimeric in nature. Our experimental observations of the mCD9-LEL are consistent with a study in which the structure of the human CD81-LEL was solved by x-ray crystallography (Kitadokoro, Bordo et al. 2001).

The hCD81-LEL structure consists of five α -helices (designated A–E) (Figure 3.1). The regions corresponding to helices A, B, and E, which appear to be conserved among all tetraspanin family members, form a dimerization (stalk) subdomain of the tetraspanin-LEL. These helices bracket a hypervariable region or head subdomain (Kitadokoro, Bordo et al. 2001). Among tetraspanins, the head subdomain varies in length and number of disulfide bonds (Boucheix and Rubinstein 2001). The two subdomains are clearly demarcated by a conserved cysteine motif characteristic of tetraspanins. Although the hCD81-LEL head subdomain consists of two α -helices (C and D), the CD9 head subdomain is not predicted to be α -helical (Seigneuret, Delaguillaumie et al. 2001). Our observation that the mCD9-LEL is approximately one-third α -helical roughly matches the predicted secondary structure content of the CD9 dimerization subdomain. Furthermore, sedimentation equilibrium data clearly show that the mCD9-LEL is a dimer at low concentrations in physiological buffer. This suggests that the dimer seen in the hCD81-LEL structure is also observed in solution and that dimer formation of tetraspanin-LELs is conserved and biologically significant.

Often, detailed structural knowledge of a protein gives a deeper understanding of the functional properties of that protein. Although both sequence and solution studies strongly suggest that the CD9-LEL adopts a similar global structure to the hCD81-LEL (Seigneuret, Delaguillaumie et al. 2001), we initiated structural studies to derive atomic level resolution of the CD9-LEL. We chose to pursue three parallel experimental methodologies: x-ray crystallography, nuclear magnetic resonance, and structural homology modeling. As the human and mouse CD9-LEL share 89% sequence similarity, we chose to use the hCD9-LEL sequence for our homology model studies.

A detailed, structural basis for mCD9-LEL function would lay the foundation for probing the molecular nature of the mCD9-LEL protein and may also serve as a template

for both the rational design of inhibitory molecules and of dominant-negative constructs.

Materials and Methods:

Crystal Trials:

The mCD9-LEL protein, devoid of salt and buffer, was prepared by dissolving lyophilized protein in H₂O at 9.5mg/ml. Protein concentration was determined using Edelhoch's reagent and monitored for aromatic absorbance at 280nm. Crystals were screened using the sitting drop method in 48-well plates. One μ l drops of protein solution were mixed with 1- μ l of each crystallization solution from the Hampton Sparse Matrix Screens I and II (Hampton Research). One hundred μ ls of mother liquor was used for vapor diffusion. All crystal trials were set up and incubated in a 20°C humidity-controlled room and crystal chambers were assayed under a dissection microscope after 2, 7, 14, and 28 days. All crystallization trials were undertaken in two independent trials.

Nuclear Magnetic Resonance Analysis

The mCD9-LEL protein, devoid of salt and buffer, was prepared by dissolving lyophilized protein in 50mM deuterated acetic acid/100mM NaCl/10%²H₂O/adjusted to pH 5.5 with NaOH. NMR experiments were performed at 760 μ M protein (~8mg/ml). ¹H NMR experiments were performed by using a Bruker (Billerica, MA) AMX spectrometer operating at 500 MHz and 25°C. Data were processed with Felix 98.0 (Molecular Simulations) on Silicon Graphics computers and all spectra were referenced using 2,2-dimethyl-2-silapentane-5-sulfonic acid (DSS) (Sigma).

After data collection from nuclear magnetic resonance analysis, the mCD9-LEL solution was recovered. Protein sample was diluted into a matching buffer as used for NMR analysis and quantified with Edelhoch's buffer by monitoring absorbance at 280 nm (Edelhoch 1967). The pH of the buffer was checked with a pH buffer strip. Circular dichroism spectra were monitored as in Chapter 2.

Homology Modeling

The hCD81-LEL and hCD9-LEL sequences were aligned with Clustal using the BLOSUM62 matrix (Jung and Lee 2000). The three-dimensional coordinates for the hCD81-LEL structure (1G8Q) were downloaded from the Protein Data Bank (PDB). This structure contains two molecules in the crystallographic asymmetric unit

(Kitadokoro, Bordo et al. 2001). As there are two protein chains (designated Chain A and Chain B) with similar, but non-identical structures, the PDB file was deconvoluted into individual protein chains prior to modeling. Two disulfide-bond constraints were placed on the hCD9-LEL model: between cysteine 41/cysteine 70, and between cysteine 42/cysteine 56 respectively. These disulfide-bond connectivities correspond to the connectivities observed in the hCD81-LEL structure. The hCD9-LEL was modeled separately onto either the hCD81-LEL ChainA or Chain B with MOE-HOMOLOGY (Chemical Computing Group), resulting in two similar, but non-identical models. Secondary structure analysis was conducted with the PHD prediction algorithm through the ProSite (Rost, Sander et al. 1994) web-based portal.

Results:

Protein Crystallization Trials of the mCD9-LEL

To explore the structural basis underlying the α -helical, dimeric nature of the mCD9-LEL molecule, we attempted protein crystal trials (Hendrickson 1991). Large quantities of the α -helical, dimeric mCD9-LEL protein were purified as described in Chapter 2 and no contaminant was detected by SDS-PAGE, reverse-phase chromatography, or mass spectrometry. For expediency we chose to use the sitting drop methodology (which is a variant of standard hanging drop methods) coupled with two commercially available sparse matrix screens (Page and Stevens 2004). In all, one hundred disparate crystallization conditions were tested. All conditions were tested in two replicates, yielding highly similar results. Protein solutions were observed over time and classified into clear (no precipitate), precipitate (appearance of “dust” in the drop chamber), and oil (appearance of a diffracting film at the surface of the protein solution). Although precipitating conditions were observed and catalogued (Figure 3.2), we determined that successful identification of crystallizing conditions would require significant amounts of time and material. Given the limited size of the murine CD9-LEL and the derivation of a workable homology model (see below), this avenue of analysis was not pursued further.

Nuclear Magnetic Resonance Studies of the mCD9-LEL

Concurrent with crystal trials, we began initial structural studies by nuclear magnetic resonance. Due to protein limitations, we used a 8mg/ml protein sample in 10% $^2\text{H}_2\text{O}$ at pH5.5. One-dimensional proton spectra revealed multiple significant peaks, although peak dispersion was far from ideal (Figure 3.3) (Evans 1995). Empirically, it has been observed that approximate global secondary structure may be measured through peak chemical shift changes, without the need for specific proton assignment (Wishart and Sykes 1994). These chemical shift regions have been designated secondary structural signature regions. Qualitatively, we see (i) no evidence for β -strands (4.85-5.9ppm), (ii) significant helical structure (3.4-4.1ppm), and (iii) significant random coil (8.2-9ppm).

Total correlated spectroscopy reveals numerous cross peaks (Figure 3.4). Focusing on the helical fingerprint region did not reveal many well-dispersed amide/alpha cross-peaks (Figure 3.5). To explore possible acid denaturation of the mCD9-LEL protein at pH5.5, we recovered our protein sample and analyzed α -helicity by circular dichroism at lowered pH (Figure 3.6). Our analysis revealed that although there was some loss of α -helicity, the protein still appeared to be significantly helical.

Homology Model Construction of the hCD9-LEL

There is significant sequence similarity among tetraspanin family members (Seigneuret, Delaguillaumie et al. 2001). For structural homology modeling, we chose to model the human CD9-LEL sequence onto the only existing tetraspanin structure: human CD81-LEL (Figure 3.1B). There are two amino-acid chains in the hCD81-LEL crystallographic asymmetric unit. For simplicity, we deconvoluted the crystal structure coordinates and modeled the hCD9-LEL molecule onto either hCD81A or hCD81B, resulting in two models, designated hCD9ModA and hCD9ModB respectively (Figure 3.7B)

A basic homology program, MOE, was able to derive an averaged hCD9-LEL model with no steric clashes. This program derived a model of the hCD9-LEL that is composed of five α -helices, similar to the published hCD81-LEL structure (Kitadokoro, Bordo et al. 2001)(Figure 3.7). However, secondary-structure prediction of the hCD9-LEL using the program PHD predicted the region modeled as helix C to be in an extended (non-helical) conformation (Figure 3.1A). Furthermore, the hCD9-LELModA and ModB minimized solvent exposure of the dimerization interface, resulting in a more compact intermolecular surface than in the hCD81-LEL interface (Figure 3.8). Although our model gives us a basis upon which to begin molecular dissection of the mCD9-LEL dimer, it clearly is not completely accurate. In summary, we believe that the tertiary structure and the majority of the secondary structural elements of our hCD9-LEL model are accurate. However, we have low confidence in the side-chain rotamers of our model. Complete coordinates of the hCD9-LEL protein modeled to both Chain A and Chain B are included in the appendix.

Discussion

In this chapter, we present three avenues of experimentation to derive detailed structural analysis of the murine CD9-LEL protein. As the mCD9-LEL protein may be readily purified in large quantities, attempts at x-ray crystallographic and nuclear magnetic resonance structural determination were initiated.

With the advent of multiwavelength anomalous diffraction techniques (Hendrickson 1991), solving a protein crystal structure has become much less labor-intensive than in previous years. However, the ability to derive well-ordered protein crystals is still a major limiting factor (Page and Stevens 2004). It is nearly impossible to determine crystallization buffer conditions intuitively. We initiated crystallization trials with the mCD9-LEL protein with this significant caveat in mind. As a result, we restricted our crystallization trial conditions to commercially available sparse matrix kits. Our ability to identify precipitating, but not crystallization conditions of the mCD9-LEL protein on a first-pass basis is not surprising. Subsequent to these crystal trials, Francoise Martin and Peter Monk (University of Sheffield) have repeated our experiments with no success. Martin and Monk are currently testing crystallization conditions for the humanCD63-LEL protein (see Chapter 6) in collaboration with us.

There are many reasons why our crystal trials may have failed. Given the small size of the mCD9-LEL protein, it is possible, that the C-terminal hexahistidine tag precluded the formation of well-ordered interchain contacts. The Bolognesi group's hCD81-LEL protein also contained an uncleaved C-terminal hexahistidine tag (Kitadokoro, Galli et al. 2001). Although their crystal trials were successful, it is difficult to extrapolate between proteins, however phylogenetically similar they are (Boucheix and Rubinstein 2001). We do note that of various tetraspanin-LEL proteins we have studied, the hCD81-LEL is the most easily purified of the family (Chapter 6).

Our nuclear magnetic resonance experiments qualitatively confirmed our circular dichroism data (Wishart, Sykes et al. 1991). However, the mCD9-LEL protein appeared to contain significant unstructured regions. Circular dichroism analysis at lowered pH did not reveal significant unfolding. Another possible reason for non-resolved cross-peaks could be due to low protein concentration. To circumvent these problems, we considered large-scale expression and purification of the mCD9-LEL protein with ^{13}C or

¹⁵N isotope metabolic labeling. However, given the relative success of our structural homology modeling, we decided not to pursue detailed structural analysis further.

CD9 is the most homologous tetraspanin to CD81, especially in respect to their sequences in the large extracellular loops (for phylogeny, see Chapter 1). Between the human CD9-LEL and human CD81-LEL, there is 18% identity and an additional 16% homology for an overall sequence similarity of 34%. In actuality, this underrepresents the similarities between the CD9-LEL and CD81-LEL as the putative dimerization subdomains have increased similarity. On the other hand, a hypervariable region in the LEL structure demarcated by a strictly conserved cysteine amino-acid residue pattern has very low sequence similarity.

By definition, our structural homology modeling resulted in a hCD9-LEL structure that was very similar to the hCD81-LEL structure. Given the sequence similarity between helix A, helix B, and helix E of the hCD81-LEL and the complementary sequence regions of hCD9-LEL (Figure 3.1A), we have confidence in our homology model of the dimerization subdomain of the hCD9-LEL. We believe that our model of this region roughly represents the buried, hydrophobic dimerization interface conserved among many tetraspanins. However, our efficient strategy of modeling the hCD9-LEL onto individual hCD81-LEL chains, whose hydrophobic dimerization interface is normally capped, while minimizing the hydrophobic effect is clearly flawed. As a result, direct molecular dissection of this interface is necessary (see Chapter 4).

More seriously, forcing the putative head domain of the hCD9-LEL protein to fit secondary structural elements of the hCD81-LEL is grossly flawed. Although we surmise that the unique disulfide bonding pattern is conserved among tetraspanins-LELs, (and thus severely restricts the global conformation of the head subdomain), we have low confidence in the ability of our homology model to predict surface exposed amino acid residues. Again, further molecular biological analysis of the head domain is necessary.

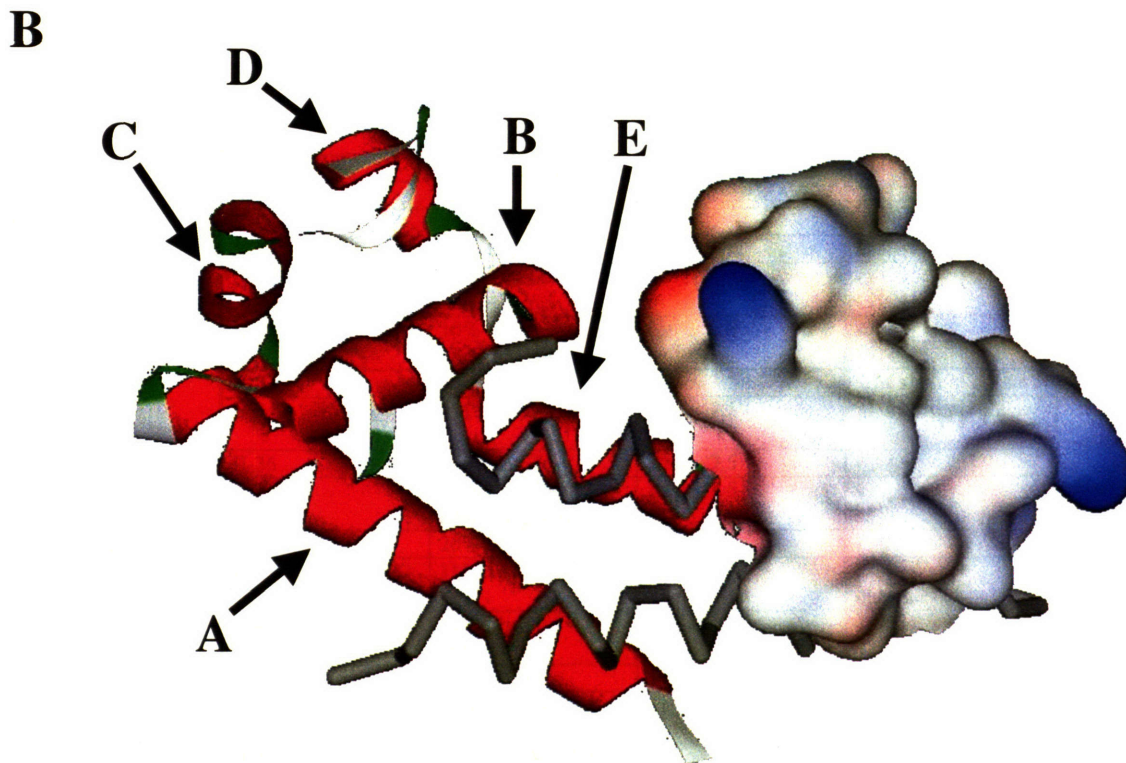


Figure 3.1 Sequence Alignment of hCD9-LEL and hCD81-LEL. A) Schematic diagrams of the primary sequence for the hCD9-LEL and hCD81-LEL are shown. These sequences were aligned in Clustal and gaps in the alignment are denoted with a hyphen. Human CD9-LEL putative disulfide-bond connectivities are indicated with lines. Human CD81-LEL disulfide-bond connectivities are as indicated in the structure shown in B. Human CD9 predictions of α -helices by the red boxes above the sequence. Observed human CD81-LEL α -helices are represented in red. Amino acid residues in the hCD81-LEL Chain B for which an electrostatic surface potential was generated (as shown in B) are indicated in a gray box. B) The hCD81-LEL Chain A is depicted in flat ribbon, with α -helices indicated in red. Helix A, B, C, D, and E are indicated by arrows on Chain A. Chain B is depicted in C α stick mode and an electrostatic surface potential was generated around the amino-acid residues indicated in A. Figure prepared using DS ViewerPro.

Precipitating conditions:			
Hampton ID #	Precipitant	Buffer	Salt
I-4	2M AS	Tris 8.5	-
I-6	30% Peg 4K	Tris 8.5	.2M Magnesium chloride
I-13	30% Peg 400	Tris 8.5	.2M trisodium citrate
I-14	28% Peg 400	Hepes 7.5	.2M CaCl2
I-16	1.5M LiSO4	Hepes 7.5	-
I-17	30% PEG 4K	Tris 8.5	.2M lithium sulfate
I-22	30% Peg 4K	Tris 8.5	.2M sodium acetate
I-23	30% PEG 400	Hepes 7.5	.2M magnesium chloride
I-33	4M sodium formate	-	-
I-38	1.4M trisodium citrate	Hepes 7.5	-
I-39	2%Peg 400/2M AS	Hepes 7.5	-
I-41	10%IP/20%PEG 4K	Hepes 7.5	-
I-45	18% PEG 8K	NaCacodylate 6.5	.2M zinc acetate
I-47	2M AS	Na Acetate 4.6	-
II-1	10% PEG 6K	-	2M NaCl
II-14	2M AS	.1M Nacitrate 5.6	.2M KnaTartarate
II-25	1.8M AS	Mes 6.5	.01M CoCl
II-27	25% PegMME550	Mes 6.5	ZnSo4
II-28	1.6M tri-sodium citrate pH6.5	-	-
II-30	10% PEG 6K/5%MPD	Hepes 7.5	-
II-32	1.6M AS	Hepes 7.5	.1M sodium citrate
II-34	1M sodium acetate	Hepes 7.5	.05M cadmium sulfate
II-36	4.3M NaCl	Hepes 7.5	-
II-37	10% PEG 8K/8% ethylene glycol	Hepes 7.5	-
II-38	20% Peg 10K	Hepes 7.5	-
II-41	1M lithium sulfate	Tris 8.5	.01M nickel chloride
II-42	12% glycerol anhydrous	Tris 8.5	1.5M AS
II-44	20% EtOH	Tris 8.5	-
II-45	20% PEG MME 2000	Tris 8.5	.01M Nickel chloride
II-46	30% PEGMME 550	Bicine 9.0	.1M NaCl

Figure 3.2 Precipitant Conditions for hCD9-LEL: Protein crystal trials were attempted using a 10mg/ml solution of the mCD9-LEL using the sitting drop method. Tabulated are conditions by which the hCD9-LEL precipitated in an unordered fashion. No conditions were found with protein crystals. Hampton Buffer ID#s are listed with roman numeral I corresponding to the Hampton Sparse Matrix Screen I. Components of the precipitating buffers, listed as precipitant, buffer, and salt components are as indicated.

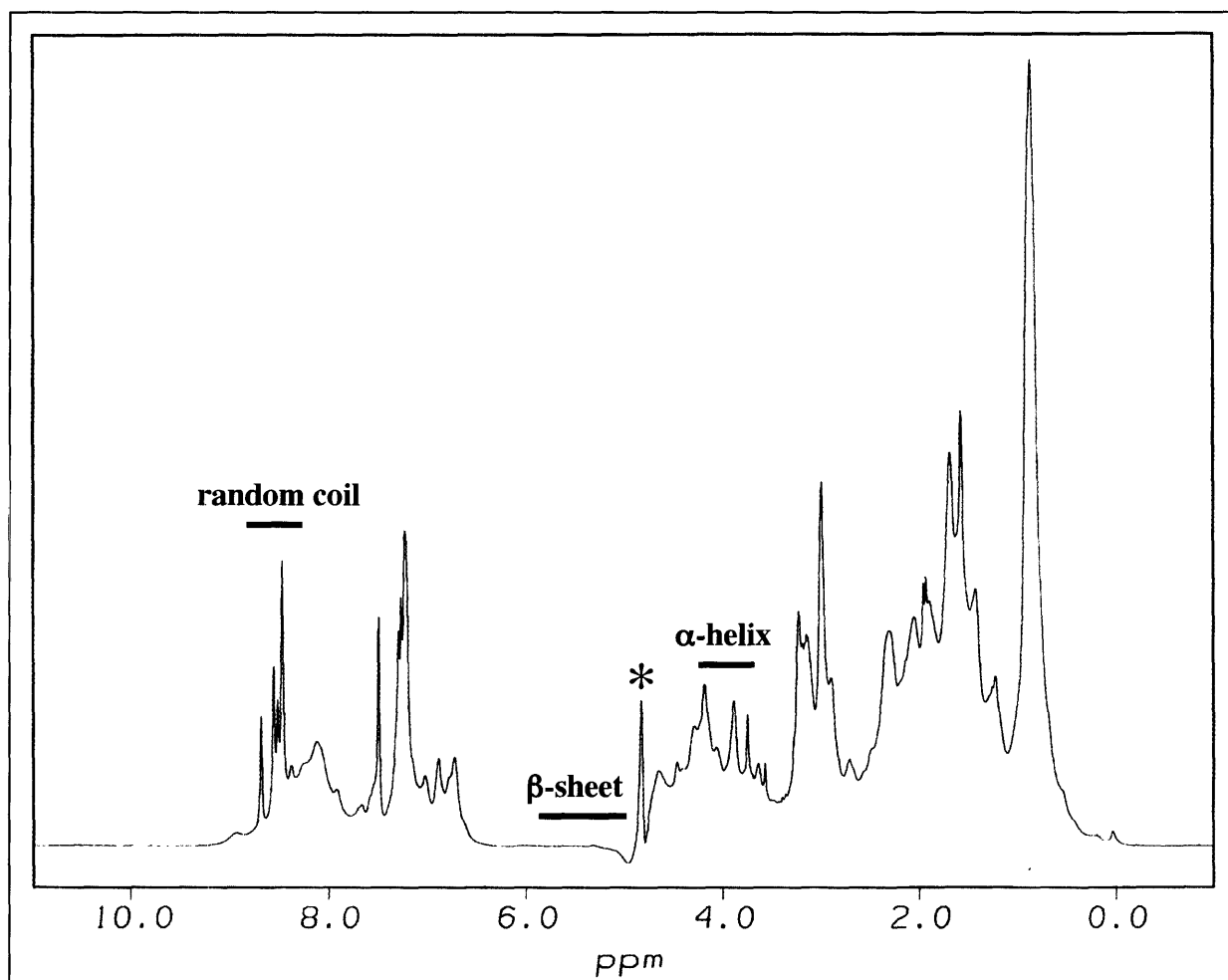


Figure 3.3 One-Dimensional ^1H Nuclear Magnetic Resonance Spectrum of the mCD9-LEL: Lyophilized mCD9-LEL was dissolved in 50mM deuterated acetic acid/100mM NaCl/10% $^2\text{H}_2\text{O}$ adjusted to pH 5.5. One-dimensional nuclear magnetic resonance was collected at 500MHz at 25°C. Fingerprint regions of peak chemical shifts due to secondary structure are indicated above the spectrum by bars. These are α -helix (3.4-4.1ppm), β -sheet (4.85-5.9ppm), and random coil (8.2-9ppm). The $^2\text{H}_2\text{O}$ peak is indicated with an asterisk.

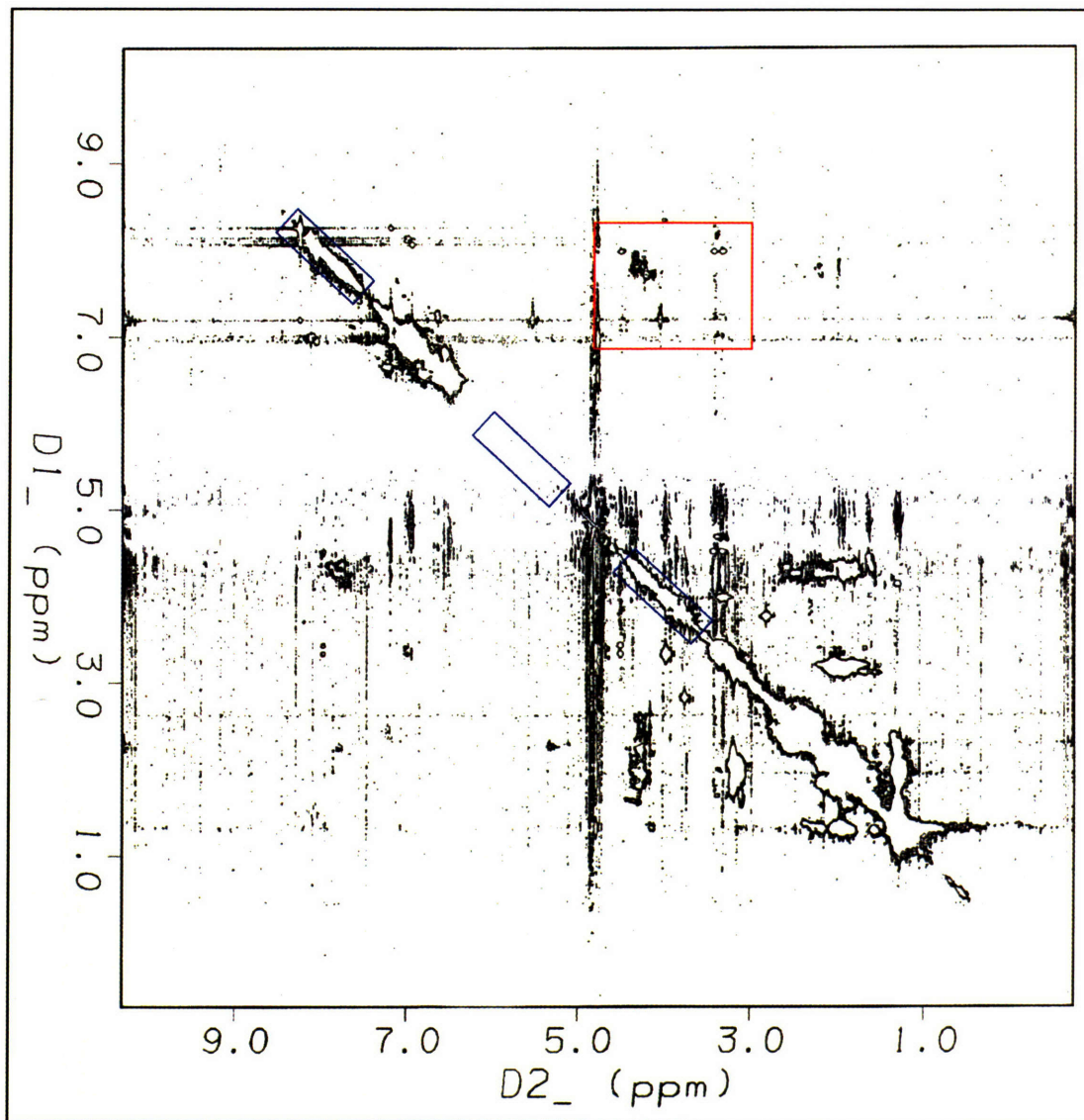


Figure 3.4 Two-Dimensional ^1H Nuclear Magnetic Resonance Spectra of the mCD9-LEL: Two-dimensional NMR spectra were collected with the first dimension plotted on the Y-axis and the second dimension plotted on the X-axis. Fingerprint regions of secondary structure corresponding to random coil (8.2-9ppm), β -sheet (4.85-5.9ppm), α -helix (3.4-4.1ppm), in order, are boxed in blue on the diagonal. The expected region for α -helical amide/ α cross-peaks is indicated with a red box.

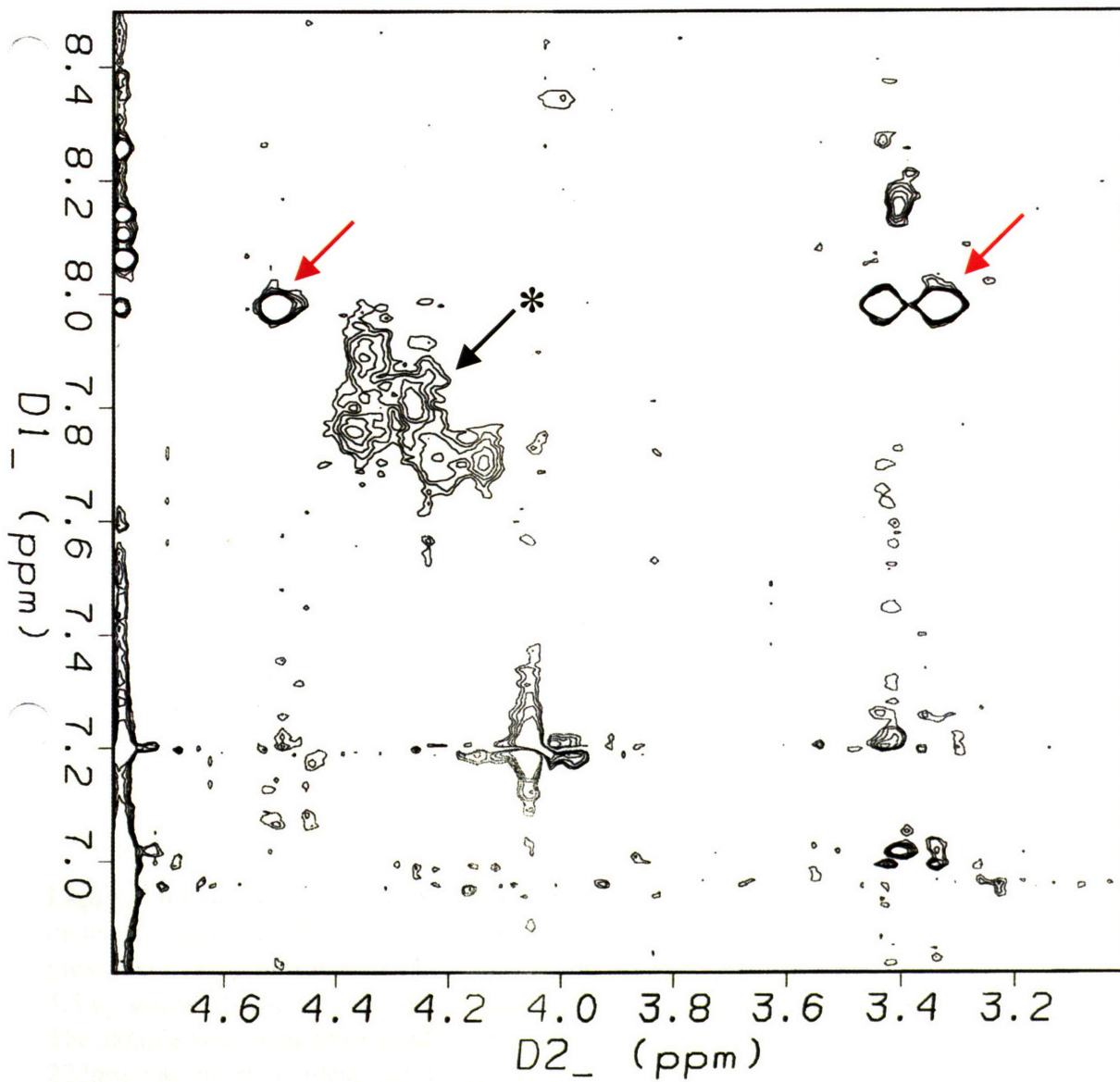


Figure 3.5 Helical Cross Peak Region of the mCD9-LEL NMR spectra: Amide/alpha cross peaks in the fingerprint α -helical region are shown. Well-dispersed stable cross-peaks are indicated with arrows. A poorly-resolved patch of cross-peaks is indicated with an asterisk.

Circular Dichroism Wavelength Scan of mCD9-LELat pH 5.5

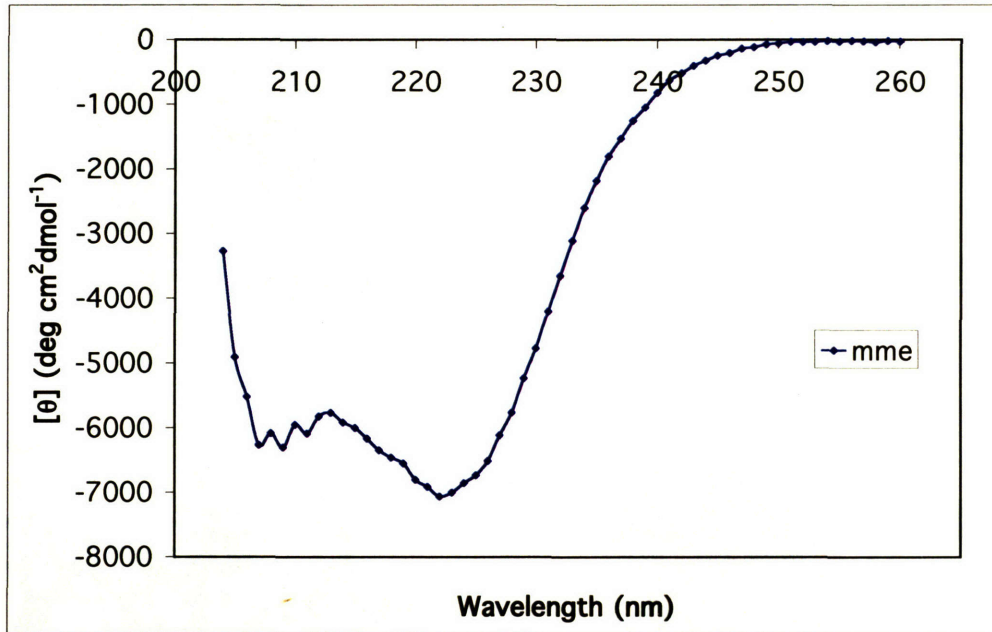


Figure 3.6 Circular Dichroism Spectrum of mCD9-LEL at pH 5.5: The circular dichroism spectrum of the murine CD9-LEL protein was analyzed as described previously. Protein was tested in 50mM acetic acid/100mM NaCl with the pH adjusted to 5.5 by sodium hydroxide (conditions used for nuclear magnetic resonance experiments). The sample was blanked to a buffer reference lacking protein. A spectral minimum at 222nm was clearly evident and the spectrum was not collected to 200nm as a high dynavoltage at low wavelengths was observed.

Figure 3.6 shows the circular dichroism spectrum of mCD9-LEL at pH 5.5. The y-axis represents the molar ellipticity [θ] in deg cm²-dmol⁻¹, ranging from 0 to -8000. The x-axis represents the wavelength in nm, ranging from 200 to 260. The spectrum shows a characteristic minimum at approximately 222 nm, indicating a high degree of alpha-helical content. The curve is labeled 'mme' in the legend. The data points are connected by a smooth line, showing a clear negative peak at 222 nm and a positive peak at approximately 240 nm. The spectrum was not collected to 200 nm due to a high dynavoltage at low wavelengths.

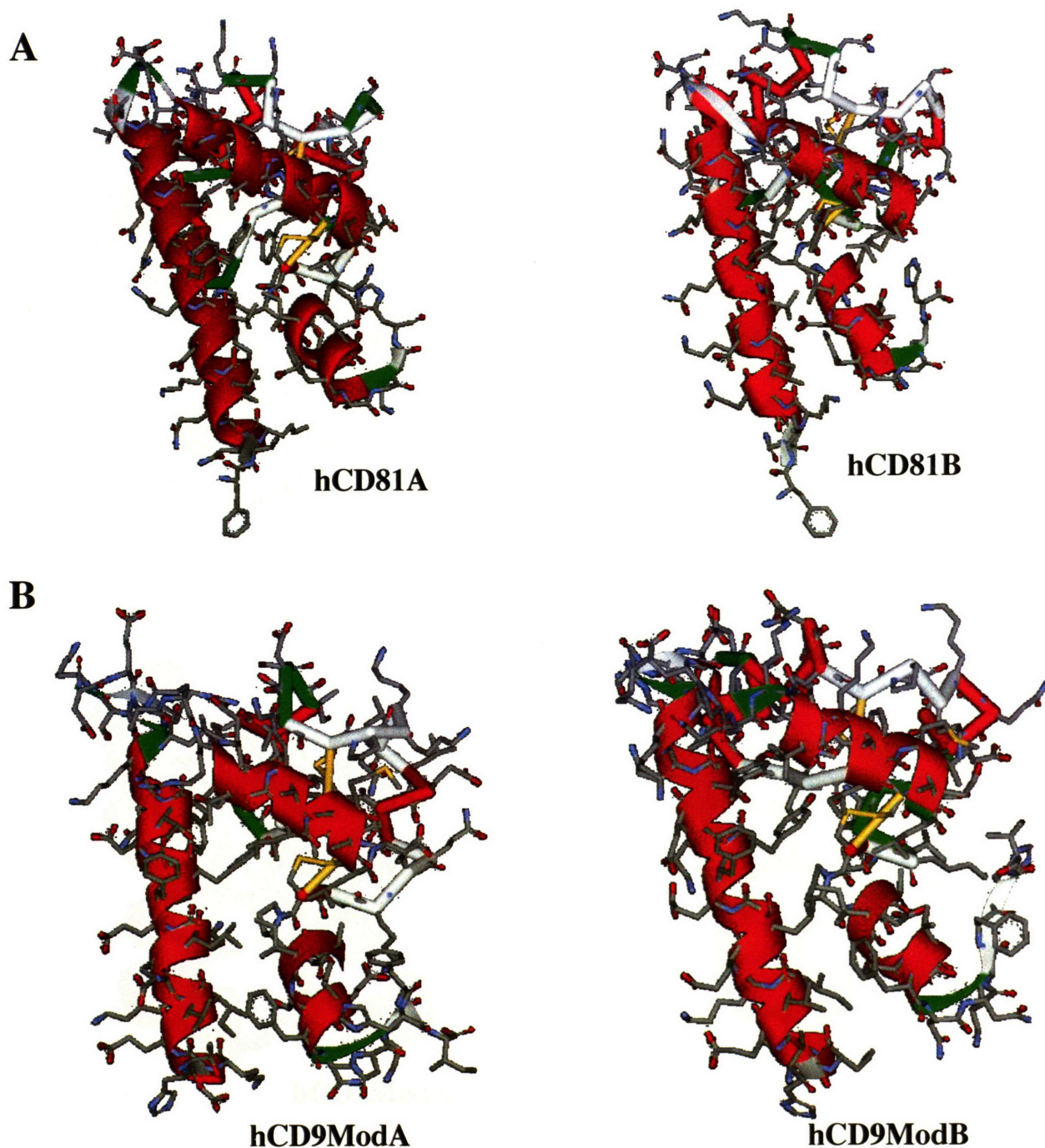


Figure 3.7 Secondary Structures of the hCD81-LEL Chain A and B and hCD9-LEL ModA and ModB: All subunits are depicted with the N- and C-terminal residues pointing to the bottom of the page. Helices A, B, and E are depicted in a flat ribbon and the remainder of the molecule is depicted in C α stick. A) Individual hCD81-LEL peptide chains extracted from the hCD81-LEL crystal structure. Helix C and Helix D are to the rear. In the structure of the dimer, a subunit would bind to the front of the indicated molecule (Helix A, B, and C). B) The structure of hCD9-LEL homology modeled onto the hCD81-LEL Chain A is shown to the left. The structure of hCD9-LEL homology modeled onto the hCD81-LEL Chain B is depicted to the right. Figure prepared using DS ViewerPro

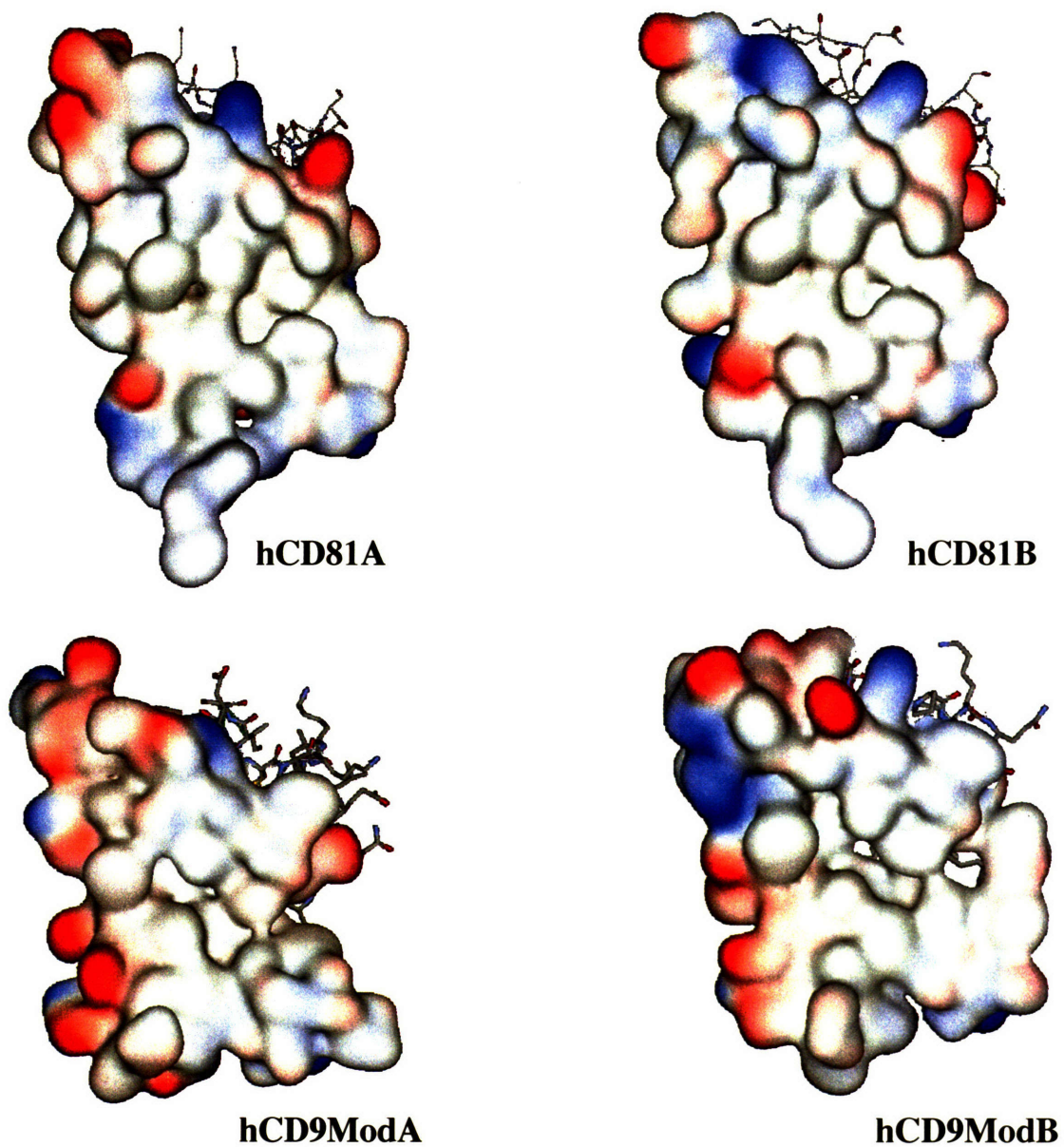


Figure 3.8 The Dimer Surface Properties of hCD81-LEL and hCD9-LEL: All protein geometries are identical to those presented in Figure 3.7. An electrostatic surface potential was generated around all residues N-terminal and C-terminal to the head domain (non-italicized amino acid residues in Figure 3.1).

Chapter 4

Molecular Biological Studies of the Murine CD9 Large Extracellular Loop

These experiments were conceived by Christopher C. Liu, Richard O. Hynes and Peter S. Kim. All experiments were carried out by Christopher C. Liu. All errors are my own.

Introduction:

The hCD81-LEL structure is a novel protein fold, with no sequence or structural homology to other known domains (Kitadokoro, Bordo et al. 2001). Our biophysical analysis of the murine CD9-LEL protein, hCD81-LEL's closest related gene, suggests that the novel dimeric fold elucidated in the hCD81-LEL structure exists in solution at biological concentrations. However, we were not able to empirically obtain detailed structural knowledge of the mCD9-LEL. Based upon our theoretical homology model, we designed a series of experiments to probe the molecular basis of the mCD9-LEL's α -helical, dimeric properties.

To probe the molecular nature of mCD9-LEL oligomerization, we replaced conserved, hydrophobic residues hypothesized to contribute to LEL-dimerization with charged mutations. As the mCD9-LEL is proposed to exist as an anti-parallel dimer, introduction of a single charged mutation presents two charged mutations into the dimer interface, one on each subunit. In addition, these designed mutations also served to promote α -helicity (Popot and Engelman 2000), which we have shown is a hallmark of the native-fold of the mCD9-LEL. This series of experiments serves both to define the contribution of the dimerization interface to the folding stability of the mCD9-LEL dimer and to test the robustness of our homology model in designing a soluble, well-folded monomeric version of the mCD9-LEL.

Concurrently, we wished to identify critical amino-acid residues for sperm-egg fusion in the mCD9-LEL protein. Toward these ends, we epitope-mapped a function-inhibiting α -CD9 antibody, clone KMC8 (Miller, Georges-Labouesse et al. 2000). The identification of key residues will also serve to: (i) illustrate our rapid recombinant protein expression and purification system in screening tetraspanin-LEL variants (ii) derive α -helical dimeric variants of the mCD9-LEL to act as negative controls in cellular inhibition assays (see Chapter 7); (iii) explore the mechanism of inhibitory antibody function.

In this chapter, we describe extensive mutagenesis over both the dimerization subdomain and the head subdomain of the mCD9-LEL protein. We also produce and purify Fab fragments of the KMC8 antibody and demonstrate that it binds the mCD9-LEL protein in a 2:2 macromolecular complex. These results are consistent with our

previous biophysical characterization of the mCD9-LEL and lend insight to both the mechanism of antibody-induced and tetraspanin-mediated cellular phenotypes.

Materials and Methods:

Monomeric mCD9-LEL trials

Multiple point mutations in the mCD9-LEL sequence were constructed with the Quik-Change Site-Directed Mutagenesis Kit (Stratagene) and confirmed by DNA sequencing. By sequence alignment, we utilized the following oligos, designated CL89 through CL100 to introduce mutations into the mCD9-LEL construct.

CL89, which mutated V115R was

5'-CGCTAGCTAGCACCCACAAGGATGAGCGCATTAAAGAACTGC-3'.

CL90, which mutated V115D, was

5'-CGCTAGCTAGCACCCACAAGGATGAGGAGATTAAAGAACTGC-3'.

CL91, which mutated L119R, was

5'-CGCTAGCTAGCACCCACAAGGATGAGGTGATTAAAGAACGCCAGGAG-3'.

CL92, which mutated L119D, was

5'-CGCTAGCTAGCACCCACAAGGATGAGGTGATTAAAGAAGAGCAGGAG-3'.

CL93, which mutated V115R/L119R, was

5'-CGCTAGCTAGCACCCACAAGGATGAGCGCATTAAAGAACGCCAGGAG-3'.

CL94, which mutated V115D/L119D, was

5'-CGCTAGCTAGCACCCACAAGGATGAGGAGATTAAAGAAGAGCAGGAG-3'.

CL95, which mutated V186R, was

5'-CCGCTCGAGGATGTGGAACCTTGTGTTGAAGCGCTCACTGATGG-3'.

CL96, which mutated V186D, was

5'-CCGCTCGAGGATGTGGAACCTTGTGTTGAACCTCCTCACTGATGG-3'.

CL97, which mutated F187R, was

5'-CCGCTCGAGGATGTGGAACCTTGTGTTTCGCGACCTCACTGATGG-3'.

CL98, which mutated F187D, was

5'-CCGCTCGAGGATGTGGAACCTTGTGTTCTCGACCTCACTGATGG-3'.

CL99, which mutated V186R/F187R, was

5'-CCGCTCGAGGATGTGGAACCTTGTGTTGCGGCGCTCACTGATGG-3'.

CL100, which mutated V186D/F187D, was

5'-CCGCTCGAGGATGTGGAACCTTGTGTTCTCCTCCTCACTGATGG-3'.

CL89 through CL94 were used individually with CL35 (Chapter 2) to mutagenize the mCD9-LEL construct. CL95 through CL100 were used individually with CL34 (Chapter 2) to mutagenesis the mCD9-LEL construct. Mutants were transformed into *E. coli* BL21/pLysS, induced with isopropyl-beta-D-thiogalactopyranoside, and insoluble fractions were purified over Ni-NTA agarose under denaturing conditions. SDS-PAGE followed by silver staining was used to assess protein expression and purity. Selected mCD9-LEL variants were further purified over reverse-phase HPLC. Biophysical analysis was conducted as described in Chapter 2.

Alanine-scanning Mutagenesis and Epitope-Mapping of the mCD9-LEL protein

Multiple point mutations in the recmCD9-LEL sequence were constructed by recombinant PCR (Higuchi 1990) and confirmed by DNA sequencing. These series of oligos, which were used in pairs in conjunction with CL34 and CL35, mutated each amino-acid residue to an alanine as follows:

To mutate L157,

CL103: 5'-GGCATAGCTGGTCCTGCCGAGCAGTTTATCTCGG-3'

CL104: 5'-CCGAGATAAACTGCTCGGCAGGACCAGCTATGCC-3'

To mutate E158A,

CL131: 5'-CATAGCTGGTCCTTTGGCGCAGTTTATCTCGGACACC-3'

CL132: 5'-GGTGTCCGAGATAAACTGCGCAAAGGACCAGCTATG-3'

To mutate Q159A,

CL133: 5'-CATAGCTGGTCCTTTGGAGGCGTTTATCTCGGACACC-3'

CL134: 5'-GGTGTCCGAGATAAACGCCTCAAAGGACCAGCTATG-3'

To mutate F160A,

CL105: 5'-CTGGTCCTTTGGAGCAGGCGATCTCGGACACCTGCCCCAAG-3'

CL106: 5'-CTTGGGGCAGGTGTCCGAGATCGCCTGCTCAAAGGACCAG-3'

To mutate I161A,

CL135: 5'-GGTCCTTTGGAGCAGTTTGCCTCGGACACCTGCCCCAAG-3'

CL136: 5'-CTTGGGGCAGGTGTCCGAGGCAAAGTCTCAAAGGACC-3'

To mutate S162A,

CL137: 5'-GGTCCTTTGGAGCAGTTTATCGCGGACACCTGCCCCAAG-3'

CL138: 5'-CTTGGGGCAGGTGTCCGCGATAAACTGCTCCAAAGGACC-3'

To mutate D163A,

CL139: 5'-GGAGCAGTTTATCTCGGCCACCTGCCCCAAGAAACAGC-3'

CL140: 5'-GCTGTTTCTTGGGGCAGGTGGCCGAGATAAACTGCTCC-3'

To mutate L170A,

CL107: 5'-CACCTGCCCCAAGAAACAGGCGTTGGAAAGTTTCCAGG-3'

CL108: 5'-CCTGGAAACTTTCCAACGCCTGTTTCTTGGGGCAGGTG-3'

To mutate L171A,

CL109: 5'-CCTGCCCCAAGAAACAGCTTGCGGAAAGTTTCCAGGTTAAGCCC-3'

CL110: 5'-GGGCTTAACCTGGAAACTTTCCGCAAGCTGTTTCTTGGGGCAGG-3'

To mutate E172A,

CL141: 5'-GCCCCAAGAAACAGCTTTTGGCAAGTTTCCAGGTTAAGCCC-3'

CL142: 5'-GGGCTTAACCTGGAAACTTGCCAAAAGCTGTTTCTTGGGGC-3'

To mutate S173A,

CL143: 5'-GCCCCAAGAAACAGCTTTTGGAAAGCTTTCCAGGTTAAGCCC-3'

CL144: 5'-GGGCTTAACCTGGAAAGCTTCCAAAAGCTGTTTCTTGGGGC-3'

To mutate F174A,

CL111: 5'-GAAACAGCTTTTGGAAAGTGCGCAGGTTAAGCCCTGCCC-3'

CL112: 5'-GGGCAGGGCTTAACCTGCGCACTTTCCAAAAGCTGTTTC-3'

To mutate Q175A,

CL113: 5'-CAGCTTTTGGAAAGTTTCGCGGTTAAGCCCTGCCCTGAAGCC-3'

CL114: 5'-GGCTTCAGGGCAGGGCTTAACCGCGAAACTTTCCAAAAGCTG-3'

To mutate V176A,

CL145: 5'-CTTTTGGAAAGTTTCCAGGCTAAGCCCTGCCCTGAAGCC-3'

CL144: 5'-GGCTTCAGGGCAGGGCTTAGCCTGGAAACTTTCCAAAAG-3'

Mutants were transformed into *E. coli* BL21/pLysS, induced with isopropyl-beta-D-thiogalactopyranoside, and whole-cell lysates were crudely analyzed by Western blot for reactivity to the antibody KMC8. Point mutants that were not recognized by the antibody

KMC8 were chosen for further purification over metal-ion chromatography and reverse-phase HPLC. Circular dichroism and sedimentation equilibrium analyses of mCD9-LEL variants were carried out as described in Chapter 2. HPLC-purified mCD9-LEL variants were reassessed for KMC8 reactivity.

KMC8 Fab generation:

Milligram quantities of purified, unconjugated KMC8 antibody (BD Pharmingen, San Diego, CA) were purchased. 2X crystallized papain (Sigma, St. Louis, MO) was activated in 1 mg/ml cysteine-HCl (Pierce)/10 mM EDTA (pH 8.0) at a concentration of 1 mg/ml for 1 hour prior to use. Antibody of the rat α -murine CD9 antibody, KMC8, was digested with papain (2% w/w) for 3 hours at 37°C in a circulating water bath (Rousseaux, Rousseaux-Prevost et al. 1986). Digestion was stopped with the addition of 15 μ M iodoacetamide (Sigma). Proteolytic digestion of KMC8 into Fab and Fc fragments was tracked by nonreducing and reducing SDS-PAGE analysis. Fab fragments were purified away from full-length IgG by gel filtration over a Superdex 200 10/30 column (Amersham Pharmacia) in PBS at a flow rate of 0.4 ml/min using an ÄKTA/FPLC (Amersham Pharmacia). Purified KMC8 Fab fragments were concentrated using a Microcon-10 (Millipore) and final protein concentrations were determined using a Micro BCA Protein Assay Kit (Pierce). Purity was assayed by SDS-PAGE and Coomassie staining.

Gel filtration Studies of KMC8Fab and mCD9-LEL interactions:

Gel filtration standards in PBS (Bio-Rad) were loaded onto a Superdex 200 10/30 column (Amersham Pharmacia) using an ÄKTA/FPLC (Amersham Pharmacia) to optimize chromatographic conditions. KMC8 Fab fragments and individual mCD9-LEL variants were analyzed for their respective apparent molecular weights at a constant flow rate of 0.4ml/min. Eluted fractions were collected every 0.5 mls. For binding studies, KMC8 Fab fragments were mixed with either mCD9-LEL_{wt} or mCD9-LEL•Q159A at a 1:1 molar ratio for 30 minutes at room temperature. Samples were spun at 14,000 rpm and decanted. There was no visible precipitate. KMC8 Fab/mCD9-LEL binding was analyzed using gel filtration with UV absorbance monitored at 280nm. Collected fractions were

also analyzed by SDS-PAGE and subsequent Coomassie staining. mCD9-LEL levels were detected by Western blotting with a biotinylated KMC8 antibody (BD Pharmingen) followed by the Vectastain ABC Kit (Vector Labs, Burlingame, CA). The membrane was developed using the ECL system and exposed to film.

Results:

The Folding Stability of the mCD9-LEL Dimer

The analysis of multiple tetraspanin sequences strongly suggested the existence of a conserved subdomain in all tetraspanin-LELs that mediates dimerization (for full discussion, see Chapter Introduction). As our homology modeling suggested that this conserved dimerization subdomain was hydrophobic in nature, we hypothesized that it might be possible to construct a well-folded, α -helical monomer by replacing conserved hydrophobic residues with basic amino acids that had a propensity to maintain an α -helical secondary structure (Popot and Engelman 2000). Identification and characterization of a monomeric mCD9-LEL would serve as a guide for studies with the whole CD9 molecule and it would be straightforward to extend this rationale to the construction of dominant-negative monomeric tetraspanin constructs.

Oligonucleotides were designed to replace conserved, buried hydrophobic residues with either arginine (R) or aspartate (D) amino acid residues (Figure 4.1). We constructed a series of mutations in the mCD9-LELwt plasmid, confirmed the cloning by sequencing, and partially purified mCD9-LEL variants as described in Chapter 2 (Figure 4.2A). Upon induction, we observed variable expression, including several point mutations that resulted only in disulfide-linked higher order oligomers. We chose mCD9LEL•V115R/L119R for further study as it was highly expressed and introduced two amino-acid charges. The mCD9-LEL•V115R/L119R protein had a similar protein elution profile to the mCD9-LEL wild-type protein and a single species was purified to homogeneity (Figure 4.2B). Circular dichroism and sedimentation equilibrium analysis revealed that the mCD9LEL•V115R/L119R protein was both α -helical (Figure 4.3) and dimeric (data not shown). These results suggested that the introduction of V115R/L119R residues is insufficient to disrupt dimerization of the mCD9-LEL.

We utilized our panel of oligonucleotides to generate mCD9LEL constructs with four mutations in each amino acid chain (eight total amino-acid substitutions for the intact dimerization interface). We chose two constructs for further analysis: mCD9LEL•V115R/L119R/V186R/F187R and mCD9LEL•V115D/L119D/V186R/F187R. Both constructs were readily expressed and purified (Figure 4.4A and 4.4C). The mCD9LEL•V115D/L119D/V186R/F187R protein

showed a clear α -helical structure (Chen, Yang et al. 1974). However, the mCD9LEL•V115R/L119R/V186R/F187R protein had a peculiar α -helical circular dichroism signal, albeit with a clear minimum at $\theta_{222\text{nm}}$ (Figure 4.4B). Monitoring the circular dichroism signal at $\theta_{222\text{nm}}$ revealed that the midpoint temperature of thermal unfolding was significantly lowered for both constructs, resulting in a significant fraction of unfolded protein at 37°C (Figure 4.5). As these results precluded the use of these variants under physiological conditions, we did not continue these studies. We conclude that the hydrophobic nature of the dimerization interface is critical to maintain the folding stability of the mCD9LELwt construct.

Epitope-Mapping of the KMC8/mCD9-LEL Binding Site

Our homology model of the head subdomain of mCD9-LEL (modeled onto the hCD81-LEL head structure) did not match secondary structure predictions for the mCD9-LEL in this region. As a result, it was not possible to predict surface-exposed amino acid residues in the region bracketed by the conserved tetraspanin cysteine motifs. Consequently, we chose to do alanine-scanning mutagenesis (Wells 1991) over much of the presumed head subdomain of the mCD9-LEL protein domain (Figure 4.1B).

We constructed a series of alanine-substitutions, checked for proper construction by sequencing, and screened for reactivity to the antibody KMC8 by Western blotting against whole *E. coli* lysates (data not shown). Only two mutations — glutamate 158 or glutamine 159 to alanine — were sufficient for loss of KMC8 binding (Figure 4.6C). These mutants were purified using the same methodology as for the wild-type protein. The glutamine 158 to alanine mutant, denoted mCD9-LEL•E158A, did not yield separable peaks (over a C18 HPLC column (Figure 4.6A) and was not pursued for further analysis. The glutamine 159 to alanine mutant, denoted mCD9-LEL•Q159A, revealed an HPLC profile similar to wild-type (Figure 4.6A), and two species were collected. CD analysis allowed us to identify a properly folded species with helical content similar to the mCD9-LELwt (Figure 4.7A), although with slightly decreased thermal stability (T_m of 53°C vs. 58°C for wild-type) (Figure 4.7B). mCD9-LEL•Q159A is dimeric at concentrations of 20 μM and 50 μM as assessed by sedimentation equilibrium (data not shown). Thus, the mutant is well-folded.

Binding of KMC8 Fab Fragments to the mCD9-LEL

Initial attempts to purify large quantities of the KMC8 antibody from its parental hybridoma were not successful (data not shown). As a result, several milligrams of purified monoclonal antibody KMC8 were purchased from BDPharmingen, where the antibody was produced in a bioreactor (BD Pharmingen, personal communication).

The antibody KMC8 was successfully digested into its respective Fc and Fab domains. Although the digestion was far from complete, yields were sufficient for our experiments. Proteolytic KMC8 Fab fragments were fully separated from the whole IgG molecule using gel filtration chromatography (Figure 4.8A). However, there remained a 20% contamination from the KMC8 Fc fragment (as assessed by Commassie SDS-PAGE) that was not resolved (Figure 4.8B). Gel filtration analysis of the KMC8 Fab fragment shows that it is a well-behaved monomer with an observed molecular weight of 37 kDa. The KMC8 Fc fragment consistently behaved as a 46-kDa protein, irrespective of protein concentration. The mCD9-LEL protein behaved as a 21-kDa dimer (theoretically 22-kDa) at the concentrations loaded onto the column. (Figure 4.9).

When a pre-mixed solution of the KMC8 Fab fragment and the mCD9-LELwt protein was analyzed by gel filtration, we observed a major complex with an apparent molecular weight of 99-kDa suggestive of a 2:2 macromolecular complex (theoretically 95-kDa) (Figure 4.10). SDS-PAGE and Western analysis of the protein content of the 99-kDa complex revealed that it was composed principally of the 37-kDa KMC8 Fab fragment and the 11-kDa mCD9-LEL. A novel protein peak with an apparent molecular weight of 46-kDa was revealed in the gel filtration analysis. SDS-PAGE analysis identified this component as the contaminating KMC8 Fc fragment, which did not exhibit a change in its apparent molecular weight upon addition of the mCD9-LELwt protein (Figure 4.11).

These results demonstrate that the mCD9-LEL presents two apposing KMC8 binding surfaces. Furthermore, it confirms our epitope mapping studies to identify residues of the mCD9-LEL critical for KMC8/CD9 interaction.

Discussion:

In this chapter, we use a combination of molecular biology and biochemistry to dissect out amino-acid residues critical for the folding stability of the mCD9-LEL protein. By replacing hydrophobic amino-acid residues posited to contribute to oligomerization, we show that dimerization of the mCD9-LEL protein is connected with the intrinsic hydrophobicity of that domain. We also show that the antibody KMC8 binds in a 2:2 complex and that this binding site is discrete from the dimerization site. The ability of the mCD9-LEL to bind KMC8 in a 2:2 macromolecular complex reinforces our conceptual model of the mCD9-LEL protein as a two sub-domain protein: a dimerization sub-domain and an antigenic, non-dimerizing sub-domain (Kitadokoro, Bordo et al. 2001).

Our inability to develop a monomeric version of the mCD9-LEL is not surprising. The large, buried, hydrophobic interface between the hCD81-LEL protein chains should contribute significantly to the folding stability of the molecule. Our homology model (Figure 3.7) and tetraspanin sequence conservation strongly suggest that this buried hydrophobic interface is conserved (Seigneuret, Delaguillaumie et al. 2001).

Experimentally, we introduced charged, disruptive mutations into the hydrophobic interface that retain a propensity to form helical secondary structures. In retrospect, the ability of our proteins to maintain helical structure, while losing thermal stability is expected. We hypothesized that the introduction of proline residues that severely perturb helical structure may eliminate both the oligomerization and the folding of the mCD9-LEL protein. Discrete from the dimerization sub-domain is a head sub-domain, delimited by conserved cysteines in the tetraspanin's large extracellular loop. This region is encoded by a single exon and is highly variable both among tetraspanin family members and among species. This region is also where the vast majority of functional amino acid residues have been pinpointed (Boucheix and Rubinstein 2001).

Through alanine-scanning mutagenesis (Wells 1991), we identified key residues in the head sub-domain that are responsible for KMC8 antigenicity. These single alanine mutants had minimal effects on the alpha-helical, dimeric nature of the mCD9-LEL, while severely abrogating KMC8 immunogenicity. Our localization of amino acid residues critical for KMC8 antigenicity to the N-terminal half of the hypervariable region

is surprising. With the human CD81-LEL, critical residues have been identified between cysteine 3 and cysteine 4, or the C-terminal half of the hypervariable region (Higginbottom, Quinn et al. 2000). To date, most functional point mutations have been localized to the region between cysteine 3/cysteine 4 (Kazarov, Yang et al. 2002) (Zhu, Miller et al. 2002). These two loops (between cysteine 2/cysteine 3 and between cysteine 3/cysteine 4) are most likely in close proximity as they are restricted by the characteristic tetraspanin disulfide connectivities.

With our gel filtration analysis, we present evidence that binding of the KMC8 antibody does not disrupt mCD9-LEL-mediated oligomerization. KMC8 is a monoclonal rat anti-murine CD9 antibody of isotype IgG2a κ . This clone was first derived by injecting the mouse bone-marrow-derived stromal cell line BMS2 into rats and selecting for monoclonal antibodies that inhibit production of myeloid, but not lymphoid cells (Oritani, Wu et al. 1996). In subsequent studies, exogenous addition of this α -mCD9 antibody has been shown to specifically inhibit sperm-egg fusion (Chen, Tung et al. 1999).

The ability of the KMC8 antibody to bind in a 2:2 complex, while preserving dimerization, allows us to speculate about the antibody inhibition experiments. Our observations suggest that KMC8 does not inhibit cellular functions by inhibiting the endogenous dimerization ability of the CD9 protein. Rather, KMC8 most likely serves to disrupt CD9-ligand interactions, mediated through the head-subdomain of its large extracellular loop. Currently, all epitope-mapped function-blocking antibodies against tetraspanins bind to tetraspanin-LELs. We speculate that the addition of other tetraspanin antibodies may serve to modulate cellular phenotypes through disruption of an endogenous tetraspanin/non-tetraspanin complex, with no effect on the endogenous tetraspanin dimer. Our studies describing key binding residues in the head-subdomain of the CD9-LEL may also assist in the deconvolution of this endogenous cell-surface complex.

Our molecular dissection of the mCD9-LEL although suggestive of a common function for tetraspanins at the cell surface, leaves many outstanding questions. What is the role of a higher-order tetraspanin cell surface complex? Are our biophysical observations of the murine CD9-LEL complex represented on the cell surface? Lastly, is

the mCD9-LEL protein itself capable of disrupting endogenous cell-surface complexes?
The remainder of this thesis outlines our attempts to explore these questions.

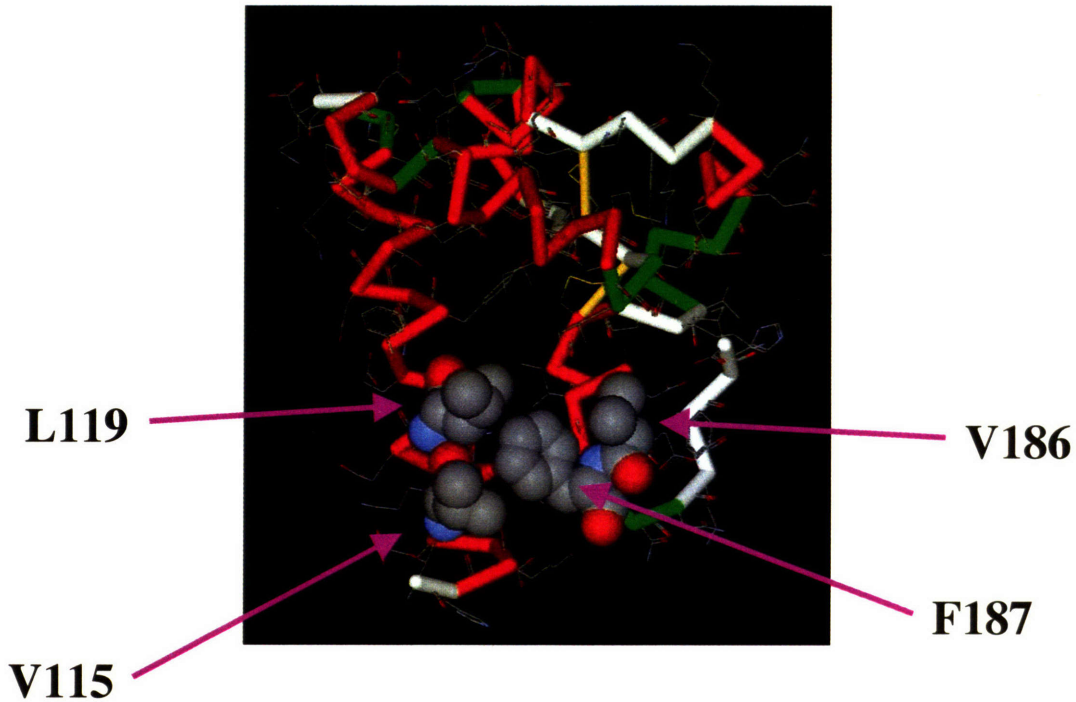
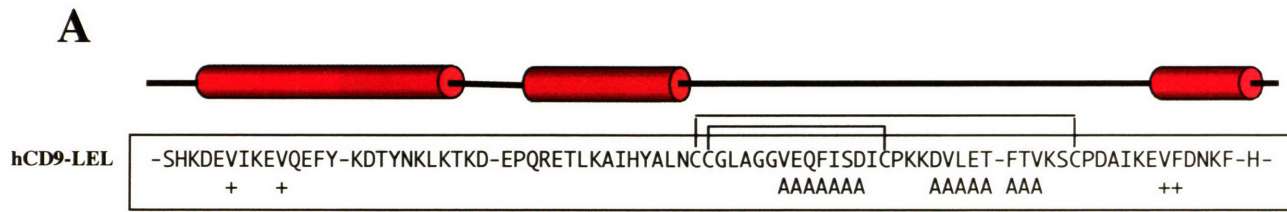


Figure 4.1 Targeted Mutagenesis of the Murine CD9-LEL. A) We schematically depict the primary sequence organization of the murine CD9-LEL structure. The conserved putative tetraspanin dimerization domain is depicted. Amino acid residues that were chosen for mutagenesis to charged lysine (K) or arginine (R) residues are depicted below the wild-type sequence with a “+”. Amino acids chosen for alanine-scanning mutagenesis are depicted with an “A”. B) We present our homology model of the human CD9-LEL sequence modeled onto Chain B of the human CD81 structure Chain B. The hCD9-LEL model is depicted in solid wire with secondary structure illustrated (α -helix in red and disulfide bonds in yellow). Amino acid side chains are illustrated in wire format. The amino acid residues on which we ultimately focused our studies are illustrated with their Van der Waals radii in space fill. These are labeled as Valine 115, Leucine 119, Valine 186 and Phenylalanine 187. These hydrophobic amino acids appear to be loosely conserved among all tetraspanin-LELs.

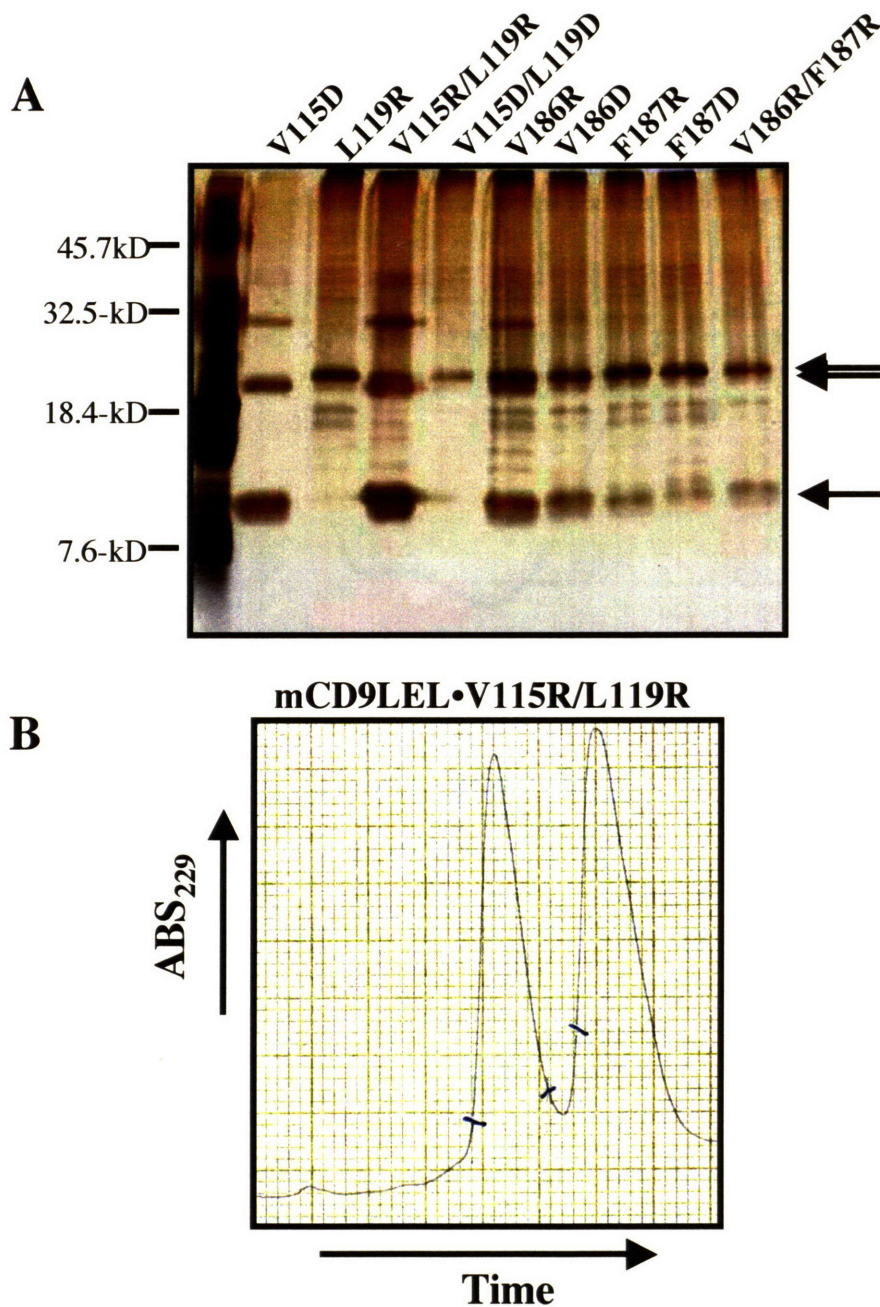


Figure 4.2 Expression and Purification of Murine CD9-LEL Dimerization Mutants. A) A series of mutations in the putative dimerization motif of the mCD9-LEL molecule was generated by PCR. These constructs were transformed into BL21/pLysS *E. Coli* cells and protein expression was induced as described in Chapter 2. Insoluble protein was solubilized and purified over a nickel-NTA drip column, eluted with imidazole, and diluted 10-fold. Protein expression was monitored by non-reducing SDS-PAGE and assessed for both purity and expression by silver-stain. Monomeric mCD9-LEL variants are indicated with an arrow. Covalent dimeric mCD9-LEL variants were also observed and are indicated with double arrows. B) A double mutation, mCD9LEL•V115R/L119R, was chosen for further study based upon high expression of the monomeric form. Large scale cultures of this variant were induced and purified by procedures as described in Chapter 2. We illustrate here a reverse-phase HPLC profile of the mCD9LEL•V115R/L119R variant as monitored at absorbance 229nm. The purification profile of this variant was similar to that of the mCD9-LEL-wt protein.

A Circular Dichroism Wavelength Scan of mCD9-LEL•V115R/L119R

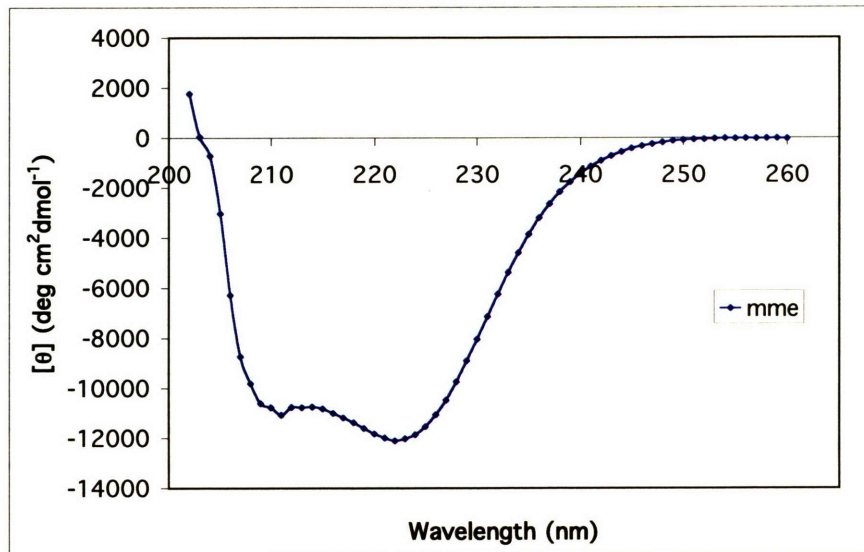


Figure 4.3 Biophysical Analysis of the mCD9LEL•V115R/L119R Variant. A) Circular dichroism spectrum was collected under standard conditions. Analysis reveals a spectral minimum at 222 and 208nm, indicative of a well folded α -helical structure. All biophysical analyses were conducted under conditions similar to those described in Chapter 2. We chose not to analyze the second peak from the reverse-phase HPLC trace, which we assume to be a disulfide-bonded variant of the α -helical form analyzed above.

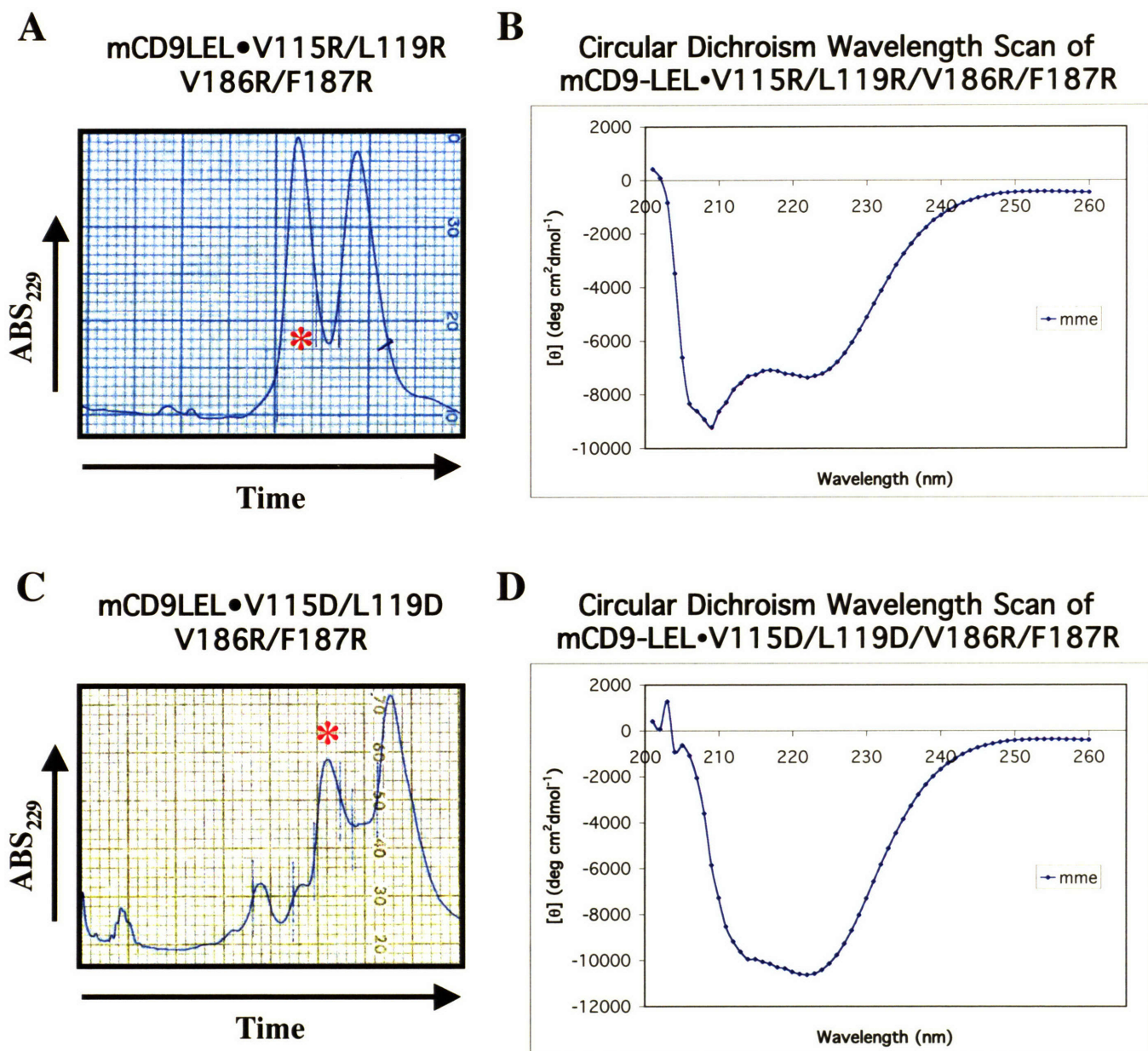


Figure 4.4 Purification and Biophysical Analysis of the mCD9LEL•V115R/L119R/V186R/F187R and mCD9LEL•V115D/L119D/V186R/F187R Variants. Large-scale amounts of the variants listed above were expressed in *E. Coli* and purified over Ni-NTA agarose as described in Chapter 2. These partially purified proteins were injected over reverse-phase HPLC and protein content was monitored by absorbance at 229nm as described. A) HPLC trace of the mCD9LEL•V115R/L119R/V186R/F187R protein, and C) HPLC profile of the mCD9LEL•V115D/L119D/V186R/F187R protein. Note in C the significant deviation from the typical C18 purification profile of the mCD9-LEL wild-type protein (see Figure 2.2). The species chosen for further analysis are indicated with a red asterisk in A and C. B and D) Circular dichroism spectra were collected under standard conditions. For both murine CD9-LEL variants, a minimum at 222nm is clearly observed. However, in B we begin to see deviation from a completely well-behaved α -helical structure.

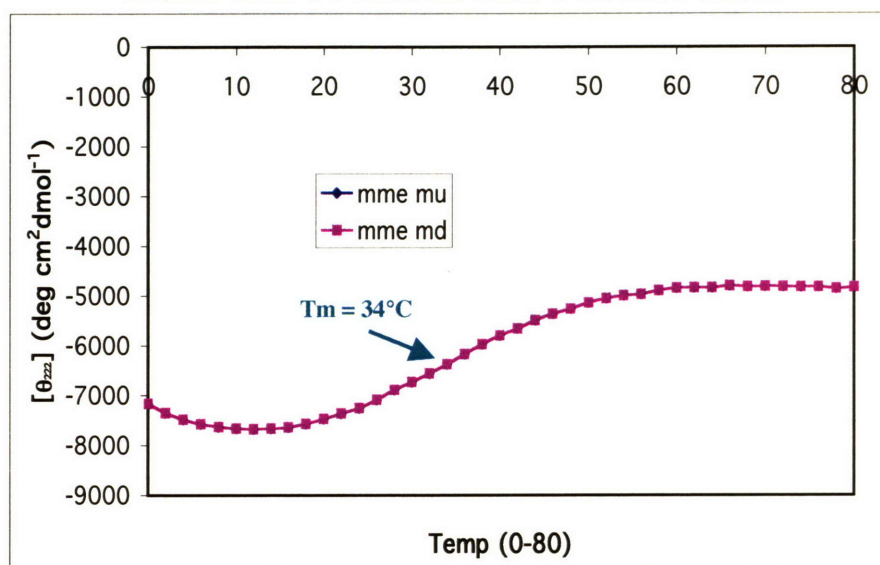
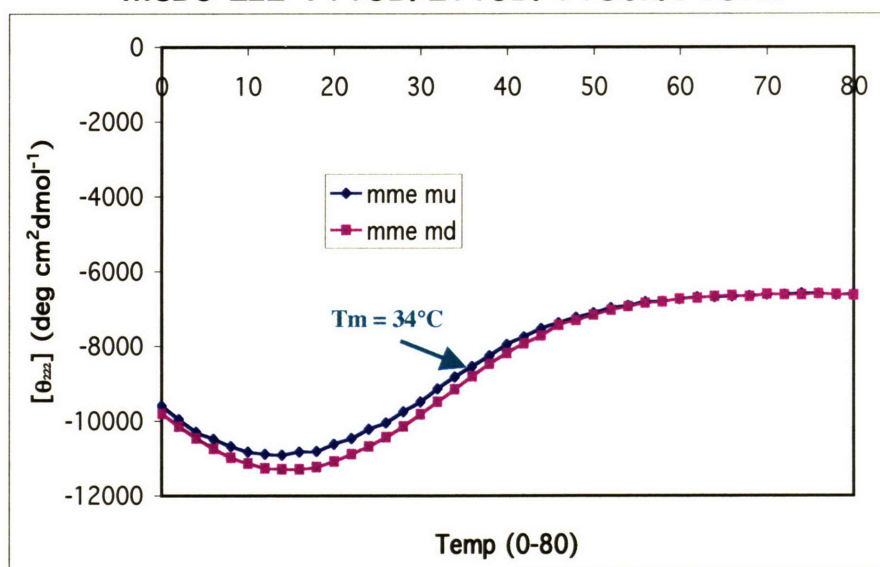
A**Thermal Denaturation/Renaturation of
mCD9-LEL•V115R/L119R/V186R/F187R****B****Thermal Denaturation/Renaturation of
mCD9-LEL•V115D/L119D/V186R/F187R**

Figure 4.5 Thermal Denaturation Profiles of the Murine CD9-LEL Variants. The thermal stability of the murine CD9-LEL variants was monitored by tracking the circular dichroism signal of the dimerization mutant constructs at 222nm. Temperature was controlled by a thermal jacket and the signal was monitored as described in Chapter 2. A) The thermal denaturation profile of the mCD9LEL•V115R/L119R/V186R/F187R protein is illustrated in pink. The midpoint temperature of thermal denaturation was derived by calculating the second moment of the thermal denaturation profile and monitoring its transition across zero. The midpoint of thermal denaturation is illustrated by a green arrow. Thermal renaturation is illustrated in blue (completely matching and overlaid by denaturation profile). B) The thermal denaturation/renaturation profile of the mCD9LEL•V115D/L119D/V186R/F187R protein. The graph is as in A.

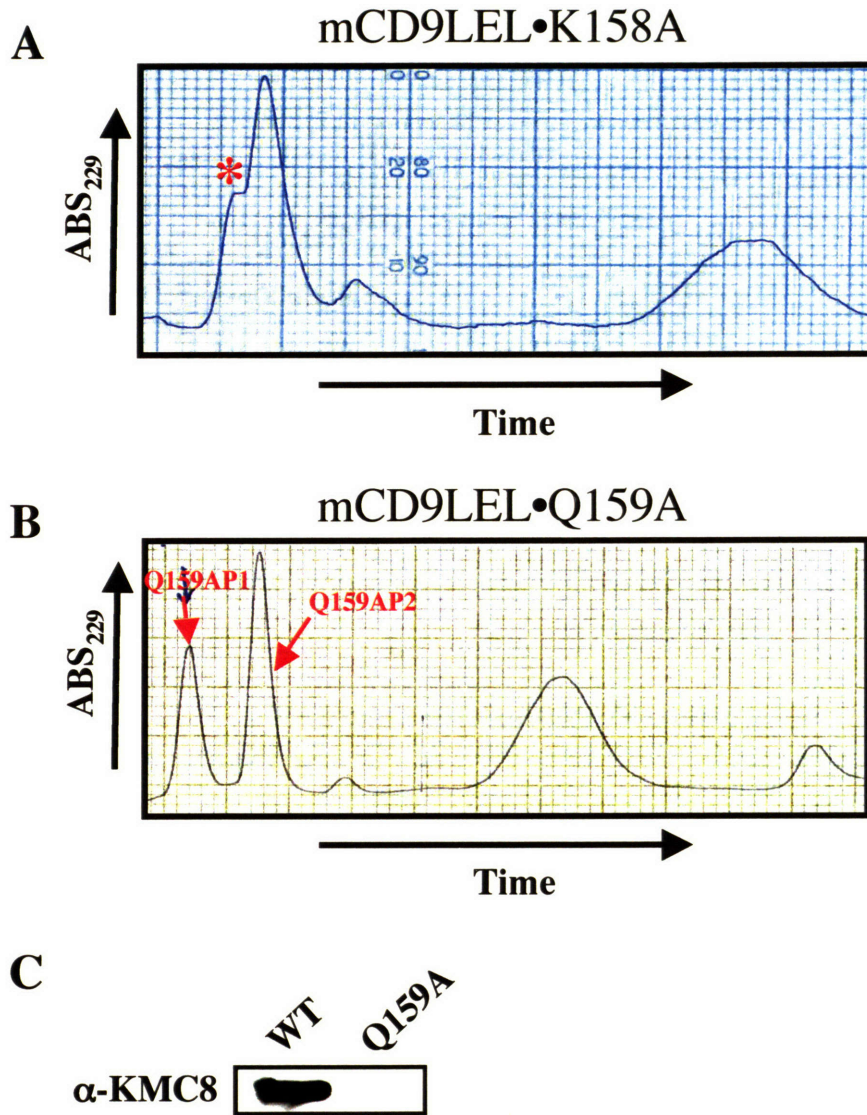
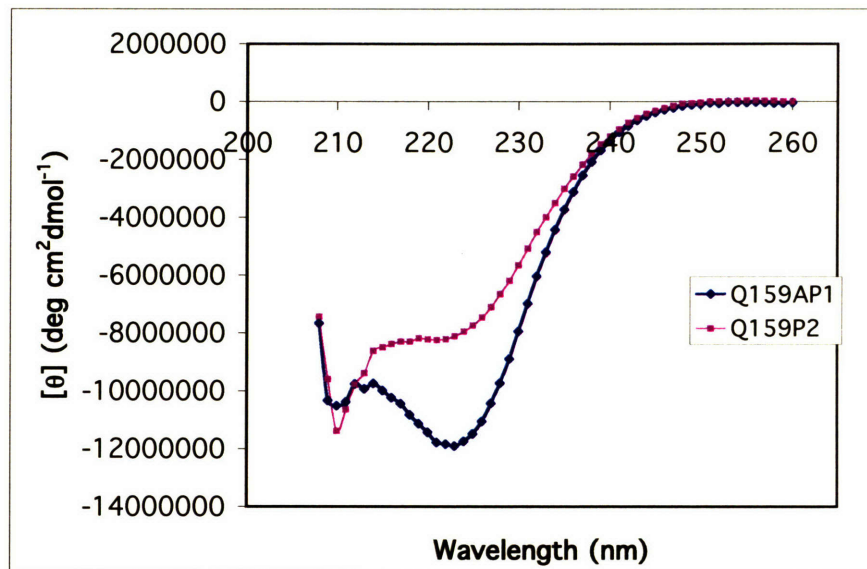


Figure 4.6 Purification and Antigenicity of murine CD9-LEL Variants. After crudely assessing KMC8 antigenicity of alanine-scanned mCD9-LEL variants, two mutations: mCD9LEL•K158A and mCD9LEL•Q159A were chosen for further study. Large-scale amounts of mCD9-LEL variants were expressed and partially purified over Ni-NTA agarose as described previously. Samples were analyzed by reverse-phase HPLC and protein content was monitored by absorbance at 229nm as described. A) The reverse-phase HPLC trace of the mCD9LEL•K158A variant revealed a recognizable, analogous profile to the mCD9-LELwt profile. However, what we suspect is the correctly-folded protein isomer (as denoted by an asterisk) could not be resolved from a second protein isomer. This protein variant was not pursued further. B) The reverse-phase HPLC trace of the mCD9LEL•Q159A variant revealed two peaks characteristic of the mCD9-LEL protein. Both peaks were purified for further analysis. C) Western blot analysis of the mCD9LELwt and mCD9LEL•Q159A protein antigenicities. Equal amounts of the proteins were analyzed on a 18% SDS-PAGE gel and probed with the KMC8 antibody. At higher exposure, trace amounts of KMC8 antigenicity of the mCD9LEL•Q159A variant could be detected. It is unclear if this is due to residual epitope antigenicity or contaminating mCD9LELwt from the adjacent well. No other bands were detected by Western analysis.

A Circular Dichroism Wavelength Scan of mCD9-LEL•Q159A-P1 and mCD9-LEL•Q159A-P2



B Thermal Denaturation/Renaturation of mCD9-LEL•Q159A-P1 and mCD9-LEL•Q159A-P2

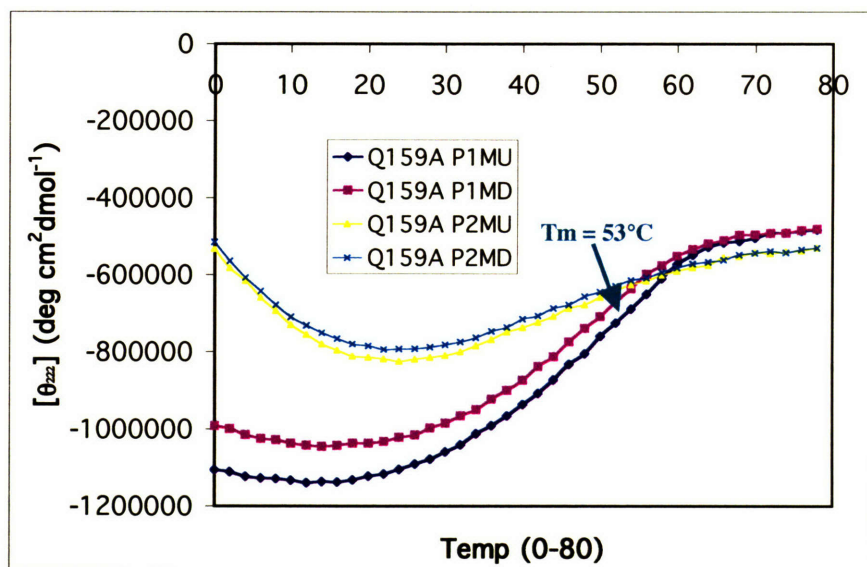


Figure 4.7 Biophysical Analysis of the mCD9LEL•Q159A Variant. A) Circular dichroism spectra were collected under standard conditions. Minima at 222 and 208nm were clearly observed. Circular dichroism spectru of the first purifiable peak of the mCD9LEL•Q159A variant, called Q159Ap1, was markedly different from the second purifiable peak, Q159Ap2. The Q159Ap2 circular dichroism spectrum is characteristic of a mix between α -helix and unfolded secondary structures. B) Thermal denaturation profiles of the non-antigenic mCD9LEL•Q159A variant reveals that it is autonomously folding. The thermal denaturation profile of Q159Ap1 is charted in blue and the renaturation profile is charted in pink. Q159Ap2 is yellow and aqua, respectively. The temperature midpoint of thermal denaturation was computed to be 53°C.

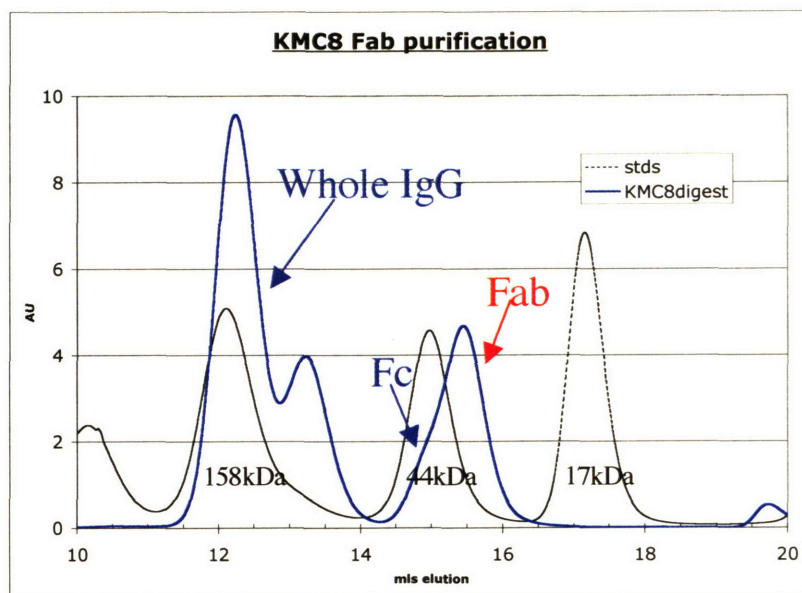
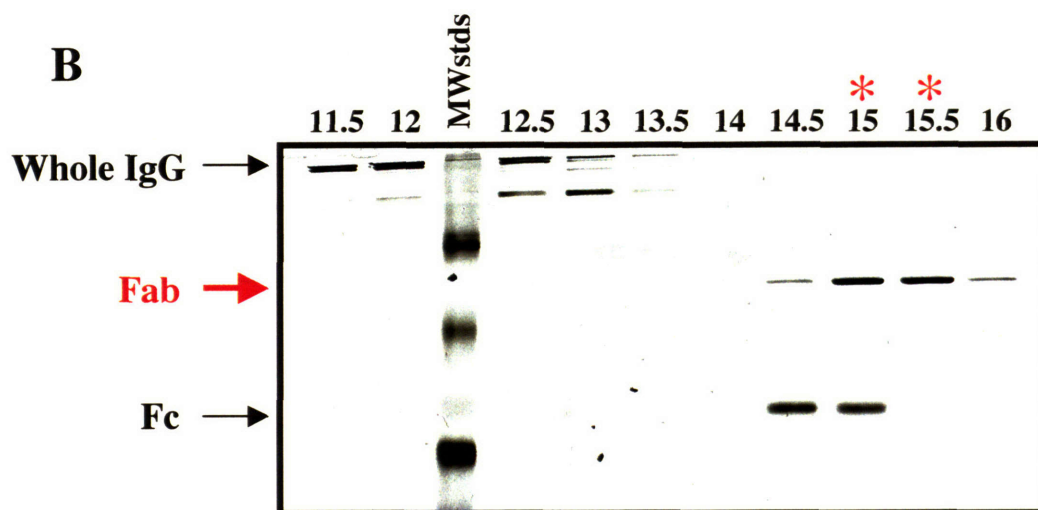
A**B**

Figure 4.8 Fab Fragment Purification of the KMC8 Antibody. Purified KMC8 antibody was digested with papain, and stopped with iodoacetamide. A) Digested KMC8 was loaded onto a Superdex 200HR 10/30 column with PBS at a flow rate of 0.4ml/min using an ÄKTA/FPLC. Protein content was monitored continuously at 280nm and mls of buffer post-sample injection is graphed on the X-axis. Absorbance at 280nm is graphed in arbitrary units on the Y-axis (profiles were multiplied by a scalar to bring all spectra into range). Protein profiles of gel filtration standards are drawn in stippled black with reference peaks labeled. The digested KMC8 protein profile is drawn in solid blue, with the whole IgG, Fc, and Fab fragments labeled. Eluted fractions were collected every 0.5mls. B) Sequential, eluted fractions were analyzed by non-reducing 12% SDS-PAGE followed (non-quantitatively) by silver stain. Whole IgG, Fc, and Fab fragments were clearly identifiable and are labeled. The migration position of the Fab fragment is labeled in red. Eluted fractions are labeled by the mls of buffer eluted from the gel filtration column post-sample injection. Samples 15 and 15.5, which were used for subsequent analyses, are labeled with red asterisks. The purification procedure was repeated several times to yield sufficient quantities of the KMC8 Fab fragment.

Stoichiometry of KMC8:mCD9-LEL Binding

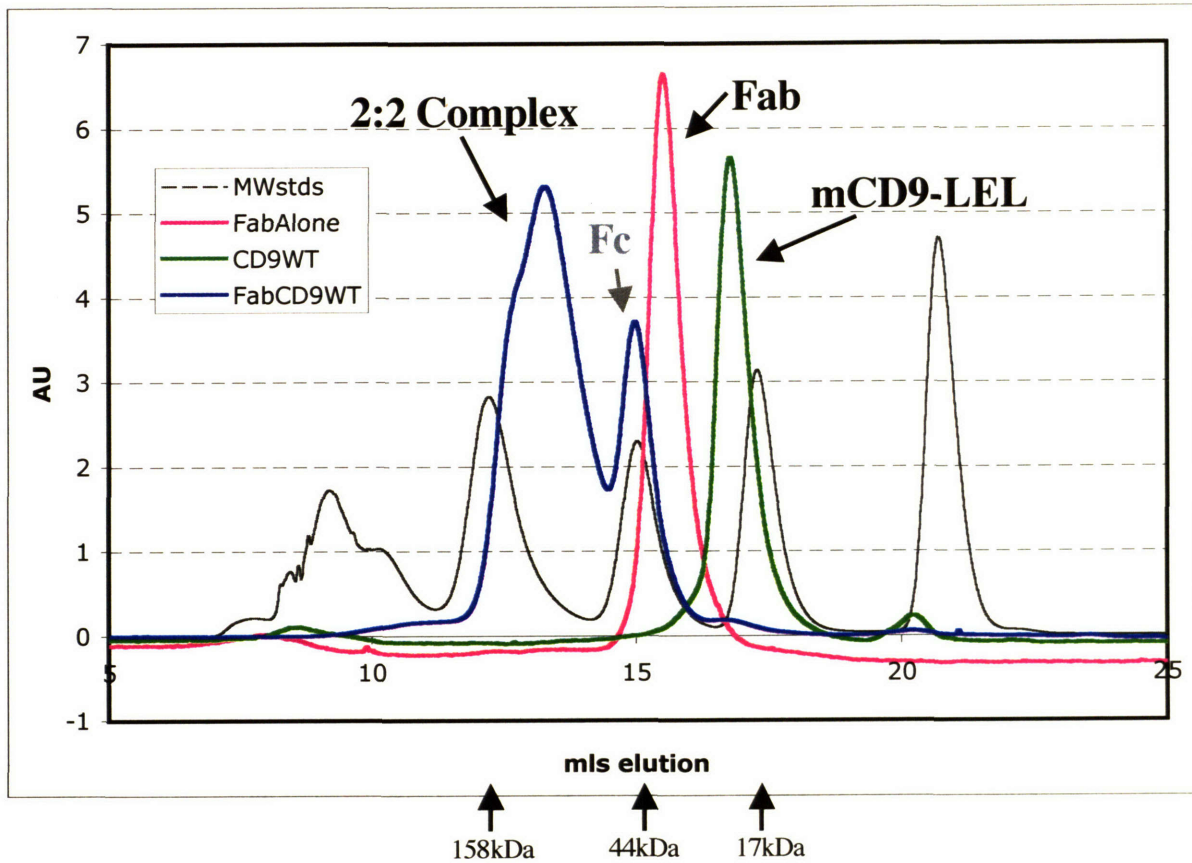


Figure 4.9 Gel Filtration Analysis of KMC8 and mCD9-LEL proteins. All proteins were analyzed by gel filtration chromatography under similar conditions to those described in Figure 4.8. Mls of buffer post-sample injection is graphed on the X-axis and arbitrary absorbance units at 280nm are graphed on the Y-axis. Molecular weight reference standards are identical to those used previously and the profiles are drawn in black. The KMC8 Fab fragment profile is drawn in red. The mCD9-LEL profile is drawn in green and the co-incubated KMC8 Fab/mCD9-LEL profile is drawn in blue. A contaminating KMC8 Fc fragment, which did not shift upon co-incubation is indicated with a gray arrow. Apparent molecular weights of each protein (as calculated relative to the gel filtration standards) is indicated with arrows below the chart.

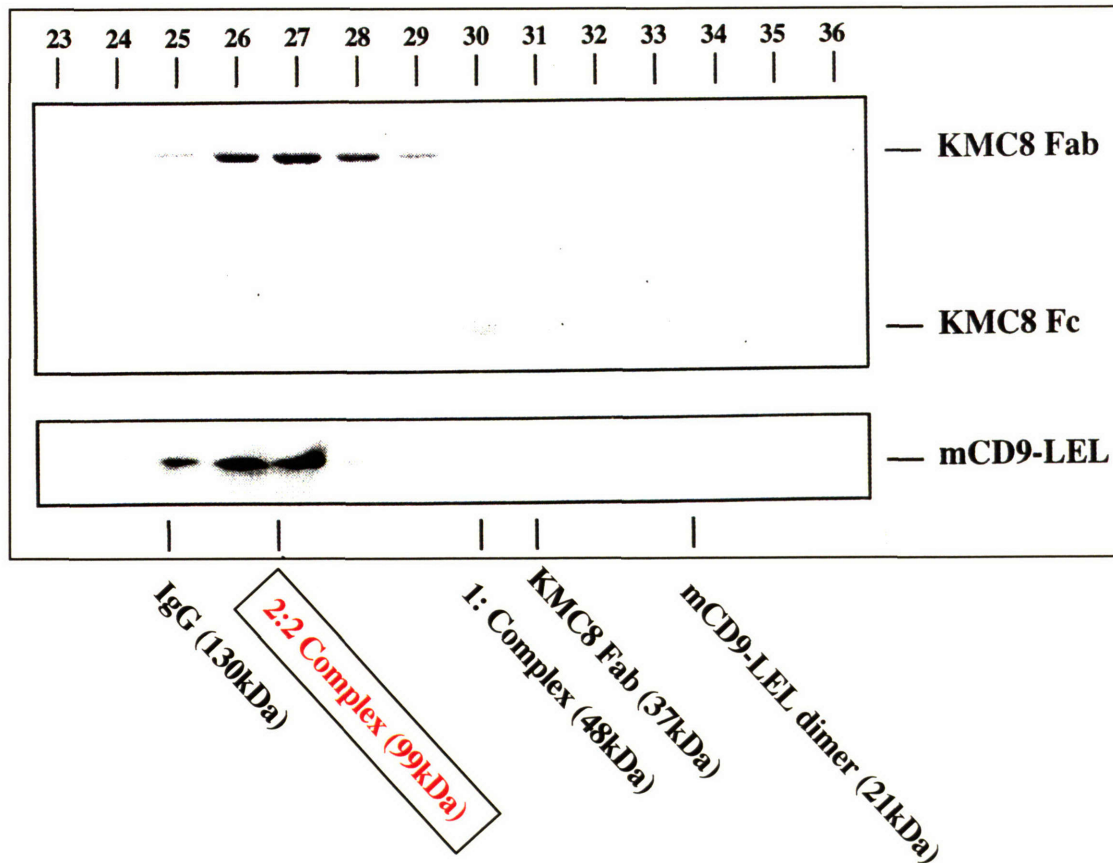


Figure 4.10 SDS-PAGE Analysis of Eluted Gel Filtration Fractions. Sequentially eluted sample were collected from the previous gel filtration run (drawn in blue in Figure 4.10) and analyzed by SDS-PAGE. The fraction number is denoted at the top of the gels, with earlier eluting fractions to the left of the gel. In the top panel, the non-reducing SDS-PAGE gel was analyzed by Coomassie analysis and the migratory positions of the KMC8 Fab and the KMC8 Fc fragments are denoted to the right. In the bottom panel, the mCD9LEL protein (which could not be detected by SDS-PAGE) was detected by assayed by Western blot analysis using the antibody KMC8 as a primary antibody. Theoretical and observed (boxed) positions of the complex relative to the eluted fractions are denoted below the bottom panel.

Chapter 5

Oligomerization Studies of the CD9 Protein

These experiments were conceived by Christopher C. Liu and Richard O. Hynes. All experiments were carried out by Christopher C. Liu. All errors are my own.

Introduction:

Previously, we have described our biophysical, biochemical and molecular characterization of the murine CD9-LEL protein. These results suggested that the mCD9-LEL protein is a α -helical dimer. This dimer consists of two subdomains: a conserved α -helical dimerization domain, and a less conserved, antigenic region which we propose is responsible for interacting with non-tetraspanin ligands.

Historically, tetraspanins were identified as the targets of monoclonal antibodies that perturbed cellular proliferation, adhesion, and differentiation (Maecker, Todd et al. 1997). As a result, there are a panoply of well-characterized antibodies directed against tetraspanins. Readily available and highly characterized antibodies against tetraspanins directed the bulk of biochemical analysis to focus on immunoprecipitation interactions. A wide range of binding partners have been proposed to interact with tetraspanins, including homotypic (tetraspanin/tetraspanin) (Rubinstein, Le Naour et al. 1996) and heterotypic (tetraspanin/non-tetraspanin) (Boucheix and Rubinstein 2001) associations. These protein complexes may be composed of integrins (Berditchevski 2001), major histocompatibility class proteins (Szollosi, Horejsi et al. 1996), signaling molecules (Hemler 2003), and other tetraspanins (Rubinstein, Le Naour et al. 1996). Given the wide range of binding partners, immunoprecipitated tetraspanin interactions have been classified into categories based upon a series of increasingly stringent detergent conditions (Hemler 2001). Very few heterotypic (tetraspanin/non-tetraspanin) and homotypic (tetraspanin/tetraspanin) interactions immunoprecipitate under standard conditions (1%TX-100). The widespread use of milder detergent conditions, such as CHAPS and Brij97, 98, and 99 result in the precipitation of a greater variety of tetraspanin-ligands including integrins, MHC proteins, CD4 (Imai, Kakizaki et al. 1995), CD8 (Imai and Yoshie 1993), and each other.

A limited number of heterotypic interactions have been characterized in TX-100 or digitonin. These interactions are robust and of high stoichiometry (Stipp, Orlicky et al. 2000). Strikingly, although there has been widespread speculation about the existence of a tetraspanin web (Levy and Shoham 2005) or tetraspanin-enriched microdomains (Cherukuri, Shoham et al. 2004), homotypic (tetraspanin/tetraspanin) interactions are not robust and are only detected under mild detergent conditions.

Given the high thermal stability of the mCD9-LEL, we hypothesized that full-length CD9 homooligomerization is robust and detectable under stringent detergent conditions. In this chapter, we present several methodologies to probe murine CD9 oligomerization. Surprisingly, we observed CD9 oligomers only under weak detergent conditions (CHAPS) (Chamberlain 2004) and not under stringent detergent conditions (TX-100 or RIPA). Although in many ways inconclusive, our results are consistent with published and unpublished data in the tetraspanin field.

Materials and methods:

Full-Length CD9 construction and Expression:

Oligonucleotides CL191 and CL207 were designed to amplify the full-length murine CD9 cDNAs with flanking EcoRI (5') and NotI (3') restriction enzyme sites.

CL191: 5'-CCGGAATTCATGCCGGTCAAAGGAGGCACC-3'

CL207: 5'-ATAAGAATGCGGCCGCGACCATCTCGCGGTTCTTG-3'

These sites were used to insert the mCD9 cDNA into the multiple cloning site of pCDNA3.1myc-HIS and pCDNA3.1V5-His eukaryotic epitope-tagged vectors (Invitrogen). Vectors were checked for proper subcloning by DNA sequencing. Large quantities of vector were purified from DH5 α ' *E. coli* cells using the Qiagen Maxi-Prep system and quantified by monitoring absorbance at 260/280nm.

Epitope-tagged vectors were transfected individually or in pairs into COS-7 cells with the Fugene transfection kit according to manufacturer's instructions. In brief, 3 μ l of Fugene transfection reagent (Roche) were mixed with 1 μ g of DNA and incubated in 100 μ l of DMEM serum-free media for 20 minutes. This mix was then added in a drop-wise fashion to freshly fed COS-7 cells in E4HG/10%FBS at 90% confluency.

Forty-eight hours post-transfection, cells were washed in PBS+Ca⁺⁺/Mg⁺⁺, lifted off the plate with a scraper, aliquoted, and lysed in buffer containing either 1%CHAP, 1%TX-100 or RIPA (150mM NaCl, 20mM Tris, .1%SDS, 1%NP-40, 0.5% deoxycholate, pH7.4). Lysates were cleared of particulates by centrifugation and murine CD9 insoluble fraction was solubilized in 1X SDS-loading buffer. Total protein content was monitored by the microBCA (Pierce) as per the manufacturer's instructions.

Immunoprecipitation of Epitope-Tagged CD9:

Anti-mouse IgG-conjugated agarose beads (Sigma) were washed in detergent buffer and incubated with two μ gs of either anti-myc or anti-V5 monoclonal antibody (Invitrogen) for 2 hours at 4°C with agitation. Excess, unbound antibody was removed from the antibody-bound beads by sequential centrifugation and washing (3X in total). Concurrently, cell lysates were pre-cleared by the addition of anti-mouse IgG-conjugated

agarose (Sigma) (without anti-epitope antibodies) for 2 hours at 4°C with agitation. Agarose beads were removed by centrifugation. Pre-cleared cell lysates were added to antibody-bound beads and rocked overnight at 4°C. Agarose beads were washed 3X with detergent buffer to clear unbound proteins. Bound proteins were eluted by the addition of 1X SDS-loading buffer (Bio-Rad) and incubation at 100°C for 10 minutes. Eluted proteins were loaded onto 12% SDS-PAGE gels and analyzed by Western blotting under non-reducing conditions.

Cell-Surface Labelling:

Forty-eight hours post-transfection, cells were washed 3X with PBS+Ca⁺⁺/Mg⁺⁺. Fresh sulfo-NHS-LC-biotin (Pierce) was added to PBS+ Ca⁺⁺/Mg⁺⁺ to a final concentration of 0.1mg/ml and allowed to react for 30' at 37°C/5%CO₂. Sequentially washing and incubation with Tris-buffered saline for a total of 10' quenched the reactions. Cells were harvested as described previously with the cross-linker-quenching TBS replacing PBS in all solutions. Immunoprecipitation reactions were carried out as previously described.

Gel Filtration Analysis:

Transfected cells were freshly lysed in RIPA buffer and cleared by centrifugation. Soluble cell lysate was loaded onto a Superdex 200HR 10/30 column (Amersham Pharmacia), pre-equilibrated with PBS at a flow rate of 0.4 ml/min using a ÄKTA/FPLC (Amersham Pharmacia). Due to the complexity of the loaded proteins, tracking protein content at 280nm did not yield meaningful information. Eluted fractions were collected every 0.3mls and analyzed for CD9 content by Western blotting as previously described.

Native Blue Electrophoresis:

Native-blue electrophoresis (NBE) is a polyacrylamide gel electrophoresis (PAGE) technique that uses the amphipathic qualities of the Coomassie Brilliant Blue (CBB) protein-binding dye instead of ionic detergent to probe native macromolecular complexes of transmembrane proteins (Schagger and von Jagow 1991). This technique bypasses the requirement for highly pure transmembrane protein necessary in traditional

analyses of protein complexes. Cells are lysed under detergent conditions and the addition of excess CBB serves both to displace non-ionic detergents and to introduce a charge onto proteins to allow electrophoresis (Schagger, Cramer et al. 1994).

For native-blue electrophoresis, a 30% acrylamide stock of 29:1 monomer to cross-linker was made from powder. A 4X buffer solution consists of 200mM BisTris pH 7.0 and 2M aminocaproic acid (Sigma). Buffer was mixed with the acrylamide stock to make a 6% and an 18% acrylamide stock respectively. TEMED was added to .05% and 10% APS was added to .5% to catalyze acrylamide cross-linking and continuous gradient gels were poured into a 5-8X10cm multi-gel caster (Hoefer) and overlaid with water-saturated butanol. Upon polymerization, a 2.5% acrylamide stacker was poured with the BisTris/amino-caproic acid buffer as above.

Transfected cells were freshly lysed in either CHAPS, TX-100, or RIPA buffers as for immunoprecipitations. An equal volume of native-blue loading buffer (5% CBB/100mM BisTris pH7.0/0.5M amino-caproic acid/pH7.0) was added and cell lysates were loaded onto the gradient gels without boiling. Anode buffer (without CBB) was composed of 25mM BisTris, 0.5M amino-caproic acid, pH7.0. Cathode buffer was composed of 50mM Tricine, 15mM BisTris supplemented with .01% CBB. When the CBB dye front reached the end of the gel, the cathode buffer was replaced without CBB and the CBB was allowed to electrophorese off the gel. Gels were washed in H₂O to remove excess dye (which can compete with protein binding) and transferred to nitrocellulose in 10mM CAPS pH11.0. Protein blots were blocked and developed with anti-Myc and anti-V5 antibodies as previous.

Cross-Linking of CD9:

Co-transfected cells were freshly lysed in either CHAPS, TX-100, or RIPA buffers as described previously. A fresh stock of 40mg/ml of dithio-bis succinimidyl propionate (DSP) (Pierce) was dissolved in dimethyl sulfoxide. Whole cell lysates were cross-linked with 0, 0.1, 0.4, or 0.8 mg/ml of DSP cross-linker (DMSO final concentration is 1%) and allowed to incubate at RT for 1 hour. Reactions were quenched with the addition of 1M Tris pH 8.0 to a final concentration of 200 μ M. 2X SDS-Loading

buffer was added immediately and samples were loaded onto SDS-PAGE gels for Western analysis.

Results:

Detergent Stability of CD9 Homooligomers

Detergents of varying stringency have been used to characterize both homotypic (tetraspanin/tetraspanin) and heterotypic (tetraspanin/non-tetraspanin) tetraspanin interactions (Berditchevski, Zutter et al. 1996). As detergents of increasing stringency are utilized, the complexity of immunoprecipitated protein complexes decreases. In the presence of weak, non-ionic detergents (CHAPS), many homotypic and heterotypic interactions occur. Under stronger, non-ionic detergent conditions (TX-100), homotypic interactions disappear and only a small subset of strong heterotypic interactions remain (Hemler 2003). With ionic detergents (RIPA), almost no interactions are detected (Figure 5.1).

We utilized this array of detergents to monitor the stringency of homotypic intraspecies tetraspanin interactions. The protein CD9 was tagged with either a V5 or Myc epitope in similar vectors (pCDNA3.1) and co-transfected into COS-7 cells. Protein production was monitored by Western blot analysis and optimal expression was at 48 hours post-transfection (data not shown). Cells were lysed and aliquoted in either CHAPS, TX-100, or RIPA buffer (Figure 5.1). We tracked fractionation of CD9 by Western blot and although a bit of CD9 was detected in the CHAPS-insoluble portion, minimal insoluble CD9 was detected in stronger detergents (Figure 5.2A). This figure overrepresents the proportion of insoluble CD9, as correcting for volume, the insoluble fraction is approximately 5 times as concentrated as the soluble portion. Cell-surface biotinylation with a membrane-impermeable biotin cross-linker revealed that a significant portion of CD9 was biotinylated and presumably reached the cell surface (Figure 5.2B).

CD9 molecules were immunoprecipitated by either anti-Myc or anti-V5 antibodies pre-bound to anti-mouse IgG agarose beads. Bound protein complexes were eluted from the beads with SDS and analyzed by SDS-PAGE and Western blot analysis. The efficiency of CD9 immunoprecipitation was analyzed by Western blot. Co-immunoprecipitation of the complementary, co-transfected CD9 molecule was also analyzed by Western blot. We observed co-immunoprecipitation only in weak, non-ionic CHAPS buffer and no co-immunoprecipitation in either TX-100 or RIPA buffer (Figure 5.2C). This detergent stringency of co-immunoprecipitation was observed regardless of

which detergent epitope-tagged CD9 was bound to agarose. The immunoreactive doublets observed in all gels are consistent with published accounts.

Gel Filtration Analysis of CD9 Oligomerization State:

As we did not observe co-immunoprecipitation of co-transfected epitope-tagged CD9 constructs under stringent detergent conditions, we attempted to get an apparent molecular weight of the CD9 molecule. The native molecular weight of monomeric CD9 is approximately 25kDa (as assessed both by SDS-PAGE and the predicted molecular weight of the protein without glycosylation).

Transfected cells were lysed in stringent, ionic detergent buffer (RIPA) and the cell lysate was cleared of particulate matter by centrifugation. Cell lysate was loaded onto a gel filtration column pre-equilibrated with RIPA buffer. Due to both the high absorbance background of the RIPA buffer and protein lysate complexity, monitoring at OD280 was not informative. As a result, protein fractions were collected, analyzed by SDS-PAGE and Western blot analysis and CD9 elution was estimated by densitometry. The CD9 elution profile was compared to gel filtration markers run under the same conditions. We derived an estimated molecular weight of 130-kDa for the CD9/micellar complex (Figure 5.3A). It is difficult to estimate an oligomeric state from these results. Although unlikely, it is plausible that the binding of detergent molecules may add 100-kDa to the native molecular weight of a CD9 monomer through binding to the four transmembrane regions, native palmitoylation sites, and possibly large, exposed hydrophobic surfaces in the CD9-LEL (Kitadokoro, Bordo et al. 2001). However, the observed 130-kDa apparent molecular weight is also consistent with a detergent-bound CD9-LEL dimer.

Native Blue Electrophoresis Analysis of CD9 Oligomerization State:

Although SDS-PAGE allows precise molecular weight analysis of a protein, it does not preserve quaternary protein complexes. One method to circumvent this is to use native-blue electrophoresis, a specialized PAGE technique (Schagger and von Jagow 1991). This technique utilizes the amphiphilic nature of the common protein dye, Coomassie Brilliant Blue R-250 (CBB), to solubilize integral membrane proteins. By

providing a negative charge to bound proteins, the Coomassie dye also allows all proteins (regardless of native pI) to electrophorese and helps to limit protein aggregation. These attractive attributes persuaded us to attempt to obtain a more precise molecular weight of the CD9 complex than gel filtration allowed (Schagger, Cramer et al. 1994).

We lysed transfected COS cells expressing CD9 in detergents of varying strengths. This allowed defined quarternary membrane protein complex solubilization. Subsequent to lysis, we added CBB loading buffer to ensure membrane solubilization in the native-blue PAGE system. After electrophoresis, proteins were transferred to nitrocellulose and analyzed by Western blotting according to standard methods (Figure 5.4).

Cell lysates prepared with detergents of varying strengths resulted in quite different electrophoretic mobilities. CHAPS lysis resulted in a wide migratory range of the CD9 complexes with a much lower apparent molecular weight complex evident when cells were lysed in stronger detergents. These results suggest that CHAPS lysis results in much greater heterogeneity of CD9 complexes than either TX-100 or RIPA solubilization. Migration of the 120-kD epitope-tagged LacZ (beta-galactosidase) is also indicated (Figure 5.4). The LacZ protein contains no transmembrane segments but is homo-tetrameric, and it is not clear if subunit binding was disrupted with CBB dye binding. Soluble, protein markers (which contained some sodium dodecyl sulfate) migrated as broad bands. However, we estimated the TX-100 solubilized CD9 complex to be between 25-50-kDas in molecular weight. Lastly, it is clear that the CD9 complexes behave differently when solubilized in CHAPS versus stronger detergent. It is difficult to draw conclusions about CD9 homooligomerization from this series of experiments.

Cross-Linking Analysis of CD9 proteins:

Chemical cross-linkers are often used to identify protein partners in close proximity. We chose to use a range of chemical cross-linkers at different concentrations to explore oligomerization of CD9 molecules (Kovalenko, Yang et al. 2004). In brief, equal amounts of the CD9 molecule were incubated with an amine-specific cross-linker

for a period of time. The reaction was then quenched with Tris buffer (which contains an amine) and protein complexes were analyzed by non-reducing SDS-PAGE.

DSP is a 12Å cross-linker that reacts with amine groups (Figure 5.5A). With a CHAPS solubilized CD9 lysate, addition of the DSP cross-linker resulted in a higher molecular weight CD9 species corresponding to a covalent dimer. Higher order complex formation was not observed when CD9 was solubilized in more stringent detergents such as TX-100 or RIPA (Figure 5.5B). Although we tried a panel of amino-specific cross-linkers with varying spacer arms, only DSP was successful in capturing a covalent dimer (data not shown). These observations are consistent with the notion that stronger detergent precludes the formation of CD9 quarternary complexes.

Detergent stability of tetraspanin-LEL proteins:

To probe the detergent stability of tetraspanin-LEL-mediated oligomerization, we chose to estimate the apparent molecular weight of CD9 in TX-100 buffer. We chose this detergent condition as it did not allow oligomerization between CD9 molecules. Our biophysical analysis of the mCD9-LEL protein in isolation suggested that LEL-mediated dimerization would be insensitive to non-ionic detergents. Gel filtration analysis of molecular weight standards in TX-100 resulted in significant noise. However, it was possible to estimate approximate molecular weights. Utilizing these standards, we estimate that the mCD9-LEL in TX-100 has an apparent molecular weight of 30-kDa suggestive of a dimer with bound detergent (data not shown). Given the hydrophobic head domain of the mCD9-LEL, it is plausible that detergent-bound molecules may have shifted the molecular weight of the mCD9-LEL. The observed apparent molecular weight of the mCD9-LEL protein in the absence of detergent is 21-kDa (Chapter 4).

Discussion.

The most common method to probe tetraspanin interactions is to observe these interactions in a range of detergent conditions. Strong interactions are characterized in stronger non-ionic detergents such as TX-100. Extraction of tetraspanin complexes under weaker detergent stringency results in many binding partners. Under weaker stringency, it is not clear if protein interactions are direct or indirect, as immunoprecipitates contain many tetraspanin and non-tetraspanin proteins. These observations have led to the hypothesis of a tetraspanin web, or a network of tetraspanin molecules that serves as an organizing nucleus at the cell surface (Rubinstein, Le Naour et al. 1996).

The goal of this chapter was to utilize a panel of detergents to observe conditions under which the CD9 molecule could form homodimers. Our biophysical analysis on the mCD9-LEL protein suggests that LEL-mediated oligomerization is very stable. Both a high midpoint of thermal denaturation and a large hydrophobic dimerization surface (in the case of hCD81-LEL structure) suggest that a constitutive tetraspanin-LEL mediated dimer sits at the center of the tetraspanin web.

Empirically, we have shown previously that the mCD9-LEL is structurally similar to the hCD81-LEL crystal structure. If the mCD9-LEL structure is represented in the whole molecule, there are several hydrophobic interfaces which may bind detergent molecules. The most prominent hydrophobic domain is the four transmembrane segments, which we assume require a desolvated environment to maintain solubility. Furthermore, the CD9 molecule has been shown to contain six potential palmitoylation sites (Charrin, Manie et al. 2002), further increasing the size of the CD9 membrane-bound domains. Therefore, unlike the mCD9-LEL, which is soluble in PBS, the CD9 molecule requires detergent solubilization. The requisite addition of detergents for our studies of the CD9 molecule have severely limited our ability to estimate a molecular weight for the CD9 complex (gel filtration studies). Native-blue electrophoresis, which should give higher resolution of transmembrane protein complex molecular weight (Schagger, Cramer et al. 1994) revealed lower approximate molecular weights than gel filtration, but still did not eliminate the possibility of a dimer. CHAPS solubilization of CD9 molecules revealed a broad heterogeneous spread of complexes, further reinforcing

the difficulties to derive meaningful information in the presence of weak detergents. It is clear that we are unable to identify a definitive oligomerization state using these assays.

Our most surprising result is the ability of strong non-ionic detergents (TX-100) to disrupt CD9 oligomerization. There are many possible reasons for these negative results. As noted in Chapter 1, studies of the CD9-LEL in isolation may not be representative of the intact molecule. The presence of four transmembrane domains (which is approximately equivalent to the molecular weight of the CD9-LEL) may perturb the structure of the CD9-LEL domain, resulting in reduced oligomerization capacity. The short extracellular loop and palmitoylation may also play critical roles in mitigating CD9 oligomerization. Inhibition of palmitoylation may play a role in lateral interactions among tetraspanins (Charrin, Manie et al. 2002).

The functional relevance of the α -helical, dimeric hCD81-LEL structure is still widely debated in the tetraspanin community (Levy and Shoham 2005). Although some role for tetraspanin-LEL mediated dimerization is not disputed, it is still unclear to what degree extracellular oligomerization is a central feature of tetraspanin function. The root of this argument lies in the amino- and carboxy-termini of the ordered portion visualized in the hCD81-LEL structure (see Figure 3.1). Although each amino-acid chain's two termini are in close proximity in the crystal structure (Kitadokoro, Bordo et al. 2001), the antiparallel nature of the dimerization interface points each set of transmembrane 3 (N-terminal) and transmembrane 4 (C-terminal) helices in opposite directions. I believe that this view can be reconciled by adding an additional half-turn to the terminus of either helix A or helix E. Given the results in this chapter, the answer may lie between complete dismissal of the dimeric crystal structure and my rationalization. Currently, I believe that inclusion of the tetraspanin transmembrane domains (as with the experiments discussed in this chapter) lowers the oligomeric stability of the mCD9-LEL. These confusing results have been discussed in more detail in Chapter 1.

Regardless of how directly our biophysical studies of the mCD9-LEL protein correlate with tetraspanin behavior at the cell-surface, the mCD9-LEL domain in isolation proves to inhibit fertilization, closely matching experimental studies with both anti-CD9 antibodies and also CD9-null mice. These experiments are described in the remainder of this thesis.

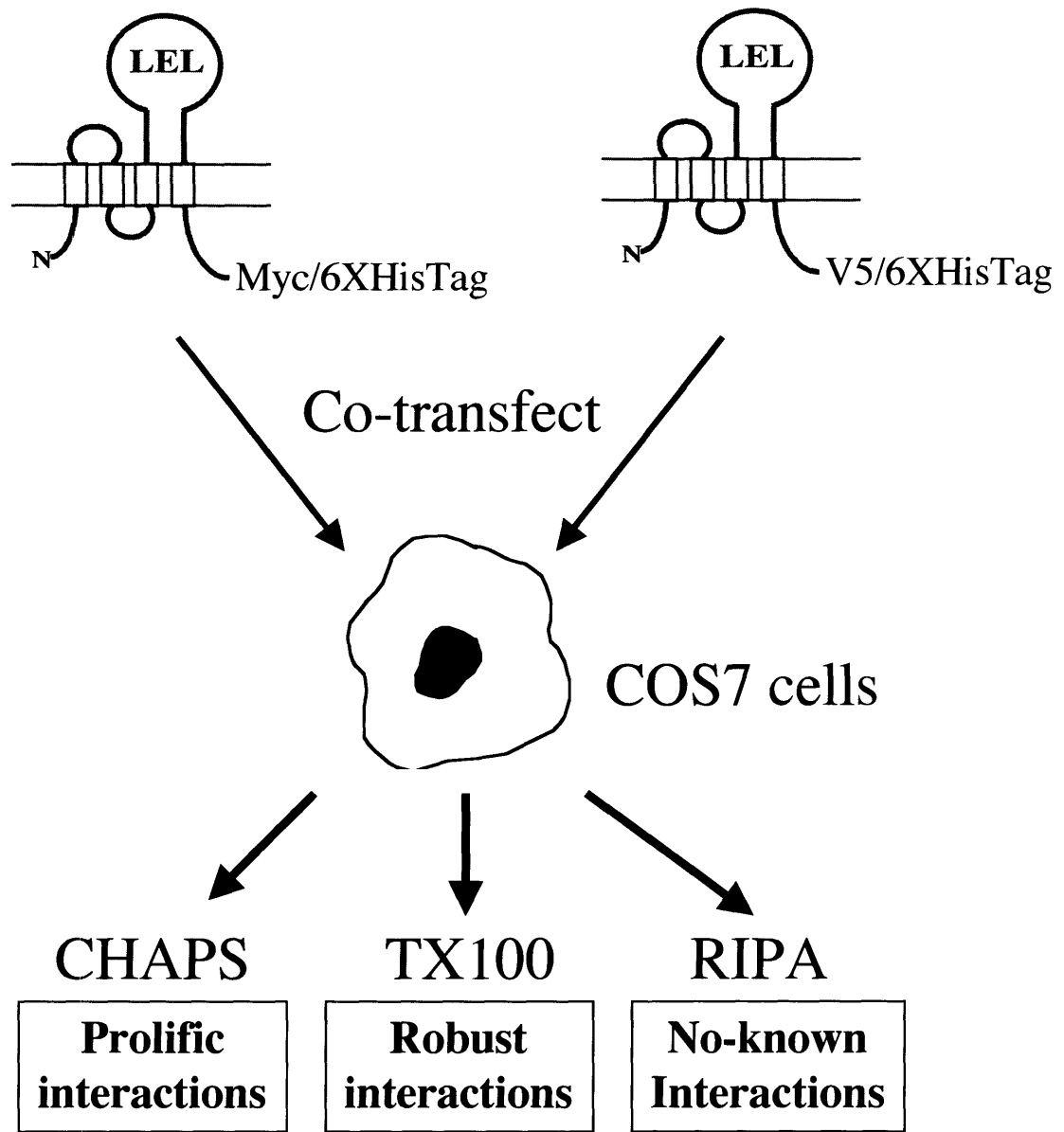


Figure 5.1 Epitope-Tagged CD9 Transfection and Lysis: Full-length cDNAs of the murine CD9 were tagged at the carboxyl-terminus with either a Myc-6XHis or a V5-6XHis. These constructs were transiently transfected into COS7 cells and ubiquitous expression was driven by the CMV promoter. Post-transfection, cells were scraped, lysed with buffer containing either CHAPS, TX100 or RIPA, and aliquoted. Tetraspanin-protein interactions have been characterized by the detergent sensitivity of their association and the detergent conditions we chose to explore are depicted.

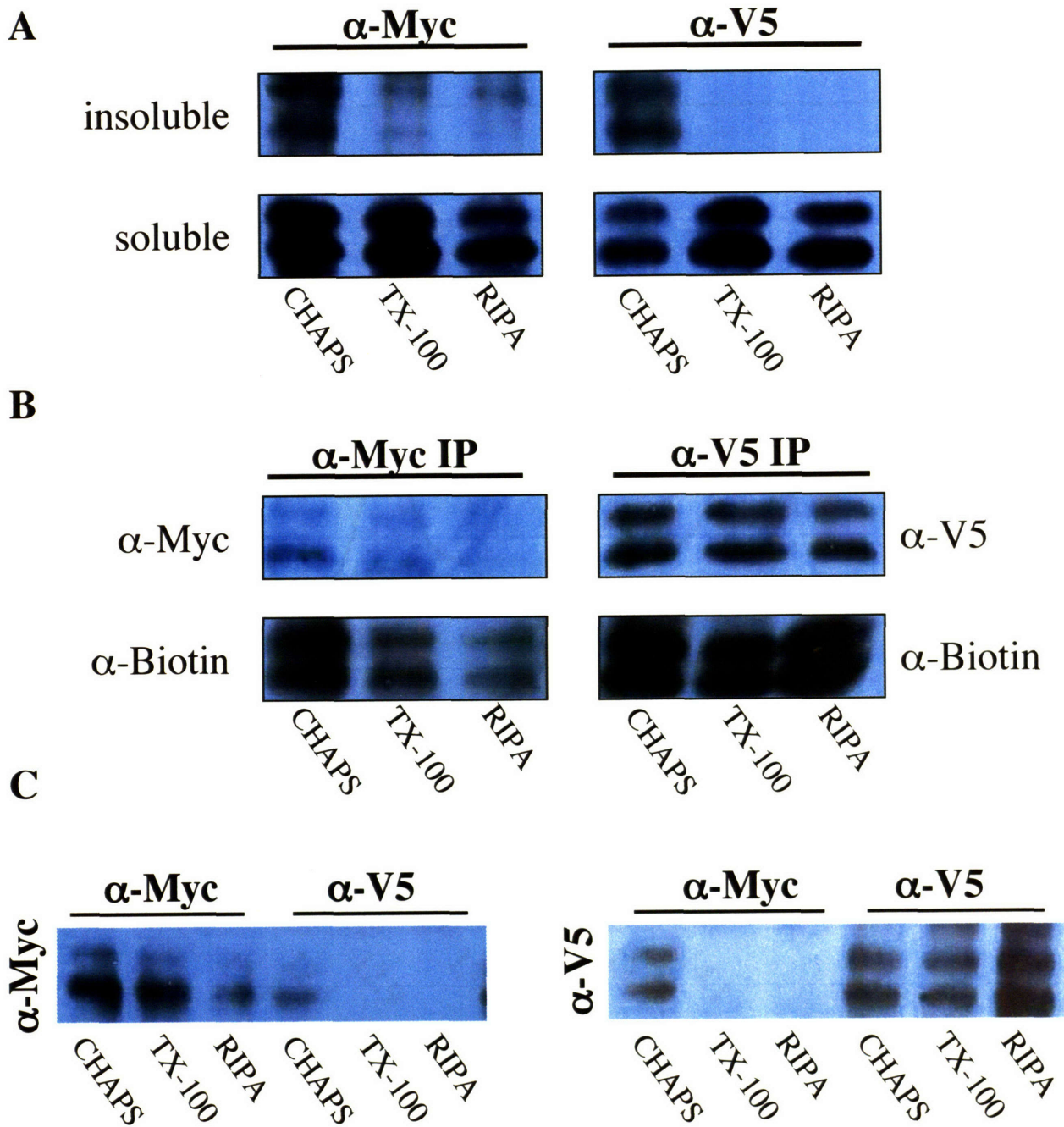


Figure 5.2 Epitope-Tagged CD9 Is Soluble, Cell-Surface Presented, and Associates Only in CHAPS A) Transfected cell lysates were separated into detergent soluble and insoluble portions and analyzed by SDS-PAGE followed by Western blot analysis against the epitope tag. We loaded approximately 5X the amount of insoluble portion as soluble. Note that the observed doublets are consistent with other publications. B) Post-transfection, cells were labeled with the membrane-impermeable NHS-LC-biotin cross-linker. Cells were then lysed under varying detergent conditions and immunoprecipitated. Bound protein was analyzed by SDS-PAGE followed by Western blotting against either the epitope-tags or the biotin label. C) Transfected cells were lysed under varying detergent conditions, aliquoted, and immunoprecipitated. Bound proteins were analyzed by SDS-PAGE followed by Western analysis against both the immunoprecipitating epitope and its complement.

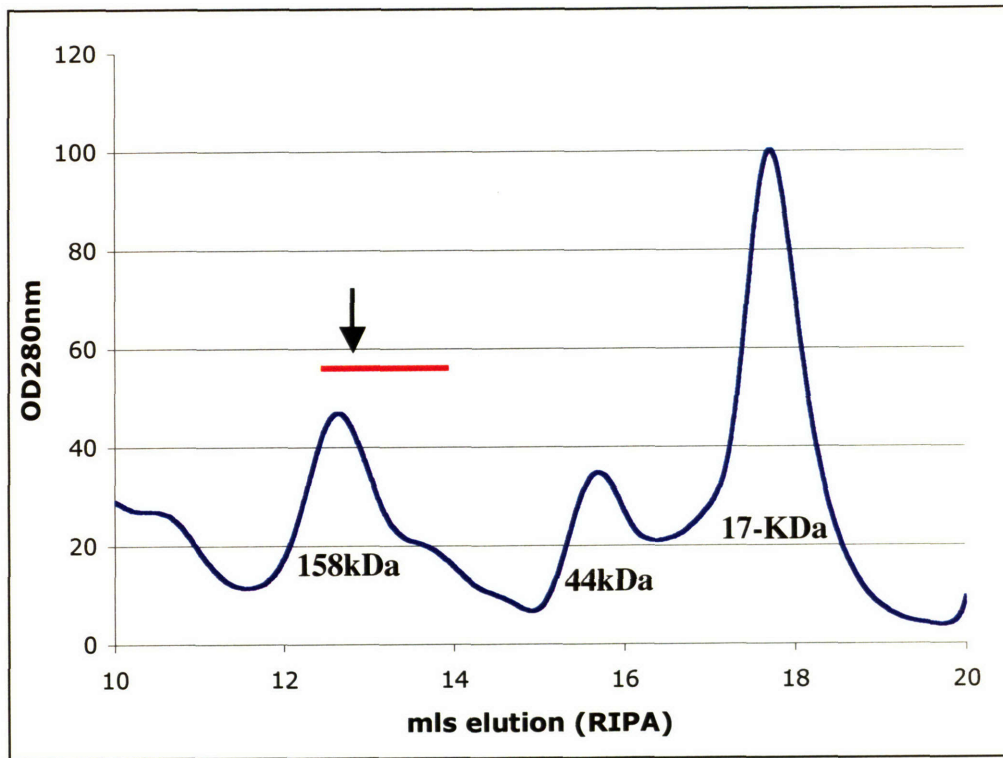
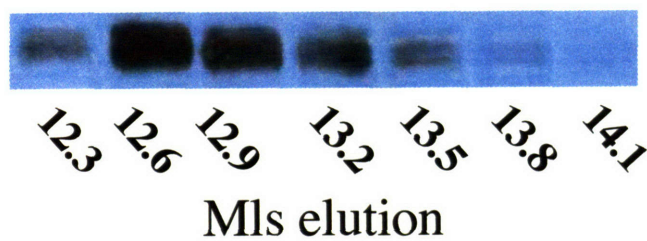
A**B**

Figure 5.3 Gel Filtration Analysis of CD9/RIPA Lysate: A) Transfected cells were lysed and cleared of particulates by centrifugation. This portion was loaded onto a Superdex200HR gel filtration column and fractions were collected every 0.3mls. Each fraction was analyzed by SDS-PAGE/Western analysis and protein was quantified by densitometry. Comparison to gel filtration standards analyzed in RIPA buffer gave an apparent molecular weight for the CD9 peak of 130-kDa. CD9 eluted over the range indicated by a red line. Maximal protein elution is indicated by the arrow. B) Western blot analysis of CD9 at various eluting fractions.

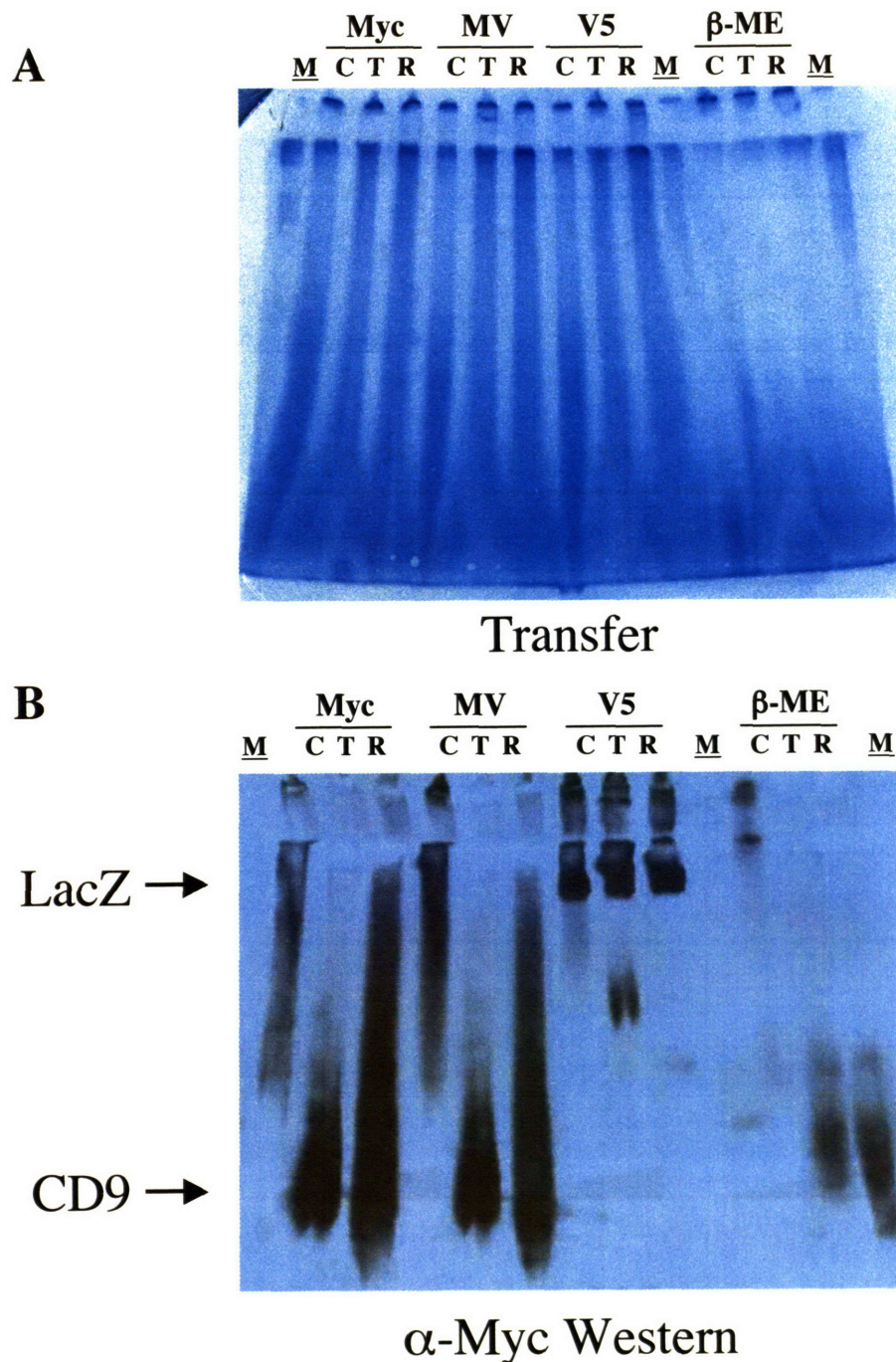


Figure 5.4 Native Blue-Electrophoresis: A) Picture of a transferred native-blue electrophoresis gel after transfer to nitrocellulose. M = marker; C = CHAPS; T = TX-100; R = RIPA. Lanes are presented in sets of three, with transfections of either Myc (M), Myc and V5 cotransfected (MV) or V5 (V) indicated. Singly epitope-tag transfections include the complementary-tagged LacZ control. The triplet lanes with β-ME had beta-mercaptoethanol added to 10-% volume prior to loading. M in the first and last lane denotes molecular weight markers. B) Western blot analysis of native-blue gel with the same lane orientation as in A. The migration position of LacZ is indicated as are myc-tagged CD9 molecules.

A

DSP
M.W. 404.42
Spacer Arm 12.0 Å

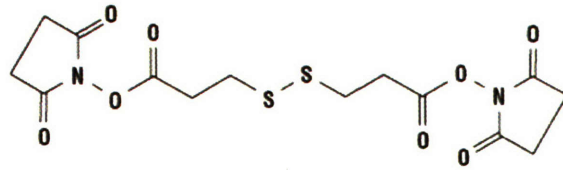
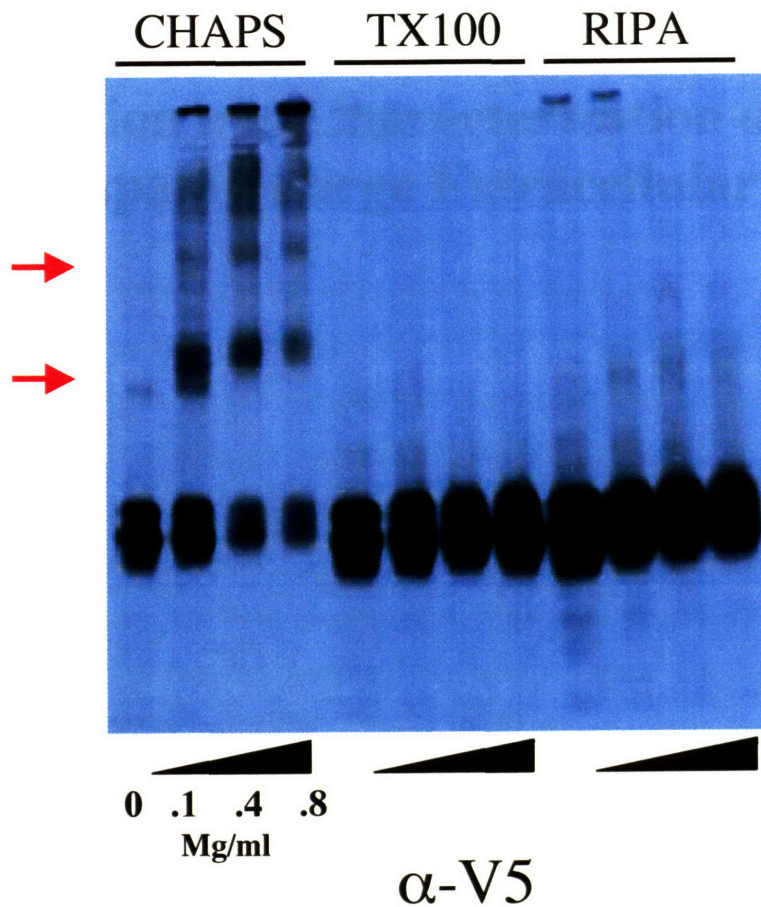
**B**

Figure 5.5 DSP Cross-linking of CD9: A) Chemical diagram of the bi-functional amine specific DSP cross-linker. B) Transfected cells expressing the V5/CD9 protein were lysed under varying detergent conditions. The concentration of DSP cross-linker is indicated below the Western blot with the negative control indicated in the leftmost lane. All samples were analyzed by 12% non-reducing SDS-PAGE/Western. Bands corresponding to a covalent dimer and trimer are indicated with red arrows to the left of the blot.

Chapter 6

Purification and Characterization of Human Tetraspanin Large Extracellular Loops

These experiments were conceived by Christopher C. Liu and Peter S. Kim. All experiments were carried out by Christopher C. Liu. All errors are my own.

Introduction:

We have described the biophysical, biochemical, and molecular analysis of the murine CD9-LEL. Our results with the large-extracellular loop in isolation have not completely translated into experiments with the intact molecule, indicating that other domains of the protein (short extracellular loop, transmembranes, palmitoylation) may contribute to the state of oligomerization of the murine CD9 protein (Charrin, Manie et al. 2002). Does our characterization of the mCD9-LEL as an α -helical dimer translate to other tetraspanin family members?

There are 28 mammalian tetraspanins, with many orthologues characterized in *Drosophila*, (Fradkin, Kamphorst et al. 2002) (Todres, Nardi et al. 2000) *C. elegans*, (Moribe, Yochem et al. 2004) and zebrafish (Maecker, Todd et al. 1997). Of this diverse family of genes, CD9 and CD81 represent two similar members with the simplest large-extracellular loops as determined by length, disulfide-bonding pattern, and glycosylation (Seigneuret, Delaguillaumie et al. 2001). More complex tetraspanin-LELs may contain six, seven, or even eight cysteine residues in this domain. Although widely expressed, there are several tetraspanin-family members that are both restricted in function and expression (Levy, Todd et al. 1998). Most notably, the uroplakins form a uroepithelial lining of the bladder and are essential for the maintenance of organellar plasticity (Wu, Lin et al. 1994). Uroplakins are expressed at such high concentrations on the bladder epithelium that they form two-dimensional lattices which are amenable to electron microscopic analysis (Min, Zhou et al. 2003).

By applying our methodology to more canonical tetraspanin family members, we explore the limits of our technology as applied to tetraspanin-LELs of greater complexity. As most tetraspanins (but not CD9 or CD81) have putative glycosylation sites in their respective large extracellular loops, what role does this have on the folding stability of the LELs? Do other tetraspanin-LELs have similar biophysical characteristics? May we develop an array of useful reagents to study the range of cellular functions in which tetraspanins are involved? Will these tetraspanin-LELs serve as functional controls in inhibition assays? With a panel of tetraspanin-LELs, we may also explore the possibility of tetraspanin-LEL-mediated hetero-oligomerization. This chapter describes the expansion of our methodology to the purification and characterization of human

tetraspanin-LELs.

Materials and methods:

Construction of human tetraspanin-LEL constructs:

Human tetraspanin cDNAs were kindly provided by Martin Hemler (Dana-Farber Cancer Institute, Harvard Medical School, Boston, MA). Oligonucleotide primers (Research Genetics) were designed to amplify the tetraspanin-LEL domain based upon the region predicted to lie between transmembrane 3 and transmembrane 4.

For cloning of the human CD9-LEL, we used

CL77: 5'-CGCTAGCTAGCTCCCACAAGGATGAGGTGATTAAGG-3'

CL78: 5'-CCGCTCGAGGTGGAATTTATTGTCGAAGACCTC-3'

For cloning of the human CD63-LEL, we used

CL87: 5'-CGCTAGCTAGCAGAGATAAGGTGATGTCAGAGTTTAATAAC-3'

CL88: 5'-CCGCTCGAGCACATTTTTTCCTCAGCCAGCCC-3'

For cloning of the human CD81-LEL, we used

CL85: 5'-CGCTAGCTAGCTTTGTCAACAAGGACCAGATCGCC-3'

CL86: 5'-CCGCTCGAGCTTCCCGGAGAAGAGGTCATCGATC-3'

For cloning of the human CD151-LEL, we used

CL79: 5'-CGCTAGCTAGCGCCTACTACCAGCAGCTGAACACGG-3'

CL80: 5'-CCGCTCGAGCCTCAGGTGCTCCTGGATGAAGGTC-3'

For cloning of the human CO-029-LEL, we used

CL127: 5'-CGCTAGCTAGCAAATCTAAGTCTGATCGC-3'

CL128: 5'-CCGCTCGAGATTTTTTGCCAAGAAGTC-3'

Human tetraspanin-LEL fragments were PCR-amplified and inserted between the *NheI* and *XhoI* restriction sites of the carboxy-terminal hexahistidine expression vector pET24a (Novagen). All resulting plasmids were sequenced to check for errors.

Plasmids were transformed into BL21/pLysS competent cells (Novagen) for protein expression as described previously (see Chapter 2). In brief, expressed proteins from inclusion bodies were solubilized in guanidine-HCl buffer and partially purified over Ni-NTA chromatography (Qiagen). The solubilized protein was then lowered to

pH2 and analyzed by reverse-phase C18 HPLC with protein content monitored as absorbance at 229nm.

Qualitative dot-blot Analysis and Purification of Human Tetraspanin-LELs:

HPLC-eluted protein peaks were collected and centrifuged under vacuum to remove the acetonitrile. For qualitative dot blots, 1 microliter of each peak was added to dry nitrocellulose membrane and air-dried. Membranes were blocked for 2 hours at room temperature and the Westerns were developed by a standard protocol (see Chapter 2). Protein immunoreactivity was probed with the following mouse anti-human monoclonal antibodies (all from BD Pharmingen): mouse anti-human CD9 clone M-L13, mouse-anti-human CD63 clone H5C6, mouse anti-human CD81 clone JS-81, and mouse anti-human CD151 clone 14A2.H1 at 1:1000 dilutions.

Simulated Disulfide-Bond Shuffling:

For simulated disulfide-bond shuffling experiments, oxidized tetraspanin-LEL proteins in denaturing buffer (6M Guanidine-HCl, pH 8.0) were diluted 10-fold into PBS containing 2mM reduced glutathione/0.5mM oxidized glutathione. The glutathione-containing protein solution was mixed overnight, brought to pH 2.0 with 5% HOAc, clarified by filtration through a 0.2 μ M syringe filter, and loaded onto a reverse-phase HPLC under standard conditions. Observed peaks were analyzed as above.

Biophysical Analysis:

Purified, immunoreactive human tetraspanin-LEL species were monitored for helicity and thermal denaturation by circular dichroism as described in Chapter 2. All proteins were monitored at 10 μ M concentrations at 25°C. For thermal denaturation and renaturation profiles, proteins were heated in a step-wise fashion to 80°C before renaturation. When an antibody was unavailable, individual tetraspanin-LEL HPLC-purified protein peaks were lyophilized and monitored for helicity by circular dichroism. For oligomerization state analysis, human tetraspanin-LELs were loaded in PBS onto a Superdex200HR column as described in Chapter 4.

Heterodimer Experiments:

To probe for heterodimer formation, lyophilized tetraspanin-LELs were resuspended in PBS and mixed individually and together to a final concentration of 10 μ M each. Samples were heated in a Stratagene Robocycler PCR machine (Stratagene) to 75°C for 10 minutes and allowed to gradually cool to room temperature. Protein samples were analyzed using a PhastGel automated electrophoresis system (Amersham Pharmacia) with precast pH 3-9 isoelectric focusing (IEF) gels (Amersham Pharmacia) with IEF standards (Amersham Pharmacia). Coomassie Brilliant Blue was used to develop IEG gels by standard techniques.

Results:

Expression of Human Tetraspanin-LEL Proteins

Previously, we had cloned and sequenced full-length human tetraspanin cDNAs into the retroviral expression vector pMig (data not shown) (Liu, Constantinescu et al. 2000). Tetraspanin-LELs were subcloned into the pET24a vector and protein expression was induced and partially purified using nickel chromatography. Protein expression and purity were monitored by 18% SDS-PAGE under non-reducing conditions (Figure 6.1). As expected, each tetraspanin-LEL was purified as a ladder of covalently disulfide-bonded species. The uniform migration pattern of each oligomer is typical of non-glycosylated proteins. Varying quantities of purified protein and ratios between individual oligomers were also observed, with the human CD81-LEL protein exhibiting very few contaminating bands. HPLC-purified hCD9-LEL was loaded onto the gel as a molecular weight comparison. Empirically, tetraspanin-LELs tend to migrate faster than their predicted molecular weights, consistent with published observations (Kovalenko, Yang et al. 2004). However, the observed migratory patterns of tetraspanin-LELs, relative to one another was as expected. The hCD151-LEL, hCD63-LEL, and hCO-029-LELs all contain six cysteines and are greater in length than either hCD9-LEL or hCD81-LEL.

Purification and Characterization of Four-Cysteine Containing Tetraspanin-LEL Proteins

Due to high sequence identity between the murine CD9-LEL and the human CD9-LEL, we concentrated our initial efforts on the hCD9-LEL. As expected, the hCD9-LEL had a similar protein elution profile over C18 reverse-phase HPLC as the mCD9-LEL protein (Figure 6.2A). By dot blot analysis, immunogenicity of an antibody directed against the hCD9-LEL protein was also restricted to a single HPLC peak, clearly distinguishable from other isomers (Figure 6.2B). This antibody had no cross-reactivity to other tetraspanin-LEL species. Circular dichroism analysis characterized the hCD9-LEL protein as a α -helical dimer (Figure 6.3A). Monitoring the circular dichroism signal of the hCD9-LEL protein over a range of temperatures revealed that this protein is

autonomously folding. A midpoint of thermal denaturation was measured at 60°C, indicative of a stably folded protein (Figure 6.3B).

The human CD81-LEL was readily purified and crystallized as a glutathione-S-transferase fusion protein by the Bolognesi group (Kitadokoro, Bordo et al. 2001). In *E. coli*, we expressed and partially purified significant quantities of the hCD81-LEL protein (Figure 6.4A). Separation of hCD81-LEL species over C18-reverse phase HPLC resulted in a significantly different elution profile from hCD9-LEL. Furthermore, hCD81-LEL species eluted at much higher concentrations of organic buffer, suggestive of a greater overall hydrophobic content.

Given the success of our anti-hCD9 antibody to recognize specific, well-folded HPLC peaks, we developed a novel, rapid assay to assess the immunogenicity of various tetraspanin-LEL peaks using dot blot analysis. Our analysis of hCD81-LEL variants revealed that the second, not the first, C18 resolvable peak was recognized by our antibody (Figure 6.4A). Unfortunately, it was not feasible to purify biochemical quantities of hCD81-LEL both due to the cross-contamination from the first (non-immunoreactive) eluting peak and low protein yield.

To resolve these problems, we turned to the disulfide-shuffling experiments previously described in Chapter 2. A rapid screen of reduced and oxidized glutathione conditions directed us to a redox mix of 2mM reduced glutathione/0.5mM oxidized glutathione. By diluting randomly oxidized hCD81-LEL protein (with an elution profile as in Figure 6.4A), we dramatically changed the protein content of individual hCD81-LEL isomers (Figure 6.4B). After disulfide shuffling, we saw five individual resolvable protein peaks. The major peak, hCD81-LEL P3, was immunogenic and clearly resolved from contaminating, non-immunoreactive hCD81-LEL isomers. Biophysical analysis of this immunoreactive hCD81-LEL species revealed that it was also a α -helical dimer (Figure 6.5A and Figure 6.5B).

Purification and Characterization of Six Cysteine-Containing Tetraspanin-LEL Proteins

The human CD63 protein is glycosylated and contains six cysteines forming three disulfide-bonds (Hotta, Ross et al. 1988). Separation of randomly-oxidized hCD63-LEL

isomers over C18-reverse phase HPLC revealed multiple peaks. Unfortunately, none of these peaks were immunoreactive to an α -hCD63 antibody (Figure 6.6A). Disulfide shuffling under similar conditions to the hCD81-LEL protein resulted in significant repositioning of hCD63-LEL peaks. Surprisingly, there was a dramatic shift of all peaks to elution at a higher organic solvent concentration. The most prominent of these peaks was immunoreactive by dot-blot analysis (Figure 6.6B), although there are presumed to be several minor, contaminating hCD63-LEL variants. Biophysical analysis of the immunoreactive hCD63-LEL protein was shown to be an α -helical dimer (Figure 6.7A). Monitoring the circular dichroism signal of the hCD9-LEL protein over a range of temperatures revealed that this protein is autonomously folding. The midpoint of thermal denaturation was measured at 64°C, slightly higher than the hCD9-LEL. There also appeared to be increased cooperativity of folding (relative to hCD9-LEL) and incubation at 80°C resulted in loss of some native-like structure (Figure 6.7B).

We also attempted to purify two different tetraspanin-LELs; the hCD151-LEL and the hCO-029-LEL (Horejsi and Vlcek 1991). Although we also had an antibody for the hCD151-LEL, we were unable to isolate an immunoreactive hCD151-LEL species (Figure 6.8A), even after extensive disulfide-shuffling experiments (Figure 6.8B). Disulfide shuffling of the hCD151-LEL protein also resulted in a shifting of the protein elution profile to higher organic solvent conditions. Irregularities in the HPLC trace are due to nonideal HPLC performance. We did not have an antibody towards the hCO-029 protein. Random oxidation of the hCO-029 protein yielded a daunting number of resolvable peaks (Figure 6.9A). Disulfide shuffling lowered the number of protein peaks and shifted resolvable proteins to more aqueous elution conditions (Figure 6.9B). Although we attempted to purify some hCD151-LEL and hCO-029-LEL species and assessed their “native-like” conformation by circular dichroism spectroscopy, we were unable to identify species that exhibited a α -helical structure (data not shown).

Heterodimer Formation of Tetraspanin-LEL Proteins

Our biophysical analysis of human tetraspanin-LELs indicates that each of our purified proteins is autonomously folding. These proteins are denatured at high temperatures and can spontaneously regain native-like α -helicity if the temperature is

lowered. Our thermal denaturation and renaturation analyses allow empirical determination of the thermal limits of tetraspanin-LEL refolding. For example, when the murine CD9-LEL is denatured to 100°C it will not spontaneously renature. These results are not surprising as under the circular dichroism conditions tested, the murine CD9 is thermally denatured for approximately 1 hour.

Our thermal denaturation profile indicates that heating tetraspanin-LELs to 75°C for 10 minutes does not restrict the reattainment of native α -helicity. As a result, we mixed CD9 and CD81 individually and in pairs at RT, thermally denatured the proteins, and allowed spontaneous renaturation. Complex formation was analyzed under native conditions by isoelectric focusing electrophoresis.

As expected, individual human CD9-LEL and CD81-LEL proteins focused as single bands. When the CD9-LEL and CD81-LEL were mixed, denatured, and renatured, we observed no novel bands (data not shown). We would expect a heterodimer to both focus to an intermediate pI and also to decrease the intensity of individual CD9-LEL and CD81-LEL focused bands. This experiment suggests that the CD9-LEL and CD81-LEL, which are phylogenetically similar tetraspanin-LELs, do not preferentially form heterodimers.

Discussion:

In this chapter, we describe our experiments to purify three human tetraspanin-LELs: hCD9-LEL, hCD63-LEL, and hCD81-LEL. These three proteins were all stable, autonomously folding, α -helical and dimeric in nature. Although we successfully expressed and partially purified the hCD151-LEL and hCO-029-LEL proteins, we were unable to purify a α -helical form of these proteins, suggesting that these nickel-purified proteins were not well folded.

Our biophysical characterization of three distinct tetraspanin-LELs strongly suggests that a conserved α -helical, dimeric sub-domain is conserved. Biophysical analysis of the folding stability of the hCD9-LEL, hCD81-LEL, and hCD63-LEL revealed that each is approximately equal in thermal stability. The denaturation and renaturation profiles of hCD81-LEL were particularly striking. Among all three tetraspanin-LELs characterized, it exhibited the most cooperativity of folding, with almost no loss of secondary structure before unfolding. This observation is consistent with high yields of the hCD81-LEL protein relative to the hCD9-LEL and hCD63-LEL.

Our methodology is not readily applicable to tetraspanin-LELs of greater complexity. There are many potential reasons for this. The CD9 and CD81 large extracellular loops are some of the simplest tetraspanin-LELs both in length and in number of disulfide connectivities. Our ability to isolate an α -helical, dimeric version of the CD63-LEL, which has three disulfide bonds, is encouraging, although we were not able to expand this methodology to the CD151-LEL, which is of comparable length and complexity to the CD63-LEL. Another reason for this deficit may be a critical contribution of glycosylation to the folding of tetraspanin-LELs. The length of the short extracellular loops (SELs) of all tetraspanins is conserved among all tetraspanins (Seigneuret, Delaguillaumie et al. 2001). Although we surmise that the SEL most likely does not contribute to the folding stability of the tetraspanin-LEL, this hypothesis can not be dismissed. We speculate that the success of our methodology with the CD9-LEL, CD81-LEL, and CD63-LEL may be expanded to closely related tetraspanin-LELs, but not to tetraspanin-LELs with sequence similarity to either the CD151-LEL or the CO-029-LEL proteins (for tetraspanin-LEL phylogeny, see Chapter 1).

Other prokaryotic expression systems have been used to study tetraspanin-LELs. Peter Monk's group has reported the purification of a panel of tetraspanin-LELs fused to glutathione-S-transferase. They report successful purification of the hCD9-LEL (Barreiro, Yanez-Mo et al. 2005), hCD81-LEL (Flint, Maidens et al. 1999), and surprisingly, the hCD151-LEL (Peter Monk, personal communication). However, attempts to express and purify the hCD63-LEL did not yield sufficient material (Peter Monk, personal communication). These proteins were affinity purified over a glutathione column and the presence of a large carrier protein precluded further analysis. By SDS-PAGE, contaminating protein or proteolytic degradation was evident (Higginbottom, Takahashi et al. 2003).

Currently, we are collaborating with Peter Monk to crystallize both the hCD9-LEL and the hCD63-LEL proteins. Initial trials with the hCD9-LEL protein have not yielded well-ordered protein crystals, consistent with our results in Chapter 3. Crystal trials with the hCD63-LEL (which would yield the first structural insight into a tetraspanin-LEL with three disulfide-bonds) are currently in progress.

If the lack of glycosylation precludes tetraspanin-folding, it will be necessary to use eukaryotic expression systems to express tetraspanin-LELs. Unfortunately, an attempt to express and purify the hCD9-LEL in S2 insect cells did not readily yield protein expression (Jack Lawler, personal communication). There are no published attempts to express tetraspanin-LELs in glycosylation-permissive eukaryotic systems.

There were multiple motivations to expand out methodology to other tetraspanin-LEL family members. One motivation was to search for heterodimers. Our observation that the murine CD9-LEL is a α -helical dimer, coupled with strong sequence conservation among tetraspanin-LELs, suggested the possibility of heterodimers. However, our experimental analysis of the human CD9-LEL and the human CD81-LEL did not corroborate this hypothesis. These results are consistent with the published literature (Charrin, Manie et al. 2002; Charrin, Manie et al. 2003). By immunoprecipitation, tetraspanins have only been observed to co-IP under mild (less stringent than TX-100) detergent conditions, suggesting that heterodimerization does not occur (Rubinstein, Le Naour et al. 1996).

Although it is imperative that we do not overinterpret our data, we believe that without biophysical and biochemical analysis of tetraspanin-LELs, results with these reagents may be difficult to interpret. Our ability to express tetraspanin-LELs that are clearly misfolded (and by analogy, nonfunctional) emphasize the difficulties in purifying tetraspanin-LEL reagents. In the remainder of this thesis, we describe experiments with our panel of folded, native-like tetraspanin-LELs in a variety of cellular assays.

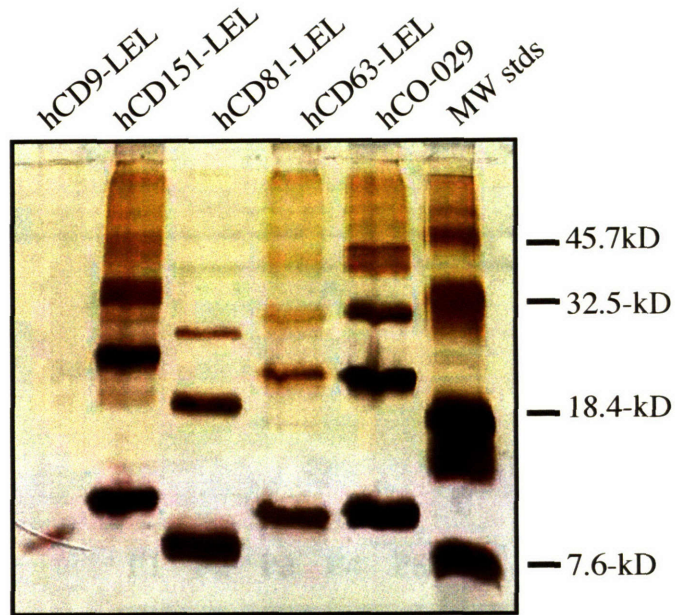


Figure 6.1 Expression and Partial Purification of Human Tetraspanin-LELs. Human-tetraspanin LELs (defined as the region between predicted transmembrane 3 and transmembrane 4 from the reference sequence) were cloned into the pET24a Histag expression vector in a similar way to the mCD9-LEL and verified by sequencing. Large-scale batches of protein were expressed in *E. Coli* and partially purified over Ni-NTA agarose as described in Chapter 2. These partially purified proteins were analyzed over 18% SDS-PAGE under non-reducing conditions, followed by silver staining. The tetraspanin name is labeled above each lane. With the hCD9-LEL, reverse-phase HPLC purified protein was loaded onto the gel as a molecular weight reference. Molecular weight standards are also included in the right-most lane. Differences between the molecular weight of the human tetraspanin-LELs correspond roughly to the predicted molecular weight of the molecule and roughly represent the complexity (length) of the respective tetraspanin-LELs. These partially purified protein fractions were utilized for subsequent purification procedures.

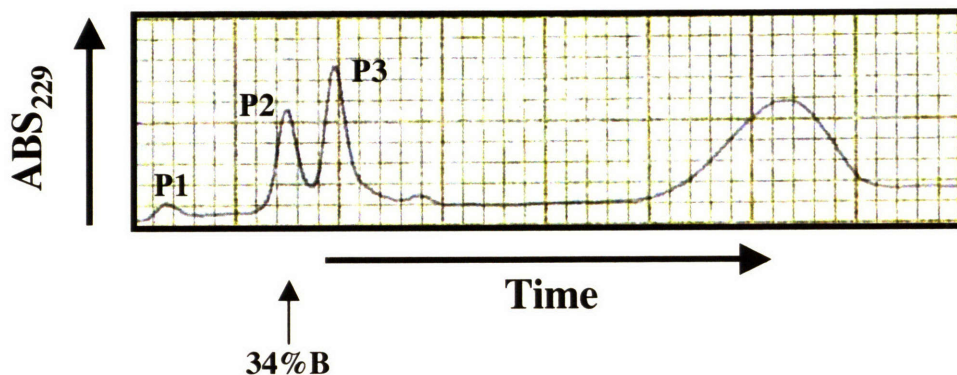
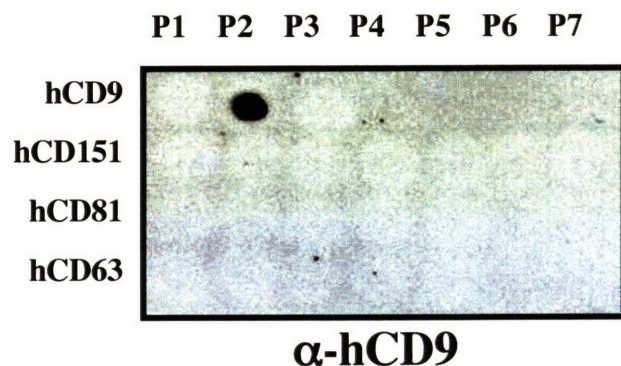
A**CD9 Random Oxidation Profile****B**

Figure 6.2 Purification of the Human CD9-LEL. A) Partially purified hCD9-LEL was resolved into individual peaks using reverse-phase C18 chromatography as described in Chapter 2. Protein content was continuously monitored at absorbance 229nm and the approximate concentration of buffer B (90%acetonitrile/10%H₂O/.1%TFA) is indicated below the trace. Protein peaks that were chosen for further study are labeled as P1, P2, etc.. B) Qualitative dot blot analysis was used to screen multiple tetraspanin-LEL peaks. In brief, protein eluted from the reverse-phase C18 column was centrifuged under vacuum to remove acetonitrile and 1 μ l was applied to dry nitrocellulose. The nitrocellulose was blocked with 4% BSA and treated as a standard Western. The peak identity(from 6.1B) is denoted above the dot blot and the molecule is denoted to the left. The Western was developed using anti-hCD9. Note that the anti-hCD9 antibody recognizes only hCD9P2, with minimal cross-reactivity both to other hCD9 peaks and also to other tetraspanin-LELs.

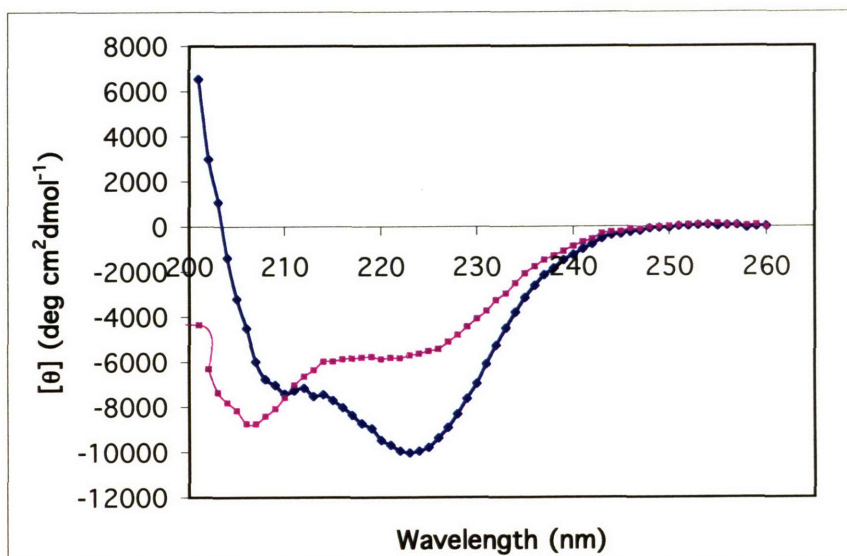
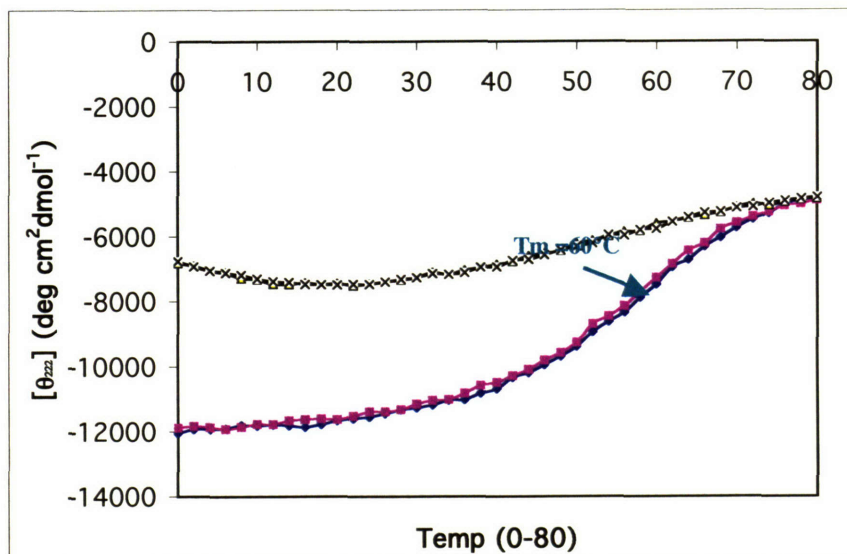
A**Circular Dichroism Wavelength Scan of hCD9-LEL-P1 and hCD9-LEL-P2****B****Thermal Denaturation/Renaturation of hCD9-LEL-P1 and hCD9-LEL-P2**

Figure 6.3 Biophysical Characterization of the Human CD9-LEL: A) Large quantities of the immunoreactive hCD9-LEL-P1 and non-immunoreactive hCD9-LEL-P2 (see Figure 6.2) were purified as described previously. Circular dichroism spectra were collected under standard conditions and revealed a spectral minima at 222nm, indicative of a well folded α -helical structure. The spectrum profile of hCD9-LEL-P1 is charted in blue and the profile of hCD9-LEL-P2 is pink. B) The thermal stability of the human CD9-LEL variants was monitored by tracking the circular dichroism signal of the proteins at 222nm as described in Chapter 2. The thermal denaturation profile for hCD9-LEL-P1 is charted in blue and the renaturation profile is charted in pink. The midpoint of thermal denaturation is indicated.

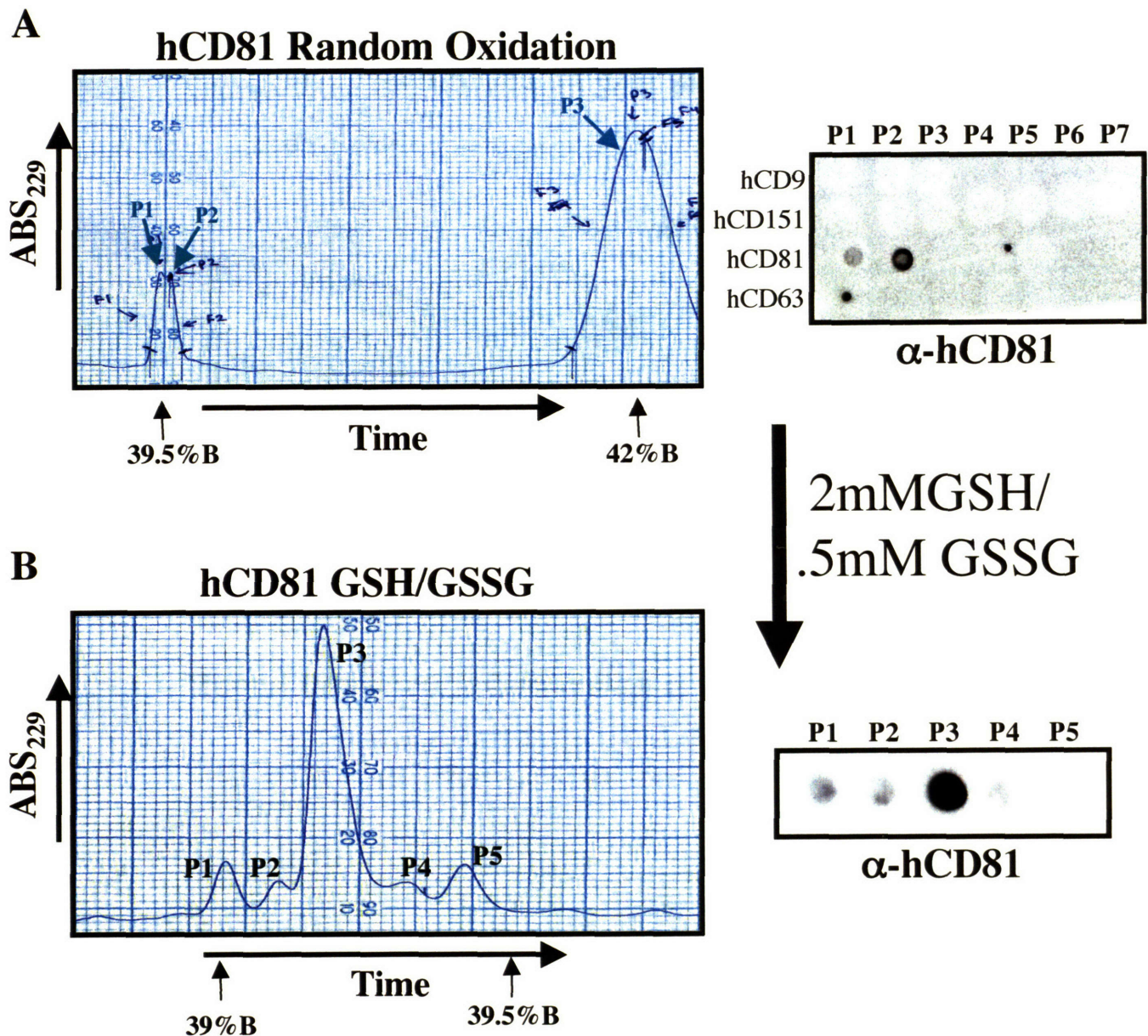


Figure 6.4 Purification of the Human CD81-LEL. A) Partially purified hCD81-LEL (see Figure 6.1) was resolved into individual peaks using reverse-phase C18 chromatography as described in Chapter 2. Protein content was continuously monitored at absorbance 229nm and the approximate concentration of buffer B (90%acetonitrile/10%H₂O/.1%TFA) is indicated below the trace. Protein peaks that were chosen for further study are labeled as P1 through P5, with P4 and P5 not shown on the HPLC trace. Qualitative dot blot analysis surprisingly revealed strong immunoreactivity in the hCD81-LEL P2, with a minor immunoreactivity from the hCD81-LEL P1, presumably through cross-contamination of collected fractions. B) An oxidized/reduced glutathione mix was used to shuffle the disulfide-bonds in hCD81-LEL. In brief, oxidized, denatured, partially-purified hCD81-LEL was rapidly diluted ten-fold into phosphate-buffered-saline containing freshly dissolved 2mM reduced glutathione and .5mM oxidized glutathione. After an overnight incubation at RT, the protein solution was clarified by both centrifugation and filtration, and analyzed by reverse-phase C18 HPLC as above. The resulting protein peaks eluted with a significantly different protein elution profile. Qualitative dot blot revealed that the the most abundant protein species (P3) was immunoreactive.

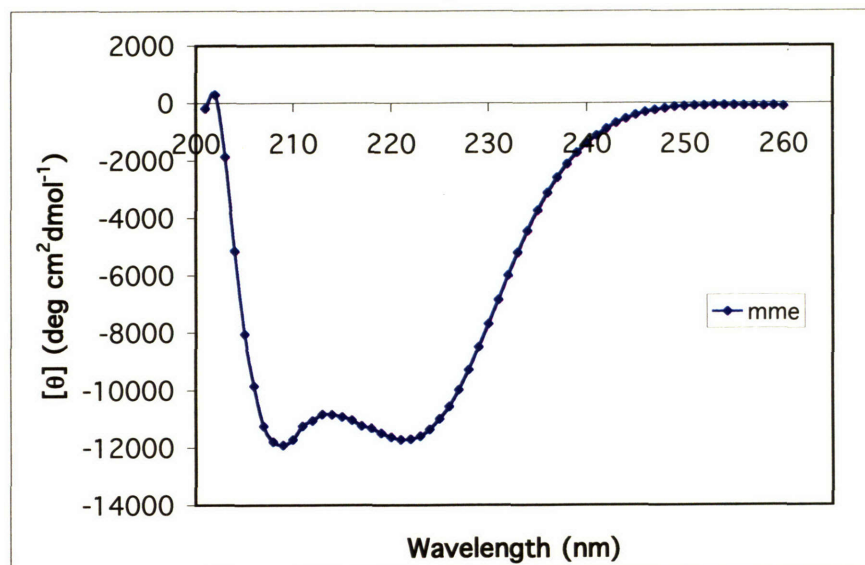
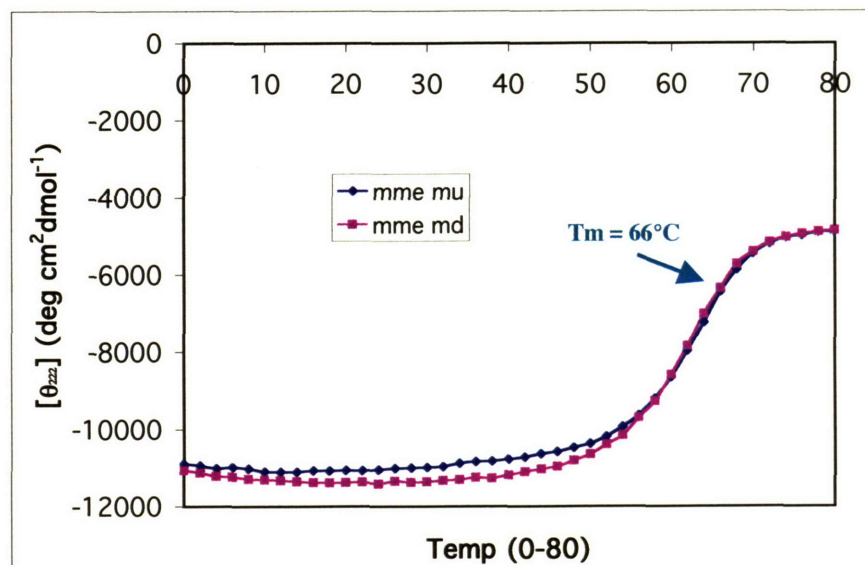
A**Circular Dichroism Wavelength Scan of hCD81-LEL-P3****B****Thermal Denaturation/Renaturation of hCD81-LEL-P3**

Figure 6.5 Biophysical Characterization of the Human CD81-LEL: A) Large quantities of the immunoreactive human CD81-LEL P3 (see Figure 6.4B) were purified as described previously. Circular dichroism spectrum was collected under standard conditions and revealed a spectral minimum at 222nm, indicative of a well folded α -helical structure. B) The thermal stability of the human CD81-LEL protein was monitored by tracking the circular dichroism signal of the tetraspanin-LEL at 222nm as described in Chapter 2. The thermal denaturation profile is charted in blue and the renaturation profile is charted in pink. The midpoint of thermal denaturation is indicated.

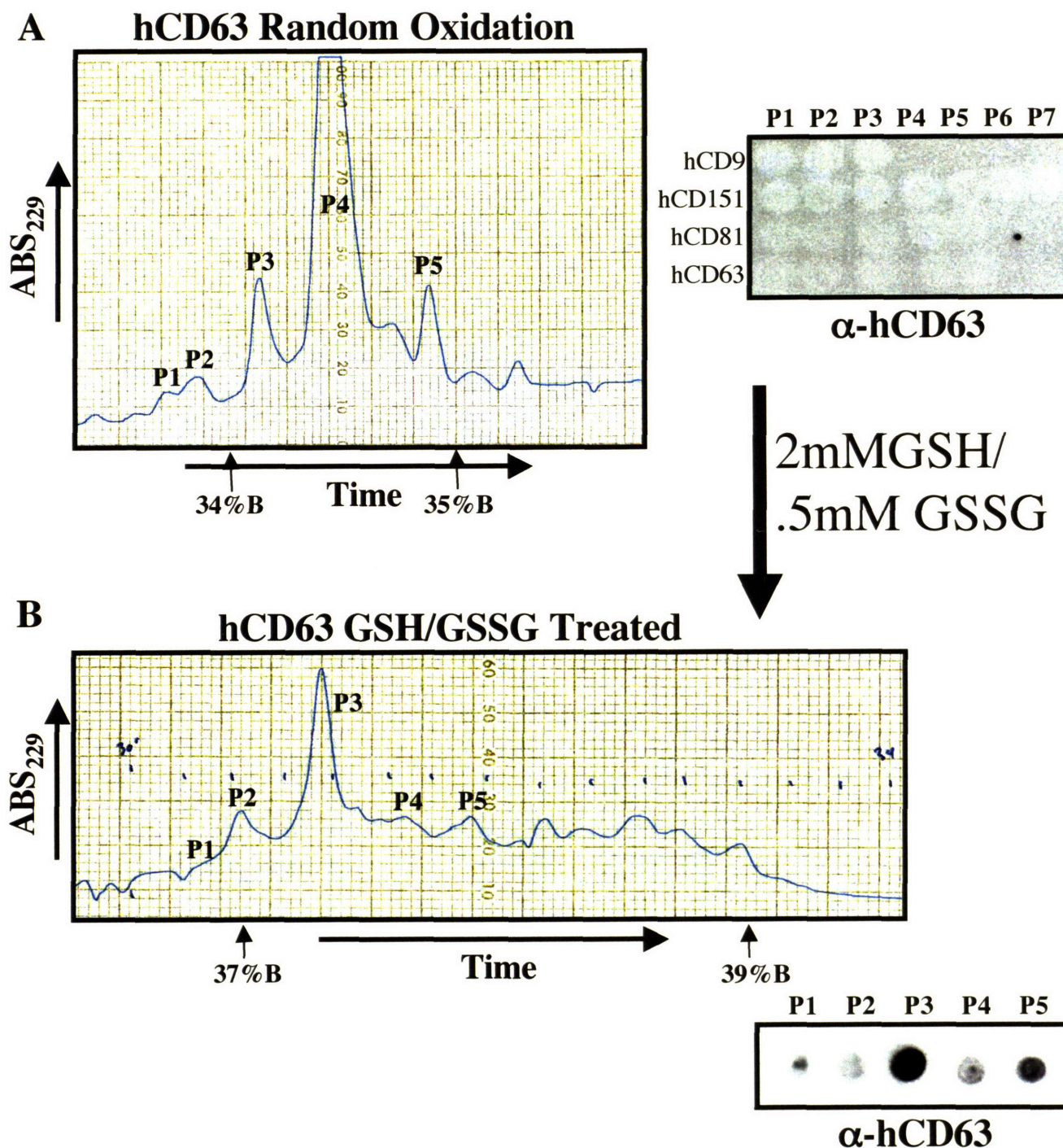


Figure 6.6 Purification of Human CD63-LEL. A) Partially purified hCD63-LEL (see Figure 6.1) was resolved into individual peaks using reverse-phase C18 chromatography as described in Chapter 2. Protein content was continuously monitored at absorbance 229nm and the approximate concentration of buffer B (90%acetonitrile/10%H₂O/.1%TFA) is indicated below the trace. Protein peaks that were chosen for further study are labeled as P1 through P5, with P4 off-scale. Qualitative dot blot analysis revealed no immunoreactivity in any of these protein peaks. B) Simulated refolding with an oxidized/reduced glutathione mix (as in Figure 6.4B) resulted in a significantly different protein elution profile, with protein peaks eluting at much higher concentrations of buffer B (indicated below the trace). Qualitative dot blot revealed that the the most abundant protein species (P3) was immunoreactive.

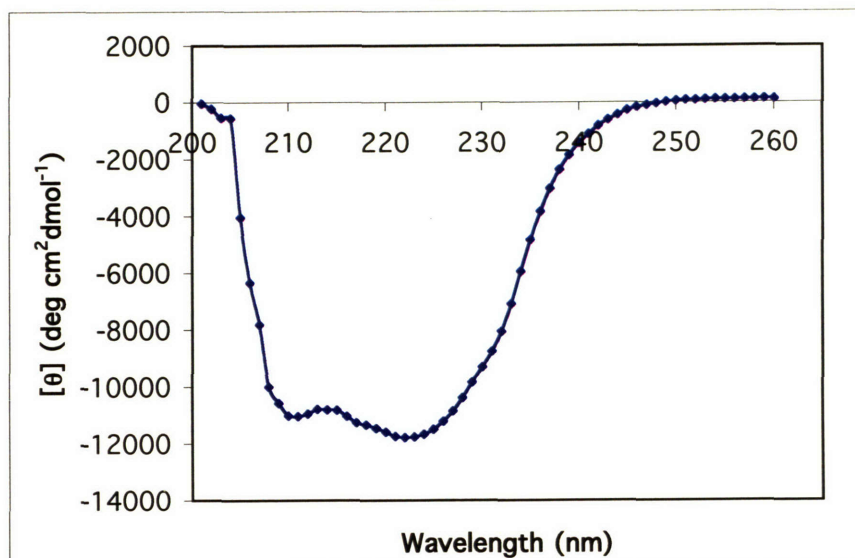
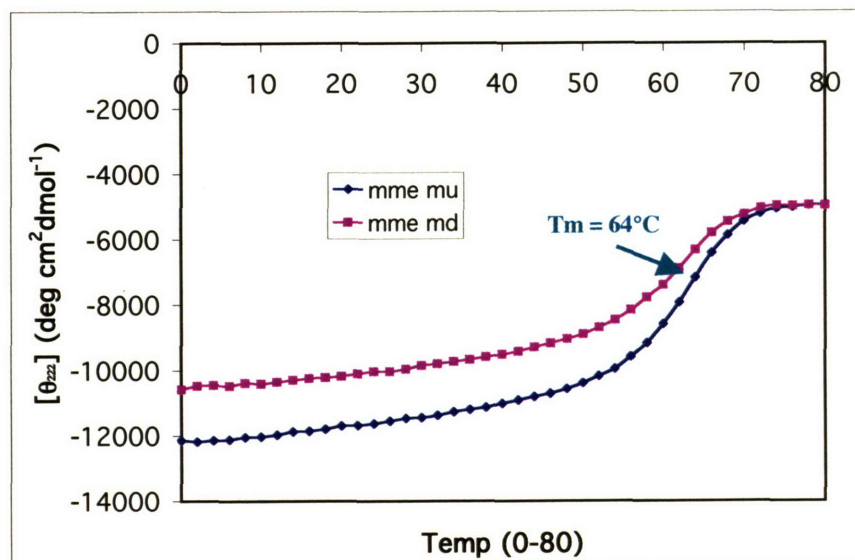
A**Circular Dichroism Wavelength Scan of hCD63-LEL-P3****B****Thermal Denaturation/Renaturation of hCD63-LEL-P3**

Figure 6.7: Biophysical Characterization of the Human CD63-LEL: A) Large quantities of the immunoreactive human CD63-LEL P3 (see Figure 6.6B) were purified as described previously. Circular dichroism spectrum was collected under standard conditions and revealed a spectral minimum at 222nm, indicative of a well folded α -helical structure. B) The thermal stability of the human CD63-LEL variants was monitored by tracking the circular dichroism signal of the tetraspanin-LEL at 222nm as described in Chapter 2. The thermal denaturation profile is charted in blue and the renaturation profile is charted in pink. The midpoint of thermal denaturation is indicated.

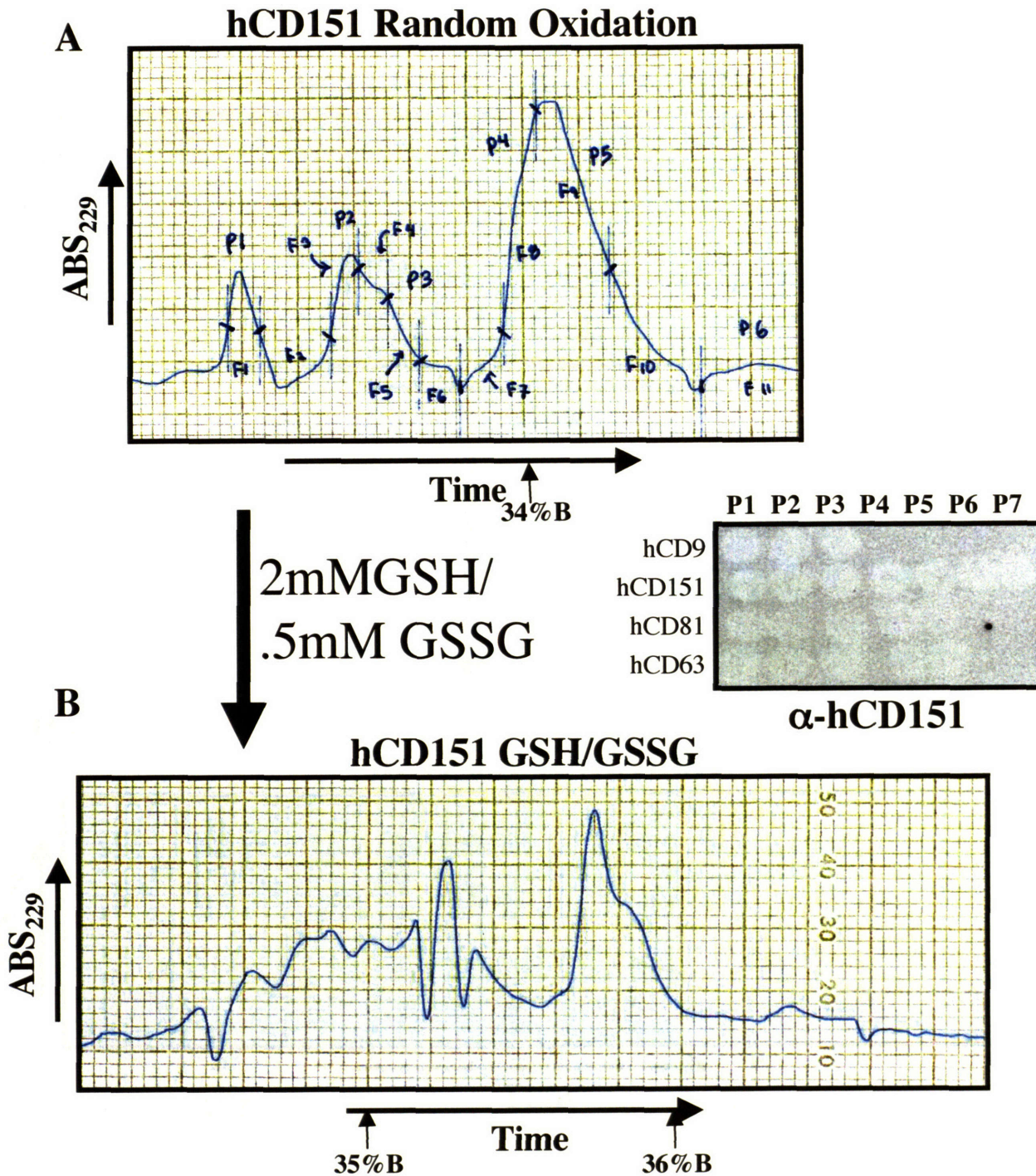


Figure 6.8 Analysis of the hCD151-LEL. A) Partially purified human CD151-LEL (see Figure 6.1) was resolved into individual peaks using reverse-phase C18 chromatography as described in Chapter 2. Protein content was continuously monitored at absorbance 229nm and the approximate concentration of buffer B (90%acetonitrile/10%H₂O/.1%TFA) is indicated below the trace. Protein peaks that were chosen for further study are labeled as P1 through P7, with P7 not shown on the HPLC trace. Qualitative dot blot analysis revealed no immunoreactivity in any of the 7 peaks. B) Simulated refolding with an oxidized/reduced glutathione mix resulted in significant shifts of protein peaks relative to randomly oxidized human CD151-LEL. However, there were still no detected immunoreactivity of the peaks, despite prolonged exposure (data not shown).

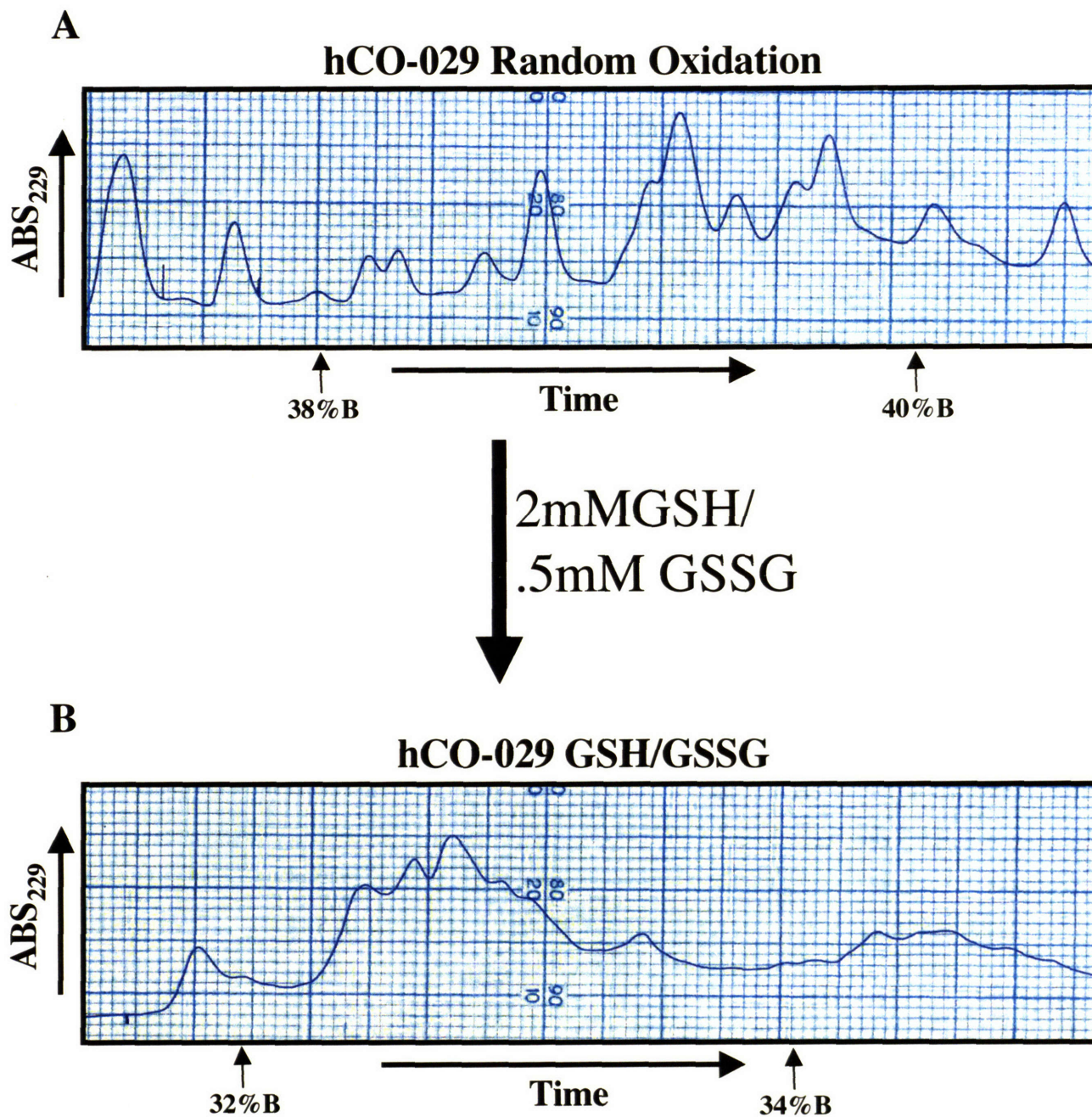


Figure 6.9 Analysis of the hCO-029 LEL. A) Partially purified human CO-029-LEL (see Figure 6.1) was resolved into individual peaks using reverse-phase C18 chromatography as described in Chapter 2. Protein content was continuously monitored at absorbance 229nm and the approximate concentration of buffer B (90%acetonitrile/10%H₂O/.1%TFA) is indicated below the trace. B) Simulated refolding with an oxidized/reduced glutathione mix resulted in significant shifts of protein peaks relative to randomly oxidized human CO-029-LEL (above). As there were no clearly resolvable peaks, this protein was not pursued further.

Chapter 7

The Role of Tetraspanins in Cell-Cell Fusion

The majority of these experiments were conceived by Christopher C. Liu, Richard O. Hynes and Peter S. Kim. CD9 inhibition of sperm-egg fusion experiments was conceived in collaboration with Guo-Zhang Zhu and Paul Primakoff. Inhibition studies of *in vitro* fertilization experiments were carried out by Guo-Zhang Zhu. Macrophage fusion experiments were conceived and carried out by Partha Varadarajan and Peter Monk. We thank Arjan van der Flier for technical assistance with myoblast fusion assays. All other experiments were carried out by Christopher C. Liu. All errors are my own.

Introduction:

Our primary interest in studying the murine tetraspanin CD9 was to use our knowledge of CD9 as a means to study mammalian sperm-egg fusion. Sperm-egg binding and fusion is the first developmental step in the creation of a new organism (Stein, Primakoff et al. 2004). Although this phenomenon has been observed to occur for well over a century, the molecular mechanisms underlying this critical developmental step have not been clearly elucidated.

For the past two decades, panels of monoclonal antibodies have functionally implicated many genes in the sperm-egg binding and fusion event (Primakoff and Myles 1983). This list most notably includes ADAM1 and ADAM2: proteins on sperm which bind to their integrin receptor partners on the egg (Myles, Kimmel et al. 1994). Antibodies against ADAM1 inhibit sperm-egg binding and fusion (Primakoff, Hyatt et al. 1987). Unexpectedly, targeted deletion of the ADAM 2 gene had no effect on sperm-egg fusion (Cho, Bunch et al. 1998) (Figure 7.1). Equally surprising, targeted deletion of the murine CD9 gene results in almost a complete ablation of sperm-egg fusion, with no effect on sperm-egg binding (Kaji, Oda et al. 2000; Le Naour, Rubinstein et al. 2000; Miyado, Yamada et al. 2000).

CD9 is expressed on oocytes (Le Naour, Rubinstein et al. 2000). Although there is also strong expression of CD9 on platelets, monocytes, and pre B cells (Clay, Rubinstein et al. 2001) (Miao, Vasile et al. 2001), CD9-null mice did not exhibit strong phenotypes in these cell types. Strikingly, CD9-null females were almost (but not completely) incapable of offspring. Studies showed that this effect was due not to a defect in sperm-migration up the female reproductive tract (as was seen with ADAM1 null-mice) or to sperm-zona pellucida interactions. Furthermore, in *in vitro* fertilization studies, sperm could bind to zona-stripped oocytes at wild-type levels. However, deletion of the CD9-gene resulted in almost no penetration of the oocyte membrane by sperm, as assessed by exit from M2 arrest and second polar body extrusion (Kaji, Oda et al. 2000). Lastly, intracytoplasmic sperm injection (ICSI) of CD9-null oocytes (bypassing the membrane fusion event) resulted in normal initiation of development (Miyado, Yamada et al. 2000).

Exogenous addition of a rat monoclonal anti-murine CD9 antibody, clone KMC8, was previously shown to effectively inhibit sperm-egg fusion, with no effect on binding in an *in vitro* fertilization assay (Chen, Tung et al. 1999; Miller, Georges-Labouesse et al. 2000). These antibody-inhibition experiments served to direct our studies to the extracellular domain of CD9, specifically the large extracellular loop (LEL). In collaboration with Paul Primakoff's laboratory (UCDavis), we tested the efficacy of our mCD9-LEL mimics in *in vitro* fertilization assays (Zhu, Miller et al. 2002). The full reprint of our studies is included in Appendix A.

Here, we also describe our attempts to expand on the fertilization inhibition studies by isolating and identifying CD9 binding partners on the oocyte. To overcome the critical biochemical limitations to the gamete-fusion model we explore a previously described role for CD9 in a myoblast fusion system (Tachibana and Hemler 1999). Currently, we do not believe the inhibition of CD9 and CD81 on the myoblast fusion system is replicable. Lastly, we describe experiments on the role of CD63 in another homotypic cell-cell fusion assay: foreign-body-induced macrophage fusion (Takeda, Tachibana et al. 2003). This series of experiments not only explore the role of tetraspanin-LELs in cell-cell fusion, but also suggest that our recombinant, soluble tetraspanin-LELs serve to disrupt endogenous tetraspanin functions.

Materials and methods

***In vitro* Fertilization Assay:**

Gametes from CD9 wild-type and null mice were collected (Zhu, Miller et al. 2002) as described in Appendix A. In brief, sperm was collected from the caudal epididymis and allowed to capacitate prior to *in vitro* fertilization. Oocytes were collected from the oviducts of super-ovulated females and cumulus cells and the zona-pellucida coat were enzymatically removed. Eggs were visually inspected for maintenance of M2 arrest. The GST-CD9-LEL was constructed and purified using standards methods as described in the appendix. Our mCD9-LEL protein was purified and characterized as described in Chapter 2. The GST-CD9-LEL and mCD9-LEL were incubated with individual gametes at 300 μ g/ml and 250 μ g/ml respectively for 3 hours. The complementary gamete was then added for a 40 minute insemination period and fertilization indices were quantified by microscopy.

For CD9-rescue of fertilization-incompetent CD9-null oocytes, CD9-null oocytes were collected as described above. Plasmids containing either the full-length murine CD9 wild-type or murine CD9 variant cDNAs fused to green fluorescent protein were linearized and mRNAs were synthesized by *in vitro* transcription. Each CD9-null oocyte was microinjected with 30pg of mRNA and allowed to express the CD9 wild-type or CD9 variant protein for 28 hours prior to *in vitro* fertilization assays as above.

mCD9F174A and mCD9SFQ(173-175)AAA Large Extracellular Loop Purification and Analysis.

Plasmids encoding full-length murine CD9 with the mCD9F174A and mCD9SFQ(173-175)AAA mutations were provided by Zhu GZ and Primakoff P; originally constructed by Rubenstein E and Boucheix C. The portion of the murine CD9 cDNA corresponding to the large extracellular loop was PCR-amplified using CL34 and CL35 (for sequence, see Chapter 2), and subcloned into pET24a . Proper subcloning was checked by DNA sequencing through the open reading frame. Protein expression was induced in BL21/pLysS cells and purified as described in Chapter 2. Circular dichroism and sedimentation equilibrium experiments were performed as described previously.

Oocyte collection and Immunoprecipitation with mCD9-LEL variants

Eight-week-old FVB females were superovulated and eggs collected by standard procedures (Hogan, Beddington et al. 1994). In brief, superovulated FVB mice were cervically dislocated and Fallopian tubes were isolated. Oocytes were collected in freshly prepared M199 media with a dissecting microscope and treated with hyaluronidase to remove cumulus cells. Oocytes were washed and treated with pronase for 6-10' to remove the zona pellucida. Oocytes washed in M199 media were then visually inspected for M2 arrest and culled. All gametes were handled and incubated under a mineral oil overlay. Oocytes were lysed in 20mM Tris-buffered saline/0.5% NP-40 (Sigma) supplemented with a protease inhibitor cocktail (Boehringer Ingelheim). Either mCD9-LELwt or mCD9SFQ(173-175)AAA were added to a final protein content of .1mg and incubated at 4°C for 3 hours. A 10 μ l bed-volume of pre-equilibrated Ni-NTA agarose (Qiagen) was added for 1 hour. The immunoprecipitate was subsequently washed in an empty spin column (Vendor). Bound proteins were eluted by boiling in SDS-Loading buffer and analyzed by SDS-PAGE.

Myoblast Fusion Assay

The murine myogenic cell line C2C12 was obtained from the American Type Culture Collection. Cells were cultured in DMEM/20% fetal bovine serum at subconfluency. For differentiation and syncytium assays, C2C12 cells were grown on sterilized coverslips coated with 2% gelatin. At confluency, DMEM/20%FBS growth medium was replaced with DMEM/2% horse serum to induce differentiation (Tachibana and Hemler 1999). At subsequent time points, coverslips were washed in PBS and fixed for 10' in 4% paraformaldehyde/PBS. Cells were stained with phalloidin-TRITC and FITC-conjugated mouse anti-desmin and visualized using both fluorescent and Nomarski optics. Antibodies recognizing murine CD9 and murine CD81 (or an isotyped antibody control) was added at 10 μ g/ml either concomitantly with the addition of horse serum or at 3 days post-differentiation. Functional activity of the anti-CD9 antibody was assayed by removing C2C12 culture medium for use as a primary antibody in standard Western analysis with the mCD9-LEL protein as antigen.

Macrophage Fusion Assay:

Peripheral blood was bled from healthy donors of both sexes with informed consent according to a protocol approved by the ethical committee, University of Sheffield.

Peripheral blood in 1% heparin was layered over a mixture of Ficoll-Hypaque (Amersham Pharmacia) at a ratio of 2:1 and centrifuged at 400g for 35 minutes. A mononuclear cell layer consisting of lymphocytes, monocytes, and platelets was cleanly separated from both blood plasma and erythrocytes with a Pasteur pipette. Mononuclear cells were washed and plated on plastic in RPMI/10%FBS for overnight incubation. Non-adherent cells (such as lymphocytes) were separated from adherent macrophages in cell-culture dishes by aspiration. The plates were washed thoroughly with 3x10ml volume of pre warmed RPMI without FBS to ensure all non-adherent cells are removed. Isolated cells were composed of 80-95% macrophages and the remainder being lymphocytes. The adherent macrophages would then be harvested or cultured further.

Macrophages were plated in either 96-well microtiter plates (Takeda, Tachibana et al. 2003) or Lab-Tek[®] chamber slides at a density of 5×10^5 /chamber. Macrophages were stimulated to undergo homotypic fusion with $10\mu\text{g/ml}$ of the lectin concanavalin A (Sigma) for 72 hours at 37°C (Takashima, Ohnishi et al. 1993). Concurrent with the addition of concanavalin A, recombinant hCD9-LEL proteins were added at a concentration of $20\mu\text{g/ml}$ (or lower concentrations as indicated). The fusion index was calculated as the ratio of total number of nuclei in fused cells/total number of nuclei by visual inspection.

Results:

CD9-LEL Inhibition Studies of Fertilization

In collaboration with Paul Primakoff's group, we tested two variants of soluble, recombinant, murine CD9-LEL mimics: our previously characterized mCD9-LEL protein with a C-terminal HisTag, and also a glutathione-S-transferase-fused mCD9-LEL (constructed and purified by Guo-Zhang Zhu and Paul Primakoff) for inhibition in a fertilization assay. Wild-type murine gametes were isolated and cultured under standard conditions. Recombinant proteins were added individually to either capacitated sperm or zona-free eggs and incubated for 3 hours prior to insemination (mixing of the gametes) for 40 minutes and quantification of fertilization. Three parameters were measured: (1) fertilization rate FR = the percentage of eggs that fuse with at least one sperm; (2) fertilization index FI = total number of fused sperm/total number of eggs; and (3) the mean number of sperm bound at the equator of the egg.

When sperm were pre-incubated with either mCD9-LEL or GST-mCD9-LEL, there was no significant effect on either fertilization rate, fertilization index, or sperm-egg binding (Figure 7.2A). However, pre-incubation of soluble recombinant CD9-LELs with eggs, resulted in significant inhibition of both fertilization rate and fertilization index, with no significant effect on sperm-egg binding (Figure 7.2A). At high concentrations, although both constructs resulted in significant inhibition, the mCD9-LEL his-tagged construct was significantly more potent than the GST-tagged construct (Figure 7.2B). Neither construct resulted in complete inhibition (see discussion).

CD9 Rescue Studies of CD9-Null Eggs

To test for recovery of fertilization potential in CD9-deficient oocytes, mRNAs encoding either the wild-type or mutant CD9 variant mRNAs were synthesized and injected into CD9-deficient oocytes. As expected, CD9-null oocytes did not allow sperm-egg fusion. This gamete-fusion defect was significantly rescued by expression of the wild-type CD9 cDNA. However, a point mutation in the mCD9-LEL, F174A abrogated the ability of the mCD9 transcript to rescue the CD9-null phenotype (Figure 7.3A). Injection of this cDNA had no effect on sperm-egg binding (Figure 7.3B). Post-injection, CD9 expression was monitored by immunofluorescent staining and Western

blot analysis (Appendix A) There was no detectable differences in CD9 expression as compared to wild-type oocytes. A triple mutation in the CD9-LEL, SFQ(173-175)AAA did not have an effect on the immunoreactivity of CD9, consistent with confirming our earlier KMC8 epitope analysis (Chapter 4). These results support the critical role of the CD9-LEL in sperm-egg fusion.

Characterization of Non-Fertilization Permissive CD9 Variants

Microinjection of full-length CD9 mRNAs rescued the CD9-null gamete fusion phenotype. Both wild-type and variant CD9 constructs were shown to be expressed and presented at the cell surface of CD9-null eggs. These variants were still recognized by the fertilization-inhibiting KMC8 antibody and were in a segment of the mCD9-LEL separate from our epitope-mapping experiments (Chapter 4 and Figure 7.4A). As a result, it was unclear if the rescue deficiency of the CD9-LEL•SFQ(173-175)AAA construct might be due to a global change in the CD9-LEL structure. To test for this possibility, we subcloned, expressed, and purified the mCD9•F174A and mCD9-LEL•SFQ(173-175)AAA variants as soluble, recombinant LELs. Circular dichroism analysis revealed that these constructs had comparable α -helical content to the wild-type mCD9-LEL (Figure 7.4B). Although the two mCD9-LEL variants had decreased thermal stability ($T_m = 52$ and 48°C), thermal denaturation analysis of α -helical content revealed significant protein stability (Figure 7.5A, B). Most importantly, the mCD9-LEL variants would have had comparable α -helical structure under the physiological conditions where the *in vitro* fertilization assay was performed. The inhibitory effect of these LEL proteins in an *in vitro* fertilization assay was not performed.

Immunoprecipitation of mCD9-LEL oocyte binding partners:

We hypothesized that the mCD9-LEL protein inhibited sperm-egg fusion by binding to and disrupting an endogenous egg surface protein complex (Zhu, Miller et al. 2002). To explore this possibility, we attempted immunoprecipitation experiments of our mCD9-LEL protein with an oocyte lysate.

Approximately 200 wild-type oocytes were collected from twelve super-ovulated FVB females. Eggs were lysed under mild detergent conditions (0.5% NP-40) and

incubated with mCD9-LELwt or the fertilization-incompetent mCD9-LEL•SFQ(173-175)AAA proteins. Nickel-NTA agarose was used to isolate both mCD9-LEL variants and their respective binding partners. Immunoprecipitates were checked for equal starting material and complete washing until binding background was negative (Figure 7.6). Upon elution, there were no significant differences between proteins immunoprecipitated by the mCD9-LELwt and mCD9-LEL•SFQ(173-175)AAA proteins (Figure 7.7). As it was necessary to silver-stain before detection of immunoprecipitated bands, these experiments were deemed intractable (also see discussion).

The Effects of Tetraspanin-LELs on Myoblast Fusion:

To further study cell-cell fusion, we turned to a system where larger biochemical quantities could be obtained. The regulated homotypic fusion of individual myoblasts to form myotubes is an essential step in muscle development (Schnorrer and Dickson 2004). Previously, it has been shown that CD9 is upregulated concomitant with myosin heavy chain and desmin, markers for myoblast differentiation (Tachibana and Hemler 1999). Furthermore, anti-CD9 and anti-CD81 antibodies inhibited and delayed homotypic myoblast fusion in the murine myogenic cell line C2C12. The ability to culture and differentiate large quantities of these cells made myoblast fusion an attractive alternative cell-cell fusion system to gamete fusion.

We obtained the C2C12 cell line and monitored in vitro differentiation into myotubes by microscopy. Greater than 60% of mononuclear C2C12 cells reproducibly fused into multinucleated myotubes (data not shown). Qualitatively, the addition of the antibodies against CD9 and CD81 did not affect either the rate or the formation of myotubes (data not shown). Addition of antibodies against CD9 and CD81 three days post-differentiation also had no effect on either the rate or the formation of myotubes, conflicting with the previously published study. When these antibodies were recovered post myoblast differentiation, they were shown to retain wild-type activity as assayed by Western analysis (data not shown). These studies suggest that the tetraspanin antibodies were not degraded over the duration of the assay. Lastly, the addition of micromolar quantities of hCD9-LEL or hCD81-LEL had no effect on myogenic ability. Without a significant difference in fusogenic ability, we did not pursue these experiments further.

The Effects of Tetraspanin-LELs on Macrophage Fusion:

A recent paper showed that antibodies to CD9 and CD81 promoted macrophage fusion (Takeda, Tachibana et al. 2003). On the other hand, preliminary studies by the Monk group showed inhibition by recombinant GST-CD63-LEL fusion proteins. To test both for the inhibitory effects of our tetraspanin-LELs and as a feasibility study for biochemical studies, we initiated a collaboration to study macrophage fusion.

We measured the index of macrophage fusion in the presence or absence of our hCD9-LEL, hCD63-LEL, and hCD81-LEL proteins. We observed significant inhibition solely in the presence of the hCD63-LEL protein, implying specificity (Figure 7.8A). Surprisingly, the hCD63-LEL protein was incredibly potent, with an IC_{50} in the nanogram/ml range (Figure 7.8B), suggestive of catalytic activity. This result was especially puzzling as we envision a structural role for tetraspanin-LELs in membrane fusion, not a catalytic one. Compared with GST-fused tetraspanin-LELs, our hexahistidine-tagged hCD63-LEL exhibited significantly higher potency.

Discussion

Sperm-egg fusion is a critical step in development (Hogan, Beddington et al. 1994). The controlled fusion of gametes to restore diploidy is essential to the formation of a proper embryo. Onset of development without sperm-egg fusion (parthenogenesis) or excess sperm-egg fusion (polyploidy) results in severe developmental defects (Gilbert 2003). The phenomenon of sperm-egg membrane fusion, which has been visualized by electron microscopy for many decades, is an intensely studied topic of interest not only to developmental biologists, but also to membrane-fusion researchers in general (Hernandez, Hoffman et al. 1996).

Until recently, the genes involved in sperm-egg fusion were not known. Although various proteins were implicated to play a role in this biological process (most notably ADAMs (Cho, Bunch et al. 1998) and integrins (He, Brakebusch et al. 2003)), mouse genetics has refined their role as non-essential (Kaji, Oda et al. 2000; Le Naour, Rubinstein et al. 2000; Miyado, Yamada et al. 2000). On the other hand, mouse genetic experiments have clearly implicated the tetraspanin CD9 as playing an essential role in this process. In the fertilization field, the identification of CD9 has been a mixed blessing. For the first time, a gene was clearly defined as being a central player in this process. On the other hand, very little is known about the role of CD9 on the egg surface and the mechanisms by which it is necessary for sperm-egg fusion. Subsequent to the identification of CD9 as an essential gene in sperm-egg fusion, research progress has been disappointingly slow.

The phenomenon of membrane fusion has been most extensively studied in viral-fusion and vesicle-fusion systems (Eckert and Kim 2001) (Jahn, Lang et al. 2003). The identification of proteins directly involved in these membrane-fusion processes has allowed the process to be both reconstituted and specifically inhibited. Extrapolating from our knowledge of viral and vesicle membrane fusion proteins, the tetraspanin CD9 does not appear to be a fusogen: a protein that directly mediates membrane apposition and mixing (for further discussion, see Chapter 1). Current hypotheses envision CD9 as playing a supporting, albeit essential, role to a sperm-egg fusogen. Currently, the identity of this hypothetical protein is unknown.

Our *in vitro* inhibition experiments indicate that the CD9 gene does not act as a receptor for sperm (Zhu, Miller et al. 2002). Although deletion of the CD9 gene had no effect on sperm-egg binding (and currently, sperm-egg binding proteins on the egg have not been identified), sperm-egg binding and fusion may be decoupled events. Our inhibition data not only shows that CD9 serves a role in cis on the egg surface, it also suggests that our mCD9-LEL protein is a specific inhibitor of endogenous CD9 function.

Extrapolating on the role of CD9 in cis on the egg surface, we hypothesized that the mCD9-LEL protein serves to disrupt endogenous heterotypic CD9/non-CD9 protein complexes on the egg surface. However, immunoprecipitation experiments with the CD9 protein and its non-functional analogue, mCD9-LEL•SFQ(173-175)AAA did not prove fruitful. It may be possible that although mutation of the mCD9-LEL SFQ residues is sufficient to inhibit rescue experiments, it is insufficient to inhibit CD9-partner interactions.

Gamete quantities are also too severely limited for this system to be biochemically tractable. In a Herculean effort, the Primakoff lab committed 8 personnel to a month of collecting oocytes to yield a lysate of approximately 100,000 eggs. An immunoprecipitation experiment with an antibody against murine CD9 yielded integrins and other known CD9-binding proteins, but no proteins with restricted oocyte expression patterns (Paul Primakoff, personal communication). These experiments prompted us to identify other, more biochemically tractable cell-cell fusion systems (Chen and Olson 2005).

Our *in vitro* inhibition experiments should be considered with several caveats in mind. The inability of several point mutations in the CD9 large extracellular loop to rescue CD9 activity suggests the importance of the CD9-LEL domain to sperm-egg fusion (Higginbottom, Takahashi et al. 2003). This result, coupled with KMC8 antibody inhibition data, also suggests that the proper presentation of the CD9-LEL is necessary for sperm-egg fusion. Ideally, we would like to see the effects of the mCD9-LEL•Q159A, mCD9-LEL•F174A, mCD9-LEL•S173A/F174A/Q175A variants on sperm-egg binding and fusion. We would also like to see dose dependence of inhibition, which was not performed.

Most importantly, although our inhibition is statistically significant, maximal inhibition was not very impressive. The inability to inhibit greater than 60% of sperm-egg fusion was also seen when GST-mCD9-LEL proteins were independently tested for inhibition activity (Higginbottom, Takahashi et al. 2003). It may be possible that the membrane-bound form of CD9, which is in a high avidity complex with cis-fusion partners, is too tightly complexed to allow complete inhibition.

Surprisingly, a recent study by the Okabe group has identified a sperm protein, izumo, to function analogously to CD9 on the sperm cell (Inoue, Ikawa et al. 2005). Genetic studies show that izumo is essential for sperm-egg fusion, not binding and this phenotype is recovered by transgenic rescue experiments. A monoclonal antibody against izumo inhibits *in vitro* fertilization (the means by which izumo was cloned) and intracytoplasmic sperm injection (to bypass sperm-egg fusion) resulted in the normal onset of development. The protein izumo consists of a single extracellular novel IgG fold and also is not presumed to directly mediate membrane fusion. Izumo does not bind the CD9-LEL as assayed by immunoprecipitation (Okabe, personal communication). Currently, an optimal strategy to identify a sperm-egg fusogen is unclear.

The closest functional analogue to the sperm-egg fusion system is a homotypic cell-cell fusion system: the fusion of single-nucleated myoblasts to multi-nucleated myotubes (Schnorrer and Dickson 2004). Upon induction, myoblasts differentiate and fuse with one another in an ordered, linear fashion. Many genes implicated in sperm-egg fusion have been characterized to have analogues in a myoblast-fusion system, such as ADAM15 (Yagami-Hiromasa, Sato et al. 1995). To date, no essential myoblast-fusion protein has been identified (although many essential myoblast differentiation genes in *Drosophila* have (Schnorrer and Dickson 2004)). Although functionally analogous, many genes involved in myoblast differentiation and fusion do not directly translate to sperm-egg fusion, and vice versa.

The proteins CD9 and CD81 have been implicated in myotube formation (Tachibana and Hemler 1999). Given the ability to grow large quantities of precursor myoblasts and the significant inhibition presented by antibodies against CD9 and CD81, we hoped to replicate these results as a source for biochemical studies on cell-cell fusion. Unfortunately, we did not see significant inhibition of myoblast fusion with antibodies

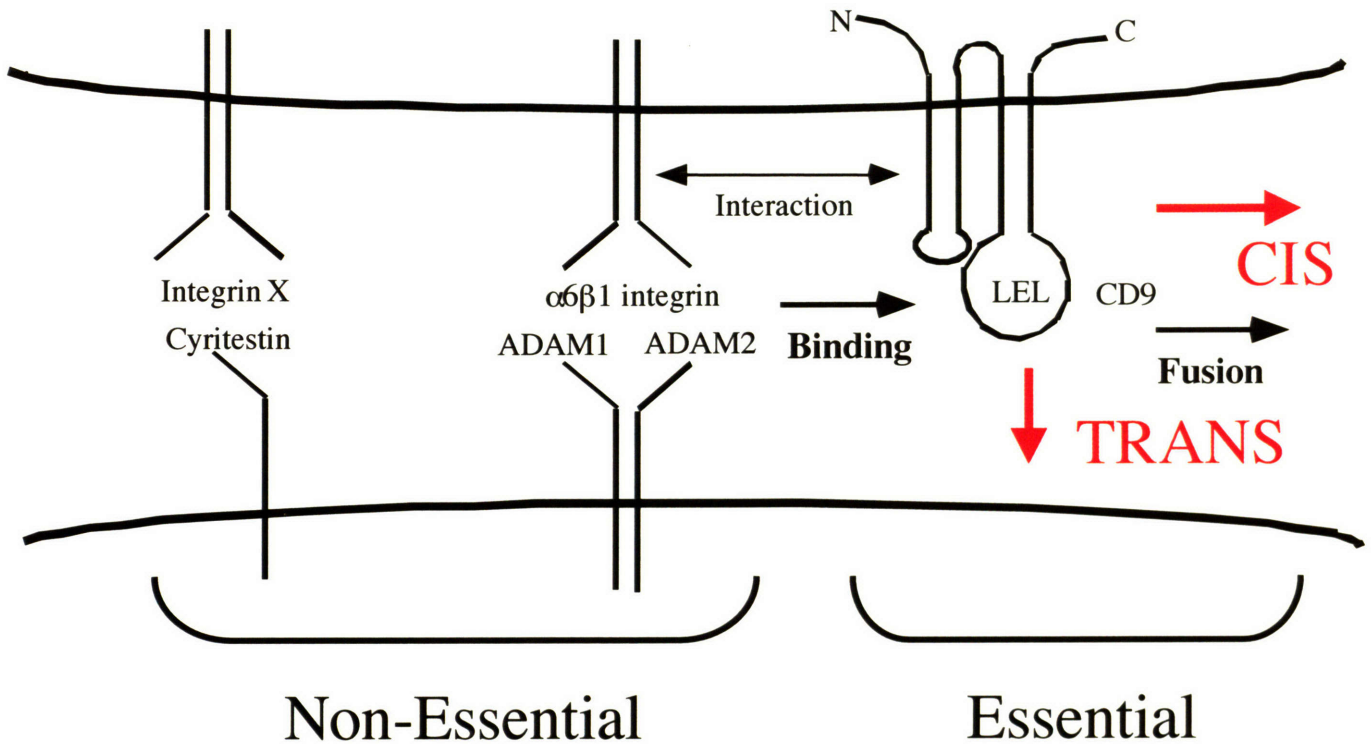
against CD9, CD81, or soluble, recombinant forms of CD9 or CD81. No other papers have implicated CD9 and CD81 in myoblast fusion and, currently, we do not believe that CD9 and CD81 play a role in myoblast fusion.

Another system for homotypic cell-cell fusion is macrophage fusion. The induction and formation of multi-nucleated macrophage giant cells (osteoclasts), cells containing several hundred nuclei after the introduction of a foreign body (such as a splinter), have been medically observed for some time (Takashima, Ohnishi et al. 1993). In vitro, this phenomenon can be reproduced by the addition of a lectin, concanavalin A, to macrophages. Whether homotypic macrophage fusion is a true cell-cell fusion event or “phagocytosis gone terribly wrong” is still wide debated to this day.

In collaboration with Peter Monk, we show a small but significant inhibition of homotypic macrophage fusion with the hCD63-LEL, but not hCD9-LEL or hCD81-LEL. There are many puzzling aspects of these results. The IC_{50} of fusion inhibition (nanogram/ml) is incredibly low. All other inhibition studies with tetraspanin-LELs have shown IC_{50} s in the microgram/ml range (see Chapter 1). Although a role for tetraspanins in macrophage fusion has previously been characterized (Takeda, Tachibana et al. 2003), these results suggested that endogenous CD9 and CD81 inhibited, not promoted, macrophage fusion, the reverse of sperm-egg fusion data. Antibodies against CD63 had no effect on macrophage fusion in their hands. Lastly, soluble CD9-LEL and CD81-LEL promoted macrophage fusion at microgram/ml quantities.

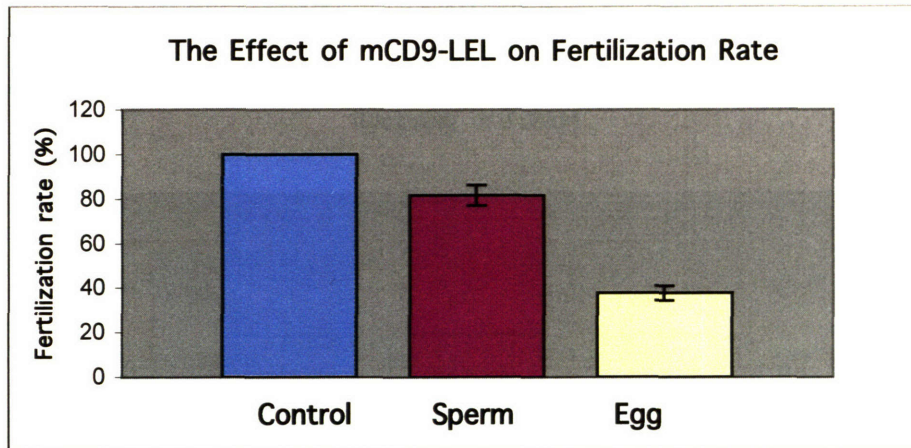
In summary, we have addressed the role of tetraspanins in three independent cell-cell fusion systems. Although our results are most significant in the sperm-egg fusion system, limited biochemical quantities preclude further exploration of the role of CD9 in this system. Our exploration of CD9 on other cell-cell fusion systems has not made significant headway. In conclusion, it is not clear if the CD9 protein will be fruitful in bootstrapping to a cell-cell fusogen in the near future. However, our addition of recombinant mCD9-LEL protein shows both that the endogenous CD9 acts in cis on the egg-surface and that tetraspanin-LELs may function to inhibit endogenous tetraspanin functions.

Oocyte Cell



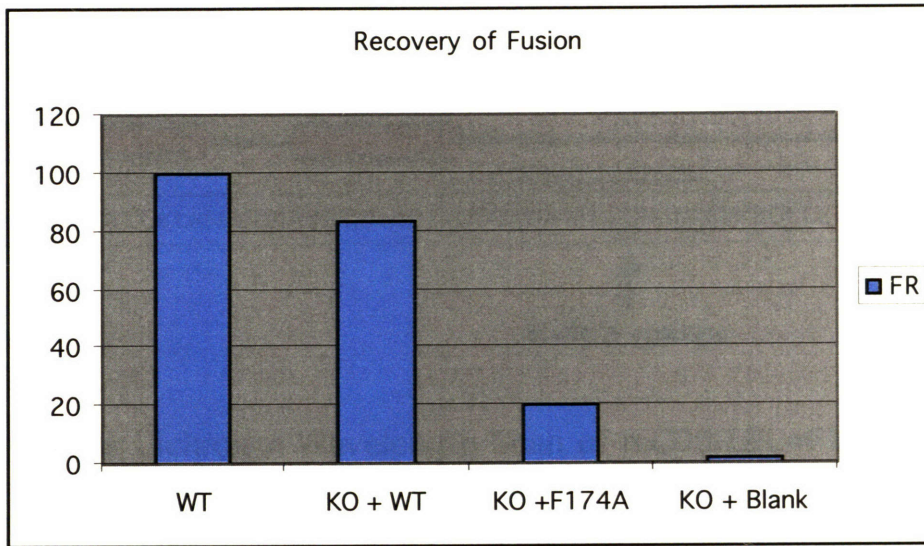
Sperm-Cell

Figure 7.1 Model of Molecules Thought to Play a Role in Sperm-Egg Fusion; A schematic of cell surface proteins on both the sperm (bottom) and the egg (top). ADAM1 and ADAM2 have been previously called fertilin- α and fertilin- β respectively. These proteins contain a disintegrin domain and have been shown to bind to the egg surface $\alpha6\beta1$ integrin heterodimer. Through gene-deletion experiments, these proteins are no longer thought to play an essential role in sperm-egg fusion. Cyritestin is an ADAM family member thought to function upstream of ADAM1/2 in the sperm-egg binding and fusion cascade. The CD9 protein is expressed on the egg and has been shown to be essential for sperm-egg fusion. Its role in mediating sperm-egg fusion is unknown.

A**B**

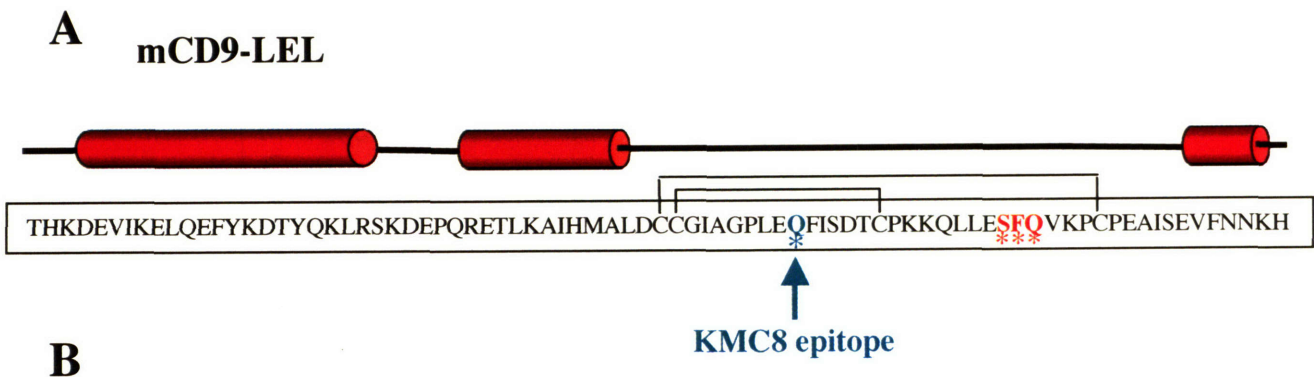
The Effect of GST-mCD9-LEL and mCD9-LEL on <i>in vitro</i> Fertilization						
Incubation Protein	Pre-incubated Gamete	Number of Eggs Tested	Fertilization Rate (%)	Fertilization Index	Sperm bound per Equator	
GST	Egg	78	100±0	1.5±0.15	6.2±0.5	
GST-mCD9-LEL	Egg	86	60±5.1	0.6±0.05	5.7±0.5	
GST-mCD9-LEL	Sperm	63	97±3.0	1.1±0.11	7.1±1.6	
Buffer (PBS)	Egg	56	83±3.5	0.83±0.04	4.6±0.3	
mCD9-LEL	Egg	76	43±2.6	0.42±0.02	4.8±0.4	
mCD9-LEL	Sperm	67	75±5.2	0.75±0.05	4.5±0.3	

Figure 7.2 The mCD9-LEL inhibits Sperm-Egg Fusion. A) Murine sperm and egg cells were isolated in defined media as described in the methods. Gametes were independently pre-incubated with the recombinant mCD9-LEL protein for 3 hours. Gametes were then mixed for 40 minutes and the fertilization rate (percentage of eggs that fuse with at least one sperm) was measured. The control sample is gametes non-incubated with recombinant proteins (and this fertilization rate (83% of eggs) was set to 100%). Pre-incubation of the mCD9-LEL protein with sperm resulted in a small and non-significant ($P>0.1$) decrease in fertilization rate. Pre-incubation of the mCD9-LEL protein with eggs resulted in a significant ($P<0.002$) decrease in the fertilization rate. *In vitro* fertilization experiments were done on multiple occasions and yielded similar results. B) Comparisons of multiple mCD9-LEL constructs on *in vitro* fertilization rate. The *in vitro* fertilization assay was similar to that conducted above. In this table, fertilization rate was quantified as above. Fertilization index was measured as the total number of fused sperm/total number of eggs. The number of sperm bound at the equator of the zona-stripped eggs were also measured. Inhibition data for Glutathion-S-transferase (GST) tagged mCD9-LELs (constructed by Guo Zhang) are also included, showing significant ($P<0.02$), but less substantial inhibition than our mCD9-LEL construct ($P<0.002$). Recombinant mCD9-LEL variants had no significant effect on sperm-egg binding ($P>0.1$). Values are means \pm s.e.m. This experiment was conducted by G-Z. Zhu with tetraspanin reagents provided by C.C. Liu.

A**B**

Incubation Protein	Fertilization Rate (%)	Fertilization Index	Sperm bound per Egg	Number of Replicates
WT eggs	66	0.83	14	5
KO eggs + WT	55	0.85	12	4
KO eggs + F174A	13	0.2	12	4
KO eggs + blank	1	0.02	14	5

Figure 7.3 Microinjection of the Full-Length Murine CD9 cDNA Rescues the Null-Phenotype. A) Wild-type sperm cells were collected as before. Eggs of varying genetic backgrounds were also harvested and used in *in vitro* fertilization assays. CD9-null eggs are denoted as KO. The fertilization rates of microinjected cDNA transcripts encoding the full-length wild-type CD9 gene (denoted WT) or with a single point mutation (denoted F174A) are also graphed. B) Tabulated data of the fertilization rate, fertilization index, sperm bound/egg and number of replicates for the conditions listed in Figure 7.2A. This experiment was conducted by G-Z. Zhu with tetraspanin reagents provided by C.C. Liu.



B

Circular Dichroism Wavelength Scan of mCD9-LEL•F174A
and mCD9-LEL•S173A/F174A/Q175A

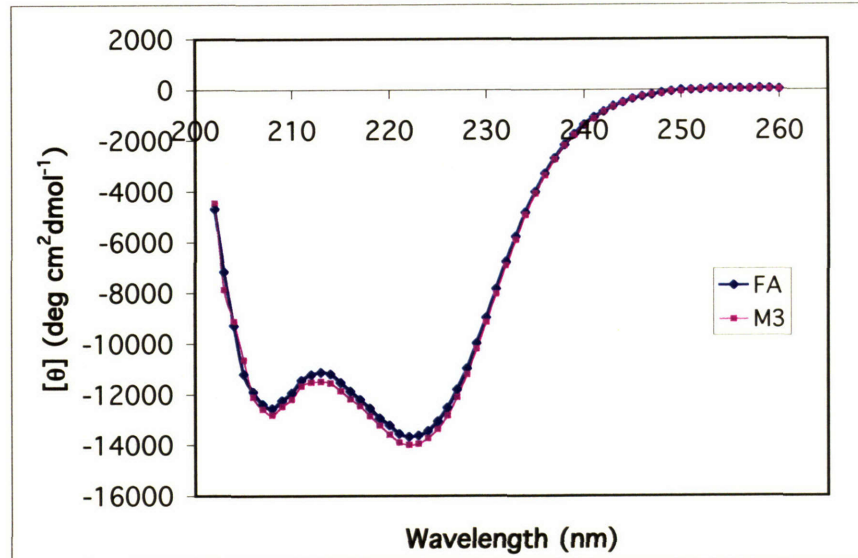


Figure 7.4 Biophysical Analysis of Fertilization Defective mCD9 Mutants: A) The murine CD9-LEL primary sequence is shown with predicted α -helical elements depicted with red bars above the sequence. The point mutation (Q159A) that abrogates KMC8 immunogenicity is denoted with a green asterisk. A series of mutations (SFQ173-175AAA) which did not allow recovery of the CD9-null phenotype are also listed as red asterisks. B) Murine CD9-LEL point mutations were subcloned into pET24a from full-length constructs by polymerase chain reaction using the oligonucleotides CL34 and CL35. Protein was expressed and purified using Ni-NTA agarose and C18 reverse-phase HPLC as described in Chapter 2. HPLC profiles did not deviate from the canonical CD9 trace (data not shown). Circular dichroism analysis revealed that both the F174A mutation (designated FA) and the SFQ triple mutant (M3) exhibited characteristic minima at 222 and 208nm, indicative of an α -helical structure. For circular dichroism data on Q159A, see Figure 4.7.

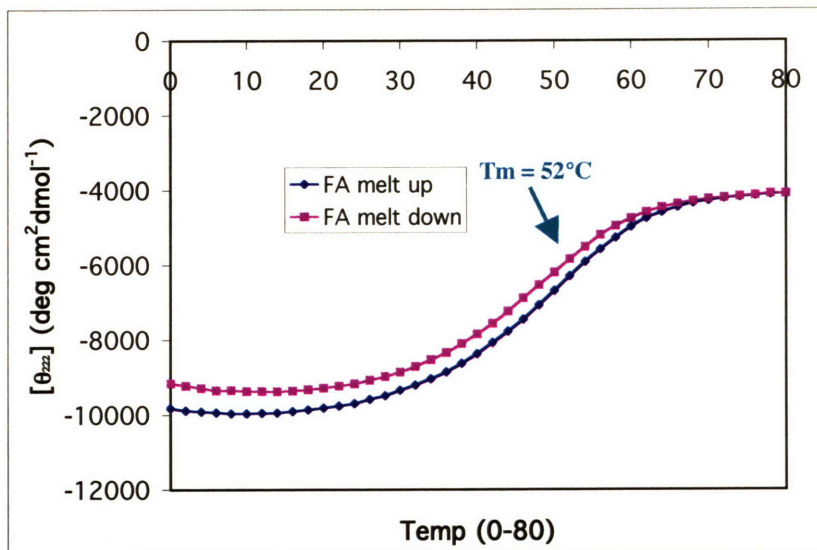
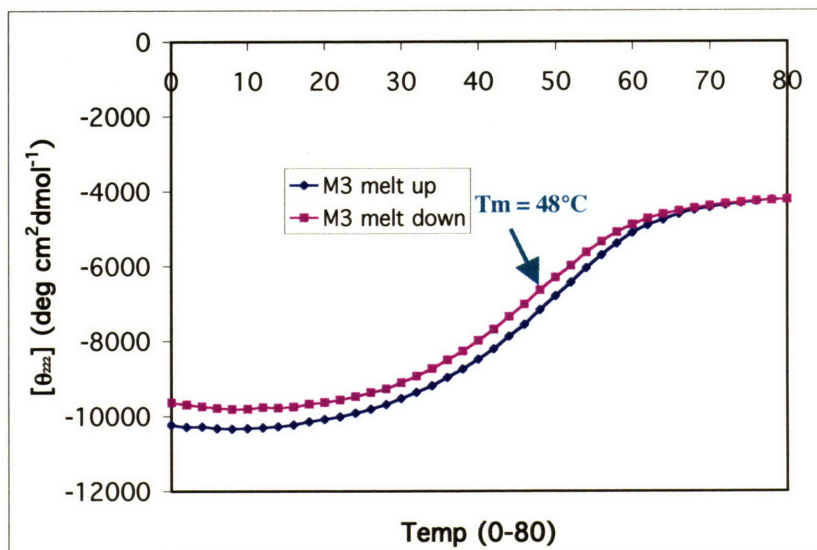
A**Thermal Denaturation/Renaturation of
mCD9-LEL•F174A****B****Thermal Denaturation/Renaturation of
mCD9-LEL•S173A/F174A/Q175A**

Figure 7.5 Thermal Stability of Fertilization defective mCD9 mutants. A) The thermal stability of the mCD9-LEL•F174A variant (FA) was monitored by tracking the circular dichroism signal of the fertilization defective mutant at 222nm as described in Chapter 2. The thermal denaturation profile is charted in blue and the renaturation profile is charted in pink. The midpoint of thermal denaturation is indicated. B) The thermal stability profile of the mCD9-LEL•S173A/F174A/Q175A triple mutant (M3). The chart is graphed as in Figure 7.4A.

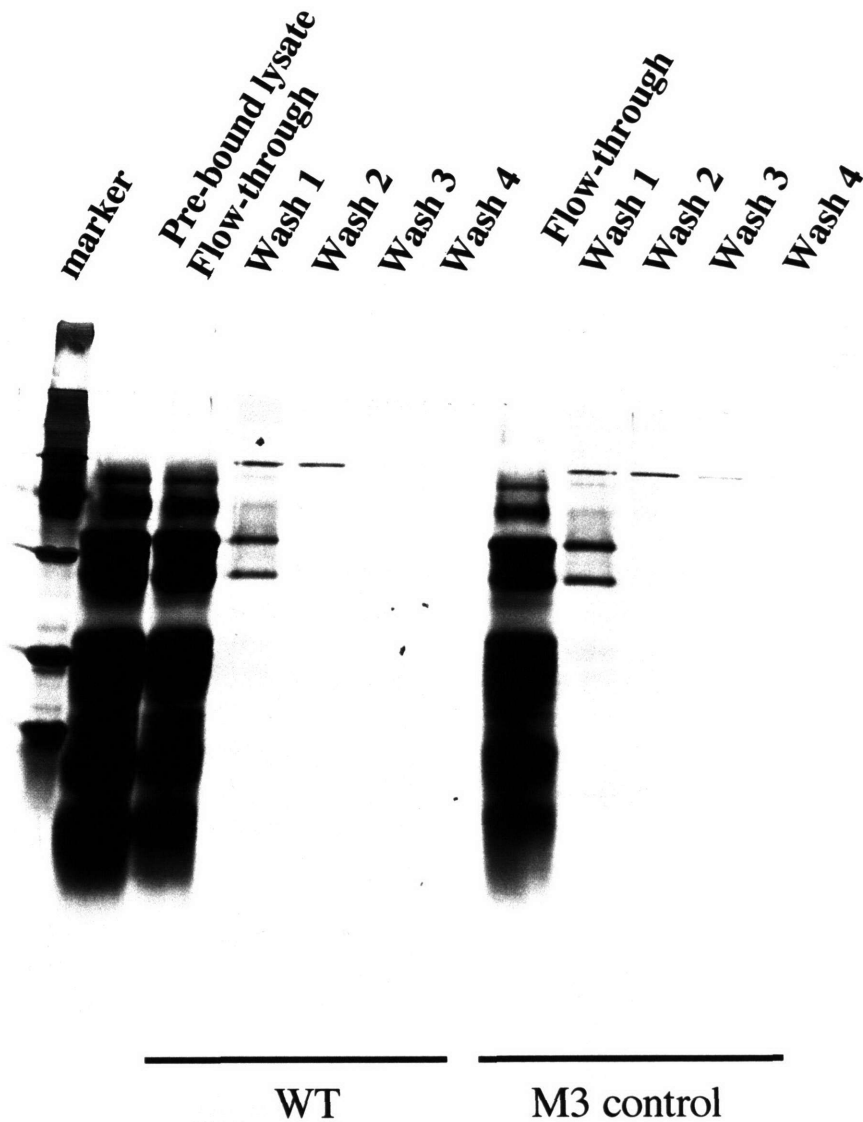


Figure 7.6 Immunoprecipitation of Egg/CD9 Interactions. Eggs from superovulated FVB female mice were harvested under standard conditions. Eggs were stripped of both cumulus cells and zona pellucida and assessed for maintenance of meiosis 2 arrest. Eggs were lysed in 1% NP-40 and cell surface protein content was assessed by SDS-PAGE and Coomassie staining (Lane 2) The supernatant was split into two aliquots, incubated with either mCD9-LELwt or the fertilization non-permissive mCD9-LEL•S173A/F174A/Q175A variant. After incubation and immunoprecipitation with Nickel-conjugated agarose beads, the non-bound fractions (lane 3; 8) and washes (lanes 4-7; 9-12) were assayed by SDS-PAGE. Molecular weight markers are in lane 1.

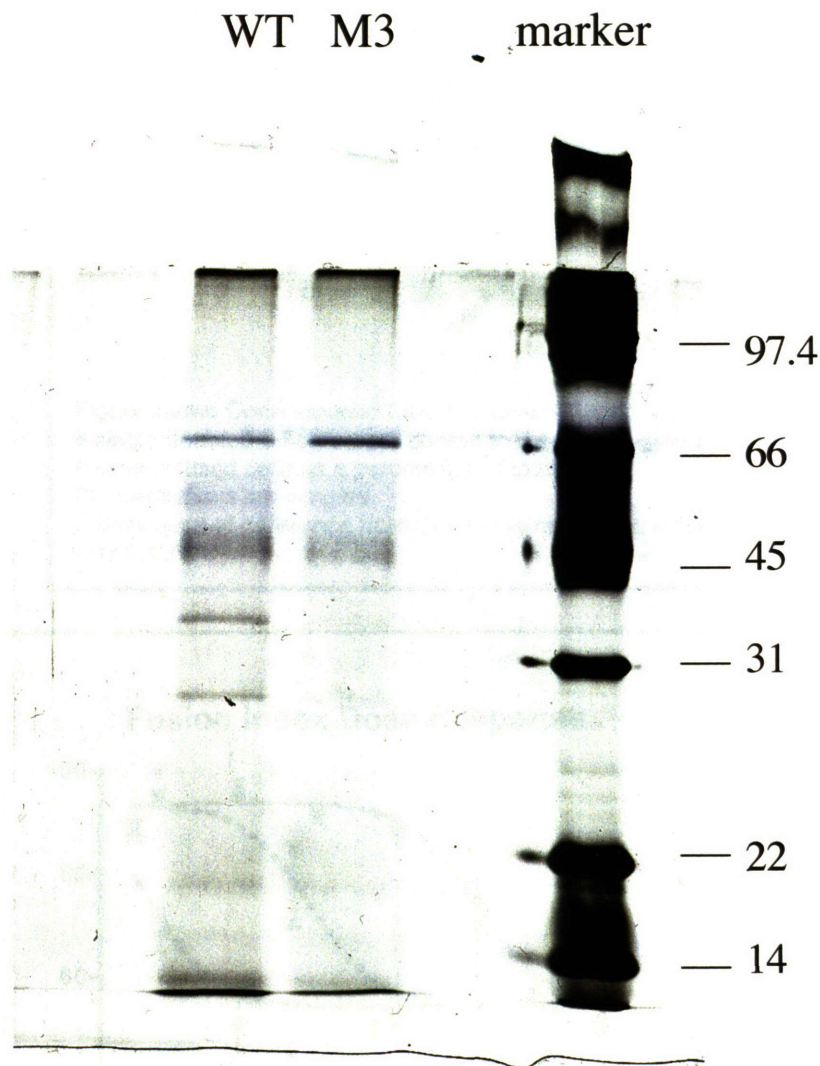
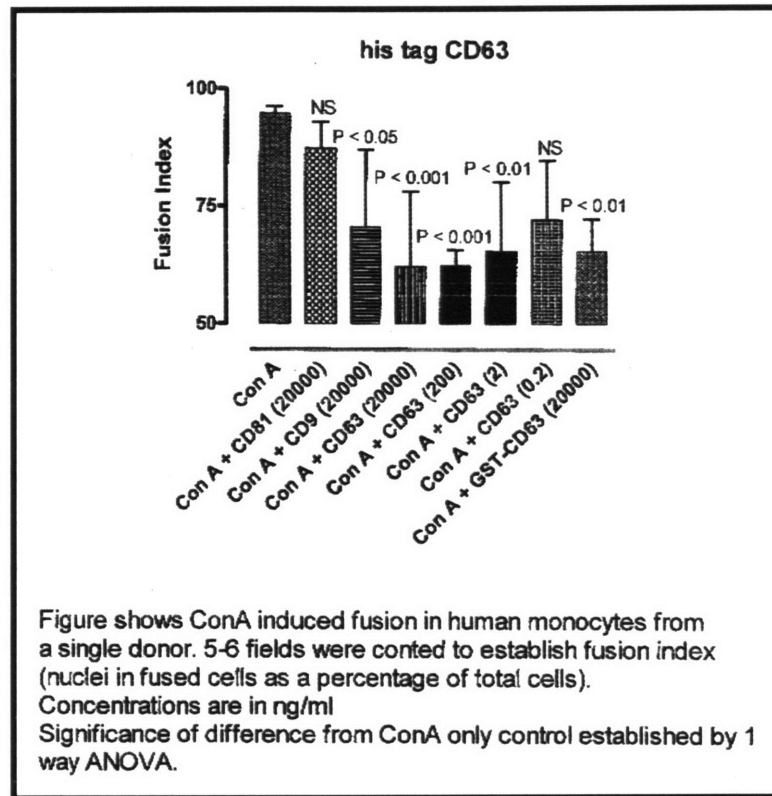


Figure 7.7 Elution Profile of CD9-LEL/egg Interactions: An egg lysate was incubated with 0.1mg of mCD9-LELwt or mCD9-LEL•S173A/F174A/Q175A protein and immunoprecipitated. Total protein content was eluted by boiling with 2X SDS-Loading Buffer and analyzed by SDS-PAGE followed by silver-staining. The stacker of the SDS-PAGE gel is included. The mCD9-LEL variants have a molecular weight of approximately 11-kDa and were allowed to run off the gel (as they would have been severely overdeveloped). The protein profile eluted from the mCD9-LELwt is labeled as WT and the protein profile eluted from the mCD9-LEL•S173A/F174A/Q175A protein is labeled as M3. Molecular weight standards are to the right of the gel.

A



B

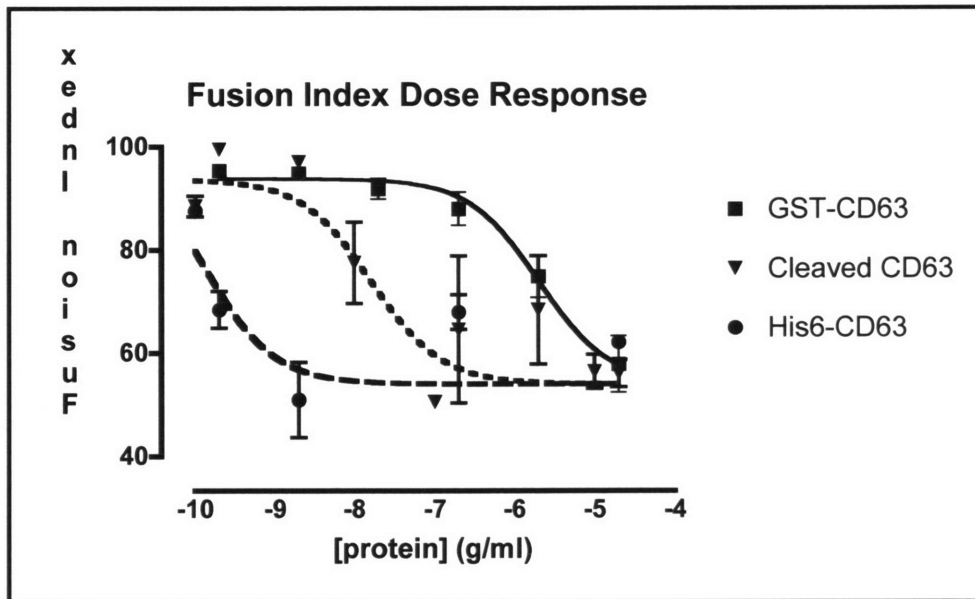


Figure 7.8 Macrophage Fusion Assay. A) Effects of recombinant tetraspanin-LELs on macrophage fusion. Concentration of all exogenously added proteins are in nanograms/ml. Standard error bars and P values are included above each bar. NS stands for not-significant ($P = >.05$). B) Dose dependence curve of hCD63-LEL inhibition. Glutathione-S-transferase fused hCD63-LEL inhibition is graphed as GST-CD63. When this construct was cleaved to remove remove the GST tag, inhibition is graphed as cleaved CD63. Our hCD63-LEL is graphed as His6-CD63. This experiment was conducted by p Varadarajan with tetraspanin reagents provided by C.C. Liu.

Chapter 8

Tetraspanins and Integrin Interactions

These experiments were conceived by Christopher C. Liu, Jun Takagi, Richard O. Hynes, and Timothy Springer. All integrin reagents were constructed by Jun Takagi and all tetraspanin reagents were constructed by Christopher C. Liu. Jun Takagi conducted all solid-phase ELISA assays. Christopher C. Liu conducted all other experiments. All errors are my own.

Introduction

Integrins are an important class of cell-surface proteins that mediate cellular adhesion to the extracellular matrix. There are 24 mammalian integrins, each comprised of an α -subunit and a β -subunit and having specific, non-redundant functions (Hynes 2002). Integrins play major roles in development, immune functions, leukocyte traffic, and human disease.

A striking feature of integrins is their ability to rapidly (<1sec) activate and mediate cellular adhesion. The abilities of integrins to change conformation (affinity), cluster (avidity), and to bind the cytoskeleton (anchoring) all may contribute to this rapid activation timeframe (Takagi and Springer 2002). Recently, several studies have emphasized the critical role of integrin transmembrane domains in the regulation of adhesion (see discussion), which may play a role in both affinity and avidity (Li, Babu et al. 2001; Luo, Springer et al. 2004). However, the majority of research describes affinity changes in the integrin extracellular domain (Takagi, Petre et al. 2002). Multiple antibodies have been described that specifically recognize, or even induce, integrin conformers in high or low affinity states (Humphries 2004).

Recently, the structure of the α V β 3 extracellular domain was solved by x-ray crystallography. Unexpectedly, the integrin structure was crystallized in a bent conformation, completely at odds with the canonical view of integrins as a headpiece attached to an extended stalk-like domain (Figure 8.1). Both electron micrographic and molecular design studies have revealed that integrins may exist in both a bent, inactive conformation and a straightened, active conformation and that these two conformers are in dynamic equilibrium. Furthermore, antibodies thought to modulate integrin affinity may also modulate integrin conformations (Takagi, Beglova et al. 2001).

In this chapter, we utilize both a panel of recombinant integrin extracellular domains and our three recombinant, tetraspanin-LELs to probe putative tetraspanin-integrin interactions. With both solid-phase ELISA and cell-based integrin binding assays, we show that tetraspanin-LELs bind integrins in a cation-dependent manner. Although there are clear rankings in integrin-tetraspanin binding, we could not decipher a pair-wise set of interactions. These interactions could be inhibited or enhanced by

antibodies that modulate integrin affinity, although a specific tetraspanin binding pattern to integrins in high or low affinity states could not be deduced.

Materials and Methods:

Recombinant Integrin Extracellular Domains:

Wild-type, human extracellular portions of integrin alpha and beta subunits were fused to the 30-residue acid and base α -helical coiled-coil peptides (also called Velcro for their specific heterodimerization properties) (O'Shea, Lumb et al. 1993) respectively, with one cysteine mutation at the N-terminal end. In the beta subunits, a seven-amino acid recognition sequence for TEV protease was inserted before the base peptide (Takagi, Erickson et al. 2001). These fragments were stably introduced into CHO lec 3.2.8.1 cells. Cell-culture supernatants containing secreted, soluble integrin fragments were purified using Ni-NTA agarose (Qiagen) followed by anion-exchange (monoQ) and gel filtration (Superdex200HR) chromatographies. Recombinant integrin fragments were stored at 0.5-1mg/ml at 4°C in TBS containing 1mM CaCl₂ and 1mM MgCl₂. release of the C-terminal clasp was achieved by incubation with 250U/ml TEV protease (Invitrogen) at 25°C for 16hr.

Recombinant tetraspanin-LEL variants:

Soluble, recombinant versions of the hCD9-LEL, hCD63-LEL, and hCD81-LEL were expressed and purified as previously described. The hCD9-LEL•Q161A and hCD9-LEL•E160A/Q161A proteins were designed by sequence alignment to the mCD9-LEL•Q159A variant described in Chapter 4. Point mutations were constructed by recombinant PCR (Higuchi 1990) and expressed and purified under similar conditions to the hCD9-LEL protein. Folding stability of the hCD9-LEL variants was monitored by circular dichroism as described in Chapter 2. Antibodies to the hCD9-LEL, hCD63-LEL, and hCD81-LEL were described in Chapter 6.

Enzyme-linked Immunosorbent Assay Analysis:

Recombinant tetraspanin-LELs were dissolved in H₂O at 2mg/ml. Protein stocks were subsequent diluted to 10 μ g/ml in TBS and 50 μ ls were bound to each ELISA well at 4°C overnight. All wells were blocked with 1% bovine serum albumin for 2 hours at RT. Soluble, recombinant integrin fragments were added to each well under varying buffer conditions for 2 hours at RT and washed once with TBS. Ten μ g/ml of biotinylated α -

velcro antibody (which recognizes the C-terminal fusion tag) was added in TBS/1mM Mn with 1% BSA for 30' at RT and washed 3X with TBS/Mn⁺⁺. Horse-radish peroxidase streptavidin/1% BSA was added for 15' at RT, washed 4X with TBS/Mn and developed using 2,2'-azino-bis-(3-ethylbenzthiazoline-6-sulfonic acid (ABTS). Absorbance was monitored at 415nm.

Tetraspanin Binding to Cell-Surface Integrins:

K562 cells are human myelogenous leukemia cells that express the $\alpha 5\beta 1$ integrin at high levels. K562 cells were stably transfected with either $\alpha \text{IIb}\beta 3$ or the $\alpha 4$ integrin (to express $\alpha 4\beta 1$) in conjunction with endogenous levels of the $\alpha 5\beta 1$ integrin. For FACS analysis, K562 cell lines were preincubated in PBS containing either 1mM CaCl_2 /1mM MgCl_2 or 5mM EDTA for 45' at RT. Cells were incubated with for 30' with .2mg/ml of hCD9-LEL and anti-CD9 antibody M-L13. Incubation with either hCD9-LEL alone or antibody M-L13 alone was used as negative controls. All samples were then incubated with PE-conjugated anti-mouse IgG for detection. All samples were analyzed in a FACS-Caliber machine, positively selected for live cells by forward and side scatter. Gated cells were then analyzed for hCD9-LEL binding by analysis along the FL2 axis with compensation adjusted to background.

For cell-binding assays, K562 variants were washed in PBS containing either 1mM CaCl_2 /1mM MgCl_2 or 5mM EDTA and then incubated with hCD9-LEL at .2mg/ml for 45' at RT. Cells were washed, lysed in RIPA buffer, and total protein was quantified using the microBCA kit (Pierce). Equal amounts of total protein were loaded onto an SDS-PAGE gel and bound hCD9-LEL protein was quantified by Western blotting.

Results:

Cation-Dependence of Tetraspanin/Integrin Binding

We used an ELISA assay to test pairwise interactions between tetraspanin-LELs and recombinant integrin fragments under a variety of conditions. As both tetraspanin-LELs and integrins contained a hexahistidine tag, this epitope could not be used to probe interactions. As a result, in all solid-phase ELISA binding assays, tetraspanin-LELs were bound to plates. Integrins were then added under a variety of conditions and the presence of bound integrin was detected with an antibody against the acid-base coiled coils (which replace the integrin transmembrane domains) (Takagi, Erickson et al. 2001).

Previously, it has been shown that Manganese (Mn) and a cyclic peptides RGD will activate integrins and EDTA, which sequesters cations, will inhibit integrin activation (Hynes 2002). Our results showed binding of tetraspanin-LELs with the α IIb β 3 integrin above non-specific bovine serum albumin (BSA) background. Pre-incubation of integrin fragments with EDTA significantly increased tetraspanin binding (Figure 8.2A). However, there did not appear to be differences between α IIb β 3 interactions with the hCD9-LEL, hCD63-LEL or hCD81-LEL. Binding of the hCD9-LEL with α 5 β 1 fragment was minimal. Given these results, we expanded our panel of integrins and restricted our cation conditions to either Calcium (low-binding) or EDTA (high-binding) buffers. Again, we observed consistently higher binding under conditions without cations (Figure 8.2B). However, there did not appear to be a specific tetraspanin/integrin binding pattern (Figure 8.2C). The hCD63-LEL consistently exhibited higher binding than either hCD9-LEL or hCD81-LEL, which both exhibited similar effects. Strikingly, tetraspanin-LELs appeared to bind as tightly to full-length α IIb β 3 integrin as to a mini- α IIb β 3 domain, which contained only the head domain.

K562 are leukemia cells that endogenously express only the integrin α 5 β 1 heterodimer. We tested hCD9-LEL binding to either K562 cells or variants stably expressing α IIb β 3 or α 4 β 1 in addition to the endogenous α 5 β 1 integrin heterodimer. We used two different techniques to analyze binding of hCD9-LEL binding to K562 variants: FACS analysis and also whole-cell lysates.

Our hCD9-LEL proteins were tagged at their C-termini with a hexahistidine tag. However, a FITC-conjugated anti-HisTag antibody did not work by FACS (data not

shown). As a result, we probed a panel of monoclonal antibodies against CD9. One monoclonal, clone M-L13, detected hCD9-LEL without interfering with binding. K562 variants were pre-incubated with PBS containing either divalent cations (+/+) or EDTA. By FACS we observed that, with all K562 variants, pre-incubation in the presence of cations increased binding of the hCD9-LEL protein (Figure 8.3). K562 variants expressing α IIB β 3 or α 4 β 1 (in addition to α 5 β 1) exhibited stronger binding. The K562/ α 4 β 1 cell line had the greatest sensitivity to cations (Figure 8.3).

We further tested binding of the hCD9-LEL protein to K562 variants using whole-cell lysates. The hCD9-LEL was bound to K562 variants incubated under varying cation conditions and equal amounts of whole-cell lysates were analyzed by SDS-PAGE and Western blotting. Again, we observed higher cell-surface tetraspanin-integrin binding in the presence of cations (Figure 8.4A). EDTA dramatically lowered hCD9-LEL binding. These results correlated with the results seen by FACS (Figure 8.3), although they are the inverse of our solid-phase ELISA results. Taken as a whole, they suggest that cations modulate tetraspanin-LEL/integrin binding.

Integrin Tail-Release Effects on Tetraspanin/Integrin Binding

All recombinant integrin fragments had their C-terminal transmembrane regions replaced with heterodimeric coiled-coil sequences. A disulfide-bond introduced into the coiled-coil further increased constitutive oligomerization, bringing the integrin stalk domains into close proximity. The close proximity of integrin stalks has been shown to hold integrins in an inactive state (Figure 8.1A). A TEV protease cleavage site was inserted between the beta integrin subunit and its base peptide fusion. Treatment with the TEV protease released the integrin stalk constraint and resulted in activation of ligand binding (Takagi, Erickson et al. 2001).

We tested whether TEV protease cleavage (and the release of the intersubunit constraint) perturbed tetraspanin/integrin interactions. Although a decrease in binding was observed when the α 6 β 4 constraint was released, in general TEV treatment (and subsequent integrin activation) had no effect on tetraspanin/integrin interactions (Figure 8.4B).

Antibody Inhibition of Tetraspanin/Integrin α IIb β 3 Binding

As tetraspanin-LELs bound most strongly to the recombinant α IIb β 3 fragment (Figure 8.2C), we tested the effects of a panel of anti- α IIb β 3 antibodies on tetraspanin/integrin interactions. A single monoclonal antibody, 10E5, inhibited α IIb β 3/CD9 interaction and reduced binding to background levels (Figure 8.5A). The 10E5 antibody not only inhibited CD9/ α IIb β 3 interactions, it reduced binding in all tetraspanin-LELs/ α IIb β 3 interactions (Figure 8.5B). In the case of the hCD63-LEL, this binding was not reduced to background, possibly suggestive of significant non-specific background. When the hCD9-LEL was tested for antibody-dependent binding to α IIb β 3 under cationic conditions, no antibody inhibition was observed (8.5C). The addition of two small molecule activators to the α IIb β 3 integrin, EF5154 and cyclic-RGD did not perturb integrin binding. These interactions were probed in Ca/Mg as the small molecule EF5154 does not bind in EDTA. These results are consistent with the notion that high affinity integrin conformers bind weakly to tetraspanins by solid-phase ELISA analysis.

Tetraspanin Specificity in Tetraspanin/Integrin Binding

To test further the specificity of tetraspanin-LEL/ α IIb β 3 integrin interactions, we utilized a panel of anti-tetraspanin antibodies. As these antibodies presumably bind the head subdomain of tetraspanin-LELs, we hypothesized that they would serve to inhibit tetraspanin/integrin interactions. Anti-tetraspanin antibodies were pre-incubated with each tetraspanin post-binding to ELISA plates and then binding was compared to anti- α IIb β 3 10E5 inhibition (Figure 8.6A). Although 10E5 consistently lowered binding to background levels, antibodies against tetraspanins had minimal effect. Only in the case of anti-CD63 was there a significant inhibition of interaction, comparable to 10E5 inhibition. Inhibition of hCD63-LEL/ α IIb β 3 interaction by the anti-CD63 antibody was specific. As expected, anti-tetraspanin antibodies did not inhibit α IIb β 3 interactions with non-recognized tetraspanins (Figure 8.6B)

With the hCD9-LEL, we constructed, expressed, and purified two hCD9-LEL variants that are analogous to the mCD9-LEL species that fail to bind KMC8 (as described in Chapter 4). The hCD9-LEL•Q161A and hCD9-LEL•E160A/Q161A variants had comparable biophysical characteristics to the hCD9-LELwt (data not

shown). These variants were tested for binding to α IIB β 3 under divalent cation conditions (Figure 8.6C). We did not observe any difference in binding among all the hCD9-LEL variants, suggesting that interaction is not mediated by this region of the hCD9-LEL head sub-domain.

Anti- α 4 β 1 Antibody Modulation of Interaction:

Using BSA background as a negative control and hCD81-LEL/ α 4 β 1 integrin binding under cationic conditions as a positive control, we tested antibody modulation of this specific interaction. A panel of antibodies revealed that one anti- β 1 antibody, clone 4B4 reduced binding to background levels (Figure 8.7A). Another anti- β 1 antibodies, clone TS2/16, actually increased binding although TS2/16 and 4B4 have overlapping epitopes and compete with each other for binding (Takada and Puzon 1993). A series of anti- α 4 antibodies also inhibited binding, although the pattern of inhibition did not match known inhibitory antibody functions (Figure 8.7A). These surprising results were reproducible, with clones TS2/16, SG7, and L25 augmenting binding and clones 4B4, 5D5, 8F2, and HP1/7 inhibiting binding (Figure 8.7B).

Specificity of Anti- α 4 β 1 Antibody Modulation of Binding:

To test for the specificity of hCD81-LEL/ α 4 β 1, binding between the hCD81-LEL protein and α 5 β 1 integrin was tested under cationic conditions. No increase by either of the augmenting antibodies, clones TS2/16 or SG7, was observed (Figure 8.8A). The inhibitory antibody 4B4 also had no effect, although this could be due to the lack of resolution under these experimental conditions. Specificity of hCD81-LEL/ α 4 β 1 interaction was also probed by testing binding between the hCD81-LEL protein and α 6 β 4 integrin under cationic conditions. Screening a panel of anti- α 6 antibodies revealed a clone, S198, that inhibited interaction (Figure 8.8B). As before, anti- β 4 antibody clones 5D5, 8F2, and HP1/7 inhibited binding. Surprisingly, inhibition by the anti- β 1 antibodies, 4B4 suggests that perhaps antibody-mediated inhibition was non-specific (Figure 8.8B). Furthermore, it was observed that the majority of inhibitory antibodies were ascites, an effect also observed with CD81 binding to α IIB β 3 integrin (data not shown).

With our cell-based binding assay, we preincubated K562 cells expressing endogenous $\alpha 5\beta 1$ integrin with a series of modulating antibodies before probing binding with the hCD9-LEL protein. All buffers contained Ca/Mg and whole-cell lysates were quantified, equated, and loaded onto 18% non-reducing SDS-PAGE. Nucleoporin was used as a loading control. The anti- $\beta 1$ antibodies, 13, AG89, TS2/16, and SG89 increased interaction (Figure 8.9). Disturbingly, the anti- $\alpha 4$ antibody, L25, which augments $\alpha 4$ binding but should have no effect in this assay, increased hCD9-LEL binding. These results were reproducible and densitometry analysis suggested that clone TS2/16 induced a 5-fold increase in hCD9-LEL binding and was dose-dependent on hCD9-LEL concentrations (data not shown).

Discussion.

In this chapter, we utilize three different techniques to show the influence of various cations on binding between tetraspanins and integrins. These cation-dependent effects were observed with a large number, but not all, of integrins tested. Furthermore, they were observed with three different, soluble, tetraspanin-LELs. Surprisingly, we observed inverted cation-dependent effects depending upon the assay used. With solid-phase ELISA binding, we observed higher binding under cation-deficient, or inactivating, conditions. However, with cell-binding assays, we observed higher binding under cation-activating conditions. The simplest explanation for this discrepancy is to assume the ELISA binding assays, which contain minimal binding components, is authentic and that tetraspanin-LELs bind inactivated integrins.

In the case of our cell-binding assays, where we see increased binding under cation-positive or integrin active conformations, our inverted observations to the ELISA binding experiments may be explained by endogenous CD9, which has been shown to be present in low copies on K562 cells (Mannion, Berditchevski et al. 1996). If interaction between CD9 and integrins is real, endogenous CD9 molecules may be constitutively bound to inactive integrins on K562 cells. Under inactivating conditions (EDTA), this endogenous cis interaction would preclude the binding of exogenous, soluble forms of the CD9-LEL. However, release of this CD9/integrin complex by cation-induced integrin activation could expose novel, low-affinity binding sites and allow interaction of soluble CD9-LELs in trans with cell-surface integrins. The low-affinity of tetraspanin-LEL interactions is also suggested by our inability to observe CD9-LEL/ α IIB β 3 integrin binding by gel filtration analysis, which only detects high affinity interactions (data not shown).

Our observed cation-dependence of tetraspanin/integrin interactions is not in concordance with several published reports (Mannion, Berditchevski et al. 1996) (Longhurst, White et al. 1999), which suggest that modulation of integrin affinity does not affect tetraspanin/integrin interactions. Longhurst *et. al.* observed the association of CD9 with α IIB β 3 (and also the GP1b/V/IX complex) using CHAPS solubilization. An activating antibody, D3, inhibited CD9/ α IIB β 3 immunoprecipitation, but the interaction was not cation dependent (Longhurst, White et al. 1999). Mannion et. al. shown the

cation independence of CD81/ α 4 β 1 interaction. However, the introduction of two point mutations to the α 4 subunit that inhibit adhesion, D346E and D408E also inhibit immunoprecipitation (Mannion, Berditchevski et al. 1996). Association between CD81 and α 4 β 1 is only observed in CHAPS or weaker detergents. The binding inhibition of extracellular antibodies (which may disrupt the tetraspanin/integrin binding site) described by Longhurst et. al. is encouraging. However, similar to the results described in this chapter, many of these observations are discordant with one another. How would an activating antibody decrease binding and yet not be cation-dependent? We hypothesize that the use of weak detergents (such as CHAPS and even weaker detergents, such as Brij58) to observe interactions causes tetraspanins and integrins to constitutively and non-specifically associate with one another through their hydrophobic domains. This constitutive effect may mask the conformational-dependence of tetraspanin-integrin interactions.

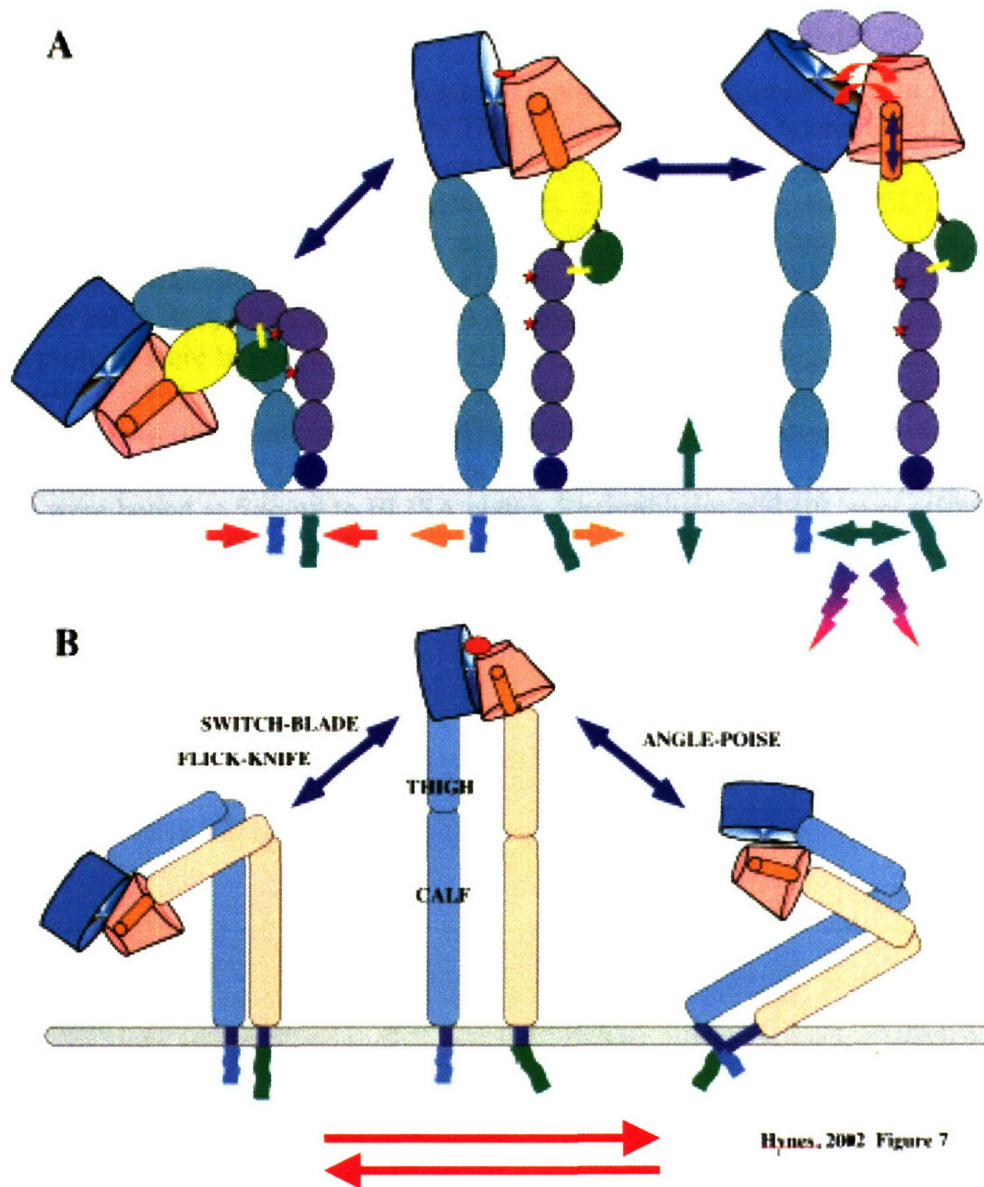
It is possible that under integrin activating conditions, extracellular tetraspanin binding to integrins is minimal. However, binding was significantly increased in the presence of inactive integrins (as with our solid-phase ELISA assays), and induction of the inactive conformation may expose a tetraspanin-LEL binding site. Cation-dependent tetraspanin-LEL/integrin binding strongly suggests that this interaction may depend upon different integrin conformations. To test this hypothesis, we used the Tev protease to activate integrins by releasing an artificial coiled-coil clasp (Takagi, Erickson et al. 2001). However, release of the integrin inactivation constraint did not significantly affect tetraspanin-LEL/integrin binding. Lastly, we queried tetraspanin-LEL/integrin interactions in both solid-phase binding and cell-binding assays with modulating antibodies. Although these antibodies were also able to modulate tetraspanin/integrin interactions, they did not suggest preferred binding of tetraspanins to either activated or inactivated integrin conformational state (Takagi, Petre et al. 2002). As we noted that a number of antibodies produced as ascites all had inhibitory effects on tetraspanin-LEL binding, regardless of their function, we have low confidence in these results.

Lastly, to test the specificity of our tetraspanin-LEL binding, we constructed two point mutations in the human CD9-LEL that we hypothesized would serve to disrupt heterotypic interactions. Unexpectedly, these mutations had no effect on the interactions

between the CD9-LEL and integrins, suggesting a lack of specificity in our observations. Furthermore, the addition of antibodies that recognize tetraspanin-LELs (and supposedly block heterotypic interactions) had no inhibitory effect on interactions. These results do not support the specificity of our tetraspanin-LEL/integrin binding experiments. However, unlikely, it may be possible that the dimeric, not the variable, subdomain of tetraspanin-LELs does not mediate our observed interactions. However, this hypothesis is not supported by our cell-binding assays, where we incubated integrin-expressing cells with tetraspanin-LELs at concentrations where the tetraspanin-LELs would be dimeric. Lastly, addition of the mCD9-LEL protein, which is thought to interact with the platelet integrin α IIB β 3 (Longhurst, White et al. 1999), had no effect on the activation or aggregation kinetics of human platelets in a aggregometer assay (data not shown).

Unlike our initial results showing the cation-dependence of tetraspanin/integrin interactions, all of our latter experiments suggest a discouraging lack of binding specificity. Regardless, many reports suggest the role of tetraspanins in regulating cell migration. For example, antibodies against CD9, CD81, α 3 integrin, and β 1 integrin inhibit in vitro keratinocyte wound-healing (Penas, Garcia-Diez et al. 2000). Antibodies against CD63 inhibit melanoma cell migration and overexpression of CD63 increased β 1 integrin mediated adhesion and migration (Radford, Mallesch et al. 1995). Whether tetraspanin-dependent modulation of integrin-mediated adhesion and migration is direct or indirect is unclear.

In summary, we have presented a series of experiments to directly reconstitute and probe tetraspanin/integrin interactions. These experiments suggest that commonly observed interactions between tetraspanins and integrins occur through the extracellular portions of these molecules. However, we were not able to decipher a pair-wise binding pattern (i.e., all tetraspanin-LELs bound equivalently to α IIB β 3), although these data did roughly correlate to published observations (none bound well to α V β 3 integrin). Most importantly, we were unable to show specificity of tetraspanin-LEL interactions either through the addition of putative function-inhibiting antibodies or the introduction of putative non-heterotypic interacting mutations.



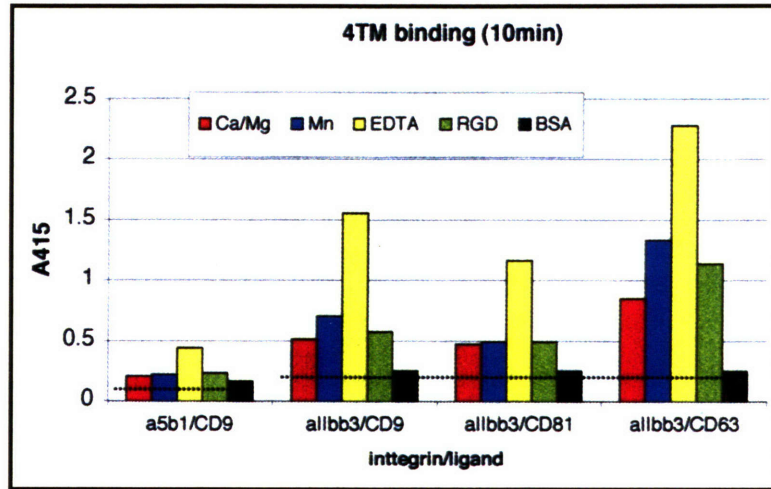
Hynes, 2002 Figure 7

Cations, tail release, modulating antibodies, **tetraspanins (?)**

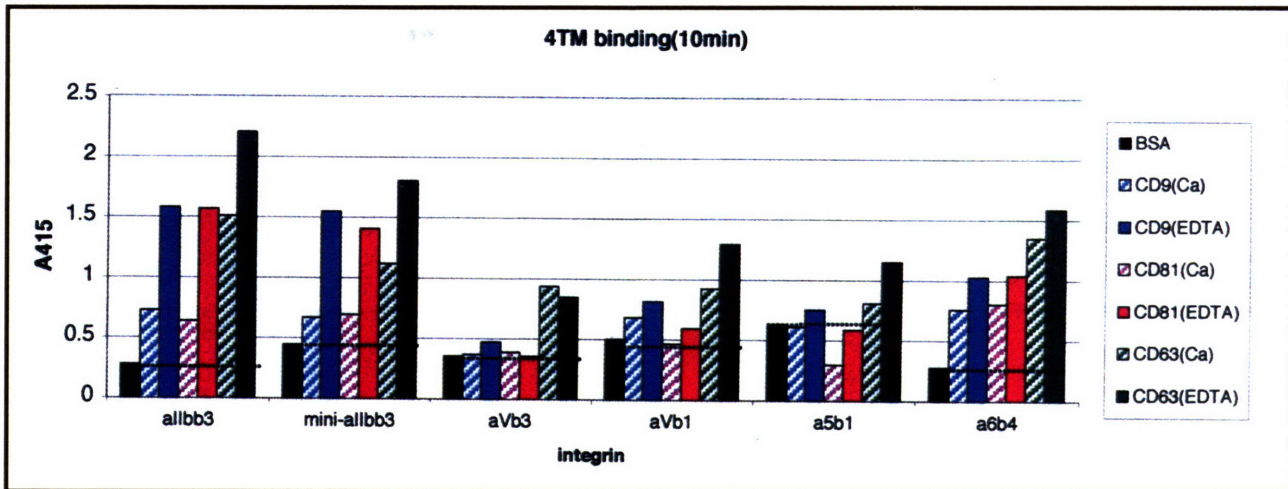
Figure 8.1 Global Conformational Rearrangements of Integrin Heterodimer Structures: A) Integrins in a bent form (left-most structure) have been shown to be inactive. Straightening of the integrin heterodimer to an active conformation can occur either by ligand binding or through the cytoplasmic domains, resulting in the straightening and the separation of the integrin legs (middle/right diagrams). B) Two proposed models for global rearrangement of integrin structure are through either the switch-blade or flick-knife model, or an angle-poise model. The orientation of the integrin heterodimer relative to their respective transmembrane domains is unknown. Experimentally, it has been shown that global integrin conformational changes can occur through either cations, tail release, or modulating antibodies. It is unknown if tetraspanin molecules regulate integrin conformations.

Figure 8.2 ELISA Analysis Reveals Cation-Dependent Tetraspanin/Integrin Interactions: A) The hCD9-LEL, hCD63-LEL, and hCD81-LEL proteins were bound to ELISA plates at 10 μ g/ml. Recombinant α 5 β 1 or α IIb β 3 integrin (10 μ g/ml) was incubated in TBS supplemented with either 1mM Ca/1mM Mg (red), 2mM Mn (blue), 4mM EDTA (yellow), 2mM Mn + 200 μ M GRGDNP for α 5 β 1 and GRGDSP α IIb β 3 (Green). Bovine serum albumin (black) was added as a negative control. The stippled lines indicate background binding, as set to BSA. B) The hCD9-LEL (blue), hCD63-LEL (red), and hCD81-LEL (green) proteins were bound at 5 μ g/ml to ELISA plates. Recombinant α IIb β 3, mini- α IIb β 3, α V β 3, α V β 1, α 5 β 1, α 6 β 4 at 5 μ g/ml were incubated in TBS supplemented with either 1mM Ca/1mM Mg (thatched) or 2mM EDTA (solid). Baseline was set to the BSA control (stippled line). C) The hCD9-LEL (blue), hCD63-LEL (red), and hCD81-LEL (green) proteins were bound at 5 μ g/ml to ELISA plates. Recombinant α IIb β 3, mini- α IIb β 3, α V β 3, α V β 1, α 5 β 1, α 6 β 4, α 4 β 1, α 4 β 7 at 5 μ g/ml were incubated to the plates in TBS supplemented with 2mM EDTA (solid). This ELISA experiment was conducted by J. Takagi using tetraspanin reagents provided by C. C. Liu.

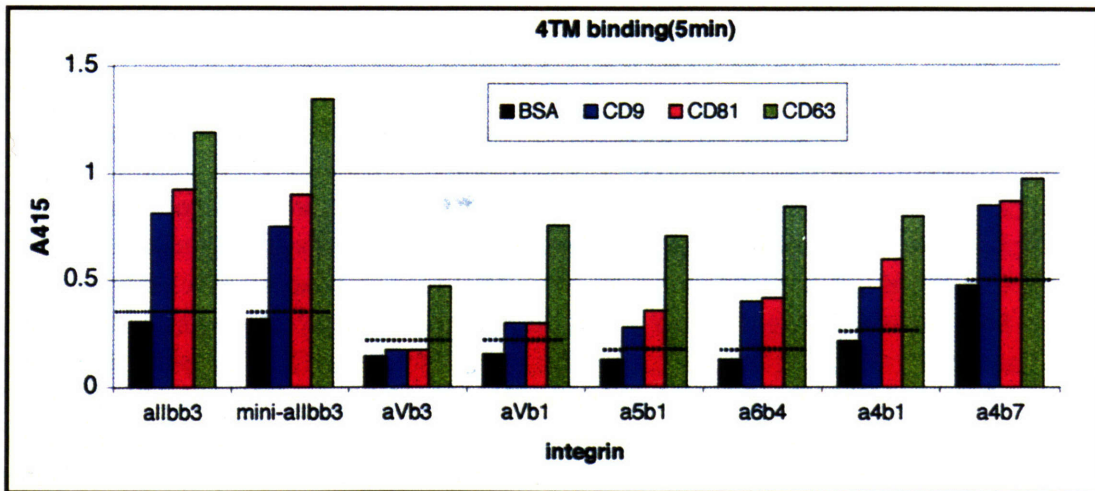
A



B



C



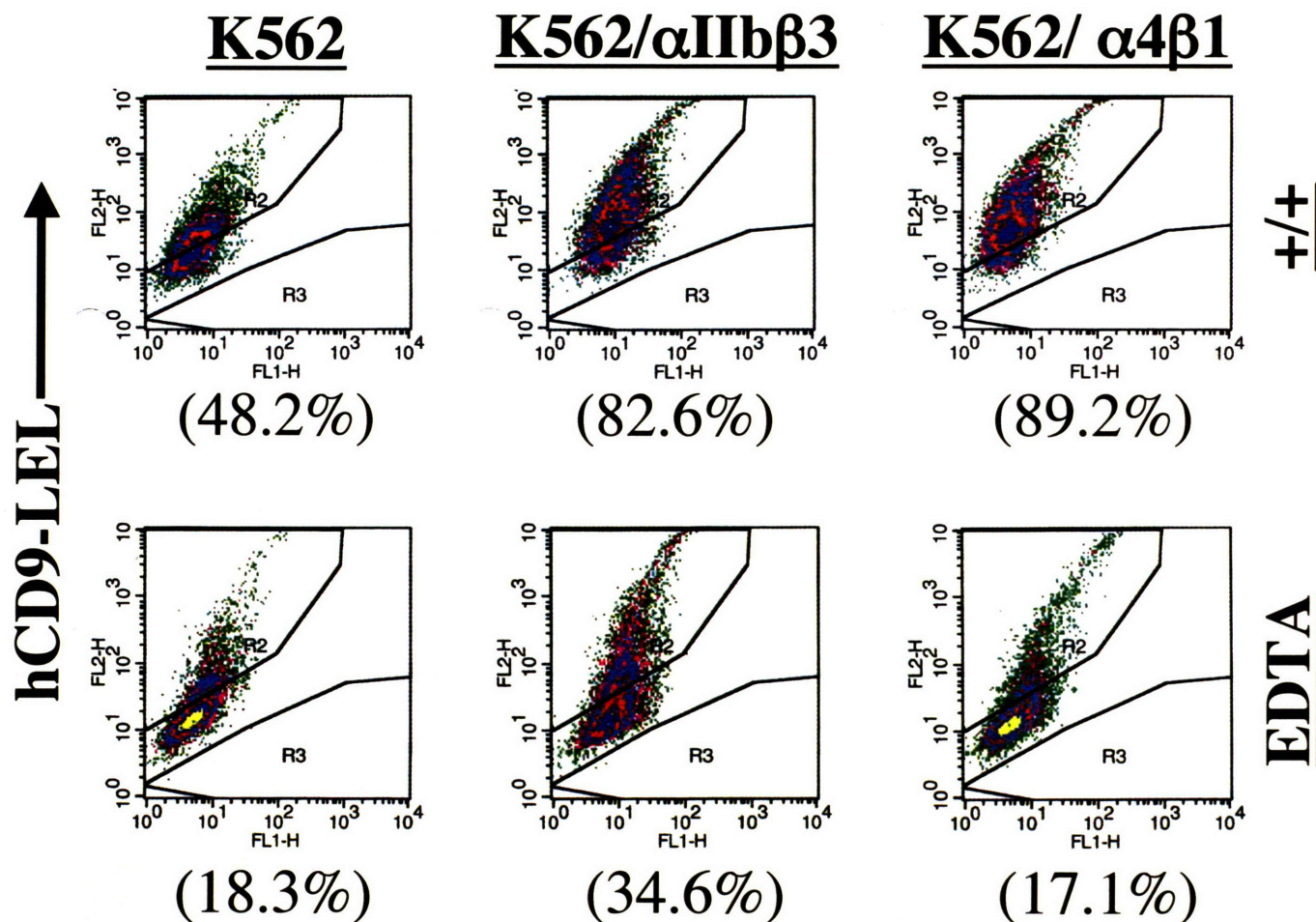
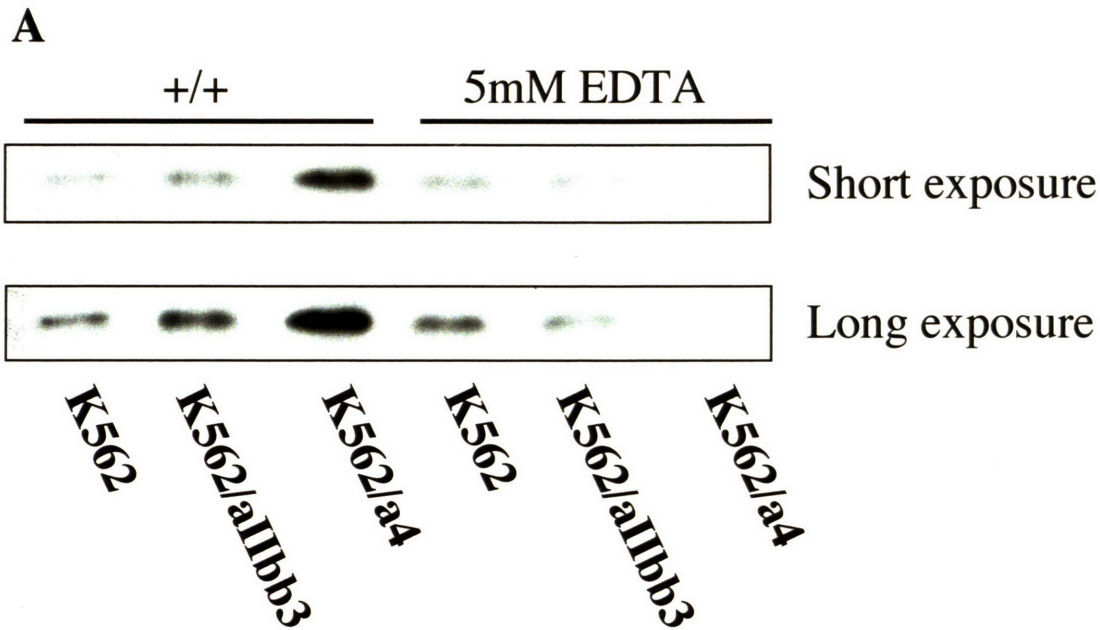


Figure 8.3 FACS Analysis of Cation-Dependent Tetraspanin/Integrin Interactions: K562 cells expressing endogenous α 5 β 1 and stably transfected α IIb β 3 or α 4(β 1) integrins were washed and incubated in phosphate-buffered saline containing either 1mM Ca^{2+} /1mM Mg^{2+} or 5mM EDTA for 1 hour at 4°C. Cells were washed and co-incubated with the hCD9-LEL protein (final concentration 2mg/ml) and a 1:100 dilution of α -CD9 antibody, clone M-L13, for 1 hour at 4°C. Subsequently, cells were washed 1X in PBS/cation and incubated with a 1:100 dilution of PE-conjugated anti-mouse IgG. Cells were washed 1X and analyzed by FACS. Forward and side scatter gates were optimized to select for live cells. Region 2 was defined by K562 samples with either no hCD9-LEL protein or no M-L13 antibody. Under these conditions, <0.5% of K562 cells fell in region 2. Increasing PE fluorescence (CD9 binding) is indicated in the FL2 range. Percentages of region 2 cells under various conditions are indicated in parentheses. This experiment was conducted by C.C. Liu using cells provided by J. Takagi.



B

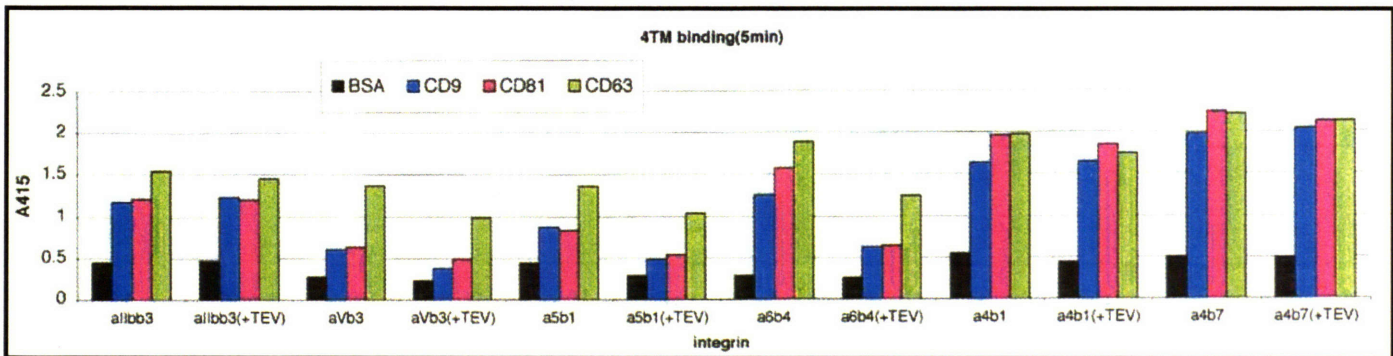


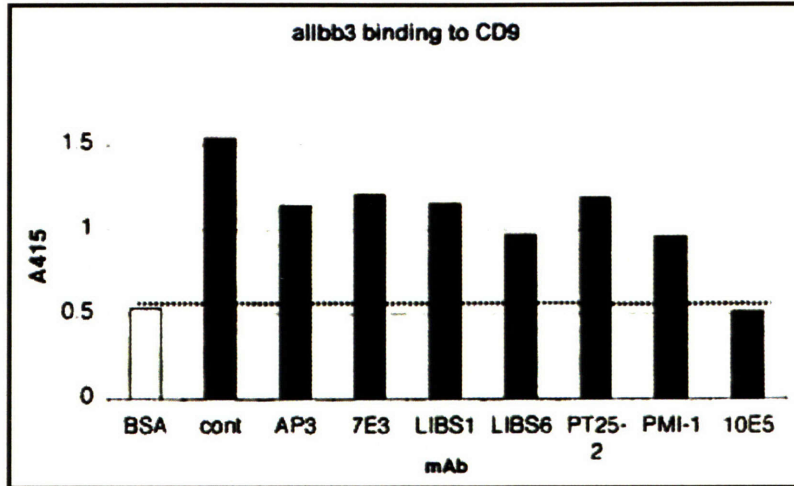
Figure 8.4 Cell-Surface Integrin Binding of Tetraspanins: A) K562 cells expressing endogenous $\alpha 5 \beta 1$ and stably transfected α IIb β 3 or $\alpha 4(\beta 1)$ integrins were washed and incubated for 1 hour at RT in phosphate-buffered saline containing either 1mM Ca^{2+} /1mM Mg^{2+} or 5mM EDTA. Cells were washed and incubated with the hCD9-LEL protein (final concentration 2mg/ml) for 1 hour, washed in PBS/cation and lysed in RIPA buffer. Insoluble portion was cleared by centrifugation and cell lysate was quantified with the microBCA kit. Equal amounts of protein were loaded on 18% non-reducing SDS-PAGE and probed for hCD9-LEL with the antibody 72F6. B) Tetraspanins were bound to ELISA plates as previously described. Integrins with C-terminal coiled-coil clasps were released with 250U/ml of TEV protease by overnight incubation at RT. Non-cleaved integrins were incubated with TEV-negative buffer. Integrins were added to tetraspanin-ELISA plates and developed under standard conditions. TEV protease addition is indicated under each set of data.

Experiment in A was conducted by C.C.Liu and ELISA in B was conducted by J. Takagi using tetraspanin reagents provided by C. C. Liu.

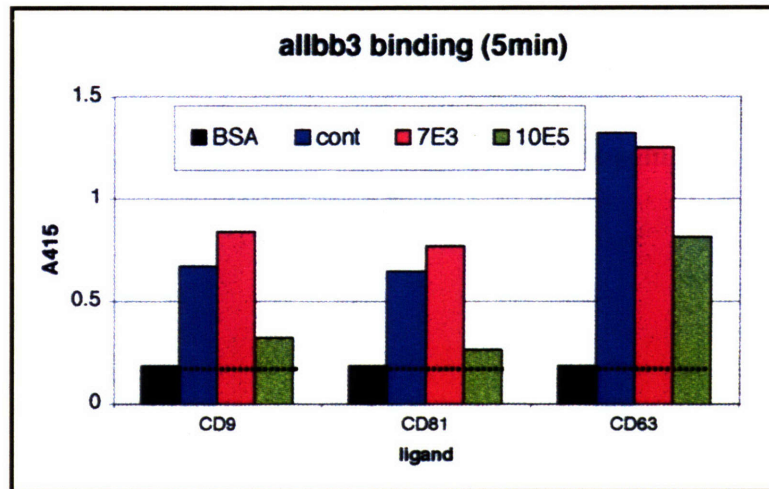
Figure 8.5 α IIB β 3 Binding to Tetraspanins: To further explore α IIB β 3 binding to tetraspanin-LELs, we used a series of anti-integrin modulating antibodies. A) The hCD9-LEL protein was bound to ELISA plates. Integrin α IIB β 3 was incubated with a panel of modulatory antibodies listed. No antibody addition is listed as cont(rol). B) To test binding inhibition by the anti- α IIB β 3 antibody 10E5, tetraspanin-LELs were bound as before. The α IIB β 3 integrin was incubated in 2mMEDTA with either no-antibody (blue), non-modulating antibody (red), or the modulating 10E5 antibody (green). Baselines are set to the BSA background control. C) To test the effects of associating drugs, the hCD9-LEL was bound to ELISA plates. Integrin α IIB β 3 binding was tested as before, except instead of 2mM EDTA, TBS was supplemented with 1mM Ca²⁺/1mM Mg²⁺. As indicated, integrin α IIB β 3 was supplemented with 100 μ M EF5154 or GFGDSP.

This experiment was conducted by J. Takagi using tetraspanin reagents provided by C. C. Liu.

A



B



C

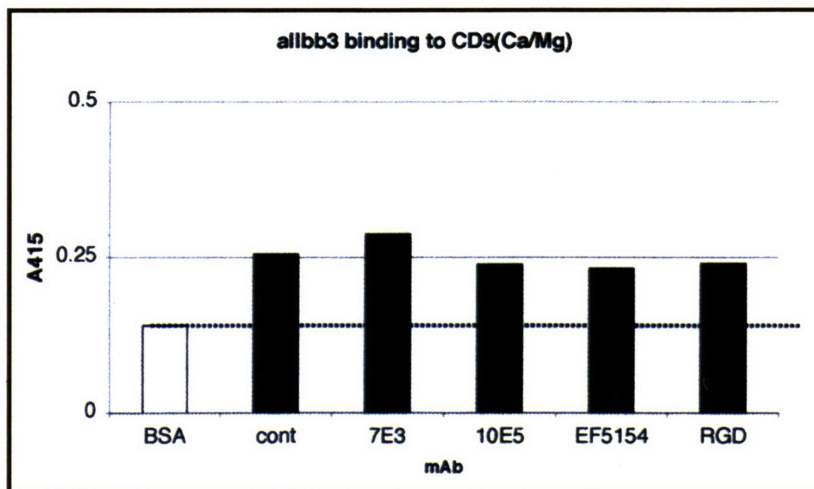
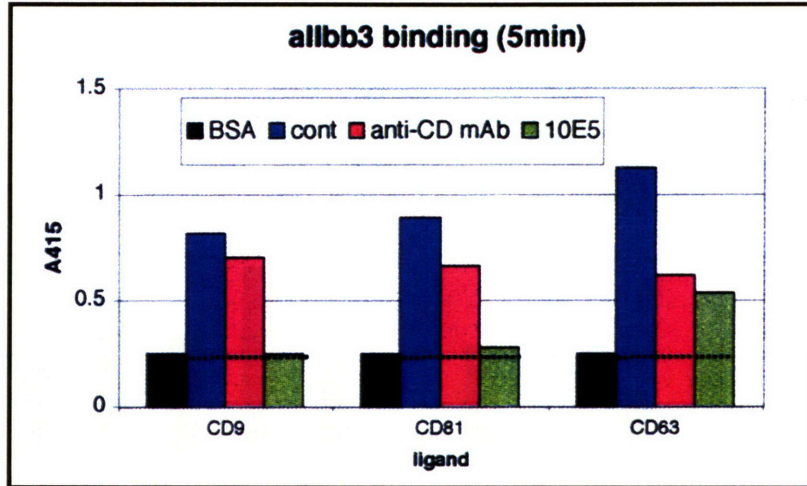


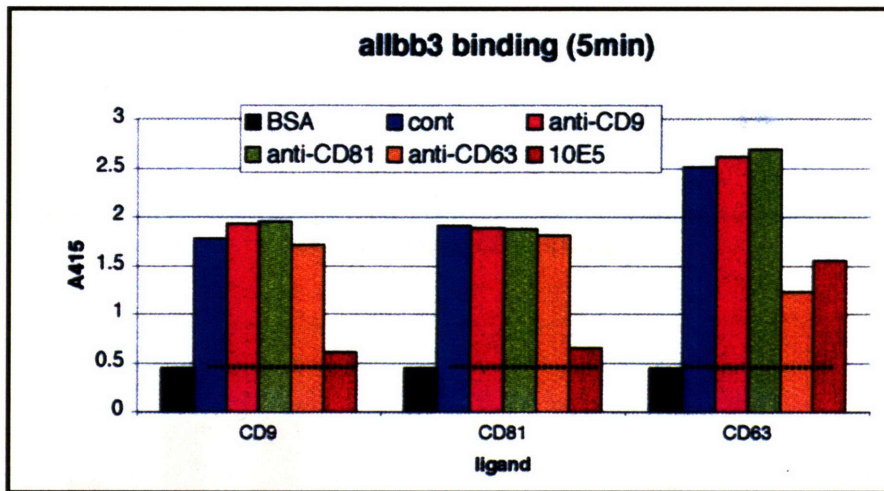
Figure 8.6 Tetraspanin Antibody and Point Mutation Effects on α IIB β 3 Binding: To test specificity of α IIB β 3/tetraspanin interactions, hCD9-LEL, hCD63-LEL, and hCD81-LEL were bound to ELISA plates as before. A) Integrin α IIB β 3 was incubated in TBS/EDTA to ELISA plates with either no antibody (blue), an antibody against the bound tetraspanin (red), or the inhibitory 10E5 antibody (green). Background is indicated with a stippled line. B) Tetraspanin-LELs were bound to the plate and incubated with α IIB β 3 integrin in TBS/EDTA. Anti-CD9 (pink), anti-CD81 (green), anti-CD63 (orange) or 10E5 (red) were added at 20 μ g/ml. No antibody addition (blue) and BSA (black) were used as positive and negative controls respectively. Background binding is indicated with stippled lines. C) To test specificity of human CD9-LEL interactions, two point mutations were constructed hCD9-LEL•Q161A and hCD9-LEL•E150A/Q161A and bound to ELISA plates. α IIB β 3 integrin was incubated with TBS/1mM Ca²⁺/1mM Mg²⁺ and background binding is indicated with a stippled line.

This ELISA experiment was conducted by J. Takagi using tetraspanin reagents provided by C. C. Liu.

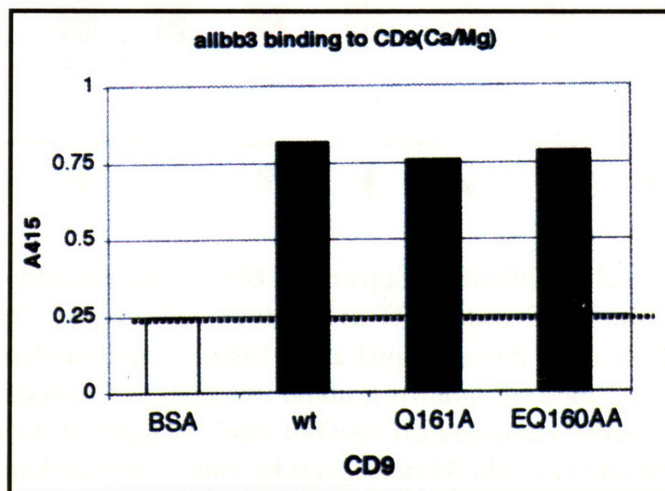
A



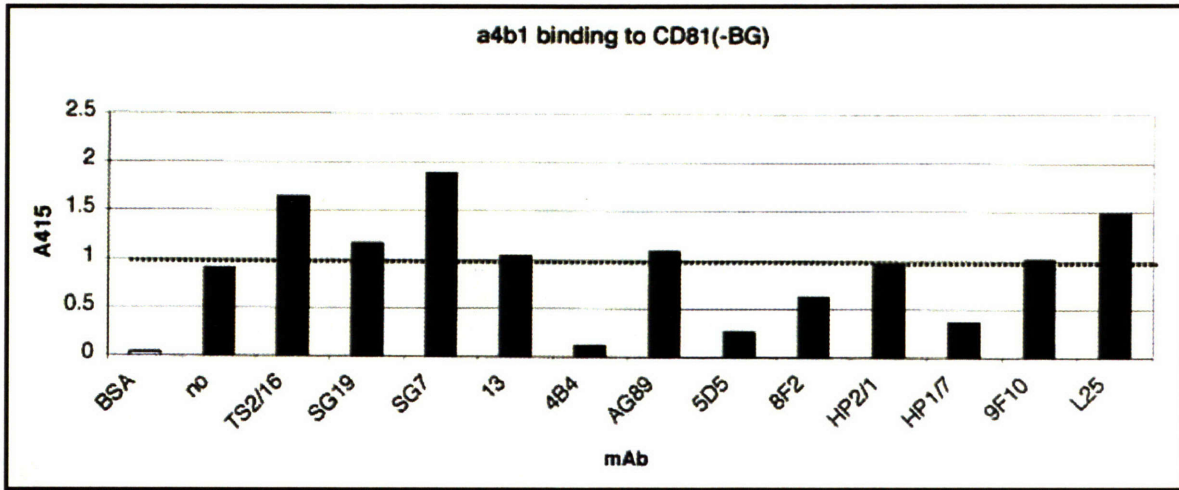
B



C

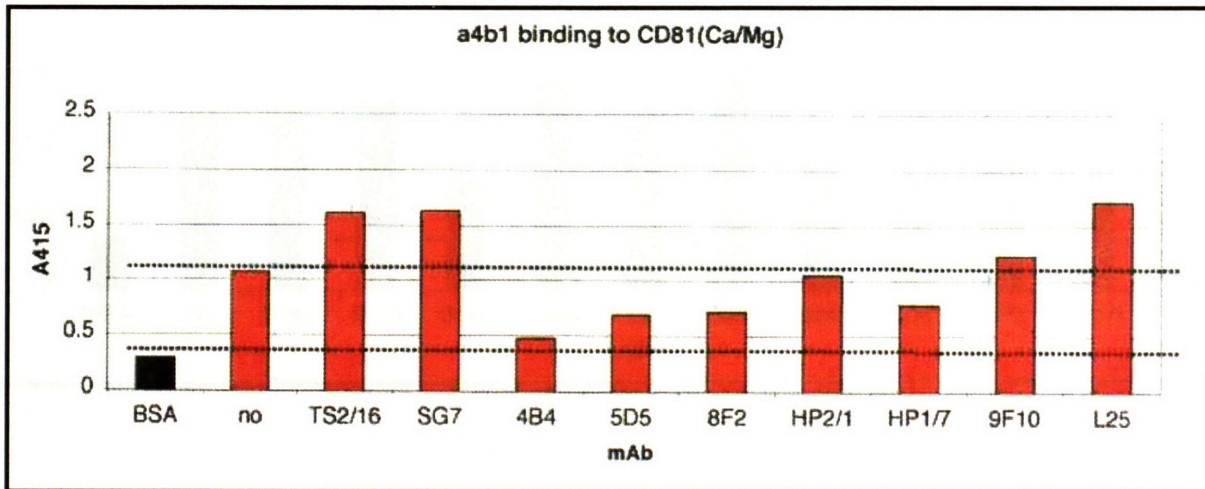


A



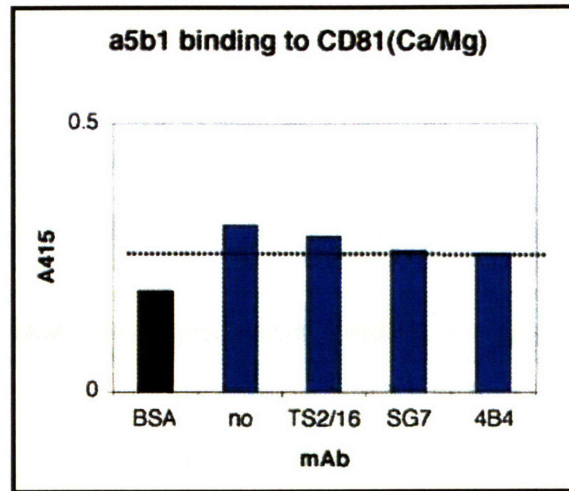
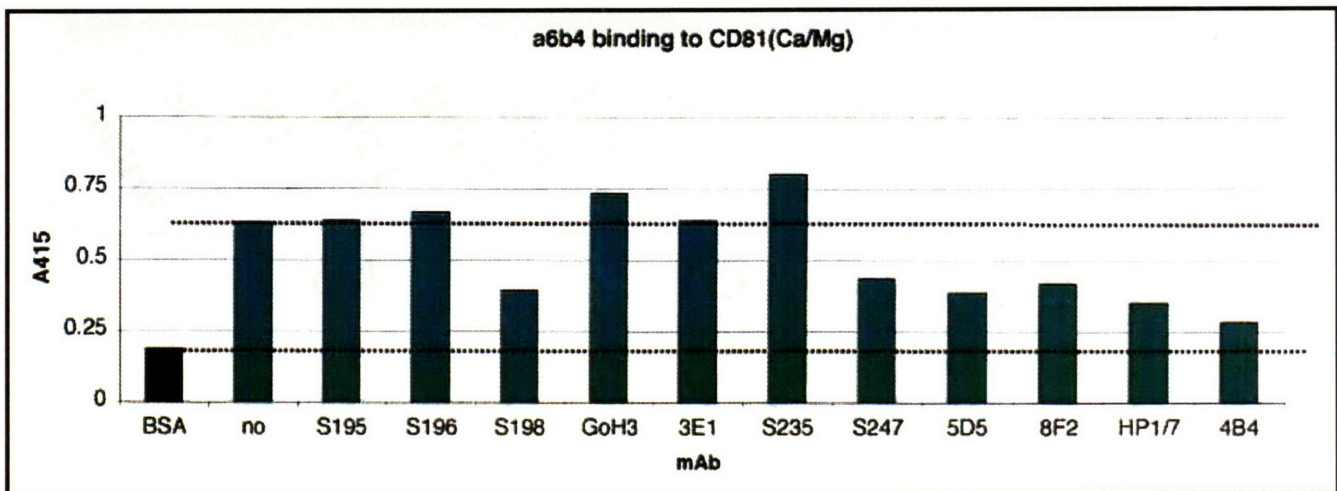
* * * I N I I N ?

B



* * I N I I N ?

Figure 8.7 Antibody Modulation of $\alpha 4\beta 1$ /Tetraspanin Binding: The hCD81-LEL was bound to ELISA plates. $\alpha 4\beta 1$ integrin was incubated in TBS/1mM Ca^{2+} /1mM Mg^{2+} with a 1:100 dilution of the indicated antibody (either from a 1mg/ml stock or ascites). A) BSA background was set to 0 and the stippled line indicates binding without the addition of antibody. B) An independent replicate of A. Stippled lines indicate background (bottom line) and baseline binding (top line). The function of anti $\alpha 4$ integrin antibodies is indicated with either an I (inhibitory) or N (non-blocking) or ? (unknown). Antibodies that have overlapping epitopes are indicated with an asterisk. This experiment was conducted by J. Takagi using tetraspanin reagents provided by C. C. Liu.

A**B**

X X X X

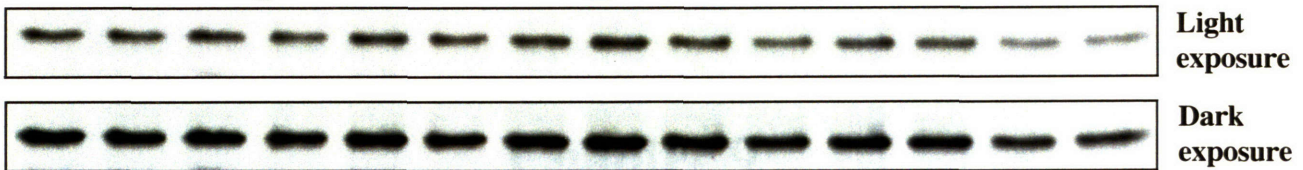
Figure 8.8 Antibody Characterization of $\alpha 4 \beta 1$ and $\alpha 6 \beta 4$ Integrins

Figure 8.8 Specificity of $\alpha 4 \beta 1$ Antibody Effects: A) To test the specificity of anti- $\beta 1$ antibodies, hCD81-LEL was bound to ELISA plates. $\alpha 5 \beta 1$ integrin heterodimer was incubated with plates in TBS/1mM Ca^{2+} /1mM Mg^{2+} with antibodies at 1:100 dilution. B) To test binding to $\alpha 5 \beta 1$, hCD81-LEL was bound to ELISA plates. $\alpha 6 \beta 4$ integrin was incubated with plates in TBS/1mM Ca^{2+} /1mM Mg^{2+} with antibodies at 1:100 dilution. Antibodies against the $\alpha 4$ integrin are indicated with a red X. Stippled lines indicate both background binding (lower line) and baseline binding (upper line). This ELISA experiment was conducted by J. Takagi using tetraspanin reagents provided by C. C. Liu.

$\alpha 5 \beta 1$ and $\alpha 6 \beta 4$ integrin antibodies are indicated with a red X.

reagents provided by J. Takagi

α -Nucleoporin (*loading control*)



α -hCD9-LEL (*experimental*)

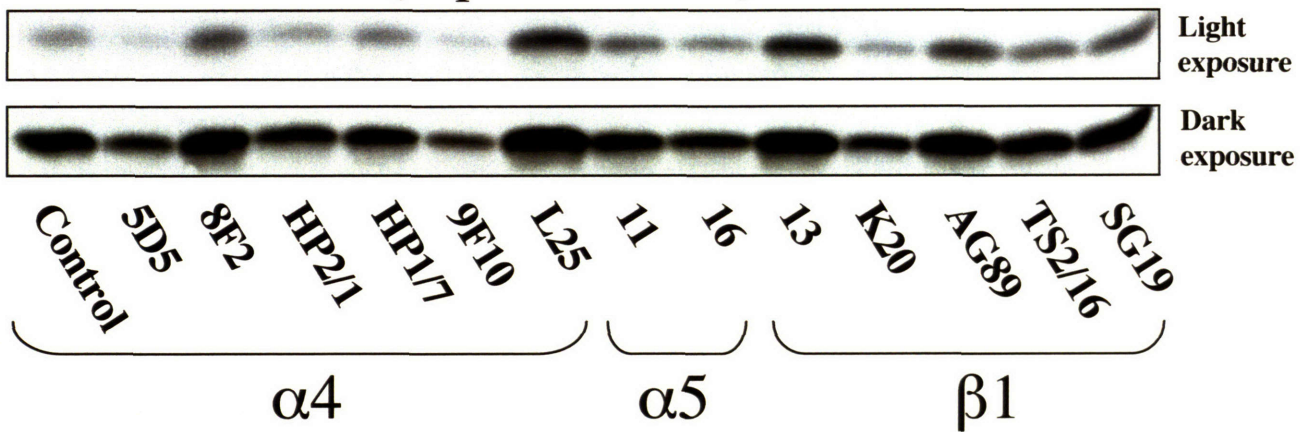


Figure 8.9 Antibody Modulation of Cell-Surface Integrin Binding: K562 cells expressing endogenous α 5 β 1 were washed in PBS/1mMCa/1mMMg, aliquoted, and incubated with a 1:25 (40mg/ml or ascites dilution) in 50 μ ls for 15' at RT. Fifty μ ls of a 2mg/ml solution of hCD9-LEL (for a final concentration of 1mg/ml protein) was added to the cells and incubated for 45' at RT. Cells were washed 3X in PBS+/. Cells were lysed in RIPA buffer with protease inhibitor cocktail (Boehringer) and insoluble portion was cleared for by centrifugation. Protein content was monitored by microBCA assay and equal amounts were loaded onto 18%SDS-PAGE. Westerns were developed using the anti-human CD9 antibody clone 9F27. Anti-nucleoporin antibody was used as a loading control. Antibodies against α 4, α 5, and β 1 integrin subunits are indicated. This experiment was conducted by C.C. Liu using reagents provided by J. Takagi.

Chapter 9

Conclusions and Future Directions

This discussion was written by Christopher C. Liu with helpful discussion and editing from Richard O. Hynes. All conclusions and errors are my own.

Introduction

This thesis has described a rapid methodology to purify and characterize tetraspanin-LELs. Biophysical and molecular biological analyses show that the CD9-LEL, CD63-LEL, and CD81-LEL are all α -helical dimers composed of a conserved dimerization subdomain and a variable subdomain, consistent with a published crystal structure of the human CD81-LEL. We are readily able to purify a single conformational species of each tetraspanin-LEL dimer. These reagents can be used to inhibit endogenous tetraspanin functions, further suggesting that our tetraspanin-LEL proteins are biologically relevant. The discussion and future directions of these inhibition studies (fertilization and hepatitis C infection) are discussed in Chapter 7 and the Appendix, respectively. In this chapter, we discuss future experiments that are both a natural extension of the work described in this thesis and may also serve to lend the most insight into tetraspanin functions.

Tetraspanin Extracellular Domains

The first area of focus of this thesis has been on the biophysical characterization of tetraspanins-LEL domains *in vitro*. We have purified and characterized three different tetraspanins-LELs, including many variants of the murine CD9-LEL. As the hCD81-LEL structure has proven to be instrumental in developing our conceptual framework for tetraspanin functions (Kitadokoro, Bordo et al. 2001), we have attempted (and failed) to derive atomic-level structures of other tetraspanin-LELs. Structural studies of other tetraspanin-LELs would add significantly to the mutagenesis analyses described in this thesis. More detailed biophysical techniques to measure the binding kinetics of one tetraspanin monomer to another, such as isothermal calorimetry, may also prove useful. Currently, we have not measured the binding and dissociation constants of tetraspanin oligomerization, although biophysical and mutagenesis studies indicate that tetraspanin-LELs are obligate homodimers.

In many ways, the global stability, small size, dimeric nature and cooperativity of folding of tetraspanin-LELs suggest that these proteins are ideal substrates for oligomeric protein folding and design studies (Cordes, Davidson et al. 1996). Based upon structural and sequence homologies (Seigneuret, Delaguillaumie et al. 2001), it may be possible to

further stabilize the tetraspanin-LEL homodimers either through introducing an interchain disulfide-bond or by designing a single-chain tetraspanin-LEL dimer (Root, Kay et al. 2001). These studies may serve both to validate further the quarternary structure of the tetraspanin-LEL dimer and to increase both the stability and potency of tetraspanin-LELs in inhibition experiments.

Our observations of well-folded homodimeric tetraspanins-LELs immediately suggested the attractive possibility of heterodimers, especially as multiple homotypic tetraspanin interactions have been observed. Experimentally, we saw no evidence of preferential heterodimerization between the hCD9-LEL and the hCD81-LEL. The role of specific protein dimerization and oligomerization is of key importance in regulating biological functions (Klemm, Schreiber et al. 1998). Protein oligomerization serves not only to increase functional diversity combinatorially, but also to regulate receptor avidity and to define spatio-temporal boundaries of signaling complexes. The small size and global stability suggests the possibility of rationally designing heterodimeric tetraspanin-LELs (Keating, Malashkevich et al. 2001).

Our initial attempts to disrupt dimerization and to design a monomeric, folded version of the murine CD9-LEL were not successful. However, we have not completely exhausted the possibilities in this avenue of research. By introducing intramolecular, buried disulfide bonds, it may be possible to stabilize further each independent tetraspanin-LEL subunit (Betz 1993). Such stabilization, coupled with a more rigorous attempt to introduce polar and charged amino acid residues into the dimerization interface may allow the design of a monomeric tetraspanin-LEL. A monomeric tetraspanin-LEL variant would allow researchers to explore the contribution of tetraspanin-LEL dimerization to inhibition experiments. Currently, we view tetraspanin-LELs as dominant negatives, serving to disrupt endogenous heterotypic complexes at the cell surface. It is unclear if the bivalent nature of the tetraspanin dimer is essential to their inhibitory effects.

As technology for peptide synthesis advances, the relatively short length of tetraspanin-LELs (~80 amino-acids) will allow chemical synthesis of these molecules (either by standard synthesis reactions or through sequential peptide ligation). The ability to synthesize tetraspanin-LELs chemically would allow the incorporation of covalent

cross-linkers into the amino acid chain that do not disrupt heterotypic interactions but allow direct cross-linking to heterotypic binding partners. The molecular dissection of the KMC8 epitope as presented in this thesis lays the groundwork for the design of these tetraspanin-LEL variants. These reagents, used in tandem with our studies on both the inhibitory effects of recombinant tetraspanins-LELs and their interactions with integrins would serve to decipher the complex roles of tetraspanins-LELs. The ability to covalently cross-link tetraspanins-LELs to their specific binding partners would also assist in clearly mapping heterotypic interaction domains.

Inhibitory Effects of Soluble Tetraspanin-LELs.

Our primary, motivating interest in tetraspanins was, and still remains, their unique roles in membrane fusion (Stein, Primakoff et al. 2004). The proteins directly responsible for cell-cell fusion remain unknown. Given the recent, significant advances in viral-cell and vesicle-vesicle fusion (Earp, Delos et al. 2005), an understanding of cell-cell fusion at the molecular level would be a giant advance towards our appreciation of this fascinating topic

CD9, which was shown to be essential for sperm-egg fusion, did not fit our view of a membrane fusogen. To further explore the role of CD9 in membrane fusion, we developed a methodology to produce and purify the CD9-LEL. A well-characterized, soluble CD9-LEL could be useful in several ways. Logically, if CD9 does not play a direct role in catalyzing membrane fusion, it may bind to either a sperm or an egg protein that does. We made the CD9-LEL and a series of folded, characterized mutants with this series of experiments in mind.

Indeed, our CD9-LEL protein exhibited significant, but far from complete inhibition of fertilization (Zhu, Miller et al. 2002). Furthermore, pre-incubation of the CD9-LEL protein with either sperm or egg cells suggested that endogenous CD9 functions on the egg surface, and not as a sperm receptor. We, and others, have attempted to identify CD9 binding partners on the egg surface with no luck.

The search for a heterotypic CD9 binding partner is far from complete. The inhibitory activity of our CD9-LEL protein has is a small, but significant step forward towards our understanding of how CD9 functions on the egg surface. As limited

numbers of egg cells is a significant technical hurdle for classical biochemistry, it may be possible to find oocyte specific binding partners through either screening a λ gt11 phage library (Mierendorf, Percy et al. 1987), or expression cloning in eukaryotic cells. The reversible effect of PSG17-mediated inhibition on CD9, suggests that CD9 does not function as a chaperone to a membrane fusogen (Ellerman, Ha et al. 2003). Our ability to rescue CD9-null oocytes with de novo expression of CD9 also suggests that CD9 may serve to increase affinity or avidity of other, essential proteins in sperm-egg fusion (Zhu, Miller et al. 2002).

The ubiquitous binding nature of tetraspanins-LELs makes the development and characterization of CD9-LEL variants described in this thesis essential for this series of experiments. Coupled with the possible generation of novel, covalent cross-linking CD9-LELs described above, we remain optimistic that CD9 may serve as a conduit to bootstrap towards a sperm-egg fusogen. Our inability to make greater headway into probing the molecular mechanisms underlying sperm-egg fusion remains a point of deep disappointment for us.

Recently, we initiated a collaboration with Jane McKeating to utilize our recombinant tetraspanins-LELs to study another membrane fusion event: the infectivity of hepatitis C. For some time, hepatitis C (HepC) envelope proteins have been known to bind to the tetraspanin CD81 (Pileri, Uematsu et al. 1998) (Flint, Maidens et al. 1999). As CD81 expression is not limited to HepC permissive cells (Levy, Todd et al. 1998), it has been hypothesized to function as a viral co-receptor (McKeating, Zhang et al. 2004). Recent advances in replicating the hepatitis C lifecycle, including genomic replication (Blight, Kolykhalov et al. 2000), viral pseudotyping (Hsu, Zhang et al. 2003), and finally, the full HepC viral lifecycle (Lindenbach, Evans et al. in press) may serve to accelerate the pace of flavivirus research. Lastly, the detailed mechanism of HepC glycoprotein mediated membrane fusion is converging with the better understood retroviral and vesicle fusion systems (Earp, Delos et al. 2005).

Our results showing specific inhibition of HepC infectivity with the CD81-LEL is not novel. Multiple groups have produced and shown inhibition with similar reagents (Flint, Maidens et al. 1999; Higginbottom, Quinn et al. 2000; Petracca, Falugi et al. 2000). However, our methodology to produce and characterize highly purified CD81-

LELs and their non-inhibitory variants results in significantly greater potency of inhibition (unpublished results). These reagents may serve to both probe hepatocyte specific CD81-LEL binding partners (in a manner similar to that described for fertilization) and also to probe the mechanism of HepC glycoprotein function. In collaboration, Jane McKeating will utilize both our reagents and the ability to produce high HepC viral titers to search for escape mutants from CD81-LEL mediated inhibition.

Lastly, the greater potency of our reagents will allow us to test inhibition of HepC virions in a SCID mouse model system transplanted with human hepatocytes (Meuleman, Libbrecht et al. 2005) in collaboration with both Jane McKeating and the Leroux-Roels laboratory. If these *in vivo* inhibition experiments are successful, I expect that the CD81-LEL protein may be commercialized.

Tetraspanin Interactions in the Membrane

Shortly after the identification of tetraspanins as a family of proteins (Oren, Takahashi et al. 1990), the concept of a tetraspanin web was raised (Rubinstein, Le Naour et al. 1996). Almost a decade after this hypothesis, the existence of a tetraspanins web, or the ability of tetraspanins to spatially organize complexes at the cellular membrane, remains contentious.

A large body of literature suggests that tetraspanins bind in a robust, stoichiometric, heterotypic fashion with other membrane proteins (integrins (Berditchevski 2001) and immunoglobulin superfamily members (Stipp, Kolesnikova et al. 2003). This interaction is mediated through the tetraspanins-LEL (Kazarov, Yang et al. 2002). When the stringency of these techniques is lowered, significantly greater numbers of interactions are also observed, including homotypic tetraspanins interactions (Berditchevski, Zutter et al. 1996), MHC proteins, CD4 (Imai, Kakizaki et al. 1995), CD8 (Imai and Yoshie 1993), CD36 (Miao, Vasile et al. 2001), and a larger array of integrins (Berditchevski 2001).

An outstanding question raised and unresolved in this thesis is the role of tetraspanin oligomerization at the cell surface. Both the structure of the CD81-LEL (Kitadokoro, Bordo et al. 2001) and our characterization of tetraspanins-LELs as helical dimers immediately suggested that tetraspanins-LELs might play a central role mediating

oligomerization at the cell surface. However, many biochemical attempts to probe this function, including some described in this thesis, have been attempted without resolving conclusively the nature or even the validity of these proposed interactions.

Our biophysical and molecular analysis of a number of tetraspanins-LELs is internally consistent and suggests that dimerization is a key factor in the folding stability of the tetraspanins-LEL. Surprisingly, we were not able to detect oligomers with intact CD9 molecules, in direct disagreement with our biophysical data. We have no choice but to conclude that either our biophysical data is incorrect, is not biologically relevant, or that the inclusion of other tetraspanin domains serves to mitigate the oligomerization of tetraspanins-LELs.

We do not believe our biophysical data to be incorrect. Our observations that the tetraspanins are α -helical dimers composed of two subdomains is consistent with a large body of literature, including structure (Kitadokoro, Bordo et al. 2001), sequence (Seigneuret, Delaguillaumie et al. 2001), and antibody-induced effects (Maecker, Todd et al. 1997). On the other hand, dimerization of tetraspanins-LELs may be biologically irrelevant. Both sequence conservation and disulfide-bonding patterns strongly suggest that a large hydrophobic patch exists in the tetraspanins-LELs (Seigneuret, Delaguillaumie et al. 2001). However, this surface does not necessarily need to mediate dimerization. It is possible, however unlikely, that the tetraspanins small extracellular loop (SEL) may serve to cap this surface. As SELs are short (Maecker, Todd et al. 1997), 15-20 amino acids in length, chemical synthesis of this tetraspanins domain and the analysis of its influence on both the biophysical properties of tetraspanins-LELs and tetraspanins-LEL mediated inhibition are intriguing. Lastly, multiple observations that tetraspanins-LELs specifically inhibit functions and that these inhibitory effects match both mouse model and antibody-induced effects support the biological relevance of our methodology.

Our experiments with the intact CD9 molecule raise the probability that other tetraspanins hydrophobic domains may serve to mitigate tetraspanin-LEL mediated oligomerization. The presence of conserved, polar residues in all tetraspanins transmembrane segments suggests an evolutionarily conserved role (Stipp, Kolesnikova et al. 2003). Although our null hypothesis is that the crystal structure the CD81-LEL is

consistent with the existence of a tetraspanins dimer on the same lipid bilayer, this assumption is still quite controversial. To reconcile, the antiparallel structure of the CD81-LEL, it is necessary to envision a flat, planar tetraspanins dimer lying in close proximity to the lipid bilayer. It is conceivable that the hydrophobic, putative dimerization interface lies embedded into the lipid bilayer, similar to a peripheral membrane protein.

To ideally resolve these issues, we propose that it is necessary to characterize tetraspanin molecules in isolation, in reconstituted lipid vesicles. Reconstitution of purified tetraspanin molecules would allow the use of both fluorescence resonance energy transfer (FRET) or fluorescence recovery after photobleaching (FRAP) to probe the oligomerization state of tetraspanins. These studies, coupled with the mutagenesis studies described in this thesis, would allow precise measurements of the contribution of each tetraspanin domain to oligomerization – if indeed it occurs. Reconstitution of tetraspanins with heterotypic partners would also explore the potential influence of heterotypic partners on oligomerization and avidity regulation. Lastly, synthesis of tetraspanin transmembrane segments in isolation and subsequent introduction into lipid vesicles would directly measure the contributions of these domains to oligomerization, which has been alluded to, but not directly explored.

Given the technical difficulties underlying reconstitution of intact tetraspanins into lipid bilayers, we also propose an alternative methodology. In parallel with the tetraspanin variants that abolish heterotypic interactions, it may be possible to use rapamycin-induced FKBP dimerization to induce tetraspanin dimers (Klemm, Schreiber et al. 1998). By artificially inducing high-avidity homo- or hetero- oligomeric tetraspanin complexes, it may be possible to decipher the contribution of oligomerization to endogenous tetraspanin functions.

The ideas and future directions described here are not novel. The study of membrane proteins, their functions, and their oligomerization states is complex. In this thesis, we have taken a traditional approach to study membrane proteins, by largely ignoring the hydrophobic domains. It appears that in tetraspanins, even more so than other transmembrane proteins, the effects of hydrophobic domains may not be ignored. However, given the complexity and contribution of different domains to the endogenous

functions of transmembrane proteins, these studies must be undertaken. Recently, the integrin field has undergone a renaissance of ideas, both with the description of global conformational changes long known to occur, and a strong indication that lateral association of transmembrane segments may modulate extracellular domain functions (Hynes 2002). The concept of lateral association between tetraspanin transmembrane segments is appealing and needs to be explored in full detail.

The idea of a tetraspanin-enriched microdomain (TEM), similar to that observed with lipid rafts, is both alluring and fraught with controversy. Various experimental approaches, including tetraspanin palmitoylation and detergent-insoluble flotation gradients hint at the existence of a TEM (Cherukuri, Shoham et al. 2004). However, current techniques lack the resolution or rigor to resolve outstanding issues. Without detailed analysis of tetraspanin partitioning into and out of high avidity complexes, this idea will remain in the hypothesis stage. In this thesis, we have presented detailed molecular analysis regarding the tetraspanin-LEL segment. These insights, in conjunction with mutations of conserved amino acid residues in each tetraspanin transmembrane segment and the techniques described above may shed light on TEMs.

Currently, an active avenue of tetraspanin research is the generation and analysis of tetraspanin knock-out mice. Targeted deletion of CD82 (a prostate metastasis suppressor (Dong, Lamb et al. 1995)) and CD63 are eagerly anticipated. Transgenic rescue of tetraspanin-null mice (which has only been described with CD9-null oocytes in Chapter 7) with multiple tetraspanin variants may also begin to decipher tetraspanin-LEL functions. Analysis of detergent-solubilized tetraspanin complexes, potential recruitment of these complexes into TEMs, and the contribution of tetraspanin palmitoylation to complex formation (Charrin, Manie et al. 2002; Charrin, Manie et al. 2003) also remain active areas of research. Detailed analysis of these hydrophobic tetraspanin domains, coupled with an increasing cognizance of tetraspanin-LEL-mediated functions, may serve to reveal the underlying function of all tetraspanins.

Over the course of this thesis it has become evident that without the reconstitution and analysis of specific tetraspanin domains in isolation and together, an inclusive understanding of endogenous tetraspanin functions will prove difficult. The approaches taken in this thesis underscore the parallel approach I have taken to explore tetraspanin

functions relative to the rest of the field. Rather than the deletion of specific genes (a reverse genetic approach (Hemler 2001)) or the sequential characterization of cellular tetraspanin complexes (a deconvolution approach), we have sought to characterize the roles of a specific tetraspanin domain (a reconstitution approach). This reconstitution approach has both allowed the development of novel hypotheses for tetraspanin functions and also the precise exploration of tetraspanin-LEL mediated inhibition.

The success of reverse genetics and deconvolution has served to reveal a panoply of exciting, novel roles for tetraspanins in many diverse cell types, functions, and model organisms (Hemler 2003). However, our reconstitution approach has yet to reach full concordance with these other approaches and a unifying theory of tetraspanin function is unclear. When these approaches meet and merge, hopefully with the completion of the experiments described in this chapter, we believe that tetraspanins will fully reveal their central roles, which we propose is in regulating both the affinity and the avidity of membrane proteins.

Appendices

Appendix A

Specific hCD81-LEL inhibition of Hepatitis C Infection

These experiments were conceived by Christopher C. Liu, Jane McKeating, and Richard O. Hynes. All tetraspanin reagents were constructed by Christopher C. Liu. All inhibition of Hepatitis C pseudotyped virions assays was performed in the laboratory of Jane McKeating. Non-pseudotyped Hepatitis C virions (HepCpp) was made and analyzed by Brett Lindenbach.

Tetraspanin CD81-LEL Inhibition of Hepatitis C Infection

The experiments described in this appendix were initiated over the summer of 2004 through a series of discussions with Jane McKeating at the FASEB Tetraspanin 2004 meeting. Since my undergraduate studies, I have followed research on Hepatitis C infectivity and the mechanisms of flaviviral membrane fusion closely and with great interest. It is quite an honor to both finally study and contribute reagents to this body of research. However, I must admit that Jane McKeating intellectually drives this collaboration and I am merely providing useful reagents. As a result, I feel the series of experiments described below are not worthy of a full chapter in this thesis. A publication, appended in this thesis, has already risen from this fruitful collaboration.

The most prominent role for a tetraspanin in infectious disease is CD81, which has been characterized as a receptor for the flavivirus Hepatitis C (Pileri, Uematsu et al. 1998).

Hepatitis C virus (HCV) is a major cause of liver disease, with over 170 million infected individuals worldwide. Currently, HCV infection is the major cause of liver transplants in the United States and current drug therapies are mostly ineffective (De Francesco and Rice 2003). A member of the flaviviridae viral family, HCV encodes two envelope genes, E1 and E2, believed to be type I transmembrane proteins that mediate viral entry (Fields 2001). These proteins have been structurally categorized as class II membrane fusion molecules (see Chapter 1) (Earp, Delos et al. 2005). It has been shown that recombinant, soluble versions of the HCV E2 proteins bind a number of cell-surface proteins, including CD81 (Pileri, Uematsu et al. 1998; Flint, Maidens et al. 1999), scavenger receptor class B1 (SR-B1) (Scarselli, Ansuini et al. 2002), dendritic cell-specific ICAM 3-grabbing nonintegrin (DC-SIGN) (Pohlmann, Zhang et al. 2003), and low-density lipoprotein (LDL) (Wunschmann, Medh et al. 2000).

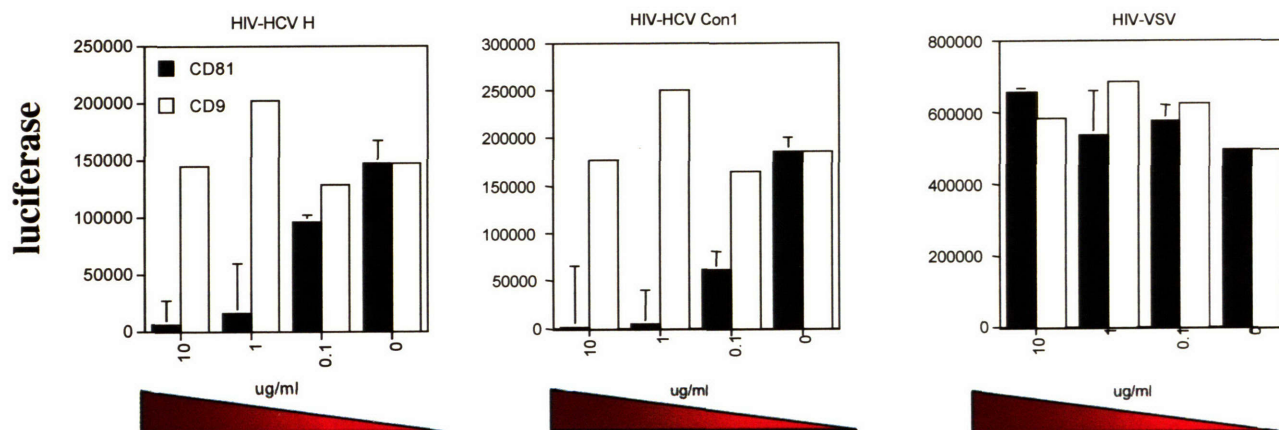
The best characterized of these putative HCV receptors is CD81. Although CD81 is necessary for HCV infection of liver cells, CD81 expression alone is insufficient to mediate viral entry, suggesting that other factors are necessary (McKeating, Zhang et al. 2004). Furthermore, CD81 is expressed on a diverse array of cell types, many of which

are not susceptible to HCV entry. As a result, CD81 has been characterized as a HCV co-receptor. Soluble, recombinant CD81-LELs have been shown to bind the pseudotyped hepatitis C virions (Pileri, Uematsu et al. 1998; Flint, Maidens et al. 1999). Binding of HepC pseudotyped virions is dependent on the CD81-LEL and mutagenesis to non-permissive CD81-LEL sequences abrogated viral entry.

In this section, we present evidence for the role of our hCD81-LEL in specific, dose-dependent inhibition of HCV entry. Our purified, recombinant hCD81-LEL protein, and not the CD9-LEL, inhibits envelope-null human immunodeficiency virus (HIV) pseudotyped with HepC H and Con1 glycoproteins (Figure A.1). Neither protein inhibited the entry of envelope-null HIV particle pseudotyped with vesicle stomatitis virus (VSV) envelope, which mediates ubiquitous cellular entry. The inhibitory effect was dose dependent with an IC_{50} in the high ng/ml range, exhibiting approximately an order of magnitude greater potency than previously observed with GST-CD81-LEL fusions.

To further test both the specificity and potency of inhibition, we constructed and purified mouse and rat hCD81-LEL. Rat CD81-LEL did not inhibit binding, similar to negative controls. As expected, none of the recombinant CD81-LEL proteins inhibited virions pseudotyped with Murine Moloney Leukemia virus. Mouse CD81-LEL inhibited virions pseudotyped with HepC envelope strain H77, but not HepC envelope strain JFH (Figure A.2).

Recently, Brett Lindenbach and colleagues were able to produce infectious non-pseudotyped HepC virions (Lindenbach, Evans et al. in press). Infection of these virions were inhibited both with a antibody against the HepC glycoprotein known to inhibit entry (clone C1) and also with our hCD81-LEL protein (Figure A.3). These inhibition experiments suggest that the HepC viral particle, called HCVcc, is similar to native HepC virions. To further study the mechanism of hCD81-LEL mediated inhibition, Jane McKeating will screen for HCVcc escape mutations. Lastly, the greater potency of our reagents will allow us to test inhibition of HepC virions in a SCID mouse model system transplanted with human hepatocytes in collaboration with both Jane McKeating and the Leroux-Roels laboratory (Meuleman, Libbrecht et al. 2005). If these *in vivo* inhibition experiments are successful, I expect that the CD81-LEL protein may be commercialized.



CD81 $\mu\text{g/ml}$	% neutralization of pseudotype infectivity		
	HIV-HCV H	HIV-HCV Con 1	HIV-VSV
10.0	96%	99%	-
1.0	89%	97%	-
0.1	34%	55%	-
CD9 $\mu\text{g/ml}$			
10.0	-	-	-
1.0	-	-	-
0.1	3	-	-

Figure A.1 Plasmids carrying Hepatitis C virus strain H or Con1 E1E2 glycoproteins were cotransfected with a luciferase plasmid containing an env-defective human immunodeficiency virus (HIV) proviral genome into 293T cells. Supernatants were collected after 48h post-transfection, HIV p24 antigen was assessed, and equal volumes of p24-antigen normalized viral supernatants were added with the indicated concentration of tetraspanin-LELs to target cells. After 4 hours, media was changed and 72 hours post-infection, cells were washed, lysed, and assayed for luciferase activity. Dose dependence of both the hCD81-LEL and hCD9-LEL is graphed at top and tabulated below.

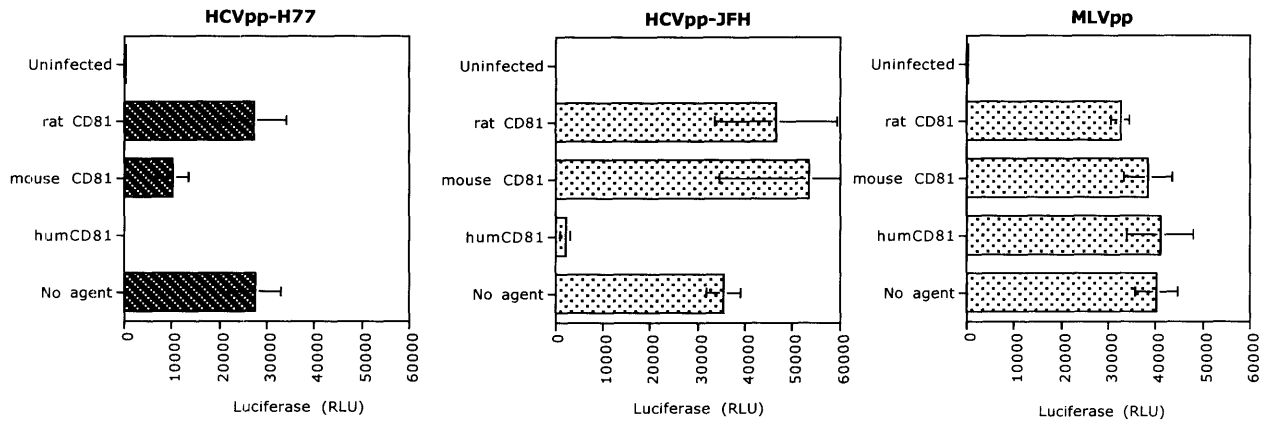


Figure A.2 Pseudotyped Hepatitis C virions were produced as described in A.1. Instead, glycoproteins from either Hepatitis C virus strain H77 or JFH were used as experimentals with the Murine Moloney Leukemia virus envelope as a negative control. All tetraspanin-LELs were tested at $5\mu\text{g/ml}$. Data with the CD9-LEL protein, which had no effect on infectivity, is not shown. Dose dependence curves are in progress.

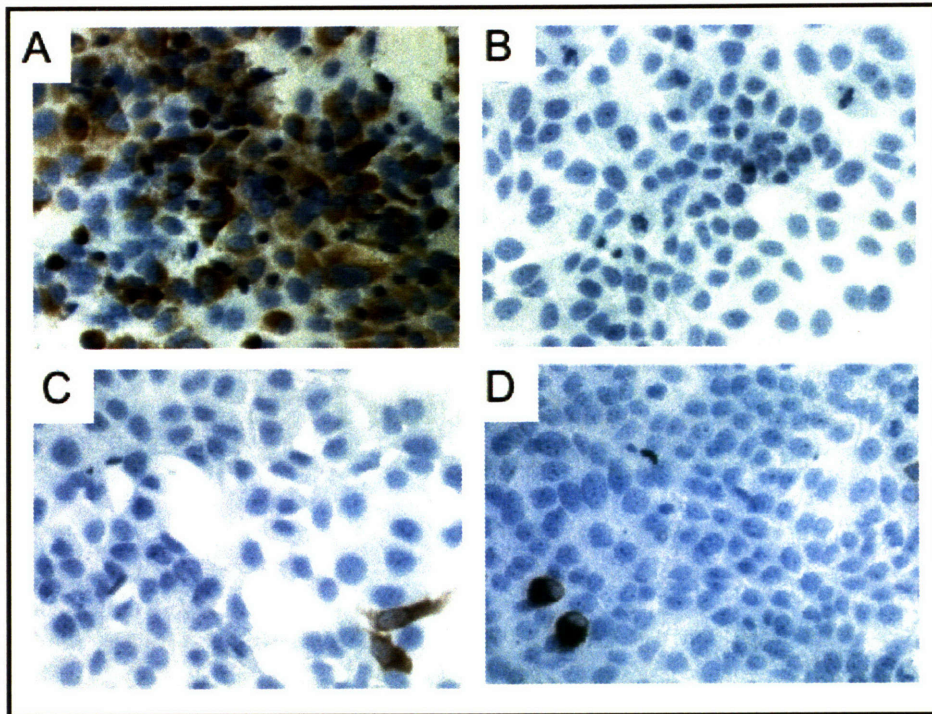


Figure A.3 Entry of the non-pseudotyped Hepatitis C virion, HCVcc, is indicated by immunohistochemical staining for epitope-tagged NS5A protein with monoclonal antibody 9E10 (brown). Huh-7 cells were treated with A) clarified, filtered culture sup containing HCVcc virions or B) untreated. To test for inhibition, HCVcc supernatants were pretreated for 1hr at 37°C with either C) inhibitor anti-E2 human monoclonal antibody C1 or D) 1 μ g/ml of hCD81-LEL. Cell nuclei are stained with hematoxylin (blue).

Appendix B

Publications

Residues SFQ (173-175) in the large extracellular loop of CD9 are required for gamete fusion

Guo-Zhang Zhu^{1,*}, Brent J. Miller², Claude Boucheix³, Eric Rubinstein³, Christopher C. Liu⁴, Richard O. Hynes⁴, Diana G. Myles² and Paul Primakoff¹

¹Department of Cell Biology and Human Anatomy, School of Medicine, University of California Davis, Davis, CA 95616, USA

²Department of Molecular and Cellular Biology, University of California Davis, Davis, CA 95616, USA

³Institut National de la Sante et de la Recherche Medicale (INSERM), Unite 268, Hôpital Paul-Brousse, 94800 Villejuif, France

⁴Howard Hughes Medical Institute, Center for Cancer Research, Massachusetts Institute of Technology, Cambridge, Massachusetts 02139, USA

*Author for correspondence (e-mail: gzhu@ucdavis.edu)

Accepted 15 January 2002

SUMMARY

Gamete fusion is the fundamental first step initiating development of a new organism. Female mice with a gene knockout for the tetraspanin CD9 (CD9 KO mice) produce mature eggs that cannot fuse with sperm. However, nothing is known about how egg surface CD9 functions in the membrane fusion process. We found that constructs including CD9's large extracellular loop significantly inhibited gamete fusion when incubated with eggs but not when incubated with sperm, suggesting that CD9 acts by interaction with other proteins in the egg membrane. We also found that injecting developing CD9 KO oocytes with CD9 mRNA restored fusion competence to the resulting CD9 KO eggs. Injecting mRNA for either mouse CD9 or

human CD9, whose large extracellular loops differ in 18 residues, rescued fusion ability of the injected CD9 KO eggs. However, when the injected mouse CD9 mRNA contained a point mutation (F174 to A) the gamete fusion level was reduced fourfold, and a change of three residues (173-175, SFQ to AAA) abolished CD9's activity in gamete fusion. These results suggest that SFQ in the CD9 large extracellular loop may be an active site which associates with and regulates the egg fusion machinery.

Key words: Gamete fusion, CD9, Tetraspanin, mRNA injection, Mutation, Mouse

INTRODUCTION

Sperm-egg binding and fusion initiate the development of a new organism, but the molecular mechanisms of gamete adhesion, gamete membrane fusion and associated signaling are still poorly understood. Recently, one egg surface protein, CD9, was shown to be essential for gamete fusion. The fertility of CD9-deficient female mice is severely reduced because membrane fusion ability is lost in CD9-deficient eggs (Kaji et al., 2000; Le Naour et al., 2000; Miyado et al., 2000). CD9 belongs to a family of proteins called tetraspanins, which contain four transmembrane domains, one small extracellular loop (EC1) and one large extracellular loop (EC2), and cytoplasmic amino and carboxyl termini (Boucheix and Rubinstein, 2001). Tetraspanins are reported to function in a variety of cell activities including cell adhesion, motility, proliferation, differentiation and signaling (Maecker et al., 1997; Lagaudriere-Gesbert et al., 1997). Immunoprecipitation and other studies suggest that tetraspanins in the plasma membrane are associated with each other and with several other cell surface molecules, including a subset of $\beta 1$ integrins and Ig superfamily members, to form a tetraspanin web (Nakamura et al., 1995; Berditchevski et al., 1996; Rubinstein et al., 1996; Serru et al., 1999; Charrin et al., 2001; Stipp et al.,

2001; Maecker et al., 1997; Boucheix and Rubinstein, 2001). Tetraspanins may organize specific cell surface molecules to form functional macromolecular complexes on the surface of the cell that express the tetraspanin (Maecker et al., 1997; Boucheix and Rubinstein, 2001). Additionally, it is possible that tetraspanins are ligands for receptors on other cells, as reported for the tetraspanin CD81 (Kelic et al., 2001).

Another egg surface protein, the integrin $\alpha 6\beta 1$, was previously proposed as the receptor for sperm on mouse eggs (Almeida et al., 1995). It was thought that $\alpha 6\beta 1$ binds to the disintegrin domain of fertilin β on the sperm surface (Chen and Sampson, 1999; Chen et al., 1999; Evans, 2001). Because it was found that $\alpha 6\beta 1$ and CD9 could be coimmunoprecipitated from mouse eggs, it was suggested that CD9 plays its crucial role in gamete fusion through involvement in a fertilin β - $\alpha 6\beta 1$ /CD9 intergamete complex (Miyado et al., 2000). This view, however, is challenged by two other reports. One shows that fertilin β -deficient sperm fuse with eggs at 50% of the wild-type level (Cho et al., 1998). The other shows that $\alpha 6\beta 1$ -deficient eggs fuse with sperm at the same level as the wild-type eggs (Miller et al., 2000). These two reports indicate that there must be other molecules on the cell surface of gametes that can act in sperm-egg fusion.

Thus, how CD9 functions in gamete fusion is still unknown. In the present study, we addressed two questions. Does CD9 work by binding to sperm or to other egg surface proteins? What is the binding site on CD9? Our data suggest that CD9 interacts through its large extracellular loop (EC2) domain with other egg surface proteins (i.e. in *cis*), and that the three residues SFQ (173-175) in EC2 are required for CD9's function in gamete fusion. These findings add to our understanding of the mechanism of the gamete fusion process and emphasize the importance of identifying the egg protein(s) that interact with the SFQ site in CD9.

MATERIALS AND METHODS

Plasmid construction

The plasmid pmCD9 was constructed by inserting the full-length mouse CD9 cDNA (GenBank accession number NM007657) into the *EcoRI* site of the pBluescript vector (Stratagene). The plasmid phCD9 was constructed by inserting the full-length human CD9 cDNA (GenBank accession number NM001769) into the *EcoRI* site of pcDNA3.1 (Invitrogen). pmCD9 was used as the parental plasmid to construct the three-amino-acid-mutant plasmid pmCD9-SFQ(173-175)AAA by PCR. Two overlapping mutated fragments were generated by two sets of primers (forward 5'-GCAGGAATTCCGGCCCTTCTGT-3' and reverse 5'-AACCgcGgcccTTCCAAAAGCTGTTTCTTGGG-3', forward 5'-GGAAGggcCgcGGTTAAGCCCTGCCCTGAAGC-3' and reverse 5'-ATCGATAAGCTTGATATCGAATTC-3', the mutated sequence in lowercase), digested with *NciI* and ligated together to form a single fragment. This fragment was digested with *EcoRI* and ligated back into the parental *EcoRI*-digested pBluescript vector.

The green fluorescent protein (GFP)-tagged chimeric plasmids were constructed as follows. The forward primer 5'-ACGTagatctAGTCACG-ACGTTGTAAAACGACGGCC-3' (*BglII* site in lower case) and the reverse primer 5'-ACGTagcttGACCATTTCTCGGCTCCTGCGGAT-3' (*HindIII* site in lower case) were used in PCR to make a construct including the T7 promoter and the open reading frame (ORF) of the mouse CD9 cDNA from the plasmid pmCD9. After digestion with *BglII* and *HindIII*, the PCR product was ligated into the vector pEGFP-N1 (Clontech) to obtain the GFP chimeric plasmid pmCD9-eGFP. This plasmid was used as the parental vector to construct the single-amino-acid-mutant plasmid pmCD9-F174A-eGFP, according to the instruction of the Quick-Change™ mutagenesis kit (Stratagene). The primers used in the mutagenesis were forward 5'-CCAAGAAAACAGCTTTTG-GAAAGTGCCAGGTTAAGCCCTGCCCTGAAGCC-3' and reverse 5'-GGCTTCAGGGCAGGGCTTAACCTGGGCACTTCCAAAAG-CTGTTTCTTGG-3'.

All constructs were sequenced to show that undesired mutations had not been introduced during the PCR and cloning steps.

In vitro synthesis of mRNA

The plasmids pmCD9, phCD9, pmCD9-SFQ(173-175)AAA, pmCD9-eGFP and pmCD9-F174A-eGFP were linearized by digestion with appropriate restriction enzymes whose recognition sites are downstream of the ORFs of the corresponding cDNAs. The linearized plasmids were used as templates to synthesize mRNA using the mMessage mMachine™ capped RNA transcription kit with T7 RNA polymerase (Ambion), according to the manufacturer's protocol. The mRNAs were dissolved in RNase/DNase-free water.

Antibodies

Antibodies used include the anti-mouse CD9 monoclonal antibodies: KMC8 (Pharmingen), 4.1F12, 1.2C4, 1.1F2 and 1.4G1, isolated and characterized in one of our laboratories (C. B. and E. R., unpublished results). The anti-human CD9 monoclonal antibody, ALB-6, has been described (Rendu et al., 1987).

Media for oocyte culture and in vitro fertilization assay

Medium 1: (M199; Gibco BRL), 3.5 mM sodium pyruvate, 1,000 i.u. penicillin-streptomycin, 0.1% polyvinyl alcohol, 2 mM L-glutamine, 0.2 mM 3-isobutyl-1-methylxanthine (IBMX, Calbiochem); Medium 2: 10 mM Hepes (N-[2-hydroxyethyl]piperazine-N'-[2-ethanesulfonic acid] in Medium 1; Medium 3: 5% fetal calf serum in Medium 1; Medium 4: Medium 3 without IBMX; Medium 5: Medium 2 without IBMX; Medium 6: 0.3% bovine serum album (BSA) in Medium 1 without IBMX; Medium 7: 3.0% BSA in Medium 1 without IBMX.

Oocyte culture and microinjection

Wild-type or CD9-deficient C57BL6 female mice (Le Naour et al., 2000) (6-8 weeks old) were primed with 10 i.u. of pregnant mare serum gonadotropin 48 hours prior to ovary isolation. Isolated ovaries were placed in Medium 1 to collect germinal vesicle (GV)-stage oocytes. After the removal of granulosa cells, the GV-stage oocytes were allowed to recover in Medium 1 at 37°C, 5% CO₂ for 2-3 hours and then loaded into a 25 µl drop of Medium 2 in a 35 mm tissue culture dish (Corning). A 0.5 µl drop of mRNA solution was placed approximately 2 mm away from the drop containing oocytes in Medium 2. Both drops were overlaid with dimethylpolysiloxane (DMPS, 20 centistokes; Sigma) to prevent evaporation. Each oocyte was injected with approximately 30 pg of mRNA. Injections were carried out on a Zeiss Axiovert 135 equipped with a bipolar temperature controller set at 37°C (Medical Systems Co.) Injected oocytes were transferred to Medium 3 for a period of approximately 12 hours at 37°C, 5% CO₂. After incubation, oocytes were allowed to incubate for approximately 16 hours in Medium 4. The metaphase II eggs among the cultured oocytes were selected for use in experiments.

In vitro fertilization assay (IVF)

Eggs, prepared as described above, were treated with acid Tyrodes solution for about 30 seconds to remove the zona pellucida and then allowed to incubate in Medium 6 at 37°C, 5% CO₂ for 3 hours. Sperm for the in vitro adhesion and fusion assay were isolated from the cauda epididymis and the vas deferens of C57BL6 male mice (10-12 weeks old) into Medium 7, and capacitated for 3 hours in Medium 7 at 37°C, 5% CO₂, resulting in a population of 60-70% acrosome-reacted sperm (Moller et al., 1990). The other steps for in vitro fertilization were carried out as previously described (Miller et al., 2000).

Indirect immunofluorescence of eggs expressing human or mouse CD9

After in vitro fertilization, the eggs were fixed in 4% paraformaldehyde and 0.1% PVA in phosphate-buffered saline (PBS, pH 7.4) for 10 minutes at room temperature. After fixation, eggs were incubated with either 10 µg/ml anti-mouse CD9 antibody KMC8 (BD Pharmingen) or 10 µg/ml anti-human CD9 antibody ALB-6 for 1 hour at 37°C, 5% CO₂ in Medium 6, followed by a 30-minute incubation with an appropriate secondary antibody conjugated to Oregon Green™ or Alexa Fluor™ 488 fluorophore (Molecular Probes Inc.). The fluorescence images were acquired with a laser scanning confocal microscope (model LSM 410; Carl Zeiss).

Visualization of CD9-eGFP fusion protein expression using confocal microscopy

For eggs injected with CD9-eGFP or CD9-F174A-eGFP mRNAs, the expression of the eGFP fusion protein on the eggs was observed with a laser scanning confocal microscope (model LSM 410; Carl Zeiss) after the eggs were incubated in Medium 4 for 16 hours and then coincubated with sperm for in vitro fertilization assay.

Preparation of glutathione S-transferase (GST)-mouse CD9 extracellular large loop (EC2) fusion protein and EC2-histidine (HT) fusion protein

The DNA fragment encoding the extracellular loop of mouse CD9 (EC2) was inserted into *EcoRI* and *BamHI* restriction sites of the PGEX-

3X vector (Amersham Pharmacia Biotech, Piscataway, NJ, USA). The GST-EC2 fusion protein and GST alone were expressed in *E. coli* BL21 cells (Amersham Pharmacia Biotech). The cells were lysed by mild sonication, and GST-EC2 or GST was allowed to bind to a glutathione affinity matrix (Amersham Pharmacia Biotech). The GST-EC2 fusion protein or GST was eluted from the affinity matrix using 10 mM reduced glutathione in 50 mM Tris-HCl (pH 8.0). The eluted proteins were used fresh in the *in vitro* fertilization assay.

The EC2 DNA fragment was also inserted into the *NheI* and *XhoI* restriction sites of the carboxy-terminal hexa-histidine expression vector pET24a (Novagen, Madison, WI, USA). The resulting plasmid, denoted pET24a-CD9EC2/HT, was transformed into *E. coli* BL21/pLysS cells for protein expression. The cells were lysed in a French press and separated into soluble and insoluble fractions by centrifugation. The insoluble portion was resuspended in 6 M guanidine-HCl, and subsequently clarified by both centrifugation and filtration. The fusion protein EC2/HT was purified by nickel-nitrilotriacetic acid metal-affinity chromatography (Qiagen, Chatsworth, CA, USA), followed by reverse-phase HPLC (Waters, Milford, MA, USA) using a Vydac C18 preparative column (Vydac, Hesperia, CA, USA) with a water/acetonitrile gradient of 0.05%/minute in the presence of 0.1% trifluoroacetic acid. Protein peaks were collected, centrifuged under vacuum to remove the acetonitrile, and lyophilized. A single oxidized species was recognized by the monoclonal antibody KMC8. Circular dichroism analysis revealed that this species had significant helical structure and was thermally stable (C. C. L. et al., unpublished results). This fraction of the EC2/HT was resuspended in PBS just before use in the *in vitro* fertilization assay.

Western blot analysis

Western blot analysis was performed according to the standard method for ECL western blotting detection reagent (Amersham Pharmacia Biotech). Protein samples were analyzed by non-reducing SDS-PAGE. Gels were transferred onto Hybond-C membranes (Amersham Pharmacia Biotech) by electroblotting. Monoclonal antibody KMC8 (BD Pharmingen) against CD9 was used as the primary antibody at a final concentration of 0.5 µg/ml. The blotting signals were developed using the ECL system (Amersham Pharmacia Biotech), using film development times that gave a signal in the linear range of blot intensities.

RESULTS

The fusion proteins GST-EC2 and EC2/HT inhibit mouse sperm-egg fusion

We first asked which region(s) of the CD9 protein is important

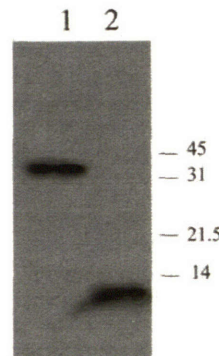


Fig. 1. Western blot of GST-EC2 and EC2/HT. Western blotting was carried out as described in Materials and Methods. Lane 1, 50 ng GST-EC2; lane 2, 10 ng EC2/HT. The molecular mass (kDa) of protein standards is indicated.

for its function in gamete fusion. The monoclonal antibody KMC8 to mouse CD9 has been reported to inhibit sperm-egg fusion but not binding (Miller et al., 2000), but the KMC8 epitope is unknown. We expressed the large extracellular loop (EC2) of mouse CD9 as a GST fusion protein (GST-EC2) and this fusion protein bound KMC8 in western blotting (Fig. 1, lane 1), suggesting that a functional site of CD9 may be in EC2. Freshly purified GST-EC2 fusion protein was tested for its effect on gamete fusion. Three parameters were measured: (1) fertilization rate FR = the percentage of eggs that fuse with at least one sperm; (2) fertilization index FI = total number of fused sperm/total number of eggs; (3) the mean number of sperm bound at the equator of the egg. When zona-free eggs were incubated with GST-EC2 for 3 hours before insemination, gamete fusion was inhibited (Table 1). The fertilization rate was reduced from 100% to 60%, and the fertilization index was reduced from 1.5 to 0.6. The average number of sperm bound to the egg plasma membrane was unaffected. When sperm were incubated with GST-EC2 for 3 hours before insemination, no significant inhibitory effect was seen (Table 1).

To test the effect of EC2 in another kind of construct, EC2 was fused with a histidine tag (HT) and purified by HPLC. EC2/HT binds KMC8 in western blots (Fig. 1, lane 2) and folds properly by biophysical criteria, e.g. it shows expected amounts of helical structure by circular dichroism and has a conformation related to the native form of CD9 on the mouse egg (C. C. L. et al., unpublished results). When zona-free eggs were incubated with the EC2/HT polypeptide for 3 hours before insemination, gamete fusion was inhibited (Table 1). The fertilization rate was reduced from 83% to 43%, and the fertilization index from 0.83 to 0.42. The average number of sperm bound to the egg plasma membrane was not affected (Table 1). When sperm were incubated with EC2/HT for 3

Table 1. The effect of GST-EC2 and EC2/HT on *in vitro* fertilization

Incubation protein	Pre-incubated gamete	Number of eggs tested	Fertilization rate (%)	Fertilization index	Sperm bound per equator
GST	Egg	78	100±0	1.5±0.15	6.2±0.5
GST-EC2	Egg	86	60±5.1	0.6±0.05	5.7±0.5
GST-EC2	Sperm	63	97±3.0	1.1±0.11	7.1±1.6
Buffer (PBS)	Egg	56	83±3.5	0.83±0.04	4.6±0.3
EC2/HT	Egg	76	43±2.6	0.42±0.02	4.8±0.4
EC2/HT	Sperm	67	75±5.2	0.75±0.05	4.5±0.3

Values are mean±s.e.m.

300 µg/ml of GST-EC2 or 250 µg/ml of EC2/HT were pre-incubated with sperm or with eggs for 3 hours. Then the EC2 construct remained present (undiluted) during a 40 minute insemination period beginning when the other gamete was added. After the 40 minute insemination, fertilization rate, fertilization index and sperm bound per equator were scored (see text).

For eggs pre-incubated with GST-EC2, significant inhibition was seen for both fertilization rate and fertilization index ($P < 0.02$).

For sperm pre-incubated with GST-EC2, fertilization rate was unaltered and fertilization index showed a slight, statistically non-significant reduction ($P > 0.1$).

For eggs pre-incubated with EC2/HT, significant inhibition was seen for both fertilization rate and fertilization index ($P < 0.002$).

For sperm pre-incubated with EC2/HT, fertilization rate and fertilization index showed statistically non-significant reduction ($P > 0.2$).

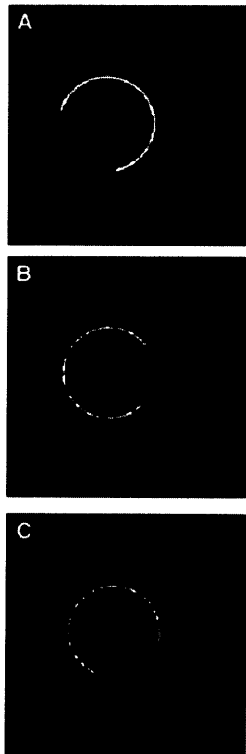


Fig. 2. Immunofluorescent staining of CD9 on the surface of CD9^{-/-} eggs injected with either mouse or human CD9 mRNAs. (A) Immunofluorescent staining using the anti-mouse CD9 antibody KMC8 on wild-type eggs. (B) Immunofluorescent staining using the anti-mouse CD9 antibody KMC8 on CD9^{-/-} oocytes injected with mouse CD9 mRNA.

(C) Immunofluorescent staining using the anti-human CD9 antibody ALB6 on CD9^{-/-} oocytes injected with human CD9 mRNA.

hours before insemination, no significant inhibition was observed (Table 1).

In the protocol used in these experiments (see legend of Table 1), the CD9 EC2 construct is preincubated with sperm or with eggs for 3 hours. Then the EC2 construct remains present (undiluted) during the 40 minute insemination period beginning when the other gamete is added. Inhibition occurs when the eggs are incubated with CD9 EC2 for

the initial 3 hours plus 40 minutes insemination but not when they are incubated with CD9 EC2 for only the final 40 minute insemination. This indicates that the preincubation time of the CD9 EC2 with the eggs is required for inhibition of gamete fusion. Overall, the results suggest that EC2 is a functional region of the CD9 molecule in gamete fusion, that sperm may lack a counter-receptor for egg CD9, and that the constructs GST-EC2 and EC2/HT may displace endogenous egg CD9 from a complex with other egg molecules, thereby inhibiting sperm-egg fusion.

Injection of CD9 mRNA into CD9-deficient oocytes restores their fusion ability

Given that the CD9 EC2 loop has a role in sperm-egg fusion, we asked what is the functional site within EC2? To address this question, we applied a mouse oocyte expression system (detailed below) using oocytes from CD9 null female mice, along with CD9 mutagenesis and IVF techniques, to investigate the key amino acid residues in EC2 required for CD9's function in sperm-egg fusion.

It has been well demonstrated that mouse oocytes can express functional proteins from injected mRNAs (Paynton et al., 1983; Kola and Sumarsono, 1996; Williams et al., 1998). The mRNAs encoding mouse or human CD9 were synthesized and injected into CD9-deficient oocytes. The injected oocytes were cultured in vitro to the metaphase II stage (see Materials and Methods). After the in vitro culture period, the mean percentages of wild-type (WT) oocytes, KO (CD9^{-/-}) oocytes, or injected KO oocytes that produced first polar bodies were in the range 61-78% and were not significantly different among the different groups (data not shown). This result indicates that CD9-deficient GV-stage oocytes, after injection with mRNA, can develop normally to metaphase II.

As expected, KO eggs, injected with CD9 mRNA, express CD9 on the egg surface as seen by immunofluorescent staining using the anti-mouse CD9 monoclonal antibody KMC8 or the anti-human CD9 monoclonal antibody ALB6 (Fig. 2B,C). The localization of staining is similar to that of WT eggs, with CD9 over the microvillar region and absent over the metaphase plate (Fig. 2A). CD9 KO eggs without mRNA injection show no surface staining (data not shown). The absence of CD9 in uninjected CD9 KO eggs and the expression of CD9 in KO eggs injected with CD9 mRNA was also confirmed by western blot (Fig. 6, lanes 1,2).

To test whether or not in ovum expression of the CD9 protein on the egg surface was capable of restoring fusion ability, GV-stage KO oocytes were injected with CD9 mRNAs, allowed to mature to metaphase II, and promptly used for in vitro fertilization assays (see Materials and Methods). The

Table 2. In vitro fertilization assay with CD9^{-/-} oocytes injected with different CD9 mRNAs

Oocyte genotype	Injected mRNA	Number of eggs tested	Fertilization rate (%)	Fertilization index	Sperm bound per equator
(A)					
CD9 ^{+/+}	None	131	83±4.3	0.89±0.07	10.0±1.3
CD9 ^{-/-}	Mouse CD9 (mCD9)	76	46±4.2	0.46±0.04	10.1±2.2
CD9 ^{-/-}	Human CD9 (hCD9)	64	48±3.3	0.58±0.08	12.1±1.0
CD9 ^{-/-}	None	140	0±0	0±0	10.2±1.2
(B)					
CD9 ^{+/+}	None	166	66±7.4	0.83±0.04	14.4±1.7
CD9 ^{-/-}	mCD9-eGFP	92	55±13.0	0.85±0.09	12.3±1.2
CD9 ^{-/-}	mCD9-F174A-eGFP	73	13±4.0	0.20±0.07	12.0±2.1
CD9 ^{-/-}	None	131	1±1.2	0.02±0.01	14.0±1.7
(C)					
CD9 ^{+/+}	None	122	80±3.3	0.81±0.04	8.3±0.8
CD9 ^{-/-}	mCD9	54	48±3.1	0.48±0.03	8.4±1.2
CD9 ^{-/-}	mCD9-SFQ(173-175)AAA	68	1±1.1	0.01±0.01	8.3±1.2
CD9 ^{-/-}	None	78	0±0	0±0	8.6±0.5

Values are mean±s.e.m.

(A) The mean fertilization rate and index for CD9^{-/-} oocytes injected with mouse CD9 mRNA are not significantly different from the values of CD9^{-/-} oocytes injected with human CD9 mRNA ($P>0.2$).

(B) The mean fertilization rate and index are reduced about fourfold after injection of mCD9-F174A-eGFP mRNA compared to mCD9-eGFP mRNA.

(C) Fertilization is almost abolished after injection of mCD9-SFQ(173-175)AAA mRNA compared to mCD9 mRNA.

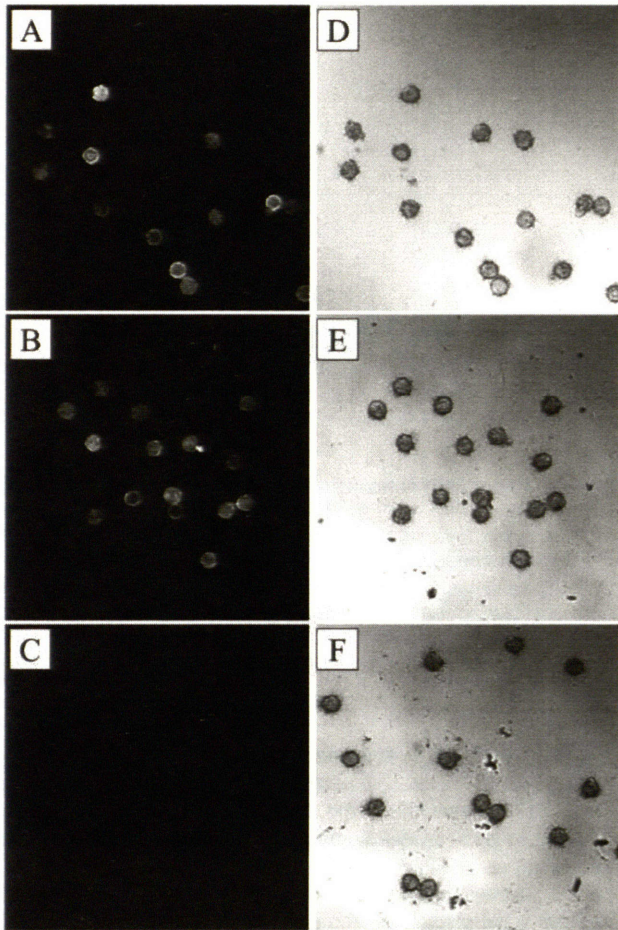


Fig. 3. CD9-eGFP fluorescence observed for CD9^{-/-} oocytes injected with either wild-type or F174A mutant mouse CD9-eGFP mRNA. (A) Fluorescence observed in CD9^{-/-} eggs injected with wild-type CD9-eGFP mRNA. (B) Fluorescence observed in CD9^{-/-} eggs injected with F174A mutant CD9-eGFP mRNA. In A and B, both intracellular and surface fluorescence are observed. (C) Fluorescence observed in uninjected CD9^{-/-} eggs. (D-F) Phase contrast images of A-C, respectively. Fluorescence levels were somewhat variable within each group of eggs injected with the identical amount and type of mRNA.

expression of mouse or human CD9 on the surface of KO eggs rescued sperm-egg fusion (Table 2A). The mean fertilization rate for WT eggs is 83±4.3%; for KO eggs expressing mouse CD9, 46±4.2%, and for KO eggs expressing human CD9, 48±3.3%. No fusion was observed in the KO eggs without mRNA injection. The fertilization index mirrors the fertilization rate (Table 2). Sperm-egg binding is not significantly different in the four groups tested (Table 2).

Reduced fusion ability of CD9-deficient oocytes injected with the CD9-F174A-eGFP mutant mRNA

To hypothesise about which CD9 EC2 residues might be critical for gamete fusion, we considered the structure of the related human tetraspanin CD81 EC2, which has been solved by X-ray crystallographic methods (Kitakodora et al., 2001). The CD81 EC2 structure reveals a ‘head domain’, delineated

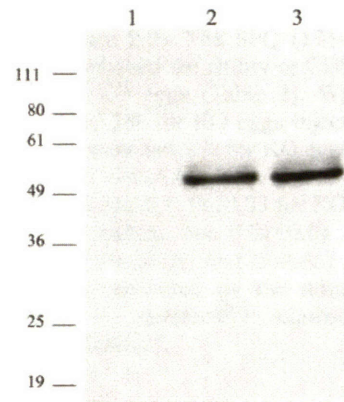


Fig. 4. Western blot assay of CD9-eGFP expression in CD9^{-/-} eggs injected with either wild-type or F174A mutant mouse CD9-eGFP mRNA. The injected eggs were allowed to develop to the M-II phase, then were lysed in non-reducing SDS-sample buffer. Western blots were carried out as described in Materials and Methods. Each lane contains 20 eggs. Lane 1, CD9^{-/-} eggs; lane 2, CD9^{-/-} eggs injected with wild-type CD9-eGFP mRNA; lane 3, CD9^{-/-} eggs injected with mutant CD9- F174A-eGFP mRNA. The molecular mass (kDa) of protein standards is indicated.

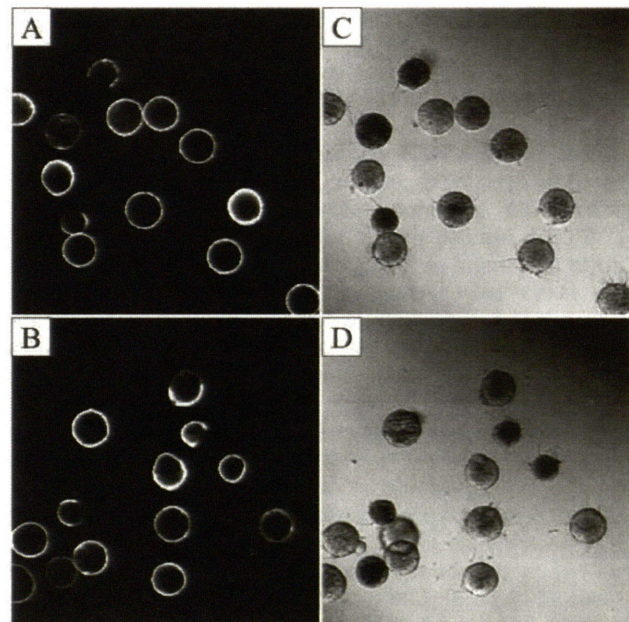


Fig. 5. Immunofluorescent staining of CD9 on the surface of CD9^{-/-} eggs injected with either wild-type or SFQ(173-175)AAA mutant mouse CD9 mRNA. After in vitro fertilization, eggs were fixed and washed as described in Materials and Methods. The fixed eggs were incubated with anti-mouse CD9 antibody KMC8 as the primary antibody, followed by a goat anti-rat IgG (H+L) conjugated with Alexa Fluor™ 488 as the secondary antibody. Immunofluorescent staining was obtained with a laser scanning confocal microscope (Carl Zeiss, LSM 410). (A) Immunofluorescent staining on CD9^{-/-} eggs injected with wild-type mouse CD9 mRNA. (B) Immunofluorescent staining on CD9^{-/-} eggs injected with SFQ-to-AAA mutated mouse CD9 mRNA. (C,D) Phase contrast images of A and B, respectively. Fluorescence levels were somewhat variable within each group of eggs injected with the identical amount and type of mRNA.

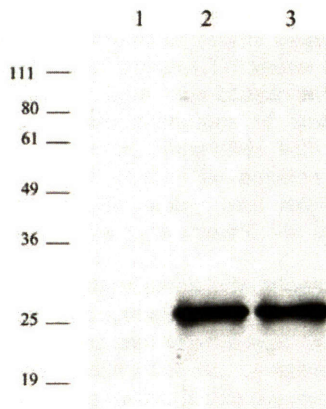


Fig. 6. Western blot assay of CD9 expression in CD9^{-/-} eggs injected with either wild-type or mutant CD9-SFQ(173-175)AAA mRNA. The injected eggs were allowed to develop to the M-II phase, then were lysed in non-reducing SDS-sample buffer. Western blots were carried out as described in Materials and Methods. Each lane contains 20 eggs. Lane 1, CD9^{-/-} eggs; lane 2, CD9^{-/-} eggs injected with wild-type CD9 mRNA; lane 3, CD9^{-/-} eggs injected with mutant CD9-SFQ(173-175)AAA mRNA. The molecular mass (kDa) of protein standards is indicated.

by disulfide bond patterning conserved in all tetraspanin family members. This head domain contains regions of the tetraspanin molecule that can associate with other surface proteins. In its head domain CD81 EC2 has a phenylalanine residue F186 in a solvent-exposed, low polarity patch. F186 is required for CD81 binding with hepatitis C virus (Higginbottom et al., 2000). CD9 F174 is present in a corresponding head domain region and we mutated CD9 F174 to alanine to determine if there would be an effect on sperm-egg fusion.

To allow direct observation of CD9 protein expression, eGFP was fused at the carboxyl terminus of the F174A mutant or wild-type CD9. The wild-type CD9-eGFP or mutant CD9-F174A-eGFP mRNAs were synthesized and injected into CD9-deficient oocytes (see Materials and Methods). In CD9-deficient oocytes, levels of expression detected by immunofluorescence and by western blot are very similar for CD9-eGFP and CD9-F174A-eGFP (Fig. 3A,B, Fig. 4, lanes 2,3). However, the F174A mutant is crippled in its ability to rescue sperm-egg fusion. The mean fertilization rate and fertilization index are reduced about fourfold after injection of mutant mRNA compared to wild-type mRNA (Table 2B). Sperm binding, measured by the number of sperm bound/egg equator, is not significantly different in any of the experimental groups (Table 2).

Lack of fusion ability of CD9-deficient oocytes injected with the CD9-SFQ(173-175)AAA mRNA

The above result indicates that residue F174 may be part of a required site necessary for CD9 function in sperm-egg fusion. To test this, we further mutated the three CD9 amino acid residues SFQ (173-175) to AAA, and determined the effect of injecting this mutant mRNA on the fusion ability of CD9-deficient oocytes. In CD9-deficient oocytes, levels of expression detected by immunofluorescence and by western

blot are very similar for CD9 and CD9-SFQ(173-175)AAA (Fig. 5A,B, Fig. 6, lanes 2,3). The SFQ (173-175) to AAA mutation essentially abolished the ability of CD9 to rescue the fusion competence of KO eggs (Table 2). While the mean fertilization rate is $48\pm 3.1\%$ for KO eggs injected with wild-type CD9 mRNA, it is only $1\pm 1.1\%$ for KO eggs injected with mutant CD9-SFQ(173-175)AAA mRNA (Table 2C). Similarly, the mean fertilization index is 0.48 ± 0.03 for KO eggs injected with wild-type CD9 mRNA, but 0.01 ± 0.01 for KO eggs injected with mutant CD9-SFQ(173-175)AAA mRNA (Table 2). Sperm binding, as measured by the number of sperm bound/egg equator, is statistically equivalent for all experimental groups (Table 2).

DISCUSSION

Previous work demonstrated that egg surface CD9 is essential for sperm-egg fusion (Kaji et al., 2000; Le Naour et al., 2000; Miyado et al., 2000), but nothing is known about how CD9 acts in this system. Egg CD9 could bind in *trans* to a counter-receptor on sperm as suggested for CD81 on astrocytes interacting with neurons (Kelic et al., 2001). Alternatively, CD9 may function by *cis* interactions on the egg surface with other egg surface molecules. One egg protein suggested to interact in a physiologically significant way with CD9 is the integrin $\alpha 6\beta 1$ (Chen et al., 1999; Miyado et al., 2000). However, eggs lacking $\alpha 6\beta 1$ fuse normally with sperm, so a role for this integrin in gamete fusion is in doubt (Miller et al., 2000).

The anti-CD9 monoclonal antibody KMC8 blocks sperm-egg fusion (Chen et al., 1999; Miller et al., 2000), and we found that KMC8 binds to constructs containing CD9 EC2, suggesting a role for EC2 in the fusion process. The EC2 constructs, preincubated with sperm, had no significant effect on fertilization rate or index, suggesting that either the constructs lack biological activity or that sperm do not have a receptor for CD9. The EC2 constructs when preincubated with eggs reduce fertilization rate and index, showing that the constructs do have biological activity. The data therefore suggest that CD9 acts in *cis* at the egg surface and that sperm lack a receptor acting as a *trans* partner for CD9.

Why do the EC2 constructs inhibit sperm-egg fusion when preincubated with eggs? The simplest interpretation is that the exogenously added EC2 can compete with endogenous CD9 for association with some key egg surface molecule(s). But the exogenous EC2, having associated and displaced endogenous CD9, cannot function to promote gamete fusion. The inability of the exogenous EC2 to exercise all CD9 functions may reflect the need for other CD9 regions for full function.

To allow further dissection of the basis of CD9 function, we tested if the fusion ability of CD9 KO oocytes could be restored after the injection of CD9 message. We found a high level of rescue of fusion ability by CD9 message injection. In the current experiments uninjected KO eggs usually did not fuse, and their fertilization rate was 0% (Table 2), though in one test uninjected KO eggs had a fertilization rate of 2%. KO eggs injected with wild-type CD9 mRNA fused at rates of 46-55%, far above the rate for uninjected KO eggs, but usually a little lower than the rate for uninjected wild-type eggs (66-83%).

We found that injection of KO eggs with wild-type mouse CD9 mRNA and wild-type human CD9 mRNA gave equivalent levels of rescue of fusion. Sequence comparison of EC2 of mouse and human CD9 shows they differ by 18 residues, including nine non-conservative substitutions, indicating that certain alterations of amino acids in the mouse EC2 structure are compatible with retention of full function. This result reveals the position of various EC2 residues where specific amino acid substitutions are not deleterious and serves as a control for mutations that do reduce function.

We found that the fertilization index obtained with CD9 null oocytes injected with mutant CD9-F174A-eGFP mRNA was reduced fourfold compared to wild-type CD9-eGFP mRNA. This result indicates that F174 plays a significant role in CD9 function in sperm-egg fusion. It also suggests that F174 might be part of a required site necessary for CD9 function. Further experiments showed that a change of three residues SFQ (173-175) to AAA essentially abolished the ability of CD9 message to restore fusion competence to CD9 KO eggs. This loss of activity is probably not due to misfolding of the mutant protein, and this conclusion is supported by three types of evidence (our unpublished data). (1) Several anti-mouse CD9 monoclonal antibodies including KMC8, 4.1F12, 1.2C4, 1.1F2 and 1.4G1 bind to the SFQ-to-AAA mutant as well as to wild-type CD9; (2) after expression in tissue culture cells, CD9 with the SFQ-to-AAA mutation associates as well as does wild-type CD9 with CD9 P-1, the major *cis* partner of CD9 in various cell types (Charrin et al., 2001; Stipp et al., 2001); (3) EC2 containing the SFQ-to-AAA mutation folds properly by biophysical criteria, e.g. it shows amounts of helical structure equivalent to wild-type by circular dichroism. Therefore, the absence of fusion activity in the SFQ-to-AAA mutant suggests that SFQ in the CD9 EC2 loop comprises a functional site, which may associate with and regulate the egg fusion machinery.

One reason to posit a close interaction of CD9 with an egg protein(s) acting in fusion is that in the *in vitro* fusion assay with CD9-null eggs, the number of sperm bound to the egg plasma membrane is the same as wild type (Kaji et al., 2000; Le Naour et al., 2000; Miyado et al., 2000). In all the experiments here, addition of EC2 constructs and the mutations in CD9 did not affect the number of sperm bound. These results suggest that CD9 may interact with the egg fusion machinery downstream of sperm adhesion.

A possible model to explain our findings is that CD9 is associated with an egg fusion protein. The process of sperm binding to the egg plasma membrane triggers and promotes the formation and stability of an association between the SFQ site of CD9 and the egg fusion protein. The egg fusion protein, upon associating with CD9, changes conformation and specifically interacts with a sperm fusion protein. Thus, relying on a portion of CD9's association repertoire, an inter-gamete functional fusion machinery composed of CD9, the egg fusion protein and the sperm fusion protein, is established and promotes membrane fusion.

This work was supported by NIH grants U54-29125 and HD 16580 (to P. P. and D. G. M.) and CA17007 (to R. O. H). We thank Lisa Mehlmann and Richard Schultz for advice on the oocyte injection procedure.

REFERENCES

- Almeida, E. A., Huovila, A. P., Sutherland, A. E., Stephens, L. E., Calarco, P. G., Shaw, L. M., Mercurio, A. M., Sonnenberg, A., Primakoff, P., Myles, D. G. and White, J. M. (1995). Mouse egg integrin alpha 6 beta 1 functions as a sperm receptor. *Cell* **81**, 1095-1104.
- Berditchevski, F., Zutter, M. M. and Hemler, M. E. (1996). Characterization of novel complexes on the cell surface between integrins and proteins with 4 transmembrane domains (TM4 proteins). *Mol. Biol. Cell* **7**, 193-207.
- Boucheix, C. and Rubinstein, E. (2001). Tetraspanins. *Cell Mol. Life Sci.* **58**, 1189-1205.
- Charrin, S., Le Naour, F., Oualid, M., Billard, M., Faure, G., Hanash, S. M., Boucheix, C. and Rubinstein, E. (2001). The major CD9 and CD81 molecular partner. Identification and characterization of the complexes. *J. Biol. Chem.* **276**, 14329-14337.
- Chen, H. and Sampson, N. S. (1999). Mediation of sperm-egg fusion: evidence that mouse egg alpha6beta1 integrin is the receptor for sperm fertilin beta. *Chem. Biol.* **6**, 1-10.
- Chen, M. S., Tung, K. S., Coonrod, S. A., Takahashi, Y., Bigler, D., Chang, A., Yamashita, Y., Kincade, P. W., Herr, J. C. and White, J. M. (1999). Role of the integrin-associated protein CD9 in binding between sperm ADAM 2 and the egg integrin alpha6beta1: implications for murine fertilization. *Proc. Natl. Acad. Sci. USA* **96**, 11830-11835.
- Cho, C., Bunch, D. O., Faure, J. E., Goulding, E. H., Eddy, E. M., Primakoff, P. and Myles, D. G. (1998). Fertilization defects in sperm from mice lacking fertilin beta. *Science* **281**, 1857-1859.
- Evans, J. P. (2001). Fertilin beta and other ADAMs as integrin ligands: insights into cell adhesion and fertilization. *BioEssays* **23**, 628-639.
- Higginbottom, A., Quinn, E. R., Kuo, C. C., Flint, M., Wilson, L. H., Bianchi, E., Nicosia, A., Monk, P. N., McKeating, J. A. and Levy, S. (2000). Identification of amino acid residues in CD81 critical for interaction with hepatitis C virus envelope glycoprotein E2. *J. Virol.* **74**, 3642-3649.
- Kaji, K., Oda, S., Shikano, T., Ohnuki, T., Uematsu, Y., Sakagami, J., Tada, N., Miyazaki, S. and Kudo, A. (2000). The gamete fusion process is defective in eggs of Cd9-deficient mice. *Nat. Genet.* **24**, 279-282.
- Kelic, S., Levy, S., Suarez, C. and Weinstein, D. E. (2001). CD81 regulates neuron-induced astrocyte cell-cycle exit. *Mol. Cell Neurosci.* **17**, 551-560.
- Kitadokoro, K., Bordo, D., Galli, G., Petracca, R., Falugi, F., Abrigiani, S., Grandi, G. and Bolognesi, M. (2001). CD81 extracellular domain 3D structure: insight into the tetraspanin superfamily structural motifs. *EMBO J.* **20**, 12-18.
- Kola, I. and Sumarsono, S. H. (1996). Microinjection of *in vitro* transcribed RNA and antisense oligonucleotides in mouse oocytes and early embryos to study the gain- and loss-of-function of genes. *Mol. Biotechnol.* **6**, 191-199.
- Lagaudriere-Gesbert, C., Le Naour, F., Lebel-Binay, S., Billard, M., Lemichez, E., Boquet, P., Boucheix, C., Conjeaud, H. and Rubinstein, E. (1997). Functional analysis of four tetraspanins, CD9, CD53, CD81, and CD82, suggests a common role in costimulation, cell adhesion, and migration: only CD9 upregulates HB-EGF activity. *Cell Immunol.* **182**, 105-112.
- Le Naour, F., Rubinstein, E., Jasmin, C., Prenant, M. and Boucheix, C. (2000). Severely reduced female fertility in CD9-deficient mice. *Science* **287**, 319-321.
- Maecker, H. T., Todd, S. C. and Levy, S. (1997). The tetraspanin superfamily: molecular facilitators. *FASEB J.* **11**, 428-442.
- Miller, B. J., Georges-Labouesse, E., Primakoff, P. and Myles, D. G. (2000). Normal fertilization occurs with eggs lacking the integrin alpha6beta1 and is CD9-dependent. *J. Cell Biol.* **149**, 1289-1296.
- Miyado, K., Yamada, G., Yamada, S., Hasuwa, H., Nakamura, Y., Ryu, F., Suzuki, K., Kosai, K., Inoue, K., Ogura, A., Okabe, M. and Mekada, E. (2000). Requirement of CD9 on the egg plasma membrane for fertilization. *Science* **287**, 321-324.
- Moller, C. C., Bleil, J. D., Kinloch, R. A. and Wassarman, P. M. (1990). Structural and functional relationships between mouse and hamster zona pellucida glycoproteins. *Dev. Biol.* **137**, 276-286.
- Nakamura, K., Iwamoto, R. and Mekada, E. (1995). Membrane-anchored heparin-binding EGF-like growth factor (HB-EGF) and diphtheria toxin receptor-associated protein (DRAP27)/CD9 form a complex with integrin alpha 3 beta 1 at cell-cell contact sites. *J. Cell Biol.* **129**, 1691-1705.
- Paynton, B. V., Ebert, K. M. and Brinster, R. L. (1983). Synthesis and secretion of ovalbumin by mouse-growing oocytes following microinjection of chick ovalbumin mRNA. *Exp. Cell Res.* **144**, 214-218.

2002 G.-Z. Zhu and others

- Rendu, F., Boucheix, C., Le Bret, M., Bourdeau, N., Benoit, P., Maclouf, J., Soria, C. and Levy-Toledano, S.** (1987). Mechanisms of the mAb ALB6(CD9) induced human platelet activation: comparison with thrombin. *Biochem. Biophys. Res. Commun.* **146**, 1397-1404.
- Rubinstein, E., Le Naour, F., Lagaudriere-Gesbert, C., Billard, M., Conjeaud, H. and Boucheix, C.** (1996). CD9, CD63, CD81, and CD82 are components of a surface tetraspan network connected to HLA-DR and VLA integrins. *Eur. J Immunol.* **26**, 2657-2665.
- Serru, V., Le Naour, F., Billard, M., Azorsa, D. O., Lanza, F., Boucheix, C. and Rubinstein, E.** (1999). Selective tetraspan-integrin complexes (CD81/alpha4beta1, CD151/alpha3beta1, CD151/alpha6beta1) under conditions disrupting tetraspan interactions. *Biochem. J.* **340**, 103-111.
- Stipp, C. S., Orlicky, D. and Hemler, M. E.** (2001). FPRP, a major, highly stoichiometric, highly specific CD81- and CD9-associated protein. *J. Biol. Chem.* **276**, 4853-4862.
- Williams, C. J., Mehlmann, L. M., Jaffe, L. A., Kopf, G. S. and Schultz, R. M.** (1998). Evidence that Gq family G proteins do not function in mouse egg activation at fertilization. *Dev. Biol.* **198**, 116-127.

ervation of both types of information in the hippocampal output may form the basis of its key role in episodic memory (2, 34).

References and Notes

1. J. O'Keefe, L. Nadel, *The Hippocampus as a Cognitive Map* (Clarendon, Oxford, 1978).
2. H. Eichenbaum, P. Dudchenko, E. Wood, M. Shapiro, H. Tanila, *Neuron* **23**, 209 (1999).
3. B. L. McNaughton, R. G. M. Morris, *Trends Neurosci.* **10**, 408 (1987).
4. J. O'Keefe, J. Dostrovsky, *Brain Res.* **34**, 171 (1971).
5. R. U. Muller, J. L. Kubie, J. B. Ranck, *J. Neurosci.* **7**, 1935 (1987).
6. B. L. McNaughton, C. A. Barnes, J. O'Keefe, *Exp. Brain Res.* **52**, 41 (1983).
7. J. J. Knierim, H. S. Kudrimoti, B. L. McNaughton, *J. Neurosci.* **15**, 1648 (1995).
8. J. O'Keefe, D. H. Conway, *Exp. Brain Res.* **31**, 573 (1978).
9. K. M. Gothard, W. E. Skaggs, B. L. McNaughton, *J. Neurosci.* **16**, 8027 (1996).
10. M. L. Shapiro, H. Tanila, H. Eichenbaum, *Hippocampus* **7**, 624 (1997).
11. E. R. Wood, P. A. Dudchenko, H. Eichenbaum, *Nature* **397**, 613 (1999).
12. E. J. Markus *et al.*, *J. Neurosci.* **15**, 7079 (1995).
13. M. A. Moita, S. Rosis, Y. Zhou, J. E. LeDoux, H. T. Blair, *J. Neurosci.* **24**, 7015 (2004).
14. E. R. Wood, P. A. Dudchenko, R. J. Robitsek, H. Eichenbaum, *Neuron* **27**, 623 (2000).
15. J. Ferbinteanu, M. L. Shapiro, *Neuron* **40**, 1227 (2003).
16. M. R. Bower, D. R. Euston, B. L. McNaughton, *J. Neurosci.* **25**, 1313 (2005).
17. S. A. Hollup, S. Molden, J. G. Donnett, M.-B. Moser, E. I. Moser, *J. Neurosci.* **21**, 1635 (2001).
18. E. Bostock, R. U. Muller, J. L. Kubie, *Hippocampus* **1**, 193 (1991).
19. C. Kentros *et al.*, *Science* **280**, 2121 (1998).
20. A. Cressant, R. U. Muller, B. Poucet, *Exp. Brain Res.* **143**, 470 (2002).
21. D. Marr, *J. Physiol.* **202**, 437 (1969).
22. S. Leutgeb, J. K. Leutgeb, A. Treves, M.-B. Moser, E. I. Moser, *Science* **305**, 1295 (2004); published online 22 July 2004 (10.1126/science.1100265).
23. Materials and methods are available as supporting material on Science Online.
24. The mean number of pretraining days in the test environment was 17 (square-circle), 14 (two rooms), and 4 (black-white).
25. The rate threshold was 0.27 Hz. Similar results were obtained with rate thresholds of 0.10 Hz and 0.50 Hz (tables S1 and S2) (23).
26. K. M. Gothard, W. E. Skaggs, K. M. Moore, B. L. McNaughton, *J. Neurosci.* **16**, 823 (1996).
27. W. E. Skaggs, B. L. McNaughton, *J. Neurosci.* **18**, 8455 (1998).
28. H. Tanila, *Hippocampus* **9**, 235 (1999).
29. If the external spatial input is strong enough, it is theoretically possible for large changes to occur in the firing rates of some cells, whereas intrinsic attractor dynamics of the network maintain the relative relations between the place fields of the ensemble (35).
30. S. A. Hollup, S. Molden, J. G. Donnett, M.-B. Moser, E. I. Moser, *Eur. J. Neurosci.* **13**, 1197 (2001).
31. In these studies, which all focused on CA1, much of the residual activity in the less active condition appeared inside the cell's place field in the more active condition [e.g., figure 8 in (30), figures 3 to 5 in (14), figures 2 to 6 in (15), figure 6 in (16), figures 6B and 9 in (12), and figure 4 in (13)], as expected if the remapping was primarily rate-based. In (30), 70% of the cells exhibited peak activity in the same quadrant in the two directions.
32. T. J. Wills, C. Lever, F. Cacucci, N. Burgess, J. O'Keefe, *Science* **308**, 873 (2005).
33. H. Markram, M. Tsodyks, *Nature* **382**, 807 (1996).
34. E. Tulving, *Annu. Rev. Psychol.* **53**, 1 (2002).
35. A. Samsonovich, B. L. McNaughton, *J. Neurosci.* **17**, 5900 (1997).

Supporting Online Material

www.sciencemag.org/cgi/content/full/309/5734/619/DC1

Materials and Methods

Figs. S1 to S5

Tables S1 and S2

25 April 2005; accepted 10 June 2005

10.1126/science.1114037

Complete Replication of Hepatitis C Virus in Cell Culture

Brett D. Lindenbach,¹ Matthew J. Evans,¹ Andrew J. Syder,¹ Benno Wölk,¹ Timothy L. Tellinghuisen,¹ Christopher C. Liu,² Toshiaki Maruyama,^{3*} Richard O. Hynes,² Dennis R. Burton,³ Jane A. McKeating,^{1†} Charles M. Rice^{1‡}

Many aspects of the hepatitis C virus (HCV) life cycle have not been reproduced in cell culture, which has slowed research progress on this important human pathogen. Here, we describe a full-length HCV genome that replicates and produces virus particles that are infectious in cell culture (HCVcc). Replication of HCVcc was robust, producing nearly 10⁵ infectious units per milliliter within 48 hours. Virus particles were filterable and neutralized with a monoclonal antibody against the viral glycoprotein E2. Viral entry was dependent on cellular expression of a putative HCV receptor, CD81. HCVcc replication was inhibited by interferon- α and by several HCV-specific antiviral compounds, suggesting that this in vitro system will aid in the search for improved antivirals.

HCV is a major cause of chronic liver disease, with over 170 million persistently infected individuals worldwide (1). HCV-associated

liver disease frequently progresses to cirrhosis, which can lead to liver failure and hepatocellular carcinoma. Current drug therapies are often poorly tolerated and effective in only a fraction of patients; there is no vaccine for HCV. A major obstacle to understanding the virus life cycle and to developing improved therapeutics is the inability to efficiently grow HCV in cell culture.

HCV is an enveloped, positive-sense RNA virus of the family *Flaviviridae*. Naturally occurring variants of HCV are classified into six major genotypes. The 9.6-kb genome encodes one large polyprotein that is processed by viral and cellular proteinases to produce the virion structural proteins (core and glycoproteins E1 and E2) as well as nonstructural (NS)

proteins (p7 through NS5B) (Fig. 1A). Subgenomic RNA replicons have been adapted for efficient RNA replication in the human hepatoma line Huh-7 and other cultured cells (2–5). However, full-length genomes containing cell culture-adaptive mutations do not produce infectious virus particles in culture and are severely attenuated in vivo (6–8). This led us to hypothesize that mutations that enhance RNA replication may have deleterious effects on virion production. To test this idea, we used a genotype 2a subgenomic replicon, SGR-JFH1, that efficiently replicates in cell culture without adaptive mutations (4). Full-length chimeric genomes were constructed with the use of the core-NS2 gene regions from the infectious J6 (genotype 2a) and H77 (genotype 1a) virus strains (Fig. 1A). Both full-length chimeras and the subgenomic RNA were competent for RNA replication, as seen by the accumulation of NS5A protein and viral RNA 48 hours after RNA transfection into the Huh-7.5 cell line (Fig. 1B). As expected, mutation of the NS5B RNA polymerase active site [GlyAspAsp to GlyAsnAsp (GND)] destroyed the ability of FL-J6/JFH to replicate (Fig. 1B). Within transfected cells, both full-length genomes expressed core, E2, and NS5A (Fig. 1C). As expected, SGR-JFH1 expressed NS5A but not core or E2. While \approx 30% of cells were productively transfected with FL-J6/JFH, FL-H77/JFH, or SGR-JFH1 RNA (Fig. 1B), >95% of FL-J6/JFH-transfected cells were positive for NS5A by 96 hours (fig. S1). This suggested that FL-J6/JFH spread within the transfected cell cultures.

To test whether infectivity could be transferred to naïve cells, we clarified conditioned

¹Center for the Study of Hepatitis C, The Rockefeller University, 1230 York Avenue, New York, NY 10021, USA. ²Howard Hughes Medical Institute, Center for Cancer Research, Massachusetts Institute of Technology, Cambridge, MA 02139, USA. ³Departments of Immunology and Molecular Biology, The Scripps Research Institute, La Jolla, CA 92037, USA.

*Present address: Alexion Antibody Technologies, San Diego, CA 92121, USA.

†Present address: Division of Immunity and Infection, Institute of Biomedical Research, University of Birmingham Medical School, Birmingham B15 2TT, UK.

‡To whom correspondence should be addressed. E-mail: ricec@rockefeller.edu

REPORTS

media from these cultures by centrifugation (9), filtered the supernatants (0.2 μ m), and incubated them with naive Huh-7.5 cells. NS5A expression could be transferred by the FL-J6/JFH-transfected culture media but not by media from cells transfected with FL-H77/JFH or SGR-JFH1 (Fig. 1B). Interestingly, the amount of FL-J6/JFH RNA released into the transfected cell culture media exceeded that of the other RNAs by a factor of >200, and only FL-J6/JFH produced an extracellular form of core (Fig. 1C, lower panel). Given that the infectivity of the genotype 2a chimera is filterable and is associated with the release of HCV RNA and core protein, we refer to this cell culture-produced virus as HCVcc. The ability of the genotype 1a/2a chimera to replicate but not spread suggests that interactions between the structural and nonstructural gene products may be important for HCVcc formation, as has been observed for other members of this virus family (10, 11).

Limiting dilution assays for NS5A expression in electroporated cells showed that 30.3 \pm 9.5% ($n = 6$) of cells were productively transfected with FL-J6/JFH, and of these, 55% produced infectivity that was detectable upon transfer to naive cells. Thus, FL-J6/JFH RNA transcripts were highly infectious and formation of HCVcc did not depend on the emergence of rare variants. Limiting dilution assays were also used to quantitate the amount of HCVcc infectivity between samples as median tissue culture infectious units per milliliter (TCID₅₀/ml). The TCID₅₀ is the dilution that infects 50% of replicate cell cultures (9). After an eclipse phase (≥ 9 hours), FL-J6/JFH infectivity could be detected in the media by 18 hours posttransfection, and it continued to accumulate until 48 hours (Fig. 1D). Interestingly, FL-J6/JFH (H2476L), which contained a weakly adaptive mutation in NS5B (4), showed slightly delayed growth kinetics but also peaked to similar levels by 48 hours. Viruses could be serially passaged, infecting 50 to 90% of cells within 5 days after two rounds of passage at a low multiplicity of infection (MOI) of 0.1 to 1.0 (Fig. 1E). The expression and subcellular localization of core, E2, and NS5A within FL-J6/JFH-infected cells was consistent with what was previously seen in full-length and subgenomic replicon-bearing cells [supporting online material (SOM) text]. Taken together, these measurements show that HCVcc replication is robust and occurs with kinetics similar to those of other *Flaviviridae*.

A classic method in virus identification is to neutralize the suspected virus with specific antisera. As shown in Fig. 2A, an E2-specific human monoclonal antibody neutralized HCVcc infectivity in a dose-dependent manner, whereas an isotype-matched control antibody had no effect on HCVcc titer. These

data affirm the viral nature of HCVcc infectivity and show that E2 is essential for virus entry.

HCV E2 has been shown to bind to the cellular surface protein CD81 (12), which is

an essential coreceptor for the entry of HCV glycoprotein-pseudotyped retroviruses (13–15). We found that HCVcc infectivity could be blocked with a soluble recombinant form of the CD81 large extracellular loop (Fig. 2B).

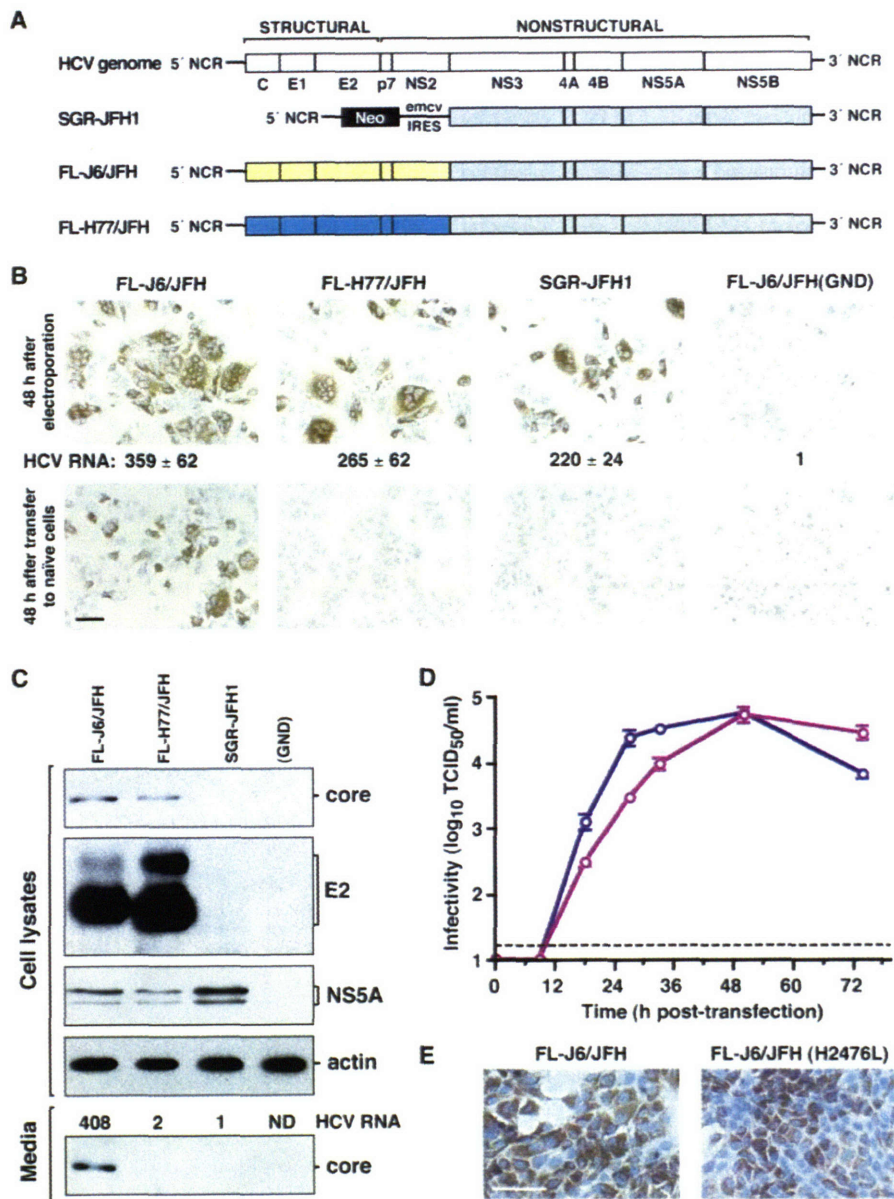


Fig. 1. Production of infectious HCV in cell culture. (A) The structures of the HCV RNA genome, the SGR-JFH1 replicon, and full-length chimeric genomes FL-J6/JFH and FL-H77/JFH. NCR, noncoding region; C, core; yellow, J6; cyan, H77. (B) Huh-7.5 cells were electroporated with RNA transcripts of the indicated genomes [or the RNA-polymerase defective mutant FL-J6/JFH(GND)] 48 hours before immunostaining for NS5A (brown, upper panel). Nuclei were counterstained with hematoxylin (blue). Below is the relative amount of HCV RNA detected in each transfected cell population at 48 hours by quantitative reverse transcription polymerase chain reaction (RT-PCR). Naive Huh-7.5 cells were incubated for 48 hours with filtered, conditioned media from the transfected cells and immunostained for NS5A expression (lower panel). (C) Western blot for HCV core, E2, NS5A, or actin protein expression at 48 hours in RNA transfected Huh-7.5 cells. Below each lane is the relative quantitative amount of HCV RNA and core detected in cell culture media by quantitative RT-PCR and Western blot, respectively. ND, not determined. (D) The accumulation of HCVcc infectivity after electroporation of FL-J6/JFH (blue) or FL-J6/JFH (H2476L) (purple) into 6×10^5 cells/timepoint, assessed by a limiting dilution assay (mean \pm SEM; $n = 4$). Dotted line, assay sensitivity. (E) Cells were immunostained for NS5A 5 days after infection with serially passaged virus. Scale bars, 100 μ m.

To further examine the role of CD81 in virus entry we used HepG2 cells, which lack CD81 expression but are capable of supporting HCV RNA replication (3). As seen in Fig. 2C, normal HepG2 cells were not infected by FL-J6/JFH, whereas CD81-expressing HepG2 cells were infected under the same conditions, albeit with reduced efficiency (~850 times less than Huh-7.5 cells). These data confirm that interactions between E2 and CD81 are important for HCV entry.

The physical nature of HCV particles has been difficult to study in the absence of an infectious culture system. In density gradients, clinical isolates of HCV exhibit a broad distribution and unusually low buoyant den-

sities [reviewed in (16)]. These properties have been partly explained by the interaction of HCV with serum components such as immunoglobulins and β -lipoproteins. We examined the profiles of RNA and infectivity associated with HCVcc particles by equilibrium centrifugation in 10 to 40% iodixanol, an iso-osmotic gradient material. A series of controls confirmed that this method accurately measured the buoyant density of HCVcc (SOM text). HCV RNA was broadly distributed through the top of the gradient, with a peak in fractions 16 and 17 (1.13 to 1.14 g/ml), and was not found beyond fraction 20 (1.18 g/ml) (Fig. 3A). HCVcc infectivity was also broadly distributed among fractions 1 to 15 (1.01 to 1.12 g/ml), and infectivity was not seen beyond fraction 18 (1.17 g/ml). Surprisingly,

fractions 16 and 17, which contained the highest levels of HCV RNA, had little infectivity associated with them. The specific infectivity of a virus preparation relates the amount of infectivity to the total number of virus particles or genomes in the preparation. Interestingly, a plot of HCVcc-specific infectivity versus buoyant density indicates that the most infectious material is at 1.09 to 1.10 g/ml (Fig. 3B), which is similar to the peak of infectivity (1.09 to 1.11 g/ml) previously seen in chimpanzees (17). In contrast, RNA-containing material with a buoyant density of 1.14 g/ml (fraction 17) had a low specific infectivity, with ~300,000 RNA molecules per infectious unit. Many groups have reported an HCV RNA peak near this density (18–20), although infectivity could not be assessed.

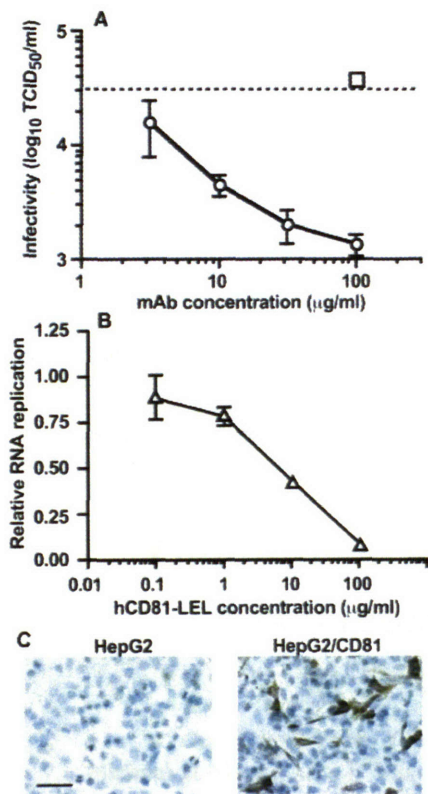


Fig. 2. HCVcc infection is dependent on HCV glycoprotein functions. (A) FL-J6/JFH (H2476L) was pre-incubated for 1 hour at 37°C with the indicated concentrations of recombinant human anti-E2 C1 (circles) or anti-dengue virus NS1 (square) immunoglobulin G1 monoclonal antibodies (mAb), then titered by limiting dilution assay (mean \pm SEM; $n = 3$). Assays for both antibodies were conducted in parallel. The dotted line indicates the titer of untreated virus. (B) FL-J6/JFH (H2476L) was preincubated with 12 μ g/ml of a recombinant form of the large extracellular loop (LEL) of CD81 and used to infect naive cells. The levels of HCV RNA, relative to an untreated control, were determined at 48 hours postinfection by quantitative RT-PCR (mean \pm SEM; $n = 4$). (C) HepG2 or HepG2/CD81 cells were infected with FL-J6/JFH for 48 hours before immunostaining for NSSA expression. Scale bar, 100 μ m.

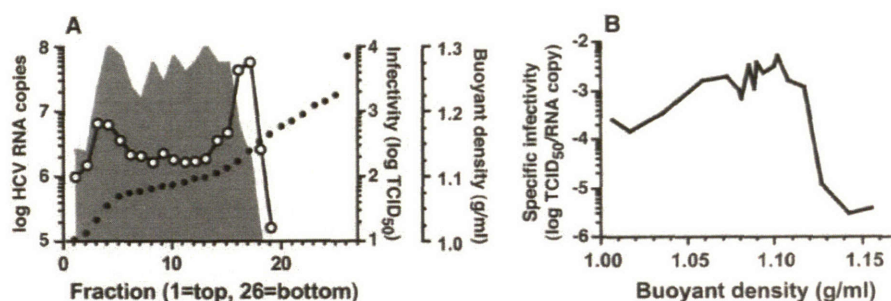


Fig. 3. Characterization of HCVcc particles. (A) The profiles of FL-J6/JFH (H2476L) RNA (open circles) and infectivity (solid gray) are shown after isopycnic centrifugation in a 10 to 40% iodixanol gradient. Closed circles indicate the buoyant density of each fraction. (B) The specific infectivity of each fraction in panel (A) was calculated as the infectivity per RNA copy and plotted against the buoyant density.

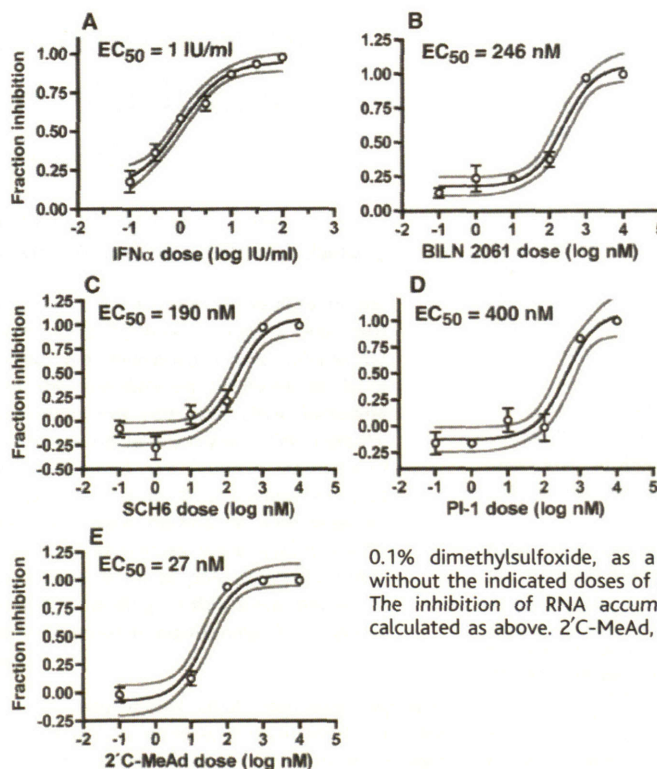


Fig. 4. Antiviral inhibition of HCVcc. (A) Huh-7.5 cells were incubated for 18 hours with the indicated doses of IFN before infection with FL-J6/JFH (H2476L) (MOI of 1.0). The fraction of inhibition was calculated from the levels of HCV RNA at 48 hours post-infection. The mean \pm SEM ($n = 3$), best-fit curve (black), and 95% confidence interval (gray curves) are shown. (B to E) After 8 hours inoculation with FL-J6/JFH (H2476L) (MOI of 0.1), Huh-7.5 cells were washed and incubated in media containing 0.1% dimethylsulfoxide, as a carrier control, with or without the indicated doses of each anti-HCV compound. The inhibition of RNA accumulation at 48 hours was calculated as above. 2'-C-MeAd, 2'-methyladenosine.

REPORTS

Thus, HCVcc exhibits physical properties similar to those that have been previously described for natural isolates of HCV.

There is an urgent need for improved HCV drug therapies. The current standard treatment, pegylated interferon- α (IFN α) and ribavirin, leads to a sustained response in only \approx 50% of genotype 1-infected patients. We examined the ability of HCVcc replication to be inhibited by IFN α and other antiviral compounds. Dose-response experiments showed that IFN α inhibited HCVcc RNA accumulation in infected cells with a median effective concentration (EC₅₀) of 1 international unit (IU)/ml (Fig. 4A). We also tested three HCV-specific inhibitors of the NS3 serine protease for their effects on HCVcc infection. As seen in Fig. 4, B to D, BILN 2061 (21), SCH6 (22), and PI-1 (23) all inhibited HCVcc RNA accumulation in the submicromolar range. In addition, a nucleoside analog inhibitor of the NS5B RNA polymerase, 2'C-methyladenosine (24), was found to inhibit HCVcc replication in the low nanomolar range (Fig. 4E). Thus, HCVcc infection can be inhibited by IFN α and several HCV-specific antiviral compounds. The specificity of these latter compounds further shows that HCVcc infection leads to authentic replication in target cells and demonstrates that this infectious system may be useful for testing current and future antiviral compounds.

We describe a full-length genotype 2a HCV genome that replicates and produces virus particles that are infectious in cell culture.

This system lays a foundation for future in vitro studies to examine new aspects of the virus life cycle and to develop new drugs for combating HCV.

Note added in proof: Full-length JFH-1 has also been recently reported to produce infectious virus in cell culture (25–27), as has a genotype 1b Com1/JFH-1 chimera (28), albeit with lower efficiency and slower growth kinetics than the system reported here.

References and Notes

1. Anonymous, *Wkly. Epidemiol. Rec.* **75**, 18 (2000).
2. K. J. Blight, A. A. Kolykhalov, C. M. Rice, *Science* **290**, 1972 (2000).
3. T. Date *et al.*, *J. Biol. Chem.* **279**, 22371 (2004).
4. T. Kato *et al.*, *Gastroenterology* **125**, 1808 (2003).
5. V. Lohmann *et al.*, *Science* **285**, 110 (1999).
6. K. J. Blight, J. A. McKeating, C. M. Rice, *J. Virol.* **76**, 13001 (2002).
7. J. Bukh *et al.*, *Proc. Natl. Acad. Sci. U.S.A.* **99**, 14416 (2002).
8. T. Pietschmann *et al.*, *J. Virol.* **76**, 4008 (2002).
9. Materials and methods are available as supporting material on Science Online.
10. E. V. Agapov *et al.*, *J. Virol.* **78**, 2414 (2004).
11. B. M. Kümmerer, C. M. Rice, *J. Virol.* **76**, 4773 (2002).
12. P. Pileri *et al.*, *Science* **282**, 938 (1998).
13. B. Bartosch *et al.*, *J. Biol. Chem.* **278**, 41624 (2003).
14. E. G. Cormier *et al.*, *Proc. Natl. Acad. Sci. U.S.A.* **101**, 7270 (2004).
15. J. Zhang *et al.*, *J. Virol.* **78**, 1448 (2004).
16. R. Bartenschlager, M. Frese, T. Pietschmann, *Adv. Virus Res.* **63**, 71 (2004).
17. D. Bradley *et al.*, *J. Med. Virol.* **34**, 206 (1991).
18. N. Fujita *et al.*, *J. Med. Virol.* **63**, 108 (2001).
19. T. Heller *et al.*, *Proc. Natl. Acad. Sci. U.S.A.* **102**, 2579 (2005).
20. M. Hijikata *et al.*, *J. Virol.* **67**, 1953 (1993).
21. D. Lamarre *et al.*, *Nature* **426**, 186 (2003).
22. A. K. Saxena *et al.*, International Patent Application WO 02/008244 (2002).

23. K. Lin, A. D. Kwong, C. Lin, *Antimicrob. Agents Chemother.* **48**, 4784 (2004).
24. S. S. Carroll *et al.*, *J. Biol. Chem.* **278**, 11979 (2003).
25. T. Wakita, T. Kato, T. Date, M. Miyamoto, paper presented at the 11th International Symposium on HCV and Related Viruses, Heidelberg, Germany, 5 October 2004.
26. T. Wakita *et al.*, *Nat. Med.* **12**, June 2005 (10.1038/nm1268).
27. J. Zhong *et al.*, *Proc. Natl. Acad. Sci. U.S.A.* **6**, June 2005 (10.1073/pnas.0503596102).
28. T. Pietschmann *et al.*, paper presented at the 11th International Symposium on HCV and Related Viruses, Heidelberg, Germany, 5 October 2004.
29. We thank P. Holst, V. Kramer, and N. Torres for technical assistance; J. Bloom, A. Gauthier, L. Dustin, and D. Bernard for careful review of the manuscript; T. Wakita for SGR-JFH1, SGR-JFH (H2476L), and SGR-JFH(GND); J. Bukh for pJ6CF; D. Moradpour for C7-50 antibody; T. von Hahn and J. Zhang for HepG2/CD81 cells; Boehringer Ingelheim for BILN 2061; The Schering-Plough Research Institute for SCH6; C. Lin and A. Kwong of Vertex Pharmaceutical, Inc. for PI-1; and D. Olsen and S. Ludmerer at Merck for 2'C-methyladenosine. Funded by grants from NIH (CA57973, CA85883, AI40034 to C.M.R., CA10702 to B.D.L., DK70497 to A.J.S., AI51820 to T.L.T., AI50798 to J.A.M.) and the Greenberg Medical Research Institute. Additional support was provided by the Charles H. Revson Foundation (M.J.E.) and the German Science Foundation (Deutsche Forschungsgemeinschaft) (B.W.). B.D.L. is a recipient of the National Cancer Institute Howard Temin Award. C.M.R. is a manager of and has equity in Apath, LLC, which has an exclusive license for the Huh-7.5 cell line.

Supporting Online Material

www.sciencemag.org/cgi/content/full/1114016/DC1

Materials and Methods

SOM Text

Figs. S1 to S3

References and Notes

25 April 2005; accepted 31 May 2005

Published online 9 June 2005;

10.1126/science.1114016

Include this information when citing this paper.

Genome-Scale Identification of Nucleosome Positions in *S. cerevisiae*

Guo-Cheng Yuan, Yuen-Jong Liu,* Michael F. Dion, Michael D. Slack,† Lani F. Wu, Steven J. Altschuler, Oliver J. Rando‡

The positioning of nucleosomes along chromatin has been implicated in the regulation of gene expression in eukaryotic cells, because packaging DNA into nucleosomes affects sequence accessibility. We developed a tiled microarray approach to identify at high resolution the translational positions of 2278 nucleosomes over 482 kilobases of *Saccharomyces cerevisiae* DNA, including almost all of chromosome III and 223 additional regulatory regions. The majority of the nucleosomes identified were well-positioned. We found a stereotyped chromatin organization at Pol II promoters consisting of a nucleosome-free region \sim 200 base pairs upstream of the start codon flanked on both sides by positioned nucleosomes. The nucleosome-free sequences were evolutionarily conserved and were enriched in poly-deoxyadenosine or poly-deoxythymidine sequences. Most occupied transcription factor binding motifs were devoid of nucleosomes, strongly suggesting that nucleosome positioning is a global determinant of transcription factor access.

Nucleosomes prevent many DNA binding proteins from approaching their sites (1–3), whereas appropriately positioned nucleosomes

can bring distant DNA sequences into close proximity to promote transcription (4). Current understanding of the primary structure of chro-

matin and its effects on gene expression comes from a handful of well-characterized loci (see examples below). High-resolution measurements of nucleosome positions over chromosome-scale distances would enhance our understanding of chromatin structure and function.

To measure nucleosome positions on a genomic scale, we developed a DNA microarray method (5) to identify nucleosomal and linker DNA sequences on the basis of susceptibility of linker DNA to micrococcal nuclease (fig. S1). Nucleosomal DNA was isolated, labeled with Cy3 fluorescent dye (green), and mixed with Cy5-labeled total genomic DNA (red). This mixture was hybridized to microarrays printed with overlapping 50-mer oligonucleotide probes tiled every 20 base pairs across chromosomal regions of interest (fig.

Bauer Center for Genomics Research, Harvard University, 7 Divinity Avenue, Cambridge, MA 02138, USA.

*Present address: Department of Molecular Biophysics and Biochemistry, Yale University, Post Office Box 208114, New Haven, CT 06520, USA.

†Present address: BAE Systems Advanced Information Technologies, 9655 Granite Ridge Drive, San Diego, CA 92123, USA.

‡To whom correspondence should be addressed. E-mail: orando@cgr.harvard.edu

References

- Allison, S. L., J. Schalich, K. Stiasny, C. W. Mandl and F. X. Heinz (2001). "Mutational evidence for an internal fusion peptide in flavivirus envelope protein E." J Virol **75**(9): 4268-75.
- Allison, S. L., J. Schalich, K. Stiasny, C. W. Mandl, C. Kunz and F. X. Heinz (1995). "Oligomeric rearrangement of tick-borne encephalitis virus envelope proteins induced by an acidic pH." J Virol **69**(2): 695-700.
- Barreiro, O., M. Yanez-Mo, M. Sala-Valdes, M. D. Gutierrez-Lopez, S. Ovalle, A. Higginbottom, P. N. Monk, C. Cabanas and F. Sanchez-Madrid (2005). "Endothelial tetraspanin microdomains regulate leukocyte firm adhesion during extravasation." Blood **105**(7): 2852-61.
- Berditchevski, F. (2001). "Complexes of tetraspanins with integrins: more than meets the eye." J Cell Sci **114**(Pt 23): 4143-51.
- Berditchevski, F., E. Gilbert, M. R. Griffiths, S. Fitter, L. Ashman and S. J. Jenner (2001). "Analysis of the CD151-alpha3beta1 integrin and CD151-tetraspanin interactions by mutagenesis." J Biol Chem **276**(44): 41165-74.
- Berditchevski, F. and E. Odintsova (1999). "Characterization of integrin-tetraspanin adhesion complexes: role of tetraspanins in integrin signaling." J Cell Biol **146**(2): 477-92.
- Berditchevski, F., E. Odintsova, S. Sawada and E. Gilbert (2002). "Expression of the palmitoylation-deficient CD151 weakens the association of alpha 3 beta 1 integrin with the tetraspanin-enriched microdomains and affects integrin-dependent signaling." J Biol Chem **277**(40): 36991-7000.
- Berditchevski, F., M. M. Zutter and M. E. Hemler (1996). "Characterization of novel complexes on the cell surface between integrins and proteins with 4 transmembrane domains (TM4 proteins)." Mol Biol Cell **7**(2): 193-207.
- Betz, S. F. (1993). "Disulfide bonds and the stability of globular proteins." Protein Sci **2**(10): 1551-8.
- Bienstock, R. J. and J. C. Barrett (2001). "KAI1, a prostate metastasis suppressor: prediction of solvated structure and interactions with binding partners; integrins, cadherins, and cell-surface receptor proteins." Mol Carcinog **32**(3): 139-53.
- Blight, K. J., A. A. Kolykhalov and C. M. Rice (2000). "Efficient initiation of HCV RNA replication in cell culture." Science **290**(5498): 1972-4.

- Blobel, C. P., T. G. Wolfsberg, C. W. Turck, D. G. Myles, P. Primakoff and J. M. White (1992). "A potential fusion peptide and an integrin ligand domain in a protein active in sperm-egg fusion." Nature **356**(6366): 248-52.
- Boucheix, C., G. H. Duc, C. Jasmin and E. Rubinstein (2001). "Tetraspanins and malignancy." Expert Rev Mol Med **2001**: 1-17.
- Boucheix, C. and E. Rubinstein (2001). "Tetraspanins." Cell Mol Life Sci **58**(9): 1189-205.
- Branden, C. and J. Tooze (1999). Introduction to Protein Structure. New York, Garland Publishing, Inc.
- Bressanelli, S., K. Stiasny, S. L. Allison, E. A. Stura, S. Duquerroy, J. Lescar, F. X. Heinz and F. A. Rey (2004). "Structure of a flavivirus envelope glycoprotein in its low-pH-induced membrane fusion conformation." Embo J **23**(4): 728-38.
- Brikhead, T. and A. Moller (1998). Sperm Competition and Sexual Selection, Academic Press.
- Carr, C. M. and P. S. Kim (1993). "A spring-loaded mechanism for the conformational change of influenza hemagglutinin." Cell **73**(4): 823-32.
- Chamberlain, L. H. (2004). "Detergents as tools for the purification and classification of lipid rafts." FEBS Lett **559**(1-3): 1-5.
- Chan, D. C., D. Fass, J. M. Berger and P. S. Kim (1997). "Core structure of gp41 from the HIV envelope glycoprotein." Cell **89**(2): 263-73.
- Chan, D. C. and P. S. Kim (1998). "HIV entry and its inhibition." Cell **93**(5): 681-4.
- Charrin, S., F. Le Naour, V. Labas, M. Billard, J. P. Le Caer, J. F. Emile, M. A. Petit, C. Boucheix and E. Rubinstein (2003). "EWI-2 is a new component of the tetraspanin web in hepatocytes and lymphoid cells." Biochem J **373**(Pt 2): 409-21.
- Charrin, S., F. Le Naour, M. Oualid, M. Billard, G. Faure, S. M. Hanash, C. Boucheix and E. Rubinstein (2001). "The major CD9 and CD81 molecular partner. Identification and characterization of the complexes." J Biol Chem **276**(17): 14329-37.
- Charrin, S., S. Manie, M. Billard, L. Ashman, D. Gerlier, C. Boucheix and E. Rubinstein (2003). "Multiple levels of interactions within the tetraspanin web." Biochem Biophys Res Commun **304**(1): 107-12.

- Charrin, S., S. Manie, M. Oualid, M. Billard, C. Boucheix and E. Rubinstein (2002). "Differential stability of tetraspanin/tetraspanin interactions: role of palmitoylation." FEBS Lett **516**(1-3): 139-44.
- Charrin, S., S. Manie, C. Thiele, M. Billard, D. Gerlier, C. Boucheix and E. Rubinstein (2003). "A physical and functional link between cholesterol and tetraspanins." Eur J Immunol **33**(9): 2479-89.
- Chen, E. H. and E. N. Olson (2005). "Unveiling the mechanisms of cell-cell fusion." Science **308**(5720): 369-73.
- Chen, M. S., K. S. Tung, S. A. Coonrod, Y. Takahashi, D. Bigler, A. Chang, Y. Yamashita, P. W. Kincade, J. C. Herr and J. M. White (1999). "Role of the integrin-associated protein CD9 in binding between sperm ADAM 2 and the egg integrin alpha6beta1: implications for murine fertilization [In Process Citation]." Proc Natl Acad Sci U S A **96**(21): 11830-5.
- Chen, Y., J. T. Yang and K. H. Chau (1974). "Determination of the Helix and β Form of Proteins in Aqueous Solution by Circular Dichroism." Biochemistry **13**(16): 3350-59.
- Cherukuri, A., T. Shoham, H. W. Sohn, S. Levy, S. Brooks, R. Carter and S. K. Pierce (2004). "The tetraspanin CD81 is necessary for partitioning of coligated CD19/CD21-B cell antigen receptor complexes into signaling-active lipid rafts." J Immunol **172**(1): 370-80.
- Cho, C., D. O. Bunch, J. E. Faure, E. H. Goulding, E. M. Eddy, P. Primakoff and D. G. Myles (1998). "Fertilization defects in sperm from mice lacking fertilin beta." Science **281**(5384): 1857-9.
- Claas, C., C. S. Stipp and M. E. Hemler (2000). "Evaluation of prototype TM4SF protein complexes and their relation to lipid rafts." J Biol Chem **11**: 11.
- Clarke, G., A. F. Goldberg, D. Vidgen, L. Collins, L. Ploder, L. Schwarz, L. L. Molday, J. Rossant, A. Szel, R. S. Molday, D. G. Birch and R. R. McInnes (2000). "Rom-1 is required for rod photoreceptor viability and the regulation of disk morphogenesis." Nat Genet **25**(1): 67-73.
- Clay, D., E. Rubinstein, Z. Mishal, A. Anjo, M. Prenant, C. Jasmin, C. Boucheix and M. C. Le Bousse-Kerdiles (2001). "CD9 and megakaryocyte differentiation." Blood **97**(7): 1982-9.
- Cordes, M. H., A. R. Davidson and R. T. Sauer (1996). "Sequence space, folding and protein design." Curr Opin Struct Biol **6**(1): 3-10.

- De Francesco, R. and C. M. Rice (2003). "New therapies on the horizon for hepatitis C: are we close?" Clin Liver Dis **7**(1): 211-42, xi.
- del Campo, J. J., E. Opoku-Serebuoh, A. B. Isaacson, V. L. Scranton, M. Tucker, M. Han and W. A. Mohler (2005). "Fusogenic activity of EFF-1 is regulated via dynamic localization in fusing somatic cells of *C. elegans*." Curr Biol **15**(5): 413-23.
- Dijkstra, S., E. E. Geisert, Jr., C. D. Dijkstra, P. R. Bar and E. A. Joosten (2001). "CD81 and microglial activation in vitro: proliferation, phagocytosis and nitric oxide production." J Neuroimmunol **114**(1-2): 151-9.
- Dong, J. T., P. W. Lamb, C. W. Rinker-Schaeffer, J. Vukanovic, T. Ichikawa, J. T. Isaacs and J. C. Barrett (1995). "KAI1, a metastasis suppressor gene for prostate cancer on human chromosome 11p11.2." Science **268**(5212): 884-6.
- Dyson, H. J. and P. E. Wright (1991). "Defining solution conformations of small linear peptides." Annu Rev Biophys Biophys Chem **20**: 519-38.
- Earp, L. J., S. E. Delos, H. E. Park and J. M. White (2005). "The many mechanisms of viral membrane fusion proteins." Curr Top Microbiol Immunol **285**: 25-66.
- Eckert, D. M. and P. S. Kim (2001). "Mechanisms of viral membrane fusion and its inhibition." Annu Rev Biochem **70**: 777-810.
- Edelhoch, H. (1967). Biochemistry **6**: 1948-1954.
- Ellerman, D. A., C. Ha, P. Primakoff, D. G. Myles and G. S. Dveksler (2003). "Direct binding of the ligand PSG17 to CD9 requires a CD9 site essential for sperm-egg fusion." Mol Biol Cell **14**(12): 5098-103.
- Evans, J. (1995). Biomolecular NMR Spectroscopy. Oxford, Oxford University Press.
- Ferlenghi, I., M. Clarke, T. Ruttan, S. L. Allison, J. Schalich, F. X. Heinz, S. C. Harrison, F. A. Rey and S. D. Fuller (2001). "Molecular organization of a recombinant subviral particle from tick-borne encephalitis virus." Mol Cell **7**(3): 593-602.
- Fields, B. N., Ed. (2001). Fields-Virology, Lippincott Williams and Wilkins.
- Flint, M., C. Maidens, L. D. Loomis-Price, C. Shotton, J. Dubuisson, P. Monk, A. Higginbottom, S. Levy and J. A. McKeating (1999). "Characterization of hepatitis C virus E2 glycoprotein interaction with a putative cellular receptor, CD81." J Virol **73**(8): 6235-44.
- Fradkin, L. G., J. T. Kamphorst, A. DiAntonio, C. S. Goodman and J. N. Noordermeer (2002). "Genomewide analysis of the *Drosophila* tetraspanins reveals a subset

- with similar function in the formation of the embryonic synapse." Proc Natl Acad Sci U S A **99**(21): 13663-8.
- Garry, R. F. and S. Dash (2003). "Proteomics computational analyses suggest that hepatitis C virus E1 and pestivirus E2 envelope glycoproteins are truncated class II fusion proteins." Virology **307**(2): 255-65.
- Geisert, E. E., Jr., R. W. Williams, G. R. Geisert, L. Fan, A. M. Asbury, H. T. Maecker, J. Deng and S. Levy (2002). "Increased brain size and glial cell number in CD81-null mice." J Comp Neurol **453**(1): 22-32.
- Geisert, E. E., Jr., L. Yang and M. H. Irwin (1996). "Astrocyte growth, reactivity, and the target of the antiproliferative antibody, TAPA." J Neurosci **16**(17): 5478-87.
- Gilbert, S. (2003). Developmental Biology. Portland, OR, Sinauer associates.
- Ha, C. T., R. Waterhouse, J. Wessells, J. A. Wu and G. S. Dveksler (2005). "Binding of pregnancy-specific glycoprotein 17 to CD9 on macrophages induces secretion of IL-10, IL-6, PGE2, and TGF- β 1." J Leukoc Biol **77**(6): 948-57.
- He, Z. Y., C. Brakebusch, R. Fassler, J. A. Kreidberg, P. Primakoff and D. G. Myles (2003). "None of the integrins known to be present on the mouse egg or to be ADAM receptors are essential for sperm-egg binding and fusion." Dev Biol **254**(2): 226-37.
- Heiman, M. G. and P. Walter (2000). "Prm1p, a pheromone-regulated multispanning membrane protein, facilitates plasma membrane fusion during yeast mating." J Cell Biol **151**(3): 719-30.
- Hemler, M. E. (2001). "Specific tetraspanin functions." J Cell Biol **155**(7): 1103-7.
- Hemler, M. E. (2003). "Tetraspanin proteins mediate cellular penetration, invasion, and fusion events and define a novel type of membrane microdomain." Annu Rev Cell Dev Biol **19**: 397-422.
- Hendrickson, W. A. (1991). "Determination of macromolecular structures from anomalous diffraction of synchrotron radiation." Science **254**(5028): 51-8.
- Hernandez, L. D., L. R. Hoffman, T. G. Wolfsberg and J. M. White (1996). "Virus-cell and cell-cell fusion." Annu Rev Cell Dev Biol **12**: 627-61.
- Higginbottom, A., E. R. Quinn, C. C. Kuo, M. Flint, L. H. Wilson, E. Bianchi, A. Nicosia, P. N. Monk, J. A. McKeating and S. Levy (2000). "Identification of amino acid residues in CD81 critical for interaction with hepatitis C virus envelope glycoprotein E2." J Virol **74**(8): 3642-9.

- Higginbottom, A., Y. Takahashi, L. Bolling, S. A. Coonrod, J. M. White, L. J. Partridge and P. N. Monk (2003). "Structural requirements for the inhibitory action of the CD9 large extracellular domain in sperm/oocyte binding and fusion." Biochem Biophys Res Commun **311**(1): 208-14.
- Higuchi, R. (1990). Recombinant PCR. PCR protocols. D. H. G. Michael A. Innis, John J. Sninsky, Thomas J. White. San Diego, California, Academic Press: 177-183.
- Hogan, B., R. Beddington, F. Constantini and E. Lacy (1994). Manipulating the Mouse Embryo. New York, Cold Spring Harbor Press.
- Horejsi, V. and C. Vlcek (1991). "Novel structurally distinct family of leucocyte surface glycoproteins including CD9, CD37, CD53 and CD63." FEBS Lett **288**(1-2): 1-4.
- Horvath, G., V. Serru, D. Clay, M. Billard, C. Boucheix and E. Rubinstein (1998). "CD19 is linked to the integrin-associated tetraspans CD9, CD81, and CD82." J Biol Chem **273**(46): 30537-43.
- Hotta, H., A. H. Ross, K. Huebner, M. Isobe, S. Wendeborn, M. V. Chao, R. P. Ricciardi, Y. Tsujimoto, C. M. Croce and H. Koprowski (1988). "Molecular cloning and characterization of an antigen associated with early stages of melanoma tumor progression." Cancer Res **48**(11): 2955-62.
- Hsu, M., J. Zhang, M. Flint, C. Logvinoff, C. Cheng-Mayer, C. M. Rice and J. A. McKeating (2003). "Hepatitis C virus glycoproteins mediate pH-dependent cell entry of pseudotyped retroviral particles." Proc Natl Acad Sci U S A **100**(12): 7271-6.
- Humphries, M. J. (2004). "Monoclonal antibodies as probes of integrin priming and activation." Biochem Soc Trans **32**(Pt3): 407-11.
- Hynes, R. O. (2002). "Integrins: bidirectional, allosteric signaling machines." Cell **110**(6): 673-87.
- Ikeyama, S., M. Koyama, M. Yamaoko, R. Sasada and M. Miyake (1993). "Suppression of cell motility and metastasis by transfection with human motility-related protein (MRP-1/CD9) DNA." J Exp Med **177**(5): 1231-7.
- Imai, T., M. Kakizaki, M. Nishimura and O. Yoshie (1995). "Molecular analyses of the association of CD4 with two members of the transmembrane 4 superfamily, CD81 and CD82." J Immunol **155**(3): 1229-39.
- Imai, T. and O. Yoshie (1993). "C33 antigen and M38 antigen recognized by monoclonal antibodies inhibitory to syncytium formation by human T cell leukemia virus type 1 are both members of the transmembrane 4 superfamily and associate with each other and with CD4 or CD8 in T cells." J Immunol **151**(11): 6470-81.

- Inoue, N., M. Ikawa, A. Isotani and M. Okabe (2005). "The immunoglobulin superfamily protein Izumo is required for sperm to fuse with eggs." *Nature* **434**(7030): 234-8.
- Ishibashi, T., L. Ding, K. Ikenaka, Y. Inoue, K. Miyado, E. Mekada and H. Baba (2004). "Tetraspanin protein CD9 is a novel paranodal component regulating paranodal junctional formation." *J Neurosci* **24**(1): 96-102.
- Iwamoto, R., S. Higashiyama, T. Mitamura, N. Taniguchi, M. Klagsbrun and E. Mekada (1994). "Heparin-binding EGF-like growth factor, which acts as the diphtheria toxin receptor, forms a complex with membrane protein DRAP27/CD9, which up-regulates functional receptors and diphtheria toxin sensitivity." *Embo J* **13**(10): 2322-30.
- Jahn, R., T. Lang and T. C. Sudhof (2003). "Membrane fusion." *Cell* **112**(4): 519-33.
- Jung, J. and B. Lee (2000). "Use of residue pairs in protein sequence-sequence and sequence-structure alignments." *Protein Sci* **9**(8): 1576-88.
- Kaji, K., S. Oda, T. Shikano, T. Ohnuki, Y. Uematsu, J. Sakagami, N. Tada, S. Miyazaki and A. Kudo (2000). "The gamete fusion process is defective in eggs of Cd9-deficient mice." *Nat Genet* **24**(3): 279-82.
- Kamath, R. S., A. G. Fraser, Y. Dong, G. Poulin, R. Durbin, M. Gotta, A. Kanapin, N. Le Bot, S. Moreno, M. Sohrmann, D. P. Welchman, P. Zipperlen and J. Ahringer (2003). "Systematic functional analysis of the *Caenorhabditis elegans* genome using RNAi." *Nature* **421**(6920): 231-7.
- Kazarov, A. R., X. Yang, C. S. Stipp, B. Sehgal and M. E. Hemler (2002). "An extracellular site on tetraspanin CD151 determines alpha 3 and alpha 6 integrin-dependent cellular morphology." *J Cell Biol* **158**(7): 1299-309.
- Keating, A. E., V. N. Malashkevich, B. Tidor and P. S. Kim (2001). "Side-chain repacking calculations for predicting structures and stabilities of heterodimeric coiled coils." *Proc Natl Acad Sci U S A* **98**(26): 14825-30.
- Kelic, S., S. Levy, C. Suarez and D. E. Weinstein (2001). "CD81 regulates neuron-induced astrocyte cell-cycle exit." *Mol Cell Neurosci* **17**(3): 551-60.
- Kitadokoro, K., D. Bordo, G. Galli, R. Petracca, F. Falugi, S. Abrignani, G. Grandi and M. Bolognesi (2001). "CD81 extracellular domain 3D structure: insight into the tetraspanin superfamily structural motifs." *Embo J* **20**(1 & 2): 12-18.
- Kitadokoro, K., D. Bordo, G. Galli, R. Petracca, F. Falugi, S. Abrignani, G. Grandi and M. Bolognesi (2001). "CD81 extracellular domain 3D structure: insight into the tetraspanin superfamily structural motifs." *Embo J* **20**(1-2): 12-8.

- Kitadokoro, K., G. Galli, R. Petracca, F. Falugi, G. Grandi and M. Bolognesi (2001). "Crystallization and preliminary crystallographic studies on the large extracellular domain of human CD81, a tetraspanin receptor for hepatitis C virus." Acta Crystallogr D Biol Crystallogr **57**(Pt 1): 156-8.
- Kitadokoro, K., M. Ponassi, G. Galli, R. Petracca, F. Falugi, G. Grandi and M. Bolognesi (2002). "Subunit association and conformational flexibility in the head subdomain of human CD81 large extracellular loop." Biol Chem **383**(9): 1447-52.
- Klemm, J. D., S. L. Schreiber and G. R. Crabtree (1998). "Dimerization as a regulatory mechanism in signal transduction." Annu Rev Immunol **16**: 569-92.
- Knobeloch, K. P., M. D. Wright, A. F. Ochsenbein, O. Liesenfeld, J. Lohler, R. M. Zinkernagel, I. Horak and Z. Orinska (2000). "Targeted inactivation of the tetraspanin CD37 impairs T-cell-dependent B-cell response under suboptimal costimulatory conditions." Mol Cell Biol **20**(15): 5363-9.
- Kohl, S., I. Giddings, D. Besch, E. Apfelstedt-Sylla, E. Zrenner and B. Wissinger (1998). "The role of the peripherin/RDS gene in retinal dystrophies." Acta Anat (Basel) **162**(2-3): 75-84.
- Kopczynski, C. C., G. W. Davis and C. S. Goodman (1996). "A neural tetraspanin, encoded by late bloomer, that facilitates synapse formation." Science **271**(5257): 1867-70.
- Kovalenko, O. V., X. Yang, T. V. Kolesnikova and M. E. Hemler (2004). "Evidence for specific tetraspanin homodimers: inhibition of palmitoylation makes cysteine residues available for cross-linking." Biochem J **377**(Pt 2): 407-17.
- L'Hernault, S. W., D. C. Shakes and S. Ward (1988). "Developmental genetics of chromosome I spermatogenesis-defective mutants in the nematode *Caenorhabditis elegans*." Genetics **120**(2): 435-52.
- Lammerding, J., A. R. Kazarov, H. Huang, R. T. Lee and M. E. Hemler (2003). "Tetraspanin CD151 regulates alpha6beta1 integrin adhesion strengthening." Proc Natl Acad Sci U S A **100**(13): 7616-21.
- Lau, L. M., J. L. Wee, M. D. Wright, G. W. Moseley, P. M. Hogarth, L. K. Ashman and D. E. Jackson (2004). "The tetraspanin superfamily member CD151 regulates outside-in integrin alphaIIb beta3 signaling and platelet function." Blood **104**(8): 2368-75.
- Laue, T. M., B. D. Shah, T. M. Ridgeway and S. L. Pelletier (1992). Analytical Ultracentrifugation in Biochemistry and Polymer Science. Cambridge, Royal Society of Chemistry.

- Le Naour, F., E. Rubinstein, C. Jasmin, M. Prenant and C. Boucheix (2000). "Severely reduced female fertility in CD9-deficient mice." Science **287**(5451): 319-21.
- Lescar, J., A. Roussel, M. W. Wien, J. Navaza, S. D. Fuller, G. Wengler and F. A. Rey (2001). "The Fusion glycoprotein shell of Semliki Forest virus: an icosahedral assembly primed for fusogenic activation at endosomal pH." Cell **105**(1): 137-48.
- Levy, S. and T. Shoham (2005). "The tetraspanin web modulates immune-signalling complexes." Nat Rev Immunol **5**(2): 136-48.
- Levy, S., S. C. Todd and H. T. Maecker (1998). "CD81 (TAPA-1): a molecule involved in signal transduction and cell adhesion in the immune system." Annu Rev Immunol **16**: 89-109.
- Li, R., C. R. Babu, J. D. Lear, A. J. Wand, J. S. Bennett and W. F. DeGrado (2001). "Oligomerization of the integrin alphaIIb beta3: roles of the transmembrane and cytoplasmic domains." Proc Natl Acad Sci U S A **98**(22): 12462-7.
- Li, R., N. Mitra, H. Gratkowski, G. Vilaire, R. Litvinov, C. Nagasami, J. W. Weisel, J. D. Lear, W. F. DeGrado and J. S. Bennett (2003). "Activation of integrin alphaIIb beta3 by modulation of transmembrane helix associations." Science **300**(5620): 795-8.
- Lindenbach, B., M. Evans, A. Snyder, B. Wolk, T. Tellinghuisen, C. C. Liu, T. Maruyama, R. O. Hynes, R. Burton, J. McKeating and C. M. Rice (in press). "Complete Replication of Hepatitis C Virus in Cell Culture." Science.
- Liu, X., S. N. Constantinescu, Y. Sun, J. S. Bogan, D. Hirsch, R. A. Weinberg and H. F. Lodish (2000). "Generation of mammalian cells stably expressing multiple genes at predetermined levels." Anal Biochem **280**(1): 20-8.
- Loewen, C. J. and R. S. Molday (2000). "Disulfide-mediated oligomerization of Peripherin/Rds and Rom-1 in photoreceptor disk membranes. Implications for photoreceptor outer segment morphogenesis and degeneration." J Biol Chem **275**(8): 5370-8.
- Longhurst, C. M., M. M. White, D. A. Wilkinson and L. K. Jennings (1999). "A CD9, alphaIIb beta3, integrin-associated protein, and GPIb/V/IX complex on the surface of human platelets is influenced by alphaIIb beta3 conformational states." Eur J Biochem **263**(1): 104-11.
- Lu, M., S. C. Blacklow and P. S. Kim (1995). "A trimeric structural domain of the HIV-1 transmembrane glycoprotein." Nat Struct Biol **2**(12): 1075-82.

- Luo, B. H., C. V. Carman, J. Takagi and T. A. Springer (2005). "Disrupting integrin transmembrane domain heterodimerization increases ligand binding affinity, not valency or clustering." Proc Natl Acad Sci U S A **102**(10): 3679-84.
- Luo, B. H., T. A. Springer and J. Takagi (2003). "Stabilizing the open conformation of the integrin headpiece with a glycan wedge increases affinity for ligand." Proc Natl Acad Sci U S A **100**(5): 2403-8.
- Luo, B. H., T. A. Springer and J. Takagi (2004). "A specific interface between integrin transmembrane helices and affinity for ligand." PLoS Biol **2**(6): e153.
- Maecker, H. T. and S. Levy (1997). "Normal lymphocyte development but delayed humoral immune response in CD81-null mice." J Exp Med **185**(8): 1505-10.
- Maecker, H. T., S. C. Todd, E. C. Kim and S. Levy (2000). "Differential expression of murine CD81 highlighted by new anti-mouse CD81 monoclonal antibodies." Hybridoma **19**(1): 15-22.
- Maecker, H. T., S. C. Todd and S. Levy (1997). "The tetraspanin superfamily: molecular facilitators." Faseb J **11**(6): 428-42.
- Mannion, B. A., F. Berditchevski, S. K. Kraeft, L. B. Chen and M. E. Hemler (1996). "Transmembrane-4 superfamily proteins CD81 (TAPA-1), CD82, CD63, and CD53 specifically associated with integrin alpha 4 beta 1 (CD49d/CD29)." J Immunol **157**(5): 2039-47.
- Mayor, S. and F. R. Maxfield (1995). "Insolubility and redistribution of GPI-anchored proteins at the cell surface after detergent treatment." Mol Biol Cell **6**(7): 929-44.
- McKeating, J. A., L. Q. Zhang, C. Logvinoff, M. Flint, J. Zhang, J. Yu, D. Butera, D. D. Ho, L. B. Dustin, C. M. Rice and P. Balfe (2004). "Diverse hepatitis C virus glycoproteins mediate viral infection in a CD81-dependent manner." J Virol **78**(16): 8496-505.
- Meuleman, P., L. Libbrecht, R. De Vos, B. de Hemptinne, K. Gevaert, J. Vandekerckhove, T. Roskams and G. Leroux-Roels (2005). "Morphological and biochemical characterization of a human liver in a uPA-SCID mouse chimera." Hepatology **41**(4): 847-56.
- Miao, W. M., E. Vasile, W. S. Lane and J. Lawler (2001). "CD36 associates with CD9 and integrins on human blood platelets." Blood **97**(6): 1689-96.
- Mierendorf, R. C., C. Percy and R. A. Young (1987). "Gene isolation by screening lambda gt11 libraries with antibodies." Methods Enzymol **152**: 458-69.

- Miller, B. J., E. Georges-Labouesse, P. Primakoff and D. G. Myles (2000). "Normal fertilization occurs with eggs lacking the integrin alpha6beta1 and is CD9-dependent." *J Cell Biol* **149**(6): 1289-96.
- Min, G., G. Zhou, M. Schapira, T. T. Sun and X. P. Kong (2003). "Structural basis of urothelial permeability barrier function as revealed by Cryo-EM studies of the 16 nm uroplakin particle." *J Cell Sci* **116**(Pt 20): 4087-94.
- Miyado, K., G. Yamada, S. Yamada, H. Hasuwa, Y. Nakamura, F. Ryu, K. Suzuki, K. Kosai, K. Inoue, A. Ogura, M. Okabe and E. Mekada (2000). "Requirement of CD9 on the egg plasma membrane for fertilization." *Science* **287**(5451): 321-4.
- Miyake, M., M. Koyama, M. Seno and S. Ikeyama (1991). "Identification of the motility-related protein (MRP-1), recognized by monoclonal antibody M31-15, which inhibits cell motility." *J Exp Med* **174**(6): 1347-54.
- Miyazaki, T., U. Muller and K. S. Campbell (1997). "Normal development but differentially altered proliferative responses of lymphocytes in mice lacking CD81." *Embo J* **16**(14): 4217-25.
- Mohler, W. A., G. Shemer, J. J. del Campo, C. Valansi, E. Opoku-Serebuoh, V. Scranton, N. Assaf, J. G. White and B. Podbilewicz (2002). "The type I membrane protein EFF-1 is essential for developmental cell fusion." *Dev Cell* **2**(3): 355-62.
- Moribe, H., J. Yochem, H. Yamada, Y. Tabuse, T. Fujimoto and E. Mekada (2004). "Tetraspanin protein (TSP-15) is required for epidermal integrity in *Caenorhabditis elegans*." *J Cell Sci* **117**(Pt 22): 5209-20.
- Mulvey, M. A., Y. S. Lopez-Boado, C. L. Wilson, R. Roth, W. C. Parks, J. Heuser and S. J. Hultgren (1998). "Induction and evasion of host defenses by type 1-piliated uropathogenic *Escherichia coli*." *Science* **282**(5393): 1494-7.
- Myles, D. G., L. H. Kimmel, C. P. Blobel, J. M. White and P. Primakoff (1994). "Identification of a binding site in the disintegrin domain of fertilin required for sperm-egg fusion." *Proc Natl Acad Sci U S A* **91**(10): 4195-8.
- Nakajima, H., L. Cocquerel, N. Kiyokawa, J. Fujimoto and S. Levy (2005). "Kinetics of HCV envelope proteins' interaction with CD81 large extracellular loop." *Biochem Biophys Res Commun* **328**(4): 1091-100.
- Nakamura, K., T. Mitamura, T. Takahashi, T. Kobayashi and E. Mekada (2000). "Importance of the major extracellular domain of CD9 and the epidermal growth factor (EGF)-like domain of heparin-binding EGF-like growth factor for up-regulation of binding and activity." *J Biol Chem* **275**(24): 18284-90.

- Neugebauer, A., C. D. Klein and R. W. Hartmann (2004). "Protein-dynamics of the putative HCV receptor CD81 large extracellular loop." Bioorg Med Chem Lett **14**(7): 1765-9.
- Newman, J. R. and A. E. Keating (2003). "Comprehensive identification of human bZIP interactions with coiled-coil arrays." Science **300**(5628): 2097-101.
- Nowak, M. and R. M. May (2000). Virus Dynamics: The Mathematical Foundations of Immunology and Virology, Oxford University Press.
- O'Shea, E. K., K. J. Lumb and P. S. Kim (1993). "Peptide 'Velcro': design of a heterodimeric coiled coil." Curr Biol **3**(10): 658-67.
- O'Shea, E. K., R. Rutkowski, W. F. Stafford, 3rd and P. S. Kim (1989). "Preferential heterodimer formation by isolated leucine zippers from fos and jun." Science **245**(4918): 646-8.
- Oren, R., S. Takahashi, C. Doss, R. Levy and S. Levy (1990). "TAPA-1, the target of an antiproliferative antibody, defines a new family of transmembrane proteins." Mol Cell Biol **10**(8): 4007-15.
- Oritani, K., X. Wu, K. Medina, J. Hudson, K. Miyake, J. M. Gimble, S. A. Burstein and P. W. Kincade (1996). "Antibody ligation of CD9 modifies production of myeloid cells in long- term cultures." Blood **87**(6): 2252-61.
- Page, R. and R. C. Stevens (2004). "Crystallization data mining in structural genomics: using positive and negative results to optimize protein crystallization screens." Methods **34**(3): 373-89.
- Pain, R., Ed. (1994). Mechanisms of Protein Folding. Frontiers in Molecular Biology. New York, Oxford University Press.
- Penas, P. F., A. Garcia-Diez, F. Sanchez-Madrid and M. Yanez-Mo (2000). "Tetraspanins are localized at motility-related structures and involved in normal human keratinocyte wound healing migration." J Invest Dermatol **114**(6): 1126-35.
- Petracca, R., F. Falugi, G. Galli, N. Norais, D. Rosa, S. Campagnoli, V. Burgio, E. Di Stasio, B. Giardina, M. Houghton, S. Abrignani and G. Grandi (2000). "Structure-function analysis of hepatitis C virus envelope-CD81 binding." J Virol **74**(10): 4824-30.
- Pileri, P., Y. Uematsu, S. Campagnoli, G. Galli, F. Falugi, R. Petracca, A. J. Weiner, M. Houghton, D. Rosa, G. Grandi and S. Abrignani (1998). "Binding of hepatitis C virus to CD81." Science **282**(5390): 938-41.

- Pileri, P., Y. Uematsu, S. Campagnoli, G. Galli, F. Falugi, R. Petracca, A. J. Weiner, M. Houghton, D. Rosa, G. Grandi and S. Abrignani (1998). "Binding of hepatitis C virus to CD81." Science **282**(5390): 938-41.
- Pohlmann, S., J. Zhang, F. Baribaud, Z. Chen, G. J. Leslie, G. Lin, A. Granelli-Piperno, R. W. Doms, C. M. Rice and J. A. McKeating (2003). "Hepatitis C virus glycoproteins interact with DC-SIGN and DC-SIGNR." J Virol **77**(7): 4070-80.
- Popot, J. L. and D. M. Engelman (2000). "Helical membrane protein folding, stability, and evolution." Annu Rev Biochem **69**: 881-922.
- Primakoff, P., H. Hyatt and J. Tredick-Kline (1987). "Identification and purification of a sperm surface protein with a potential role in sperm-egg membrane fusion." J Cell Biol **104**(1): 141-9.
- Primakoff, P. and D. G. Myles (1983). "A map of the guinea pig sperm surface constructed with monoclonal antibodies." Dev Biol **98**(2): 417-28.
- Primakoff, P. and D. G. Myles (2000). "The ADAM gene family: surface proteins with adhesion and protease activity." Trends Genet **16**(2): 83-7.
- Radford, K. J., J. Mallesch and P. Hersey (1995). "Suppression of human melanoma cell growth and metastasis by the melanoma-associated antigen CD63 (ME491)." Int J Cancer **62**(5): 631-5.
- Rey, F. A., F. X. Heinz, C. Mandl, C. Kunz and S. C. Harrison (1995). "The envelope glycoprotein from tick-borne encephalitis virus at 2 Å resolution." Nature **375**(6529): 291-8.
- Root, M. J., M. S. Kay and P. S. Kim (2001). "Protein design of an HIV-1 entry inhibitor." Science **291**(5505): 884-8.
- Rost, B., C. Sander and R. Schneider (1994). "Redefining the goals of protein secondary structure prediction." J Mol Biol **235**(1): 13-26.
- Rousseaux, J., R. Rousseaux-Prevost and H. Bazin (1986). "Optimal conditions for the preparation of proteolytic fragments from monoclonal IgG of different rat IgG subclasses." Methods Enzymol **121**: 663-9.
- Rubinstein, E., F. Le Naour, M. Billard, M. Prenant and C. Boucheix (1994). "CD9 antigen is an accessory subunit of the VLA integrin complexes." Eur J Immunol **24**(12): 3005-13.
- Rubinstein, E., F. Le Naour, C. Lagaudriere-Gesbert, M. Billard, H. Conjeaud and C. Boucheix (1996). "CD9, CD63, CD81, and CD82 are components of a surface

- tetraspan network connected to HLA-DR and VLA integrins." Eur J Immunol **26**(11): 2657-65.
- Rubinstein, E., V. Poindessous-Jazat, F. Le Naour, M. Billard and C. Boucheix (1997). "CD9, but not other tetraspans, associates with the beta1 integrin precursor." Eur J Immunol **27**(8): 1919-27.
- Sanyal, S., A. De Ruiter and R. K. Hawkins (1980). "Development and degeneration of retina in rds mutant mice: light microscopy." J Comp Neurol **194**(1): 193-207.
- Scarselli, E., H. Ansuini, R. Cerino, R. M. Roccasecca, S. Acali, G. Filocamo, C. Traboni, A. Nicosia, R. Cortese and A. Vitelli (2002). "The human scavenger receptor class B type I is a novel candidate receptor for the hepatitis C virus." Embo J **21**(19): 5017-25.
- Schagger, H., W. A. Cramer and G. von Jagow (1994). "Analysis of molecular masses and oligomeric states of protein complexes by blue native electrophoresis and isolation of membrane protein complexes by two-dimensional native electrophoresis." Anal Biochem **217**(2): 220-30.
- Schagger, H. and G. von Jagow (1991). "Blue native electrophoresis for isolation of membrane protein complexes in enzymatically active form." Anal Biochem **199**(2): 223-31.
- Scherberich, A., G. Giannone, E. Perennou, K. Takeda, C. Boucheix, E. Rubinstein, F. Lanza and A. Beretz (2002). "FAK-mediated inhibition of vascular smooth muscle cell migration by the tetraspanin CD9." Thromb Haemost **87**(6): 1043-50.
- Schnorrer, F. and B. J. Dickson (2004). "Muscle building; mechanisms of myotube guidance and attachment site selection." Dev Cell **7**(1): 9-20.
- Seigneuret, M., A. Delaguillaumie, C. Lagaudriere-Gesbert and H. Conjeaud (2001). "Structure of the tetraspanin main extracellular domain. a partially conserved fold with a structurally variable domain insertion." J Biol Chem **276**(43): 40055-64.
- Shemer, G., M. Suissa, I. Kolotuev, K. C. Nguyen, D. H. Hall and B. Podbilewicz (2004). "EFF-1 is sufficient to initiate and execute tissue-specific cell fusion in *C. elegans*." Curr Biol **14**(17): 1587-91.
- Shoham, T., R. Rajapaksa, C. Boucheix, E. Rubinstein, J. C. Poe, T. F. Tedder and S. Levy (2003). "The tetraspanin CD81 regulates the expression of CD19 during B cell development in a postendoplasmic reticulum compartment." J Immunol **171**(8): 4062-72.
- Simons, K. and W. L. Vaz (2004). "Model systems, lipid rafts, and cell membranes." Annu Rev Biophys Biomol Struct **33**: 269-95.

- Singson, A., K. B. Mercer and S. W. L'Hernault (1998). "The *C. elegans* spe-9 gene encodes a sperm transmembrane protein that contains EGF-like repeats and is required for fertilization." Cell **93**(1): 71-9.
- Springer, T. A. (1997). "Folding of the N-terminal, ligand-binding region of integrin alpha-subunits into a beta-propeller domain." Proc Natl Acad Sci U S A **94**(1): 65-72.
- Stein, K. K., P. Primakoff and D. Myles (2004). "Sperm-egg fusion: events at the plasma membrane." J Cell Sci **117**(Pt 26): 6269-74.
- Stiasny, K., S. L. Allison, C. W. Mandl and F. X. Heinz (2001). "Role of metastability and acidic pH in membrane fusion by tick-borne encephalitis virus." J Virol **75**(16): 7392-8.
- Stipp, C. S. and M. E. Hemler (2000). "Transmembrane-4-superfamily proteins CD151 and CD81 associate with alpha 3 beta 1 integrin, and selectively contribute to alpha 3 beta 1-dependent neurite outgrowth." J Cell Sci **113** (Pt 11): 1871-82.
- Stipp, C. S., T. V. Kolesnikova and M. E. Hemler (2001). "EWI-2 is a major CD9 and CD81 partner and member of a novel Ig protein subfamily." J Biol Chem **276**(44): 40545-54.
- Stipp, C. S., T. V. Kolesnikova and M. E. Hemler (2003). "Functional domains in tetraspanin proteins." Trends Biochem Sci **28**(2): 106-12.
- Stipp, C. S., D. Orlicky and M. E. Hemler (2001). "FPRP, a major, highly stoichiometric, highly specific CD81- and CD9-associated protein." J Biol Chem **276**(7): 4853-62.
- Stipp, C. S., D. J. Orlicky and M. E. Hemler (2000). "FPRP: A major, highly stoichiometric, highly specific CD81 and CD9- associated protein." J Biol Chem **275**: 21.
- Sudhof, T. C. (2004). "The synaptic vesicle cycle." Annu Rev Neurosci **27**: 509-47.
- Sugiura, T. and F. Berditchevski (1999). "Function of alpha3beta1-tetraspanin protein complexes in tumor cell invasion. Evidence for the role of the complexes in production of matrix metalloproteinase 2 (MMP-2)." J Cell Biol **146**(6): 1375-89.
- Szollosi, J., V. Horejsi, L. Bene, P. Angelisova and S. Damjanovich (1996). "Supramolecular complexes of MHC class I, MHC class II, CD20, and tetraspan molecules (CD53, CD81, and CD82) at the surface of a B cell line JY." J Immunol **157**(7): 2939-46.

- Tachibana, I. and M. E. Hemler (1999). "Role of transmembrane 4 superfamily (TM4SF) proteins CD9 and CD81 in muscle cell fusion and myotube maintenance." J Cell Biol **146**(4): 893-904.
- Takada, Y. and W. Puzon (1993). "Identification of a regulatory region of integrin beta 1 subunit using activating and inhibiting antibodies." J Biol Chem **268**(23): 17597-601.
- Takagi, J., N. Beglova, P. Yalamanchili, S. C. Blacklow and T. A. Springer (2001). "Definition of EGF-like, closely interacting modules that bear activation epitopes in integrin beta subunits." Proc Natl Acad Sci U S A **98**(20): 11175-80.
- Takagi, J., H. P. Erickson and T. A. Springer (2001). "C-terminal opening mimics 'inside-out' activation of integrin alpha5beta1." Nat Struct Biol **8**(5): 412-6.
- Takagi, J., B. M. Petre, T. Walz and T. A. Springer (2002). "Global conformational rearrangements in integrin extracellular domains in outside-in and inside-out signaling." Cell **110**(5): 599-11.
- Takagi, J. and T. A. Springer (2002). "Integrin activation and structural rearrangement." Immunol Rev **186**: 141-63.
- Takashima, T., K. Ohnishi, I. Tsuyuguchi and S. Kishimoto (1993). "Differential regulation of formation of multinucleated giant cells from concanavalin A-stimulated human blood monocytes by IFN-gamma and IL-4." J Immunol **150**(7): 3002-10.
- Takeda, Y., I. Tachibana, K. Miyado, M. Kobayashi, T. Miyazaki, T. Funakoshi, H. Kimura, H. Yamane, Y. Saito, H. Goto, T. Yoneda, M. Yoshida, T. Kumagai, T. Osaki, S. Hayashi, I. Kawase and E. Mekada (2003). "Tetraspanins CD9 and CD81 function to prevent the fusion of mononuclear phagocytes." J Cell Biol **161**(5): 945-56.
- Talbot, P., B. D. Shur and D. G. Myles (2003). "Cell adhesion and fertilization: steps in oocyte transport, sperm-zona pellucida interactions, and sperm-egg fusion." Biol Reprod **68**(1): 1-9.
- Tanford, C. (1980). The Hydrophobic Effect, John Wiley and Sons.
- Tarrant, J. M., J. Groom, D. Metcalf, R. Li, B. Borobokas, M. D. Wright, D. Tarlinton and L. Robb (2002). "The absence of Tssc6, a member of the tetraspanin superfamily, does not affect lymphoid development but enhances in vitro T-cell proliferative responses." Mol Cell Biol **22**(14): 5006-18.
- Todres, E., J. B. Nardi and H. M. Robertson (2000). "The tetraspanin superfamily in insects." Insect Mol Biol **9**(6): 581-90.

- Tsitsikov, E. N., J. C. Gutierrez-Ramos and R. S. Geha (1997). "Impaired CD19 expression and signaling, enhanced antibody response to type II T independent antigen and reduction of B-1 cells in CD81-deficient mice." Proc Natl Acad Sci U S A **94**(20): 10844-9.
- Tu, B. P. and J. S. Weissman (2004). "Oxidative protein folding in eukaryotes: mechanisms and consequences." J Cell Biol **164**(3): 341-6.
- van der Flier, A. and A. Sonnenberg (2001). "Function and interactions of integrins." Cell Tissue Res **305**(3): 285-98.
- Waterhouse, R., C. Ha and G. S. Dveksler (2002). "Murine CD9 is the receptor for pregnancy-specific glycoprotein 17." J Exp Med **195**(2): 277-82.
- Wells, J. A. (1991). "Systematic mutational analyses of protein-protein interfaces." Methods Enzymol **202**: 390-411.
- Wishart, D. S. and B. D. Sykes (1994). "Chemical shifts as a tool for structure determination." Methods Enzymol **239**: 363-92.
- Wishart, D. S., B. D. Sykes and F. M. Richards (1991). "Relationship between nuclear magnetic resonance chemical shift and protein secondary structure." J Mol Biol **222**(2): 311-33.
- Wolf, E., P. S. Kim and B. Berger (1997). "MultiCoil: a program for predicting two- and three-stranded coiled coils." Protein Sci **6**(6): 1179-89.
- Wright, M. D., S. M. Geary, S. Fitter, G. W. Moseley, L. M. Lau, K. C. Sheng, V. Apostolopoulos, E. G. Stanley, D. E. Jackson and L. K. Ashman (2004). "Characterization of mice lacking the tetraspanin superfamily member CD151." Mol Cell Biol **24**(13): 5978-88.
- Wu, L. C. and P. S. Kim (1997). "Hydrophobic sequence minimization of the alpha-lactalbumin molten globule." Proc Natl Acad Sci U S A **94**(26): 14314-9.
- Wu, X. R., J. H. Lin, T. Walz, M. Haner, J. Yu, U. Aebi and T. T. Sun (1994). "Mammalian uroplakins. A group of highly conserved urothelial differentiation-related membrane proteins." J Biol Chem **269**(18): 13716-24.
- Wu, X. R., J. J. Medina and T. T. Sun (1995). "Selective interactions of UPIa and UPIb, two members of the transmembrane 4 superfamily, with distinct single transmembrane-domained proteins in differentiated urothelial cells." J Biol Chem **270**(50): 29752-9.

- Wu, X. R., T. T. Sun and J. J. Medina (1996). "In vitro binding of type 1-fimbriated *Escherichia coli* to uroplakins Ia and Ib: relation to urinary tract infections." Proc Natl Acad Sci U S A **93**(18): 9630-5.
- Wunschmann, S., J. D. Medh, D. Klinzmann, W. N. Schmidt and J. T. Stapleton (2000). "Characterization of hepatitis C virus (HCV) and HCV E2 interactions with CD81 and the low-density lipoprotein receptor." J Virol **74**(21): 10055-62.
- Xiong, J. P., T. Stehle, B. Diefenbach, R. Zhang, R. Dunker, D. L. Scott, A. Joachimiak, S. L. Goodman and M. A. Arnaout (2001). "Crystal structure of the extracellular segment of integrin alpha Vbeta3." Science **294**(5541): 339-45.
- Xu, H., S. J. Lee, E. Suzuki, K. D. Dugan, A. Stoddard, H. S. Li, L. A. Chodosh and C. Montell (2004). "A lysosomal tetraspanin associated with retinal degeneration identified via a genome-wide screen." Embo J **23**(4): 811-22.
- Yagami-Hiromasa, T., T. Sato, T. Kurisaki, K. Kamijo, Y. Nabeshima and A. Fujisawa-Sehara (1995). "A metalloprotease-disintegrin participating in myoblast fusion [see comments]." Nature **377**(6550): 652-6.
- Yanez-Mo, M., A. Alfranca, C. Cabanas, M. Marazuela, R. Tejedor, M. A. Ursa, L. K. Ashman, M. O. de Landazuri and F. Sanchez-Madrid (1998). "Regulation of endothelial cell motility by complexes of tetraspan molecules CD81/TAPA-1 and CD151/PETA-3 with alpha3 beta1 integrin localized at endothelial lateral junctions." J Cell Biol **141**(3): 791-804.
- Yanez-Mo, M., R. Tejedor, P. Rousselle and F. Sanchez -Madrid (2001). "Tetraspanins in intercellular adhesion of polarized epithelial cells: spatial and functional relationship to integrins and cadherins." J Cell Sci **114**(Pt 3): 577-87.
- Yang, X., C. Claas, S. K. Kraeft, L. B. Chen, Z. Wang, J. A. Kreidberg and M. E. Hemler (2002). "Palmitoylation of tetraspanin proteins: modulation of CD151 lateral interactions, subcellular distribution, and integrin-dependent cell morphology." Mol Biol Cell **13**(3): 767-81.
- Yang, X., O. V. Kovalenko, W. Tang, C. Claas, C. S. Stipp and M. E. Hemler (2004). "Palmitoylation supports assembly and function of integrin-tetraspanin complexes." J Cell Biol **167**(6): 1231-40.
- Yauch, R. L. and M. E. Hemler (2000). "Specific interactions among transmembrane 4 superfamily (TM4SF) proteins and phosphoinositide 4-kinase." Biochem J **351 Pt 3**: 629-37.
- Yauch, R. L., A. R. Kazarov, B. Desai, R. T. Lee and M. E. Hemler (2000). "Direct extracellular contact between integrin alpha(3)beta(1) and TM4SF protein CD151." J Biol Chem **275**(13): 9230-8.

- Zemni, R., T. Bienvenu, M. C. Vinet, A. Sefiani, A. Carrie, P. Billuart, N. McDonell, P. Couvert, F. Francis, P. Chafey, F. Fauchereau, G. Friocourt, V. des Portes, A. Cardona, S. Frints, A. Meindl, O. Brandau, N. Ronce, C. Moraine, H. van Bokhoven, H. H. Ropers, R. Sudbrak, A. Kahn, J. P. Fryns, C. Beldjord and J. Chelly (2000). "A new gene involved in X-linked mental retardation identified by analysis of an X;2 balanced translocation." Nat Genet **24**(2): 167-70.
- Zhang, X. A., A. L. Bontrager and M. E. Hemler (2001). "Transmembrane-4 superfamily proteins associate with activated protein kinase C (PKC) and link PKC to specific beta(1) integrins." J Biol Chem **276**(27): 25005-13.
- Zhu, G. Z., B. J. Miller, C. Boucheix, E. Rubinstein, C. C. Liu, R. O. Hynes, D. G. Myles and P. Primakoff (2002). "Residues SFQ (173-175) in the large extracellular loop of CD9 are required for gamete fusion." Development **129**(8): 1995-2002.



Room 14-0551
77 Massachusetts Avenue
Cambridge, MA 02139
Ph: 617.253.5668 Fax: 617.253.1690
Email: docs@mit.edu
<http://libraries.mit.edu/docs>

DISCLAIMER OF QUALITY

Due to the condition of the original material, there are unavoidable flaws in this reproduction. We have made every effort possible to provide you with the best copy available. If you are dissatisfied with this product and find it unusable, please contact Document Services as soon as possible.

Thank you.

Some pages in the original document contain color pictures or graphics that will not scan or reproduce well.